ISSN:2146-0957
eISSN:2146-5703

Volume:12 Number:2
July 2022

An International Journal of Optimization and Control: Theories & Applications

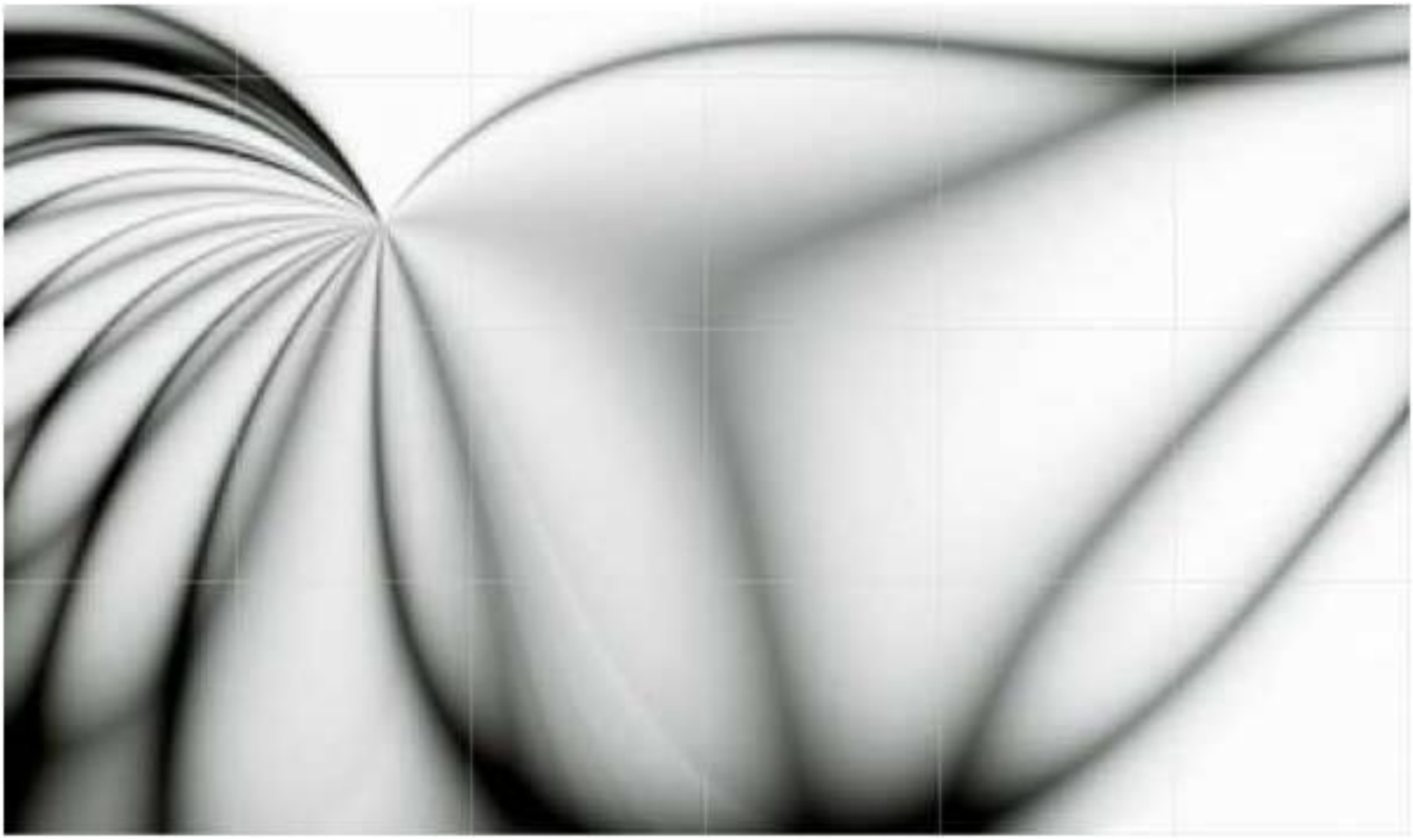

www.ijocta.org

http://www.ijocta.org
editor@ijocta.org

An International Journal of Optimization and Control:
Theories & Applications

Volume: 12, Number: 2
July 2022

Publisher & Owner *(Yayımcı & Sahibi)*:

Prof. Dr. Ramazan YAMAN
Atlas Vadi Campus 2020, Anadolu St.
No. 40, Istanbul, Turkey
Atlas Vadi Kampüsü 2020, Anadolu Cad.
No. 40, Avcılar, İstanbul, Türkiye

ISSN: 2146-0957
eISSN: 2146-5703

Press *(Basımevi)*:

Bizim Dijital Matbaa (SAGE Publishing),
Kazım Karabekir Street, Kültür Market,
No:7 / 101-102, İskitler, Ankara, Turkey
Bizim Dijital Matbaa (SAGE Yayıncılık),
Kazım Karabekir Caddesi, Kültür Çarşısı,
No:7 / 101-102, İskitler, Ankara, Türkiye

Date Printed *(Basım Tarihi)*:

July 2022
Temmuz 2022

Responsible Director (Sorumlu Müdür):

Prof. Dr. Ramazan YAMAN

IJOCTA is an international, bi-annual, and peer-reviewed journal indexed/abstracted by *(IJOCTA, yılda iki kez yayımlanan ve aşağıdaki indekslerce taranan/dizinlenen uluslararası hakemli bir dergidir)*:

- Scopus - Applied Mathematics
- Scopus - Control and Optimization
- Zentralblatt MATH
- ProQuest - Electronics & Communications Abstracts
- Proquest - Computer & Information Systems Abstracts
- Proquest - Mechanical & Transportation Eng. Abstracts
- EBSCOHost
- MathSciNet
- TR Dizin - Ulakbim (Science Database)
- Directory of Open Access Journals (DOAJ)

iThenticate plagiarism check service is granted by Balikesir University.

An International Journal of Optimization and Control:
Theories & Applications
Volume: 12 Number: 2
July 2022

CONTENTS

RESEARCH ARTICLES

An International Journal of Optimization and Control: Theories & Applications
ISSN: 2146-0957 eISSN: 2146-5703
Vol.12, No.2, pp.79-89 (2022)
https://doi.org/10.11121/ijocta.2022.1158

RESEARCH ARTICLE

Optimizing seasonal grain intakes with non-linear programming: An application in the feed industry

Alperen Ekrem Çelikdin

Planning and Logistics Manager, Tarfaş Aksaray Integrated Facilities, Aksaray, Turkey
a.celikdin@gmail.com

ARTICLE INFO

Article history:
Received: 11 September 2021
Accepted: 31 May 2022
Available Online: 12 June 2022

Keywords:
Financial optimization
Non-linear programming
Purchase planning

AMS Classification 2010:
90B05, 90B50

ABSTRACT

In the feed sector, 95% of the input costs arise from the supply of raw materials used in feed production. The selling price is determined by competition in free market conditions. Due to the use of similar technologies and the very small share of production costs in total costs, it is unlikely that a competitive advantage will be gained through innovations in production. Between 30% and 50% of grain products are used in feed ration analysis. Cereals can only be harvested at a certain time of the year. Due to this limited time frame, feed production enterprises have to balance their financial burdens with their operational needs while making their annual stocks. The study was carried out to cover all the relevant businesses of the company, which has feed factories in four regions of Turkey. Based on the season data of the year 2020-2021, the grain purchase planning for the year 2021-2022 was tried to be optimized with non-linear programming. While creating the mathematical model, grain prices, interest rates, production needs according to production planning, sales according to sales forecasts, factory stocking capacities, licensed warehouse rental, transportation, handling and transshipment costs were taken into account.

With this unique paper, in the cattle feed production sector, storage, transportation and handling costs will be minimized. Cost advantage will be provided with optimum purchase planning in the season. According to the grain pricing forecast and market data for the 2021-2022 season, model can provide a cost advantage of 0.7%. Model will also provide insight to the managers for additional storage space investments.

1. Introduction

Grain production is a strategic input of critical importance for both human and animal nutrition. The price of this strategic input is shaped under the influence of many factors. The most important factors affecting the price of grain products are the food industry price index, oil price, international food price, dollar and euro exchange rates, respectively [1]. Physical factors affecting harvest yield are also important in price formation. It is known that the grain group is the most important input in the content of animal feed rations. In this respect, cost items such as transportation, stock keeping and operating expenses should be purchased by considering the cost-benefit ratios. Grain prices reach their lowest level with the start of the harvest season and increase throughout the year due to the factors mentioned above. In addition, the availability of raw materials is limited and, due to seasonality, their prices and quality change over time.

Grain purchasing decisions in the feed sector are based on the experience of purchasing officials and their interpretations of market data in this direction, rather than analytical approaches. With this study, it is aimed to be affected by price changes at the minimum level during the year and to create a decision support model that will keep the financial burdens originating from stock holding at an optimal level. All constraints were taken into account while creating the model so that the dimensions encountered in business processes address real problems.

As far as we know, due to the generally accepted way of doing business in the feed industry, we have not encountered a decision support method that makes annual purchase planning within the framework of the factors determined in the mathematical model. The main contribution of this study is to fill this gap with a realistic and industry-independent purchasing planning optimization model.

*Corresponding author

The rest of the paper is structured as follows. A literature review is provided in Section 2. The formal problem is defined in Section 3. In Section 4 mathematical model is given. Section 5 summarizes computational results reached by running the model based on grain price estimations and financial input estimations for the current year, sensitivity analyzes and insights for magement related with the possible investments are given. In Section 6, the conclusions are mentioned as well as future research directions.

2. Literature review

In the modeling studies in the literature, it is seen that the general approach encountered is to model the entire supply chain instead of planning seasonal purchases. Soysal et al. [2] analyzed the quantitative studies in the food supply chain management, found that 54% of the distribution of methods in 36 studies was mixed integer programming, 20% was analytical studies, 11% was simulation techniques, 6% was linear programming, 6% was multi-objective programming. It is been stated that the remaining 3% is solved by goal programming. Most models were constructed with linear variables, and heuristic methods are developed due to overcome the complexity.

Agent-based simulation approaches and analytical models applied to supply chain management are studied by Ge et al. [3]. In order to determine the wheat quality testing, it was tried to decide how to structure and optimize the entire wheat supply chain. The creation of the wheat supply chain with the analytical model and the simulation approach were compared. This comparison was made between solutions and procedures. While the two approaches offer different solutions, in many respects similar conclusions have been reached regarding the general testing and quality control issue in wheat processing and handling.

While presenting a new analytical model in Hosseini et al. [4], the total cost of wheat supply chain network design has been tried to be optimized. The proposed model simultaneously integrates the harvesting, production, inventory and distribution dimensions of the wheat supply chain. The role of uncertainty in the analytical optimization model is emphasized and then a robust optimization approach is used to remove the uncertainty of the parameters. It is seen that the results obtained from the robust optimization model outperform the deterministic model. The study highlights that uncertainties over demand and supply can have a direct impact on the total cost of the supply chain.

In Mirzapour et al. [5], the problem of multi-regional, multi-period, multi-product mass production planning under uncertainty is discussed. It is designed as a supply chain that includes multiple suppliers, manufacturers and customers, respectively. In the first multi-objective robust mixed integer nonlinear programming model, the cost parameters and demand fluctuations of the supply chain are subject to uncertainty. The first objective aims to minimize the total losses in the supply chain, including the cost of production, the cost of hiring, firing and training, the cost of holding raw materials and finished products, the cost of transportation and shortages. The second objective function, on the other hand, is to ensure customer satisfaction by minimizing the sum of the maximum amount of deficiency among customers' regions in all periods. The LP-metric method was used to solve the model. The results show that the designed model can fulfill a compromise approach to satisfy an efficient production planning in the supply chain.

A general production and financial planning model is introduced in Satır and Yıldırım [6]. This model is realistic and strategic because of all the divisions in a complex poultry integration (including the feed mill, breeder houses, hatcheries, broiler houses, abattoirs and distribution centres) and the relationships between these divisions. The model appears to have made it a strategic level plan for the fast moving chicken industry due to the planning horizon taken into account over the years. It is seen that linear programming is used in the model, aiming to provide valuable management understanding by making sensitivity analysis at the expense of loosening the integrity requirement on some decision variables (egg, chick, chicken, number of workers). Experiments with various end-customer demand scenarios have found that the amount of broiler chicks to be purchased at certain times over the planning horizon is the sound key decision variable in the overall system.

Mogale et al. [7] examined the entire supply chain in terms of transportation and storage of grain during the harvest season. The researchers aimed to minimize operating costs by using a mixed integer nonlinear programming (MINLP) model with a large number of binary and integer variables with various complex constraints. Due to complexity, exact algorithms could not help with the optimal solution. Therefore, it is seen that the Hybrid Particle-Chemical Reaction Optimization (HP-CRO) algorithm is used to solve the MINLP model. It is stated that the hybrid model outperforms both particle swarm and chemical reaction optimization.

Razmi et al. [8] created a dynamic mixed integer linear programming (DMILP) model by addressing the problem in three separate sections, such as facility location selection, the decision to open and close the facilities during the season, supplier selection, and determination. The problem is categorized in the large size group. For this reason, it has been preferred to use heuristic algorithms, stating that the optimal solution cannot be obtained using the exact solution procedure. The solution has been searched by genetic algorithm and it can be seen as a satisfactory approach to divide the problem into three subproblems without losing the total optimization approach. Despite the comprehensive modeling approach, it was seen that the part of determining the lot sizes was not taken into account in order to minimize the inventory costs in the study.

Nourbakhsh et al. [9] proposed an optimum network design and total system cost minimization model, taking into account unit rail transport cost, pre-processing plant capital cost, raw grain price and post-harvest losses. Some operational assumptions have been made, such as that the loss of quality during transport and handling is directly proportional to the travel time. In the model, it is seen that the loss of dry matter over time due to the effect of initial humidity and temperature is not taken into account. In addition, inventory holding costs are neglected in the model and a simplified linear assumption is made. It can be said that it is beneficial to have the harvest time frame in the model as a new dimension.

Dwivedi et al. [10] developed a MINLP model in order to minimize total transportation cost and corbon emission tax so as to maintain a sustainable network design. Genetic algorithm (GA) and quantum-based genetic algorithm (Q-GA) and LINGO are employed for problem solving. The computational experiments concede that the performance of LINGO was better than meta-heuristics in terms of solution obtained, but opposite to solution, computational time was longer analogically.

Teixeira et al. [11] developed a MINLP model to provide decision support to the relevant unit management in the planning of purchases of a business operating in the retail sector. The step functions are designed to analyze different scenarios, mathematical programming modeling language (AMPL) is used. The solution found by the KNITRO solver is compared with the current operation. It was stated that the delivery methods of the products were rearranged by meeting with the suppliers every two weeks and a cost advantage of 19.41% was achieved.

Other than MILP and MINLP models discrete optimization had been utilized for the sake of applicable decision support for the supply chain management. Smith et al. [12] proposed a methodology for developing an optimal promotional plan that maximizes total season profit, subject to promotional resource constraints and a set of possible market scenarios, by selecting from a discrete set of candidate ads and markdowns. By the use of the model, optimal planning of the inventory levels, timely usage of ads and markdowns and less operational cost had been reached.

Deciding what quantity of material to procure is critical to improving the supply chain performance. [13] Tries to solve problem of wrong time and sizing of inventory orders in bakery industry. Profitability is mainly affected by the fluctuating cost of inputs together with rising operational and maintenance costs. To overcome these challenges researchers conducted ABC inventory analysis, optimized the total holding and ordering costs where it's suitable for the bakery industry operations as an approach which is close to economical order quantity procedure. As a result monthly purchasing quantities had been optimized with respect to monthly production forecasts. Also it includes recommendations for researchers on integrated inventory model for lead-time variability in order to cut down safety stock requirements.

The survey shows that numerical modeling is used effectively in supply chain management and provides decision support for significant profit margins and lower costs. However, lot size determination studies, except for [12], do not seem to focus on seasonal purchase planning as widely by researchers.

During the researches, only two studies were encountered that included both purchase/production lot sizes and plant storage capacities in the modeling at the same time [14-15]. Supply chain modeling/stock management with inter-facility transfers (transshipment) is covered in three related studies [16-18].

The contribution of this study to the literature can be seen as attempting to model production/purchasing lot-lot size, facility storage capacities and transfer between factories together, considering all possible alternatives in the calculations since it is designed to solve the relevant problem in real life.

3. Problem definition

Since the harvest period of grain products takes place in a limited time period and production can be made once a year, price fluctuations of the products are at a high level during the year. Successful stock management will ensure that these price fluctuations have minimal impact. Optimization of purchasing quantities is on the agenda as an important problem to be solved by purchasing decision makers, as stock holding investments are expensive and stocking can be done for a limited time. The purchases to be made during the season should include financial parameters, facility storage capacities, warehouses to be rented and the costs that will arise from these leasing transactions. Purchasing management will be an innovative approach that will allow scientific inferences to be made within the framework of the proposed decision support model, while making decisions based on market data and past experience. A model based on real-life data with all its dimensions will make it easier to make the right decisions. The problem has been evaluated in this context. As stated in the literature review in Section 2, no model was found for this purpose.

The basic approach in the model is to calculate the positioning return to be obtained by meeting the total needs with the purchases to be made in the previous monthly periods. It includes the comparison of the prices in the period when the position is taken with the estimated prices in the future periods when the need has to be met, and the comparison of this return remaining after the inventory holding costs arising from previous purchases deducted.

The company where the research was conducted has feed mill facilities in four different locations in Turkey. With the model, it is tried to find a solution about which grain type, which factory, which monthly period, in which quantity and at which unit price should be purchased. Based on this solution, it is aimed to plan external warehouse agreements, budget determination analyzes and operational actions. The healthy results of the study largely depend on the accuracy of price forecasts, interest rate forecasts and factory consumption analysis. Supply chain schema can be seen from Figure 1.

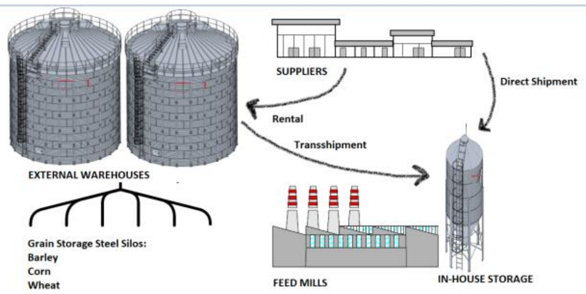

Figure 1. Supply chain schema

As can be seen from Figure 1, purchases from suppliers can be made directly to feed mills or to external warehouses. There will be rental costs in external warehouses as well as transshipment costs. Buying directly to the factory grain silos will minimize both rental fees and handling costs. For this reason, it is essential to optimize the capacity of the grain silos in the factories. To solve the problem described, the analytical model described in the next section was designed.

4. Mathematical model

As mentioned in Section 1, Frontline Analytic Solver software was used in this study to study the model designed to solve the mentioned problem in the computer environment. An NLP model is formulated for grain purchase planning and the results are analyzed using Microsoft Excel on a computer with a 2.0 GHz processor and 8 GB of RAM. All parameters and sets of the proposed NLP model are presented as follows.

Sets & parameters

f: factories = *{1,..,F}*

t: monthly periods = *{1,..,T}*

h: grain types used = *{1,..,H}*

sm^{dd}_{fht} , sa^{fb}_{fht} : for the factory f, inventory holding cost of the h type raw material in the outer warehouse in the period t, inventory transfer cost to the factory respectively.

$hm^{s}_{fht}, hm^{k}_{fht}$: for the factory f, at period t of the h type raw material, amount sold and used respectively.

av_h: Purchase deferment of h type raw material.

af_{fht}: Purchase price of h type raw material to factory f in period t.

an_{fh}: Raw material of type h received from the supplier is sent to the outer warehouse of the f factory, transshipment cost per ton.

dfn_{fh}: Per ton shipping cost of raw material h in the outer warehouse of factory f from warehouse to factory.

km_h: Rental cost per ton of keeping raw material h in an external warehouse.

em_h: Cost of handling raw material h in the outer warehouse.

dk_{fh}: Storage capacity for raw material h in factory f.

ddk_{fh}: Storage capacity for raw material h in the external warehouse of factory f.

$fo_t, dovk_{ht}$: Estimation of interest rate for period t, T.C.M.B. dollar exchange rate forecast in TL respectively.

4.1 Non-linear programming (NLP) model

The decision variables of the NLP model are defined as follows:

Decision variables

$hm^{a}_{fht}, hm^{i}_{fht}$: to factory f, the amount of raw material h type received and stocked in month t respectively.

dd^{i}_{fht} , $dd^{ç}_{fht}$, dd^{k}_{fht}: the amount of h type raw material stock, amount taken from the external warehouse to the factory f and amount stored at the outside warehouse at month t respectively.

X_{fht}: Purchase amount of raw material h for location f, in month t.

xv_{ht}: Remaining deferment of h type raw material in period t.

sfm_{fht}: Inventory financing cost for raw material h at month t of factory f/external warehouse.

PAG_{fht}: Return on positioning (early watch advantage) for raw material h at month t of factory f.

TNG_{fht}: Total net return from raw material h at factory f in month t.

The objective function and the constraints of the NLP model are presented below.

Objective function

$$\text{Maximize} \quad TNG_{fht} = PAG_{fht} - sfm_{fht} - sa^{fb}_{fht} - sm^{dd}_{fht}\ ;\ \forall t \in T\ ;\ \forall f \in F\ ;\ \forall h \in H \qquad (1)$$

Constraints

$$hm^{i}_{fht\ t=1,..,T,h=1,..,H,f=1,..F} \geq 0\ ,\ \forall t \in T\ ;\ \forall f \in F\ ;\ \forall h \in H \qquad (2)$$

$$hm^{i}_{fht-1} + hm^{a}_{fht} + dd^{ç}_{fht} = hm^{s}_{fht} + hm^{k}_{fht} + hm^{i}_{fht};\quad t = 1,..,T, h = 1,..,H, f = 1,..F;\ \forall t \in T\ ;\ \forall f \in F\ ;\ \forall h \in H \qquad (3)$$

$dd^{i}_{fht-1} - dd^{ç}_{fht} + dd^{k}_{fht} = dd^{i}_{fht};\quad t = 1,..,T, h = 1,..,H, f = 1,..F;\ \forall t \in T;\ \forall f \in F;\ \forall h \in H$ (4)

$hm^{i}_{fht} \geq hm^{k}_{fht} + hm^{s}_{fht};\ t = 1,..,T, h = 1,..,H, f = 1,..F;\ \forall t \in T;\ \forall f \in F;\ \forall h \in H$ (5)

$hm^{i}_{fht} \leq dk_{fh};\ t = 1,..,T, h = 1,..,H, f = 1,..F;\ \forall t \in T;\ \forall f \in F;\ \forall h \in H$ (6)

$\sum_{h=1}^{H} dd^{i}_{fht} \leq ddk_{fh};\ t = 1,..,T;\ f = 1,..F;\ \forall t \in T;\ \forall f \in F;\ \forall h \in H$ (7)

$\frac{hm^{i}_{fht}}{hm^{k}_{fht}}\ h \in H \leq 180;\ t = 1,..,T, h = 1,..,H, f = 1,..F;\ \forall t \in T;\ \forall f \in F;\ \forall h \in H$ (8)

$\frac{hm^{i}_{fht}}{hm^{k}_{fht}}\ h \in H \geq 10;\ t = 1,..,T, h = 1,..,H, f = 1,..F;\ \forall t \in T;\ \forall f \in F;\ \forall h \in H$ (9)

$\frac{X_{fht}}{hm^{k}_{fht}}\ h \in H \leq 365;\ t = 1,..,T, h = 1,..,H, f = 1,..F;\ \forall t \in T;\ \forall f \in F;\ \forall h \in H$ (10)

$X_{fht} = hm^{a}_{fht} + dd^{k}_{fht};\ t = 1,..,T, h = 1,..,H, f = 1,..F;\ \forall t \in T;\ \forall f \in F;\ \forall h \in H$ (11)

$sm^{dd}_{fht} = \sum_{f=1}^{F}\sum_{h=1}^{H}\sum_{t=1}^{T}[(dd^{k}_{fht} * an_{fht}) + (dd^{i}_{fht} * km_{ht}) + (em_{ht} *, dd^{ç}_{fht})];\quad \forall t \in T;\ \forall f \in F;\ \forall h \in H$ (12)

$sa^{fb}_{fht} = \sum_{f=1}^{F}\sum_{h=1}^{H}\sum_{t=1}^{T}(dfn_{fht} * dd^{ç}_{fht});\ \forall t \in T;\ \forall f \in F;\ \forall h \in H$ (13)

$sfm_{fht} = \sum_{f=1}^{F}\sum_{h=1}^{H}\sum_{t=1}^{T}(X_{fht} * fo_{t} * dovk_{ht} * af_{fht} * xv_{ht} * 30/36000)$ (14)

$xv_{ht} = \frac{X_{fht}}{hm^{k}_{fht}} - av_{h} \begin{cases} xv_{ht} > 0;\ xv_{ht} \\ xv_{ht} < 0;\ 0 \end{cases};\ \forall t \in T;\ \forall f \in F;\ \forall h \in H$ (15)

$PAG_{fht} = \sum_{f=1}^{F}\sum_{h=1}^{H}\sum_{t=1}^{T}\left(X_{fht}\right) * (af_{fht\left(t=t+\frac{X_{fht}}{hm^{k}_{fht}}\right)} - af_{fht});\ \forall t \in T;\ \forall f \in F;\ \forall h \in H$ (16)

The objective function of the NLP model given in Eq. (1) maximizes the net return resulting from the operations represents the gain remaining after the return on positioning is deducted from the cost of stock financing, the cost of transferring stock from the external warehouse and the costs of holding stock. The second constraint Eq. (2) ensures that for all monthly periods t, the stocked quantity in all factories and all types of raw materials cannot be negative. The third constraint Eq. (3) guarantees that the inventories at the beginning of the period are added to the purchases in the relevant period and the amount withdrawn from the external warehouse, deducting sales and uses, and the remaining inventory is transferred to the next period. With constraint number four, Eq. (4), the amount put in the external warehouse in the relevant period is added to the stocks in the outer warehouse at the beginning of the period, the amount withdrawn to the factory is deducted, and the remaining stock is transferred to the next period. Eq. (5) maintains the amount of raw material h stocked in the f factory in period t should not be less than the amount that is envisaged to be used and sold in the same period. The constraint (6) ensures the amount of raw material h stocked in factory f in period t should not be more than the warehouse capacity allocated for this raw material. With the constraint (7) in the external warehouse of factory f, the total amount of raw material stocked in period t cannot exceed the capacity of the outer warehouse. The number of days of stocking of raw materials stocked in factory f in period t should not exceed 180 days, see Eq. (8).

The number of stock days of raw materials stocked in factory f in period t should not fall below the critical stock level of 10 days (Eq. (9)). The number of stock days cannot exceed a one-year period in proportion to the amount of raw materials purchased in factory f in period t (Eq. (10)). Dispatch planning constraint (Eq. (11)) guarantees raw material h purchased in period t should be shipped to the f feed factory or to the external warehouse of this factory. External warehouse inventory holding cost consists of intermediate shipping + rental cost + handling cost, Eq. (12). Cost of transferring inventory from external warehouse to factory f, Eq. (13). Constraint (14) defines the stock holding cost and Constraint (15) defines the remaining purchase deferment period. The last equation, Eq. (16), stands for return on positioning which can be defined as, the product of the unit gain arising from the price difference that would occur if the long-term raw material purchased when the raw material was cheap, instead of if it was purchased at the very required time t. The problem is considered as a nonlinear programming model because of the nonlinear constraints (14), (15) and (16) where decision variables are multiplied and divided by each other.

5. Case study

Experiment design includes optimization of the analytical model in the light of real-life data. The study was designed and implemented by using real-life data for the optimization of grain purchases of the enterprise, which has factories in four regions of Turkey. The model was designed to include the purchasing optimizations of all raw material items of feed mills and analyzed as a real-life problem.

Experiment design are divided into three subsections. In the first part, the data generation procedure is explained in detail. Then, the computational results of the NLP model are given in the second subsection. The third subsection includes sensitivity analyzes and the profitability of investments that can be made in the axis of these analyzes and possible decision sets.

5.1 Data generation

Making the annual grain purchase planning correctly depends on the correct estimation of the financial data, as it will directly affect the solution of the model. The financial inputs of the model consist of grain market price forecasts, exchange rate and interest rate forecasts for periods t. Apart from these, it consists of external warehouse rental fee, handling and transshipment cost, which are operational costs. Time series analysis was used to estimate the grain market prices. The actual purchase prices of the previous year's data entered into the SPSS program, the price information that may occur at the beginning of the season of the planned year and in the next twelve-month purchase period are estimated as in Table 1.

Table 1. Forecasted price data for grains (time series t, raw material h – Currency *Turkish Liras*)

Month t	*h / barley*	*corn*	*wheat*
t.1	2.700	2.600	2.550
t.2	2.500	2.600	2.550
t.3	2.600	2.450	2.600
t.4	2.600	2.300	2.650
t.5	2.700	2.300	2.700
t.6	2.900	2.350	2.850
t.7	3.000	2.400	3.000
t.8	3.100	2.600	3.100
t.9	3.200	2.800	3.200
t.10	3.400	2.950	3.400
t.11	3.600	3.150	3.550
t.12	3.700	3.300	3.650
Average	*3.000*	*2.650*	*2.983*

Another financial input is the monthly interest rate data, which is the determinant of the cost of holding stock. The rates based on the results of the market participants survey published by the Central Bank of the Republic of Turkey (T.C.M.B.) are given in Table 2.

Table 2. Interest rate estimates (monthly time series t)

Month t	InterestRate %	*Month t*	Interest Rate %
t.1	19	*t.7*	15
t.2	19	*t.8*	15
t.3	18	*t.9*	14,5
t.4	17	*t.10*	14,5
t.5	16	*t.11*	14
t.6	16	*t.12*	14

The final financial input is exchange rates, which indirectly affect market prices for substitute products. Due to the fact that imports are carried out in dollar exchange rates, estimates are given in Table 3 based on the dollar exchange rate estimates made by T.C.M.B.

Table 3. Dollar exchange rate estimates in Turkish Liras

	t.1	t.2	t.3	t.4	t.5	t.6
$ / TL	8,5000	8,5850	8,6279	8,6711	8,7144	8,7580
	t.7	t.8	t.9	t.10	t.11	t.12
$ / TL	8,8018	8,8458	8,8900	8,9345	8,9791	9,0240

Operational cost items can be specified as warehouse rental cost, handling cost, warehouse-factory transshipment cost, supplier-factory transportation costs. All parameters listed in Table 4 below include all cost items calculated per ton for the raw materials being used.

Table 4. Operational cost items

	Rental Cost TL / Ton	Handling Cost TL / Ton	Trans shipment Cost TL / Ton	Direct Shipment Cost TL / Ton
Factory f=1	10	7	50	50
Factory f=2	10	7	100	100
Factory f=3	10	7	120	120
Factory f=4	10	7	270	270

Table 5. Estimated grain usages

Grain Type Period t	Estimated Usage (Ton)			
	Factory f=1	Factory f=2	Factory f=3	Factory f=4
Barley .t1	1.006	597	556	0
Barley .t2	1.168	866	580	0
Barley .t3	1.041	558	514	119
Barley .t4	434	482	423	125
Barley .t5	425	382	416	139
Barley .t6	343	322	167	153
Barley .t7	284	168	144	168
Barley .t8	263	151	118	185
Barley .t9	254	143	270	203
Barley .t10	280	214	166	223
Barley .t11	289	212	174	246
Barley .t12	355	217	180	270
Corn .t1	1.173	746	602	0
Corn .t2	1.168	692	589	0
Corn .t3	1.041	744	682	260
Corn .t4	1.880	964	1.504	274
Corn .t5	2.409	1.146	1.480	304
Corn .t6	2.469	1.501	1.713	334
Corn .t7	2.553	1.906	1.779	368
Corn .t8	2.368	1.767	1.449	404
Corn .t9	2.290	1.387	1.310	445
Corn .t10	2.523	1.659	1.493	489
Corn .t11	2.530	1.536	1.564	538
Corn .t12	2.202	1.517	1.081	592
wheat .t1	2.011	1.412	1.223	-
wheat .t2	1.836	1.212	1.197	-
wheat .t3	1.636	1.324	1.168	-
wheat .t4	1.302	1.068	517	-
wheat .t5	709	1.091	509	-
wheat .t6	754	750	509	-
wheat .t7	780	617	529	-
wheat .t8	724	505	431	-
wheat .t9	700	765	401	-
wheat .t10	701	696	498	-
wheat .t11	723	795	521	-
wheat .t12	923	867	1.081	-

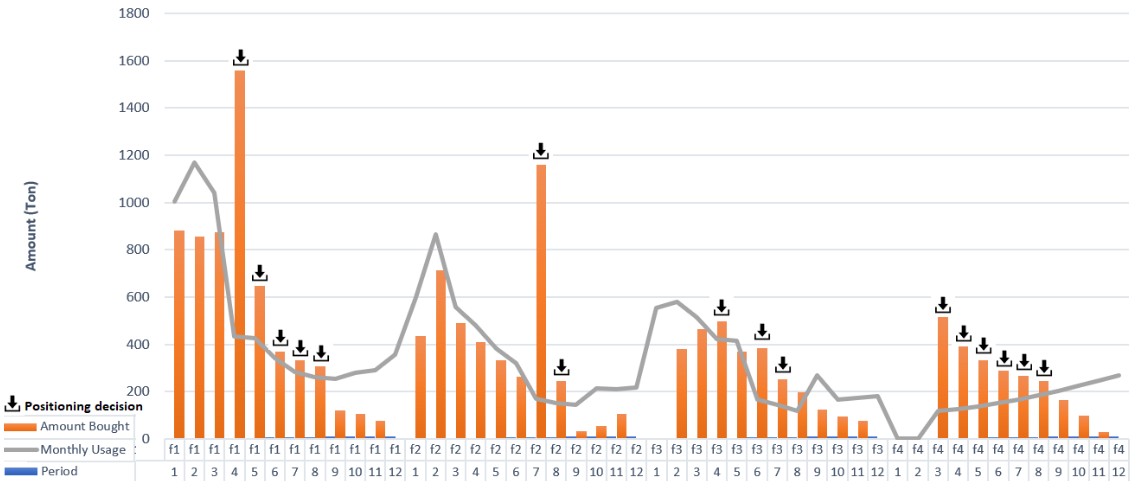

Figure 2. Purchase plan vs. monthly usage of barley

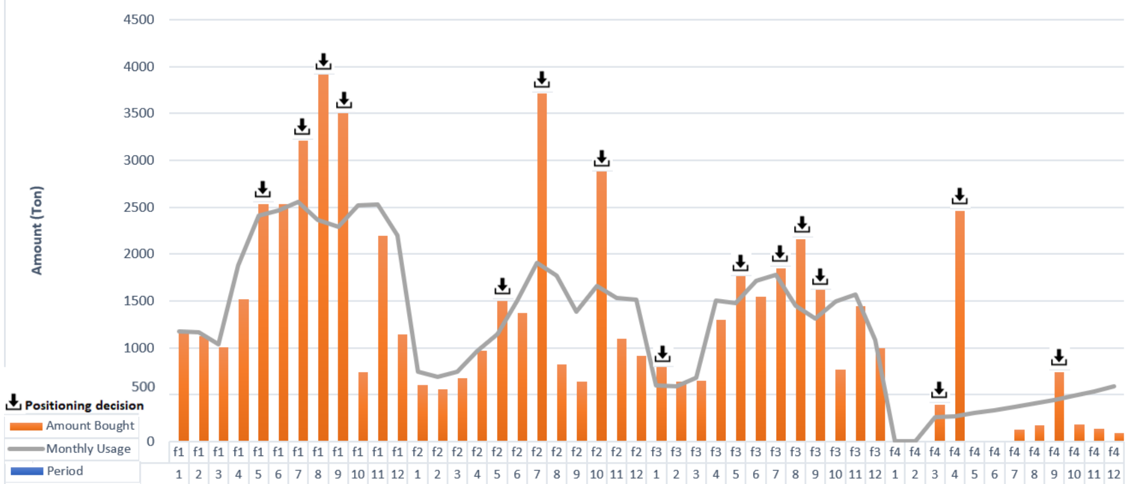

Figure 3. Purchase plan vs. monthly usage of corn

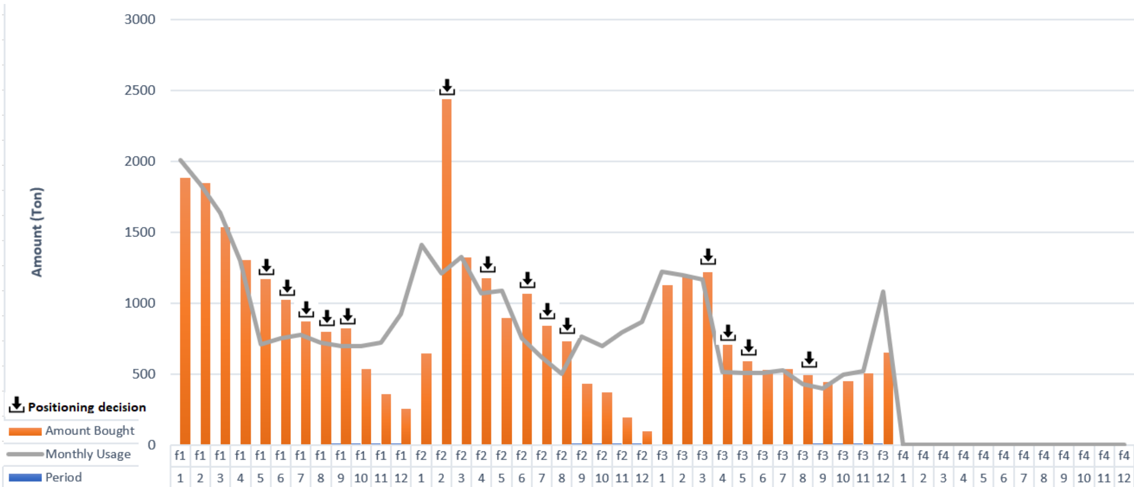

Figure 4. Purchase plan vs. monthly usage of wheat

Feed rations are prepared by the formulation department. While preparing the formula, the stock amounts of the raw materials in the existing stocks, market prices and feed target values are taken as basis. Production amounts of feeds are determined according to sales forecasts. According to the estimated grain prices, estimation recipes were prepared with the help of Brill recipe optimization program and estimated grain usage in the factories throughout the year was calculated. Estimated uses are given in Table 5.

Thus, all the necessary data for the model to provide a solution are determined.

5.2 Computational results

Model was coded in the GAMS program, in order to determine the purchase quantities and to avoid the problem of infeasibility which is eminating from start up stock quantities.

The initial stock quantities were captured. And using the initial feasible stock quantities, model solved with Excel Analytic Solver of Frontline Systems using the Gurobi engine with "General Constraint Helper Functions" available in Gurobi that will linearise the nonlinear constraints in the background. The mathematical model has 1.440 variables and 1.296 constraints. With the model, it takes an average of 4.8 seconds to reach a solution for a factory, which is a moderate time frame.

The main decision variables of the model are to determine how many tons of raw material h should be taken to factory f in which period t. The amount of raw material to be taken directly to the factory or to the external warehouse for later transfer to the factory is another variable that needs to be decided.

The values of the purchase amount decision variable on the basis of factories are given in Figures 2, 3 and 4 in comparison with the monthly usage amounts for the various grain types respectively. As it can be seen from the figures, some of the periods show some peaks in the amount bought. Those buying decisions which are higher amounts compared to the related monthly usage has some cost decreasing function. Those are positioning points. points are the optimum buying amounts just before some upward trend in the market prices of the grains. In those points, positioning gains and stock holding and handling cost are optimized.

Due to the feed usage habits in the region of the factory number 4, no wheat purchase planning has been made for this factory in the model, since wheat is not used in the ration content. This is why the purchase and estimated usage section in Figure 4 is empty. The financial results based on the purchase decisions made after the optimization are given in Table 6.

A gain of 11.6 million was achieved in return for 7.2 million TL investment, which is the sum of the storage, handling and financial costs incurred in order to take the position. 60% more return was obtained compared to the cost incurred. It is seen that the amount of return in factory number 3 is negative. Although this situation seems like a handicap in terms of the model and its solution, as can be seen from Table 7, it can be said that the negative amount would have been higher if this positioning had not been done.

Table 7. Financial results without positioning

	Factory 3
Total Amount Purchased (TON)	26.589,65
Total External Storage Amount (TON)	3.474,02
Total Purchasing Cost (TL)	72.783.925,99
Total External Storage Cost (TL)	59.058,39
Total Transshipment Cost (TL)	416.882,73
Total Financing Cost (TL)	977.537,99
Total Storage Cost (TL)	1.453.479,10
Total Gross Positioning Gain (TL)	1.304.277,17
Total Net Positioning Gain (TL)	***- 149.201,93***

The reason for the negative return in factory number 3 is that external storage solutions are needed more because the factory stocking area is lower than the stock area and usage forecast of other factories.

For this reason, the extra stocking and handling costs reduce the amount of return to a negative level. The subject will be examined in more detail in the sensitivity analysis and investment analysis section.

5.3 Sensitivity and investment analysis

Sensitivity analyzes were conducted to measure the effect of increasing the installed capacity on profitability and to determine to what extent it increased/decreased. The results are given in Figure 5.

The installed storage capacities of the factories are as given in Table 8.

Table 8. Installed storage capacities (Units in Ton)

	Factory 1	*Factory 2*	*Factory 3*	*Factory 4*	*Overall*
Barley	1.800	1.698	1.000	1.260	5.758
Corn	4.400	1.724	2.000	1.950	10.074
Wheat	1.800	2.560	1.000	-	5.360
Overall	8.000	5.982	4.000	3.210	21.192

Table 6. Financial results

	Factory 1	***Factory 2***	***Factory 3***	***Factory 4***	***Overall***
Total Amount Purchased (TON)	43.150,05	30.196,29	26.841,94	6.644,49	106.832,77
Total External Storage Amount (TON)	8.948,55	6.382,31	7.033,61	1.335,35	23.699,82
Total Purchasing Cost (TL)	115.752.441,97	81.604.833,84	73.005.150,61	17.361.083,81	287.723.510,24
Total External Storage Cost (TL)	152.125,27	108.499,21	119.571,45	22.700,94	402.896,86
Total Transshipment Cost (TL)	447.427,27	638.230,62	844.033,74	251.234,01	2.180.925,63
Total Financing Cost (TL)	1.791.119,70	1.493.840,04	1.000.196,89	363.310,53	4.648.467,15
Total Storage Cost (TL)	2.390.672,24	2.240.569,86	1.963.802,07	637.245,47	7.232.289,65
Total Gross Positioning Gain (TL)	3.876.989,97	2.915.465,10	1.820.547,54	3.006.571,78	11.619.574,39
Total Net Positioning Gain (TL)	***1.486.317,73***	***674.895,24***	***- 143.254,54***	***2.369.326,31***	***4.387.284,74***

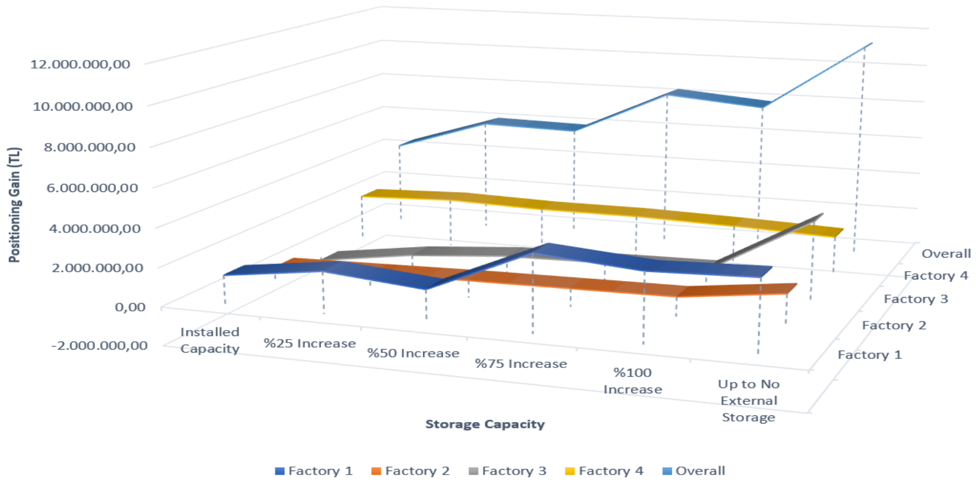

Figure 5. In-house storage capacity increase vs. positioning gain increase

In the model operated with the installed storage capacities, a positioning return of 4.3 million TL was achieved, while sensitivity analyzes of 25%, 50%, 75%, and 100% in-house capacity increase were performed, and it was observed that the return on positioning reached up to 7.8 million TL. The maximum achievable return installed capacity constraint was changed with a Big M number, and the model was revised, which provides a solution without the need for external storage. It has been observed that the maximum positioning return that can be achieved is 10,9 million TL.

Although the installed capacity is changed with a large number, the limits of the model have been determined due to the limitation that the maximum number of instant stock days cannot exceed 180 (constraint number 8) and the seasonal purchase cannot exceed a one-year period (constraint number 10). The required installed capacity determinations for the upper limit of the model are given in Table 9. Required extra storage space investments are given in Table 10.

Table 9. Maximum in-house capacity requirement (Units in Ton)

	Factory 1	*Factory 2*	*Factory 3*	*Factory 4*	*Overall*
Barley	1.800	1.698	1.666	1.260	6.424
Corn	8.575	4.043	7.302	2.573	22.493
Wheat	3.320	3.092	2.420	-	8.832
Overall	13.695	8.833	11.388	3.833	37.750

Table 10. Required Storage Space Investments (Units in Ton)

	Factory 1	*Factory 2*	*Factory 3*	*Factory 4*	*Overall*
Barley	-	-	666	-	666
Corn	4.175	2.319	5.302	623	12.419
Wheat	1.520	532	1.420	-	3.472
Overall	5.695	2.851	7.388	623	16.558

The investment return rate analysis for the determined steel silo requirements can be made as given in Table 11.

Table 11. Return on investment analysis

Steel Silo Investment Analysis	Unit	Amount
Investmet Cost (906,66 x 16.558)	**TL**	**15.012.476**
Positioning Gain Return / Yearly	TL	6.590.695
Interest Rate	%	19
Financial Cost	**TL**	**2.852.370**
Total Cost	**TL**	**17.864.847**
Total Savings (Useful Lifetime)	**TL**	**52.725.560**
ROI		**1,95**
Useful Lifetime	**Year**	**8,00**
Annual Savings of Investment	**TL**	**6.590.695**
Investment Cost Payback Time	**Month**	**32,53**
Return on invested capital	**%**	**36,89**

Although there is no consensus in the literature about the ideal figure for the return on investment [19] or minimum acceptable return rate, suggestions [20] have been made ranging from 9% to 22.5%. The company where the study is conducted sees investments with a return period of less than three years, starting with a return above the annual interest rate value, as low risk and is decided as acceptable. As a result of the analysis, the return period of the investment is determined as 32.5 months and the return rate is 36.89%, which is more than 19%, which is the current annual interest rate, thus meeting the investment feasibility conditions.

6. Conclusion

This study transforms the seasonal grain purchasing studies, which are generally carried out according to the market comments of the purchasing managers experienced in the feed industry, into an analytical non-linear optimization model in which experience is taken into account. In this way, it has been tried to develop an institutional tool that allows the simulation of different scenarios and alternatives. In the current situation, it is seen that the organization, which is the whole of the four enterprises, needs to increase its installed capacity as soon as possible.

As the first harvest period is approaching, it is not possible for the investment to be done this year. But it is beneficial to make an investment decision so that more positioning returns are possible to be reached. It is beneficial to make an investment decision so that the positioning gain is not low due to external warehouse leasing and transshipment fees. Hence cost-effective purchases can be provided in the future.

Since the model created enables the purchase planning of the grain types separately, it provides the opportunity to examine both the purchase and additional storage space investment for each grain type in detail. With simple changes that can be made in the model, a solution can be provided for all raw material inputs that can be used in feed content. With the model, it can be said that a useful tool has been created for the use of purchasing and planning executives in the feed sector.

The aspect of the study that is open to improvement is that the part where instant factors and free market conditions determine raw material prices in an environment of uncertainty is based on forecasts. Our suggestion for future studies may be to add to the model to allow price determinations with stochastic variables.

References

[1] Tay Bayramoğlu, Y. D. D. A. & Koç Yurtkur, Y. D. D. A. (2016). Türkiye'de Gıda ve Tarımsal Ürün Fiyatlarını Uluslararası Belirleyicileri. *Anadolu Üniversitesi Sosyal Bilimler Dergisi*, 15 (2) , 63-73.

[2] Soysal, M., Bloemhof-Ruwaard, J., Meuwissen, M., & Van der Vorst, J. (2012). A Review on Quantitative Models for Sustainable Food Logistics Management. I*nternational Journal of Food System Dynamics*. 3. 136-155.

[3] Ge, H., Gray, R. & Nolan, J. (2015). Agricultural supply chain optimization and complexity: A comparison of analytic vs simulated solutions and policies. *International Journal of Production Economics*, 159(C), 208-220.

[4] Hosseini, S.M., Motlagh, M.R.G., Samani, F. & Abbasi S. (2019). *Strategic optimization of wheat supply chain network under uncertainty: a real case study.* Springer Berlin Heidelberg.

[5] Mirzapour A., Malekly, H. & Aryanezhad, M.B. (2011). A multi-objective robust optimization model for multi-product multi-site aggregate production planning in a supply chain under uncertainty. *International Journal of Production Economics*. 134. 28-42.

[6] Satır, B. & Yıldırım, G. (2020). A General Production and Financial Planning Model: Case of a Poultry Integration, *Arabian Journal for Science and Engineering*. 45, 6803–6820.

[7] Mogale, D., Kumar, S. & Tiwari, M. (2018). An MINLP model to support the movement and storage decisions of the Indian food grain supply chain. *Control Engineering Practice.* 70. 98-113.

[8] Razmi, J., Kazerooni, M. P., & Sangari, M. S. (2016). Designing an integrated multi-echelon, multi-product and multi-period supply chain network with seasonal raw materials. *Economic Computation & Economic Cybernetics Studies & Research*, 50(1).

[9] Nourbakhsh, S. M., Bai, Y., Maia, G. D., Ouyang, Y., & Rodriguez, L. (2016). Grain supply chain network design and logistics planning for reducing post-harvest loss. *Biosystems Engineering*, 151, 105-115..

[10] Dwivedi, A., Jha, A., Prajapati, D., Sreenu, N., & Pratap, S. (2020). Meta-heuristic algorithms for solving the sustainable agro-food grain supply chain network design problem. *Modern Supply Chain Research and Applications.* 2 (3), 161-177

[11] Teixeira, A., Costa e Silva, E., & Lopes, I. C. (2021). A mixed integer nonlinear multiperiod model for supply chain management of a company in the retail sector. *RAIRO-Operations Research*, 55(2), 997-1013.

[12] Smith, S. A., Agrawal, N., & McIntyre, S. H. (1998). A discrete optimization model for seasonal merchandise planning. J*ournal of Retailing*, 74(2), 193-221.

[13] Nwanya, S. (2015). Material inventory optimization in bakery supply chain: Implications for food security in Nigeria. *International Journal of Supply and Operations Management*, 2(2), 683-699.

[14] Bilgen, B., & Günther, H. O. (2010). Integrated production and distribution planning in the fast moving consumer goods industry: a block planning application. *Or Spectrum*, 32(4), 927-955.

[15] Rong, A., Akkerman, R., & Grunow, M. (2011). An optimization approach for managing fresh food quality throughout the supply chain. *International Journal of Production Economics*, 131(1), 421-429.

[16] Brown, G.G., Keegan, J., Vigus, B., & Wood, R.K. (2001). The Kellogg Company Optimizes Production, Inventory, and Distribution, *Interfaces*, 31, 1-15.

[17] Wouda, F. H., van Beek, P., van der Vorst, J. G., & Tacke, H. (2002). An application of mixed-integer linear programming models on the redesign of the supply network of Nutricia Dairy & Drinks Group in Hungary. *Or Spectrum*, 24(4), 449-465.

[18] Ioannou, G. (2005). Streamlining the supply chain of the Hellenic sugar industry. *Journal of Food Engineering*, 70(3), 323-332.

[19] Jeynes, P. H. (1964). Minimum acceptable return. *The Engineering Economist*, 9(4), 9-25.

[20] Sinha, M. K., & Poole, A. V. (1987, September).

Selection of a discount rate or minimum acceptable IRR. In SPE Annual Technical Conference and Exhibition. OnePetro.

Alperen Ekrem ÇELİKDİN *currently works as a planning and logistics professional in the dairy feed industry. He received his B.S. degree from Çankaya University Industrial Engineering department. He received his MSc and Ph.D. degrees from the Business Administration Department of Aksaray University. His research interests include, supply chain planning, vehicle routing, heuristic optimization and organizational studies.*

https://orcid.org/0000-0002-2215-3812

An International Journal of Optimization and Control: Theories & Applications
ISSN: 2146-0957 eISSN: 2146-5703
Vol.12, No.2, pp.90-98 (2022)
https://doi.org/10.11121/ijocta.2022.1181

RESEARCH ARTICLE

Rotor design optimization of a synchronous generator by considering the damper winding effect to minimize THD using grasshopper optimization algorithm

Aslan Deniz Karaoglan [a] *, Deniz Perin [b]

[a] *Department of Industrial Engineering, Balikesir University, Turkey*
[b] *Department of R&D, ISBIR Electric Company, Turkey*
deniz@balikesir.edu.tr, tsr16@isbirelektrik.com.tr

ARTICLE INFO

Article history:
Received: 16 October 2021
Accepted: 31 January 2022
Available Online: 13 June 2022

Keywords:
Grasshopper optimization algorithm
Rotor design optimization
Synchronous generator
Total harmonic distortion
Damper winding

AMS Classification 2010:
13P25, 68T20

ABSTRACT

The aim of this study is to calculate the optimum factor levels for the design parameters namely slot pitch, center slot pitch, and damper width to keep the magnetic flux density distribution in a desired range while minimizing the total harmonic distortion (THD). For this purpose, the numerical simulations are performed in the Maxwell environment. Then by the aid of regression modeling over this simulation results; the mathematical equations between the responses (THD and magnetic flux density distribution) and the factors are calculated. After the modeling phase, grasshopper optimization algorithm (GOA) is run through these regression equations to determine the optimum values of the rotor design parameters (factors). The confirmations are also performed in the Maxwell environment and the result indicated that the THD is minimized and the magnetic flux density distribution on the teeth is kept in a desired range.

1. Introduction

Effect of damper winding in synchronous generator (SG) is investigated by many researchers. In these studies, total harmonic distortion (THD) and the magnetic flux density distribution are widely selected performance criteria those are tried to be improved. The output voltage's form is expected to be a sinusoidal. This means that THD is equal to zero. But because of various harmonic distortion components the output signal is distorted and THD increases. The chance of damage to the electrical machine increases as THD increases. For quality and sustainability, it is important to minimize THD in electric machine design. Magnetic flux density distribution is another important performance criterion which must be kept in a particular range to provide the high efficiency for the electric machine [1-3].

The related remarkable studies about the effect of damper winding in SG design are as follows: Matsuki et al. [4] investigated the effect of slot ripples on damper windings of SG. Two years later, they considered the oscillatory conditions of the power system and investigated the damper winding performance of a SG [5]. Vetter and Reichert [6] presented a study on damper winding currents of a SG with a solid iron rotor. Knight et al. [7] presented a study for predicting the force-density harmonics in salient-pole SG. For this purpose they used combined finite element method (FEM) and analytical modeling technique by considering the induced currents in the damper winding cage and their effects on force-density. Arjona [8] used FEM for simulating 2D nonlinear transient condition of 150 MVA two poles turbine generator and proposed an electrical circuit structure with 1D-axis damper winding. Lundstrom et al. [9] considered the effect of damper winding in the design of 74MVA synchronous hydropower generator. They used time-stepping FEM. Kinnunen et al. [10] studied on designing of damper windings for a permanent magnet SG (PMSG). They used 2D time transient field element analysis (FEA) to analyze the effects of damper winding constructions changes. Despalatovic et al. [11] studied on on-line parameter estimation of 34 MVA SG by considering damper winding. Rahimian and Butler-Purry [12] proposed an analytical method for the modeling SG with damper windings that is based on winding function approach

*Corresponding author

(WFA). Traxler-Samek et al. [13], proposed an algorithm to calculate the currents and corresponding losses in the damper winding of a large salient-pole SG. Zarko et al. [14] analyzed the effects of the stator winding parallel paths and the rotor damper winding of a salient-pole on attenuation of unbalanced magnetic pull. Matsuki et al. [15] investigated the effect of damper windings on the transient conditions of 4- pole SG by considering the magnetic flux. Wallin et al. [16] investigated the effect of three different damper winding configurations on unbalanced magnetic pull (UMP) in salient pole SG by considering the magnetic flux. They used FEM for the simulations. Nuzzo et al. [17] presented a study on improved damper cage design for salient-pole SG. Qiu et al. [18] studied on determining the influence factors to affect eddy current loss of damper windings in salient-pole 24 MW SG. They used FEM for the simulations. Elez et al. [19] presented a study on optimization of salient-pole SG. To that end they combined slot skew and damper winding pitch methods. Mandrile et al. [20] studied on the damping of the mechanical part of virtual SG (VSG) using only a damper winding in the q-axis. Nuzzo et al. [21] presented a simplified damper cage circuital model for modeling symmetric damper cages of salient-pole SG. Vanco et al. [22] investigated the effects of harmonic pollution on salient-pole SG by considering the currents induced on damper windings, on the field current and the disturbances on the load angle etc. Perin et al. [23] studied on minimizing the voltage THD of a salient-pole SG. They used grey wolf optimizer (GWO) to calculate the optimum design parameters (namely center slot pitch, slot pitch, and damper width) to minimize THD.

Besides these studies; the nature-inspired optimization algorithms such as genetic algorithm (GA) [24-30], particle swarm optimization (PSO) [31-35], ant-lion optimizer (ALO) [36], mosquito blood search algorithm (AMBS) [37] are previously used for THD minimization.

According to the studies presented in the literature damper winding effect is investigated in several studies. This study aims to calculate the optimum rotor design of 4-poled 1500 rpm 200 kVA SG by considering the damper winding effect. To that end, we studied on determining the optimum factor levels for the rotor parameters namely center slot pitch, slot pitch, and damper width to provide the desired magnetic flux density distribution while minimizing the total harmonic distortion (THD). THD (all voltage harmonics show THD values in this study) and magnetic flux density distributions are measured from Maxwell simulations. Regression modeling is used for the mathematical modelling, and then grasshopper optimization algorithm (GOA) is used for multi objective-optimization.

The grasshopper optimization algorithm (GOA) is a recently invented and very effective swarm based optimization algorithm [38]. GOA is not previously used for optimizing THD and magnetic flux density distribution. Using the design parameters namely: slot pitch, center slot pitch, and damper width together for multi-objective optimization of THD and magnetic flux distribution together with the aid of GOA, is the novelty direction of this study.

The motivation of this study is to present the readers that how the THD minimization can be performed effectively (while adjusting the magnetic flux density distribution to a desired tesla value) by considering the effect of damper winding by using minimum number of experimental runs. The reason is to avoiding dimensional design changes that will result in the new design of the production line. By considering only these parameters, we aimed to less affect the serial production line layout and its operations (such as the redesign of the assembly parts that may affect the standard production, body design, cooling design and etc.).

Another motivation of this study is to present the reader the usefulness of GOA for this type of design problems. As the No-Free-Lunch (NFL) has been shown, none of the literature's proposed algorithms can solve all problems with optimization [39, 40].

2. Mathematical modeling with regression

This paper aims to calculate the optimum factor levels of slot pitch, center slot pitch, and damper width to minimize the THD while keeping the magnetic flux density distribution in a desired range. To do this, in the first stage the mathematical relationship between these factors and the responses must be determined (then GOA will be run over these mathematical models to perform optimization). This is performed by using regression modeling. Regression models can be composed of linear terms, quadratic terms, and interaction terms. If a model has these three terms together then this model is called full quadratic model. The model is generally represented in Eq. (1) and it will be calculated from the experimental runs given in Section 4 which are obtained from the Maxwell simulations.

$$Y_u = \beta_0 + \sum_{i=1}^{n} \beta_i X_{iu} + \sum_{i=1}^{n} \beta_{ii} X_{iu}^2 + \sum_{i<j}^{n} \beta_{ij} X_{iu} X_{ju} + e_u \quad (1)$$

$$\boldsymbol{\beta}^{\mathrm{T}} = [\beta_0, \beta_1, \beta_2, \ldots, \beta_n] \quad (2)$$

Y_u represents the response value for uth experimental run. In this study responses are the THD and Magnetic flux density distribution, which means that we will calculate 2 different regression equations in Section 4. X terms are the values of the factors (in this study the factors are: X_1 :center slot pitch, X_2 : slot pitch, and X_3 : damper width). $X_{iu}X_{ju}$ terms represents the interaction terms in the model (in this study there can be maximum 3 interaction terms such as X_1X_2, X_1X_3, X_2X_3). e_u is the prediction error for the *u*th experimental run. The coefficients of this model will be calculated by regression modeling. β vector – that is given in Eq. (2) includes the coefficients of the models given in Eq. (1) and calculated as given below [41-44]:

$$\beta=\left(X^T X\right)^{-1}\left(X^T Y\right) \tag{3}$$

where Y represents a column vector that is composed of the observed response values. X represents the input matrix. The 1st column of X matrix is composed of 1s for the constant term (β_0) of the model. In a model that contains 3 factors; the 2nd, 3rd, and the 4th columns includes the factor values of X_1, X_2, and X_3 respectively . The 5th column is composed of the squares of X_1 and etc. That is to say the X matrix is arranged to include all columns in the model [41-44]. When the data given in Section 4 are examined, it will be seen that for the regression model of THD the X matrix with dimensions of 10x7 will be obtained for 10 runs and 7 model coefficients (β). Similarly, for the regression model of magnetic flux we will need a X matrix with dimensions of 10x5 will be obtained for 10 runs and 5 model coefficients. After the mathematical modeling, R^2 (coefficient of determination) is calculated to determine if the factors those are used in the mathematical model is sufficient to explain the change in the response. That is to say, R^2 is the strength level between the regression model and the factors.

$$R^2=\frac{\beta^{\mathrm{T}} X^T Y-n\bar{Y}^2}{Y^T Y-n\bar{Y}^2} \tag{4}$$

In order to use the mathematical model – that is calculated by the formulas given in Eqs. (1-3) – in the optimization phase; R^2 needs to be nearer to 1 (which means 100 percent). Because it means in this case that the modelling factors are sufficient to explain the Y change and there is no need to add additional factors to the model. If the R^2 is closer to 1, then in the last step before the optimization; the significance of the model must be determined. To do this “Analysis of Variance (ANOVA)” is used. ANOVA is a statistical hypothesis test – that uses F-test – to determine the model’s significance. ANOVA has two hypotheses (H0, H1). H0 means the regression model is insignificant, while H1 means it is significant. So to use the regression model in optimization phase, H1 must be true. If the test statistic that is calculated from the observations (F_0) is greater than the critical value obtained from F-statistical table ($F_{\alpha,m-1,N-m}$: where m is the number of coefficients estimated for regression, and N is the number of runs) or the “p-value” (in this study it is calculated by Minitab statistical package) is lower than the α (type I error) then this means H1 is true and the model is significant. ANOVA table is given in Table 1 [41-44]. In this table, df : degrees of freedom, SS: sum of squares, and MS: mean squares.

We selected the confidence level as 95%. This means the type-I error= α=0.05 (5%). After the modeling stage is completed, grasshopper optimization algorithm (GOA) was utilized to minimize the voltage THD under the desired magnetic flux density distribution by calculating the optimum factor levels for slot pitch, center slot pitch, and damper width.

Table 1. Analysis of variance (ANOVA) table.

Source	df	*SS*	*MS*=SS/df	*F*
Regression	m-1	$SS_{\text{Treatments}}$ (SS_{Tr})	MS_{Tr}	F_o=(MS_{Tr}/MS_E)
Residual Error	N-m	SS_{Error} (SS_E)	MS_E	

3. Grasshopper optimization algorithm (GOA)

Optimization methods mainly depend on gradient search. The local optima is one of the disadvantages of such methods. Stochastic methods use random operators for avoiding from local optima. Nature-inspired stochastic methods have become the most prominent in recent decades among these stochastic methods. GOA is presented by Saremi et al. [38]. GOA is a powerful optimization tool that uses a swarm-based metaheuristic optimization method inspired by nature. The ideal factor levels that give maximum efficiency and the required magnetic flux density distribution for SG are calculated using GOA in this work. To do this, GOA is run through the second order regression models those represent the mathematical relation between the rotor design parameters and the responses. By this way GOA is used as a search method on these response surfaces (regression models). The problem is represented by multi-objective and continuous mathematical equations (goal function). GOA mimics the grasshopper swarms’ behaviours in the nature. Numerous of them behave like rolling cylinders (by moving and jumping around the crops). Logically, nature-inspired algorithms divide the searching process into two phases. These are exploration and exploitation. In exploration phase the search agents of the optimization algorithm move abruptly. However in the exploitation phase, they tend to move locally. The following are the mathematical equations that express the combination of grasshopper natural behaviour with this optimization search logic [38, 45]:

$$X_i=r_1 S_i+r_2 G_i+r_3 A_i \tag{5}$$

The position of the *i*th grasshopper is defined by X_i. S_i, G_i, and A_i are the social interaction, gravity force, and wind advection on the ith grasshopper, respectively. The *r* parameters are the random numbers between [0,1]. The social interaction (which includes attraction and repulsion) is calculated as given in Eq. (6) [38, 45]:

$$S_i=\sum_{\substack{j=1\\ j\neq i}}^{N} s\left(d_{ij}\right)\hat{d}_{ij} \tag{6}$$

where s is the function ($s_r = fe^{-r/l}-e^{-r}$) that represents the strength of social forces. *f* and *l* are the intensity of attraction, and attractive length scale, respectively (please review [38] for better understanding of using s function). N represents the number of the grasshoppers. d_{ij} is the distance ($d_{ij} = \left|x_j - x_i\right|$) between *i*th and the *j*th grasshopper, and $\hat{d}_{ij}$ is a vector ($\hat{d}_{ij} = \left(x_j - x_i\right)/d_{ij}$) between two grasshoppers. s function has impact on the social interaction. This function divides the space between two grasshoppers into three parts (repulsion region, comfort zone, attraction region). Saremi et al. [38] considered the distances from 0 to 15 and they observed that the repulsion occurred between [0 2.079]. They suggested that when an artificial grasshopper is 2.079 unit away from another then this is called the comfort distance (in this comfort zone there is no attraction or repulsion). *l* and *f* parameters change this comfort zone. However at the distance values greater than 10, *s* function goes to zero. Because of this reason this function cannot apply strong forces between the grasshoppers at large distances. Another component of X_i is the G_i (gravity force) and calculated by the formulae given in Eq. (7) [38, 45]:

$$G_i = -g\hat{e}_g \tag{7}$$

g represents the gravitational constant, while the $\hat{e}_g$ represents a unity vector towards the center of the earth. Finally, A_i is the last component of X_i :

$$A_i = u\hat{e}_w \tag{8}$$

where *u* is a constant drift and $\hat{e}_w$ is a unity vector in the direction of wind. In the conventional swarm-based algorithms, the swarm is modeled as exploring and exploiting the search space surrounding a solution. The mathematical model of grasshopper algorithm utilized for the swarm is in free space. Therefore the model of X_i simulates the interaction between grasshoppers in a swarm. The expanded version of Eq. (5) that simulates the behaviour of grasshoppers in the 2D, 3D, and hyper dimensional spaces are given in Eq. (9) [38, 45].

$$X_i^d = c\left(\sum_{\substack{j=1 \\ j\neq i}}^{N} c\frac{ub_d - lb_d}{2} s\left(\left|x_j^d - x_i^d\right|\right)\frac{x_j - x_i}{d_{ij}}\right) + \hat{T}_d \tag{9}$$

c coefficient decreases to shrink the zones of comfort, repulsion, and attraction. The upper and lower bounds in the *D*th dimension s_r are represented by ub_d and lb_d respectively. $\hat{T}_d$ is the best solution. According to GOA, there is only one position vector for every search agent (in particle swarm optimization (PSO) – which is the pioneer and widely used swarm based optimizer- there is position and velocity vectors). Also in GOA all search agents are used in defining the next position of each search agent. This is another difference of GOA from PSO. The first term of Eq. (9) (the summation) considers the position of other grasshoppers and mathematically simulates the interaction of grasshoppers in nature. The second term ($\hat{T}_d$) represents their proclivity to migrate towards food sources. Finally, the parameter c is utilized to simulate grasshoppers decelerating as they approach the food source. and presented in Eq. (10) [38, 45].

$$c = c\max - l\frac{c\max - c\min}{L} \tag{10}$$

The maximum and minimum values are represented by *cmax* and *cmin*, respectively, whereas *l* denotes the current iteration and *L* is the maximum number of iterations. In their study, Saremi et al. [38] used *cmax*=1 and *cmin*=0.00001, and we utilized the same settings. In summary, the swarm converges gradually towards a stationary target by reducing the comfort zone by *c* parameter. Also the swarm properly chases a mobile target by $\hat{T}_d$. Over the course of iterations, the grasshoppers will converge on the objective. The GOA pseudo code is shown in Figure 1 below [38].

Initialize X_i, cmax, cmin, and max number of iterations
Calculate the fitness of each search agent
Assign T=the best search agent
While *l*<max number of iterations
    Update c by $c = cmax - l((cmax - cmin)/L)$
        For each search agent
            Normalize the d_{ij} between grasshoppers in [1,4]
            Update the position of the current search agent by X_i^d
            Bring the current search agent back if it goes outside the boundaries
        End For
    If there is a better solution **Then Update** T
    l=*l*+1
End While
Return T

Figure 1. Pseudo code for GOA

4. Experimental results and discussions

In this study we used 4-poled 1500 rpm 200 kVA SG. The design of this SG is performed in Maxwell environment and values of the design parameters for this SG are listed in Table 2. The SG is designed with 0.8 rated power factor. In the Maxwell design, all winding material is used as standard copper. Si-Fe is used for lamination. Finally H-Class insulation material is selected. In the first stage the aim is to determine the mathematical relation between the factors (center slot pitch, slot pitch, and damper width) and the responses (THD and magnetic flux density distribution) by using regression modeling. To perform this phase, an experiment is designed. The factor levels for this experimental design are displayed in Table 3.

The regression models will be calculated for both coded and uncoded factor levels. We actually need the coded model in the optimization phase. However to present the readers the real mathematical relation, the original models with uncoded factor levels are also calculated. Therefore, uncoded and coded factor levels are given together in Table 4. The coding is performed by using Eq. (11):

$$X_{coded} = \frac{X_{uncoded} - \left(\left(X_{\max} + X_{\min}\right)/2\right)}{\left(X_{\max} - X_{\min}\right)/2} \tag{11}$$

Table 2. General design parameters for 200 kVA SG.

Name	Value	Unit	Part	Description
Inner Ø of stator	350	mm	Stator	Core diameter on gap side
Outer Ø of stator	500	mm	Stator	Core diameter on yoke side
Length	310	mm	Stator	Length of core
Skew width	1	units	Stator	Range number of slot
Slots	48	units	Stator	Number of slots
Slot type	3	N/A	Stator	Circular (slot type: 1 to 6)
Hs0	1	mm	Stator	Slot opening height
Hs2	20	mm	Stator	Slot height
Bs0	4.2	mm	Stator	Slot opening width
Bs1	12	mm	Stator	Slot width
Bs2	13	mm	Stator	Slot width
Rs	5	mm	Stator	Slot bottom radius
Inner Ø of rotor	90	mm	Rotor	Core diameter on gap side
Length	310	mm	Rotor	Core length
Poles	4	-	Rotor	Number of poles
Pole-shoe width	181	mm	Rotor	One pole max width
Pole-shoe height	32.61	mm	Rotor	One pole max height
Pole-body width	113	mm	Rotor	One pole max width
Pole-body height	42.9	mm	Rotor	One pole max height
Number of Dampers	8	units	Rotor	Damper winding # per pole

Table 3. Factor levels.

Factors	Sym.	Unit	Levels 1	2	3
Center Slot Pitch (CSP)	X_1	degree	12	13	14
Slot Pitch (SP)	X_2	degree	6	8	-
Damper Width (DW)	X_3	mm	6	8	-

Ten experimental runs are performed by Maxwell simulations, and the results are given in Table 4. By this way the drawback of producing real SG prototypes – which is uncertain because of the costs – is eliminated.

Table 4. The experimental design and Maxwell simulation results.

Run	Factors (uncoded levels)			Factors (coded levels)			Responses THD	MFDD
i	X_{i1}	X_{i2}	X_{i3}	X_{i1}	X_{i2}	X_{i3}	Y_{i1}	Y_{i2}
1	12	6	6	-1	-1	-1	1.186	1.39040
2	12	8	6	-1	1	-1	2.411	1.32087
3	12	8	8	-1	1	1	1.383	1.34142
4	13	6	6	0	-1	-1	2.070	1.39651
5	13	6	8	0	-1	1	2.894	1.46600
6	13	8	6	0	1	-1	1.460	1.31892
7	14	6	8	1	-1	1	5.600	1.45451
8	14	8	6	1	1	-1	1.269	1.34685
9	14	8	8	1	1	1	4.071	1.36511
10	14	6	6	1	-1	-1	2.310	1.38768

After several preliminary trials, the regression model is derived by linear terms & interaction terms for THD, and linear terms & quadratic terms for magnetic flux density distribution (abbreviated as MFDD for ease of display). Calculations for regression modeling and the tests for model significance are performed by Minitab which is a well-known statistical package program. The original models are given in Eqs. (12) and (13).

$$\begin{aligned} THD_{uncoded} &= 20.9219047619047 - 1.75128571428571X_1 \\ &+ 7.85442857142858X_2 - 12.1850952380952X_3 \\ &- 0.599214285714286X_1X_2 + 0.990214285714285X_1X_3 \\ &- 0.0226071428571435X_2X_3 \end{aligned} \tag{12}$$

$$\begin{aligned} MFDD_{uncoded} &= -0.0684531381566749 \\ &+ 0.232632622055178X_1 - 0.0384676824433984X_2 \\ &+ 0.0225562435535113X_3 - 0.00861471623057757X_1^2 \end{aligned} \tag{13}$$

Matlab program is used for coding GOA, and optimization. In order to use these equations in Matlab environment for GOA optimization, the models must be derived for coded factor levels between -1 and 1. By this way the models become independent from the units and the multi-objective optimization can be performed easily. The regression models for coded factor levels are given in Eqs. (14) and (15).

$$\begin{aligned} THD_{coded} &= 2.31377380952381 + 0.985714285714286X_1 \\ &- 0.0936071428571428X_2 + 0.529440476190476X_3 \\ &- 0.599214285714286X_1X_2 + 0.990214285714285X_1X_3 \\ &- 0.0226071428571428X_2X_3 \end{aligned} \tag{14}$$

$$\begin{aligned} MFDD_{coded} &= 1.38850383336381 \\ &+ 0.00865000006016067X_1 - 0.0384676824433985X_2 \\ &+ 0.0225562435535113X_3 - 0.0086147162305774X_1^2 \end{aligned} \tag{15}$$

The R^2 statistics associated with the regression models of models THD and MFDD are 99 and 93.76% respectively. The prediction performance of the regression models are presented in Table 5. In this table, the $\hat{Y}_i$ values are the predicted responses by using Eqs. (14) and (15). The prediction error percentage (PE(%)) is also given for each response.

Table 5. The prediction performance of the models.

Run	THD			MFDD		
i	Y_{i1}	$\hat{Y}_{i1}$	$PE_{i1}(\%)$	Y_{i2}	$\hat{Y}_{i2}$	$PE_{i2}(\%)$
1	1.186	1.261	5.9	1.390	1.387	0.2
2	2.411	2.317	4.1	1.321	1.310	0.8
3	1.383	1.350	2.4	1.341	1.355	1.0
4	2.070	1.855	11.6	1.397	1.404	0.6
5	2.894	2.959	2.2	1.466	1.450	1.1
6	1.460	1.713	14.8	1.319	1.327	0.6
7	5.600	5.535	1.2	1.455	1.450	0.3
8	1.269	1.110	14.4	1.347	1.328	1.5
9	4.071	4.104	0.8	1.365	1.373	0.5
10	2.310	2.450	5.7	1.388	1.404	1.2

Table 6. ANOVA Table.

Response	Source	df	SS	MS
THD	Regression	6	17.8411	2.97352
	Residual Error	3	0.1804	0.06012
MFDD	Regression	4	0.02195	0.005488
	Residual Error	5	0.00146	0.000292

Table 6 (Continues).

Response	F_0 vs $F_{0.05,m-1,\ N-m}$	P-Value vs α=0.05	Result
THD	49.46> $F_{0.05,6,\ 3}$ (=8.9406)	0.004<0.05	Significant
MFDD	18.79> $F_{0.05,4,\ 5}$ (=5.1922)	0.003<0.05	Significant

The model significance is tested with ANOVA. The result of ANOVA is given in Table 6 (confidence level: 95%). The main effects plot and interaction plot for THD and MFDD are given in Figures 2 and 3, respectively.

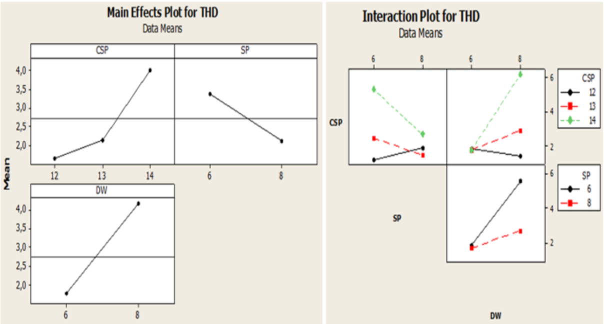

Figure 2. Main effects and interaction plot for THD.

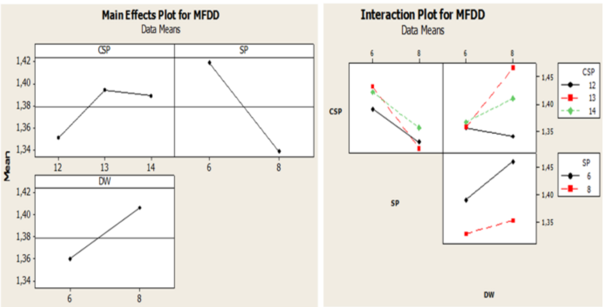

Figure 3. Main effects and interaction plot for MFDD.

According to the results, the regression models those are given in Eqs. (12) and (13) (also same as in Eqs. (14) and (15)) are significant.

Matlab program is used for coding GOA [38, 45]. In the algorithm, it is decided to use 100 search agents. Maximum number of iterations is 200. The number of search agents and the number of iterations were determined through a set of preliminary experiments. These preliminary experiments were carried out by trying different combinations by gradually changing the number of search agents between 20 and 200 and the maximum number of iterations between 100 and 1000. The problem is modeled as a constrained continuous optimization problem. For this purpose the regression models given in Eqs. (14) and (15)) are used and then the GOA algorithm is run through this model under the given constraint to optimize the factors.

$$Z = -\left|Y_{1,\,coded} / \max\left(Y_{i1}\right)\right| + \left|Y_{2,\,coded} / \max\left(Y_{i2}\right)\right| \tag{16}$$

$$Min\ Z\ s.t.\ X_1 \in [-1,1];\ X_2 \in [-1,1];\ X_3 \in [-1,1] \tag{17}$$

Note that the signs given in the equation of Z have to be reversed at Matlab code (see [45] for details). The CPU time is calculated as 32 seconds at a PC with a processor with Intel i5 2.4 GHz - 4 GB RAM. GOA is calculated the optimized factor levels as X_1=12 (coded value: -1), X_2=6 (coded value: -1), and X_3=8 (coded value: +1). For this optimized factor level combination; the THD is calculated as 0.3843, and magnetic flux density distribution is calculated as 1.4323 by GOA. For the confirmations, Maxwell simulations are performed. At the end of the simulations THD is calculated as 0.418, and magnetic flux density distribution is calculated as 1.4729. Structure of the optimized rotor, magnetic flux density distribution of optimized SG, and voltage graph of optimized SG are given in Fig. 4-6 respectively. The results indicate that minimum THD is obtained and magnetic flux density distribution is in the acceptable limits (green zone in Figure 5: 1-1.6 Tesla range).

The lamination used in this study can be used below 1.8 Tesla. As it reaches the value of 1.8 Tesla, SG is forced and above 1.8 Tesla is called the red zone where the efficiency decreases. As seen in Figure 5, the slot surface (on the surface of the lamination) between the rotor and the stator remains in the green zone from top to bottom. In addition, in the range of 1.6 – 1.7 Tesla, which we can call the forced zone, the yellow and orange zones are under full load and do not adversely affect the efficiency as they do not return to the red zone. Generally speaking, since the red areas are superficial and the green areas are predominant, there is no negative magnetic flux effect that will cause the efficiency of the SG to decrease.

Results also indicate that the increase in DW absorbs the fugitive magnetic fluxes in the windings, reducing the formation of inverse electromotive force (EMF) and harmonics. When DW is increased and mounted close to each other (SP is decreased), the probability of catching leakage fluxes increases.

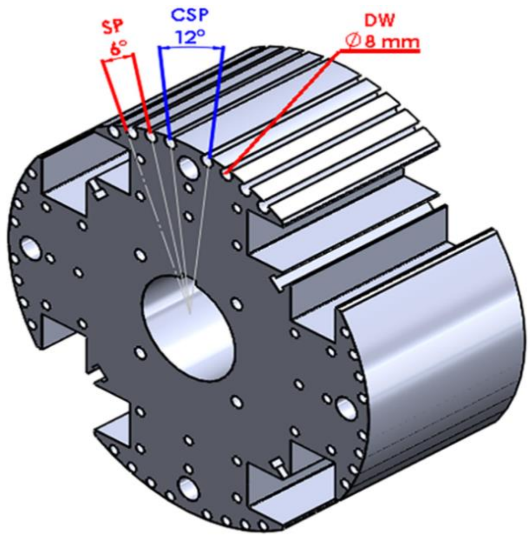

Figure 4. Structure of the optimized SG.

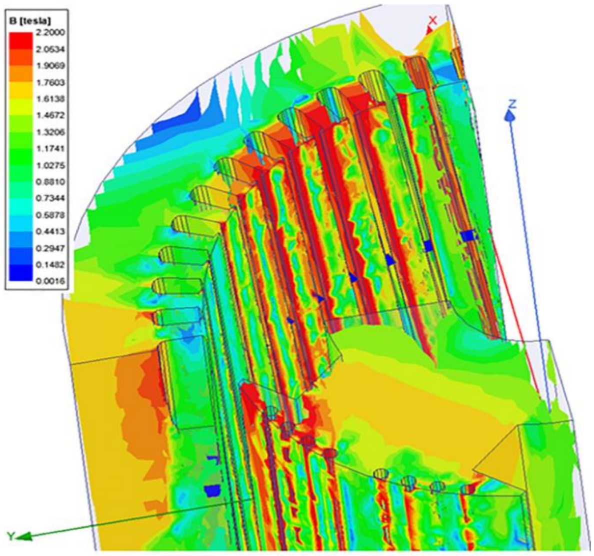

Figure 5. Magnetic flux density distribution of the optimized SG.

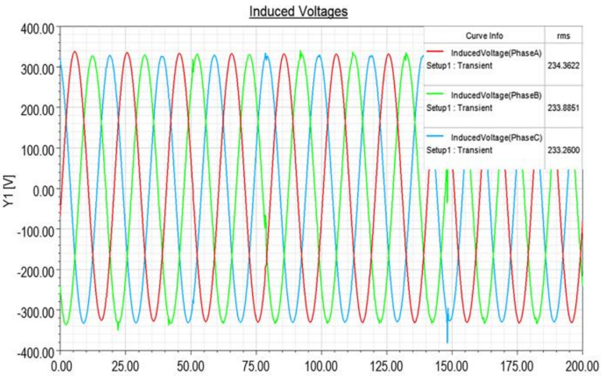

Figure 6. Voltage graph of the optimized SG.

5. Conclusion

In this study rotor design optimization of 4-poled 1500 rpm 200 kVA SG is performed. The aim is to determine the optimum factor levels of CSP, SP, and DW for minimizing THD and keeping the magnetic flux density distribution in a desired range. The regression models are fitted to the simulation results of Maxwell and GOA – which is an effective and recently invented nature-inspired optimization algorithm – is run through these regression models for optimization. The motivation is to present the readers that how THD and magnetic flux density distribution can be optimized by considering the effect of damper winding by using minimum number of experimental runs. THD of the SG is minimized to 0.38% and the magnetic flux density distribution is determined as 1.43 Tesla. The optimum factor levels for CSP, SP, and DW are calculated as 12, 6, and 8 respectively. For the confirmation one more Maxwell simulation is run and for this optimum factor levels the THD is calculated as 0.418, and magnetic flux density distribution is calculated as 1.4729 (which are very close to the predicted values). Results proved that regression modeling and GOA can be effectively used for this type of problem. Also one of the remarkable difference of GOA over previously used nature-inspired algorithms (such as GA, PSO, and etc.), is can be perform optimization with a very small number of iterations (200 iterations for this problem). So we can conclude that GOA can also be used effectively for optimization in this field such as the previously presented nature-inspired algorithms. As a future research we will expand the work for higher power groups.

Acknowledgments

We would like to thank Isbir Electric Company Research & Development Department for giving us the opportunity to use its facilities and softwares. We also gratefully thank to Kemal Yilmaz and Mehmet Baki Dogru for their support.

References

[1] De La Rosa, F. (2006). *Harmonics and Power Systems.* Taylor & Francis, Hazelwood, Missouri, USA.

[2] Arrillaga, J., & Watson, N.R. (2003). *Power System Harmonics* (2nd ed.). John Wiley & Sons, USA.

[3] Bakshi, U.A., & Godse, A.P. (2008). *Electronic Circuits and Applications* (3rd ed.). Technical Publications Pune, Pune, India.

[4] Matsuki, J., Katagi, T., & Okada, T. (1992). Effect of slot ripples on damper windings of synchronous machines. *Proc. of the IEEE International Symposium on Industrial Electronics*, 2, 864-865, Xian, China.

[5] Matsuki, J., Katagi, T., & Okada, T. (1994). Damper windings phenomena of synchronous machines during system oscillations. *IEEE Transactions on Energy Conversion*, 9(2), 376-382.

[6] Vetter, W., & Reichert, K. (1994). Determination of damper winding and rotor iron currents in convertor and line-fed synchronous machines. *IEEE Transactions on Energy Conversion*, 9(4), 709-716.

[7] Knight, A.M., Karmaker, H., & Weeber, K. (2002). Use of a permeance model to predict force harmonic components and damper winding effects in salient-pole synchronous machines. *IEEE Transactions on Energy Conversion*, 17(4), 478-484.

[8] Arjona, M.A. (2004). Parameter calculation of a turbogenerator during an open-circuit transient excitation. *IEEE Transactions on Energy Conversion*, 19(1), 46-52.

[9] Lundstrom, L., Gustavsson, R., Aidanpaa, J.O., Dahlback, N., & Leijon, M. (2007). Influence on the stability of generator rotors due to radial and tangential magnetic pull force. *IET Electric Power Applications*, 1(1), 1-8.

[10] Kinnunen, J.A., Pyrhonen, J., Niemela, M., Liukkonen, O., & Kurronen, P. (2007). Design of damper windings for permanent magnet synchronous machines. *International Review of Electrical Engıneering-IREE*, 2(2), 260-272.

[11] Despalatovic, M., Jadric, M., & Terzic, B. (2009). Influence of saturation on on-line estimation of synchronous generator parameters. *Automatika*, 50(3-4), 152-166.

[12] Rahimian, M.M., & Butler-Purry, K. (2009). Modeling of synchronous machines with damper windings for condition monitoring. *2009 IEEE International Electric Machines and Drives Conference*, 577-584, Miami, FL.

[13] Traxler-Samek, G., Lugand, T., & Schwery, A. (2010). Additional losses in the damper winding of large hydrogenerators at open-circuit and load conditions. *IEEE Transactions on Industrial Electronics*, 57(1), 154-160.

[14] Zarko, D., Ban, D., Vazdar, I., & Jaric, V. (2012). Calculation of Unbalanced Magnetic Pull in a Salient-Pole Synchronous Generator Using Finite-Element Method and Measured Shaft Orbit. *IEEE Transactions on Industrial Electronics*, 59(6), 2536-2549.

[15] Matsuki, J., Taoka, H., Hayashi, Y., Iwamoto, S., & Daikoku, A. (2014). Improvement of three-phase unbalance due to connection of dispersed generator by damper windings of synchronous generator. *Electrical Engineering in Japan*, 186(1), 43-50.

[16] Wallin, M., Bladh, J., & Lundin, U. (2013). Damper winding influence on unbalanced magnetic pull in salient pole generators with rotor eccentricity. *IEEE Transactions on Magnetics*, 49(9), 5158-5165.

[17] Nuzzo, S., Degano, M., Galea, M., Gerada, C., Gerada, D., & Brown, N. (2017). Improved damper cage design for salient-pole synchronous generators. *IEEE Transactions on Industrial Electronics*, 64(3), 1958-1970.

[18] Qiu, H., Fan, X., Feng, J., & Yang, C. (2018). Influence factors to affect eddy current loss of damper winding in 24 MW bulb tubular turbine generator. *COMPEL-The International Journal for Computation and Mathematics in Electrical and Electronic Engineering*, 37(1), 375-385.

[19] Elez, A., PetriniC, M., PetriniC, M., Vaseghi, B., & Abasian, A. (2018). Salient pole synchronous generator optimization by combined application of slot skew and damper winding pitch methods. *Progress in Electromagnetics Research M*, 73, 81-90.

[20] Mandrile, F., Carpaneto, E., & Bojoi, R. (2019). Virtual synchronous generator with simplified single-axis damper winding. *28th IEEE International Symposium on Industrial Electronics (IEEE-ISIE)*, Vancouver, Canada, Jun. 12-14.

[21] Nuzzo, S., Bolognesi, P., Gerada, C., & Galea, M. (2019). Simplified damper cage circuital model and fast analytical-numerical approach for the analysis of synchronous generators. *IEEE Transactions on Industrial Electronics*, 66(11), 8361-8371.

[22] Vanco, W.E., Silva, F.B., de Oliveira, J.M.M., & Monteiro, J.R.B.A. (2020). Effects of harmonic pollution on salient pole synchronous generators and on induction generators operating in parallel in isolated systems. *International Transactions on Electrical Energy Systems*, 30(6), Article Number: e12359.

[23] Perin, D., Karaoglan, A.D., & Yilmaz, K. (2021). Using grey wolf optimizer to minimize voltage total harmonic distortion of a salient-pole synchronous generator. *Scientia Iranica*. DOI: 10.24200/SCI.2021.57657.5349 *(Inpress)*.

[24] Sayyah, A., Aflaki, M., & Rezazade, A.R. (2006). Optimization of THD and suppressing certain order harmonies in PWM inverters using genetic algorithms. *IEEE International Symposium on Intelligent Control*, Munich, Germany, Oct. 4-6.

[25] De Almeida, A.M.F., Pamplona, F.M.P, Braz, H.D.M., da Silva, J.A.C.B., & Barros, L.S. (2014) Multiobjective optimization for volt/THD problem in distribution system. *6th World Congress on Nature and Biologically Inspired Computing (NaBIC)*, Porto, Portugal, Jul 30-Aug 01.

[26] Pradigta, S.R.L., Asrarul, Q.O., Arief, Z., & Windarko, N.A. (2017). Reduction of total harmonic distortion (THD) on multilevel inverter with modified PWM using genetic algorithm. *Emitter-International Journal of Engineering Technology*, 5(1), 91-118.

[27] Rodriguez, J.L.D., Fernandez, L.D.P., & Penaranda, E.A.C. (2017). Multiobjective genetic algorithm to minimize the THD in cascaded multilevel converters with V/F control. *4th Workshop on Engineering Applications (WEA)*, Univ Tecnologica Bolivar, Cartagena, COLOMBIA, Sep. 27-29.

[28] Fernandez, L.D.P., Rodriguez, J.L.D., & Penaranda, E.A.C. (2018). Optimization of the THD and the RMS voltage of a cascaded multilevel power converter. *IEEE International Conference on Automation (ICA) / 23rd Congress of the Chilean-Association-of-Automatic-Control (ACCA)*, Concepcion, CHILE, Oct. 17-19.

[29] Fernandez, L.D.P., Rodriguez, J.L.D., & Penaranda, E.A.C. (2019). A multiobjective genetic algorithm for the optimization of the THD and the RMS output voltage in a multilevel converter with 17 levels of line voltage. *IEEE Colombian Conference on Applications in Computational Intelligence (ColCACI)*, Barranquilla, Colombia, Jun 5-7.

[30] Booln, M.B., & Cheraghi, M. (2019). THD Minimization in a Five-Phase Five-Level VSI Using a Novel SVPWM Technique. *10th International Power Electronics, Drive Systems and Technologies Conference (PEDSTC)*, Shiraz Univ, Shiraz, Iran, Feb. 12-14.

[31] Alinejad-Beromi, Y., Sedighizadeh, M., & Sadighi, M. (2008). A particle swarm optimization for sitting and sizing of distributed generation in distribution network to improve voltage profile and reduce THD and losses. *43rd International-Universities-Power-Engineering Conference*, Padova, Italy, Sep. 1-4.

[32] Gallardo, J.A.A., Rodriguez, J.L.D., & Garcia, A.P. (2013). THD optimization of a single phase cascaded multilevel converter using PSO technique. *Workshop on Power Electronics and Power Quality Applications (PEPQA)*, Bogota, Colombia, Jul 6-7.

[33] Kanth, D.S.K., & Lalitha, M.P. (2014). Mitigation of real power loss, THD & enhancement of voltage profile with optimal DG allocation using PSO & sensitivity analysis. *Annual International Conference on Emerging Research Areas -*

Magnetics, Machines and Drives (AICERA/iCMMD), Kottayam, India, Jul. 24-26.
[34] Memon, M.A., Memon, S., & Khan, S. (2017). THD minimization from H-bridge cascaded multilevel inverter using particle swarm optimization technique," *Mehran University Research Journal of Engineering and Technology*, 36(1), 33-38.
[35] Dhanalakshmi, M.A., Ganesh, M.P., & Paul, K. (2016). Analysis of optimum THD in asymmetrical H-bridge multilevel inverter using HPSO algorithm. *2nd International Conference on Intelligent Computing and Applications (ICICA)*, KCG Coll Technol, Chennai, India, Feb. 5-6.
[36] Francis, R., & Meganathan, D. (2018). An Improved ANFIS with Aid of ALO Technique for THD Minimization of Multilevel Inverters. *Journal of Circuits Systems and Computers*, 27(12), Article Number: 1850193.
[37] Khalid, S., & Verma, S. (2019). THD and compensation time analysis of three-phase shunt active power filter using adaptive mosquito blood search algorithm (AMBS). *International Journal of Energy Optimization and Engineering (IJEOE)*, 8(1), 25-46.
[38] Saremi, S., Mirjalili, S., & Lewis, A. (2017). Grasshopper optimisation algorithm: theory and application. *Advances in Engineering Software*, 105, 30-47.
[39] Wolpert, D.H., & Macready, W.G. (1997). No free lunch theorems for optimization. *IEEE Transactions on Evolutionary Computation*, 1, 67–82 .
[40] Mirjalili, S., Gandomi, A.H., Mirjalili, S.Z., Saremi, S., Faris, H., & Mirjalili, S.M. (2017). Salp Swarm Algorithm: A bio-inspired optimizer for engineering design problems, Salp Swarm Algorithm: A bio-inspired optimizer for engineering design problems. *Advances in Engineering Software*, 114, 163-191.
[41] Montgomery, D.C. (2013). *Design and analysis of experiments* (8th ed.). John Wiley & Sons, New Jersey, USA.
[42] Mason, R.L., Gunst, R.F., & Hess, J.L. (2003). *Statistical Design and Analysis of Experiments* (2nd ed.). John Wiley & Sons, New Jersey, USA.
[43] Ileri, E., Karaoglan, A.D., & Akpinar, S. (2020). Optimizing cetane improver concentration in biodiesel-diesel blend via grey wolf optimizer algorithm. *Fuel*, 273, article number:117784.
[44] Karaoglan, A.D., Ocaktan, D.G., Oral, A., & Perin, D. (2020). Design Optimization of Magnetic Flux Distribution for PMG by Using Response Surface Methodology. *IEEE Transactions on Magnetics*, 56(6), 1-9, article number: 8200309.
[45] Mirjalili, S. (2020). *Grasshopper optimisation algorithm [online]*. Available from: http://www.alimirjalili.com. Accessed 01 June 2020.

Aslan Deniz Karaoglan *received a diploma degree in industrial engineering from Gazi University in 2001 (Turkey), MSc. in industrial engineering from Balikesir University in 2006 (Turkey), and Ph.D. in industrial engineering from Dokuz Eylul University in 2010 (Turkey). His research interests are design of experiments, statistical process control, artificial intelligence, and optimization. He is an associate professor at Balikesir University (Turkey), Department of Industrial Engineering.*
http://orcid.org/0000-0002-3292-5919

Deniz Perin *received MSc. and Ph.D. Degrees in Physics from Balikesir University in 2015 (Turkey). He has studied magnetic flux leakage (MFL) and magnetic non-destructive testing in Ph.D. and in research program of Cardiff University Wolfson Centre for magnetics. From 2017 till now, he is working on magnetic design & simulations of synchronous generators with ANSYS Maxwell in Isbir Electric Co Research & Development Department as a research and development expert.*
http://orcid.org/0000-0003-3697-3499

An International Journal of Optimization and Control: Theories & Applications
ISSN:2146-0957 eISSN:2146-5703
Vol.12, No.2, pp.99-112 (2022)
http://doi.org/10.11121/ijocta.2022.1166

RESEARCH ARTICLE

A belief-degree based multi-objective transportation problem with multi-choice demand and supply

Vandana Kakran*, Jayesh Dhodiya

Department of Mathematics and Humanities, S.V. National Institute of Technology, Surat, Gujarat, India
vandana.kakran98@gmail.com, jdhodiya2002@yahoo.com

ARTICLE INFO

Article History:
Received 21 September 2021
Accepted 1 June 2022
Available 12 July 2022

Keywords:
Multi-objective transportation problem
Multi-choice
Uncertain programming
Fuzzy programming technique

AMS Classification 2010:
90B50; 90C31; 91B06 ;90C70

ABSTRACT

This paper focusses on the development of a Multi-choice Multi-objective Transportation Problem (MCMOTP) in the uncertain environment. The parameters associated with the objective functions in MCMOTP are regarded as uncertain variables and the other parameters associated with supply capacity and demand requirements are considered under the multi-choice environment. In this paper, two ranking criteria have been utilized to convert the uncertain objectives into their crisp form. Using these two ranking criteria for the uncertain MCMOTP model, two deterministic models have been developed namely, Expected Value Model (EV Model) and Optimistic Value Model (OV Model). The multi-choice parameters in the constraints are converted to a single choice parameters with the help of binary variable approach. The EV and OV models are solved directly in the LINGO 18.0 software using minimizing distance method and fuzzy programming technique. At last, a numerical illustration is provided to demonstrate the application and algorithm of the models. The sensitivity of the objective functions in OV Model is also examined with respect to the confidence levels to investigate variation in the objective functions.

1. Introduction

In the business sector, transportation is one of the most significant concerns. The Transportation Problem (TP) consists of many warehouses (sources) and delivery locations (destinations). The basic objective of this problem is to find the quantity of items that should be supplied from each warehouse to each consumer while reducing the transportation cost. The concept of TP was first introduced by Hitchock [1] in 1941. In real life applications, the decision-makers wish to optimize multiple objectives simultaneously instead of a single objective. Many researchers have addressed the multi-objective environment in a wide range of applications because it is better adapted to real-world scenarios than a single-objective environment. Some of the authors such as [2–4] have considered multi-objective environment to deal with various real world problems. When the multi-objective environment is incorporated in the transportation theory, it results in Multi-objective Transportation Problem (MOTP) which is more applicable in the real world. These multiple objectives can be inherently conflicting in nature, so they cannot be optimised at the same time. For example, a transportation problem may require minimising overall transportation cost and transportation time while transporting the items. Zimmermann [5] introduced the Fuzzy Programing Technique (FPT) to solve multi-objective linear programming problems. FPT has wide number of applications in the field of optimization problems such as [6–8]. The MOTPs can involve different types of multiple objective functions like transportation cost, transportation time, damage cost, profit, CO_2

*Corresponding Author

emissions etc.

In traditional TP, the supply, demand and cost parameters for transportation problems were assumed to be precisely defined. However, this is not the case while handling real-world applications because not all of the parameters in the TP can be defined precisely. Consequently, a number of theories have been developed to represent imprecise TP parameters such as fuzzy set theory [9], probability theory [10], and interval theory [11]. Transportation problems are distinguished by the parameter space or variable space in which they are defined. For example, the TPs with variables/parameters considered as fuzzy numbers are known as fuzzy TPs and the TPs with parameters considered in the random space are known as the stochastic TPs. Likewise, the TP with variables as interval numbers are known as interval TPs. These theories are suitable when historical information is available for estimating imprecise values. These notions (historical data available) have been studied by several researchers in the transportation problem. Many researchers like Bhargava et al. [12], Giri et al. [13], Ali Ebrahimnejad [14] have considered the multi-objective TP under the fuzzy logic and obtained the compromise solution using the different solution approaches. Maity et al. [15] presented the study of TP with interval goal under multiple objective environment and obtained the solution using utility function approach. Roy et al. [16] analysed MOTP under fuzzy intutionistic environment in his paper. Gupta et al. [17] presented the multi-objective capacitated TP under both the certain and uncertain environments and obtained their solution using fuzzy goal programming approach. Singh et al. [18] studied the three dimensional MOTP under the stochastic environment and the solutions were obtained using FPT. Gupta et al. [19] presented a paper on extended capacitated MOTP with mixed constraints under the fuzzy environment.

Research works cited so far gives the application of theories which are suitable when the historical data is available for the situations. In 2007, Liu [20] introduced a new theory for handling the imprecise or uncertain data known as Uncertainty theory. This theory is best suited in the situations where we face problems in accessing the historical data and have no adequate samples available. When there is lack of adequate samples, this theory deals with the degree of belief for each event to happen which is estimated by some experts of the related domain area. This theory finds a wide number of applications in the transportation problems. In the past years, a TP with uncertain values for time taken during transportation was considered by Mou et al. [21]. In 2017, a very commonly used goal programming approach was considered by Chen et al. [22] for solving a bi-objective Solid Transportation Problem (STP) under uncertainty to deal with an additional constraint for mode of transportation along with the source and destination constraints. Liu et al. [23] considered a solid TP with multiple items and fixed-charges under the assumption of data with uncertain numbers. Dalman [24] tackled an uncertain multi-item solid TP and obtained its solution using minimizing distance and convex-combination method. Mahmoodirad et al. [25] modelled a TP with fractional objectives where the uncertain parameters are taken as uncertain variables. Chen et al. [26] and Dalman [27] proposed an entropy based STP and multi-item STP in the uncertain environment. Recently, Zhao and Pan [28] in 2019 generalized the existing uncertain transportation models and proposed a new uncertain transportation model with transfer costs in which all the variables along with transfer costs are supposed to be uncertain numbers.

In addition to the imprecise parameter values of the TPs, it is also possible that multiple number of choices for a parameter are provided by the decision maker. In this context, the study of transport problems leads to the emergence of a new direction known as the multi-choice problem of multi-objective transport. In 2007, Chang [29] primarily introduced the multi-choice programming model. In his paper, he introduced a new idea of programming the problem having multiple choices for a parameter from which one choice of a parameter is to be selected and stated it as multi-choice goal programming. Biswal and Acharya [30] has done illustrious amount of work in the field of multi-choice theory which is capable of accommodating upto sixteen multi-choice parameters. Acharya et al. [31] gave generalized transformation techniques for multi-choice linear programming problems. Acharya and Biswal [32] solved the MCMOTP using interpolating polynomials and solved it using the fuzzy technique. The multi-choice TP under the stochastic environment has been studied by various researchers such as [33–35] with cost coefficients as multi-choice type and supply and demand parameters following different probabilistic distributions. Maity and Roy [36] obtained the solution of TP having non-linear cost and multi-choice demand in the multi-objective environment. Gupta et al. [37] have also studied the multi-choice multi-objective capacitated TP with the uncertain demand and supply. Roy et al. [38] introduced the conic scalarization approach to solve the multi-objective TP with an interval goal under a multi-choice environment. Nasseri [39] solved MOTP with multi-choice parameters where the alternative choices of the parameters were taken as random variables. They converted the multi-choice parameters into a single choice using the interpolating polynomials and obtained the solution by utilizing fuzzy approach. Nayak et al. [40] studied the TP with transportation cost as multi-choices and other parameters like supply and demand as fuzzy trapezoidal numbers. They used binary variable approach to choose a single choice among the multiple choices of the parameters. Agarwal et al. [41] presented a methodology for finding the solution of multi-choice TP with multi-choices as random variables. Vijayalakshmi et al. [42] contributed in the study of eco-friendly MOTP under the fuzzy environment and obtained its solution using goal programming approach. Agarwal and Ganesh [43] focussed on obtaining the solution of stochastic TP involving multi-choice random parameter using Newton's divided difference interpolation.

As seen from the literature survey, it is noted that the major amount of research work with multi-choice programming in TPs is mainly focused under the uncertain environments like stochastic or fuzzy or interval-valued environment (environments which require the historical data). Our paper proposes a new model, an uncertain multi-choice programming model for multi-objective transportation problem known as Uncertain Multi-choice Multi-objective Transportation Problem (UMCMOTP). The UMCMOTP considered in this paper is an extension of the basic transportation problem and we all are very much familiar that transportation problems find a wide number of applications in the economic and industrial and business sector for reducing the transportation cost and time, maximizing the profit etc. Such extension of the transportation problem (i.e MCMOTP) finds applications in the real world when we have multiple objective functions, various sources and destinations. Additionally, the MCMOTP with uncertain variables is more applicable in the real world when the decision maker finds difficulty in providing the precise value of the parameters associated with the objective functions and constraints due to various reasons like lack of information, weather conditions, road conditions etc. The uncertain multi-choice multi-objective transportation problem assumes uncertain variables in the objective functions and multi-choice parameters in the constraints. To obtain the solution of the UMC-MOTP, we have developed two different models: an EV Model and OV Model, by using concepts of uncertainty theory and multi-choice programming techniques. Further, the deterministic conversion of the uncertain objective functions is done by utilizing the expected and optimistic value criteria given by Liu [44] and the multi-choices in the constraints are converted to single choice using the binary variable approach suggested by Acharya and Biswal [30]. The formulated multi-objective models are then converted to single-objective models using the fuzzy programming and minimizing distance technique. Lastly, the compromise solution of the single-objective models is obtained with the help of LINGO 18.0 software.

The main motivations of this paper can be listed as below:

1. None of the researchers have considered the complex environments like uncertain multi-choice environment for transportation problem with objective parameters as uncertain variables and constraint parameters as multi-choice variables.
2. The expected value model has been widely adopted to convert the uncertain model into its crisp model whereas the optimistic value model has not yet been considered to deal with uncertain problems.
3. To solve the MOTP under uncertain multi-choice environment, we are the first to consider the minimizing distance method and fuzzy programming technique solution approaches.
4. The sensitivity of the objective functions with respect to confidence levels in the optimistic value model of multi-objective transportation problem under uncertain multi-choice environment has not yet been done.

The structure of the paper proceeds in the following manner. Section 2 discusses some key concepts in uncertainty theory that are essential for understanding this paper and Section 3 states the mathematical description of MCMOTP. Section 4 introduces the uncertain model for the MCMOTP and its conversion procedure for obtaining the deterministic model is discussed. Section 5 gives the two solution methodologies used for solving the deterministic models of MCMOTP. Section 6 provides a numerical illustration to depict the application of the models along with the sensitivity of the objective functions involved in the OV Model. Section 7 shows the obtained results and their comparison with other models. Finally, the last section gives the concluding remarks and summarizes the overall study of the paper.

2. Introduction to uncertainty theory

This section introduces some prime definitions and theoretical notions of uncertainty theory useful for the better understanding of the paper.

Definition 1. *(Liu [20]) A function $\mathcal{M}$: $\mathcal{F} \to [0,1]$ (here $\mathcal{F}$ is a σ-algebra defined on Ω and $\Omega \neq \phi$), is known as an uncertain measure if it meets the stated axioms:*

Axiom 1: $\mathcal{M}\{\Omega\} = 1$.
Axiom 2: $\mathcal{M}\{\upsilon\} + \mathcal{M}\{\upsilon^c\} = 1$, *for event* $\upsilon \in \mathcal{F}$.
Axiom 3: $\mathcal{M}\left\{\bigcup_{j=1}^{\infty} \upsilon_j\right\} \leq \sum_{j=1}^{\infty} \mathcal{M}\{\upsilon_j\}$, *for any countable sequence of events* $\{\upsilon_j\}$.

Here, the space denoted by the triplet $(\Omega, \mathcal{F}, \mathcal{M})$ is known as an uncertainty space.

Definition 2. *(Liu [20]) A measurable function ζ from $(\Omega, \mathcal{F}, \mathcal{M})$ to the real line $\mathcal{R}$ is said to be an uncertain variable if $\{\zeta \in \mathcal{B}\Big\}$ is an event for any Borel set $\mathcal{B}$ of real numbers.*

Definition 3. *(Liu [20]) The uncertainty distribution $\Psi : \mathcal{R} \to [0,1]$ for any uncertain variable ζ is defined as $\Psi(y) = \mathcal{M}\{\zeta \leq y\}$, for any real number y.*

Definition 4. *(Liu [20]) An uncertain variable ζ with $\Psi(y)$ defined as*

$$\Psi(y) = \begin{cases} 0, & if\, y \leq l, \\ \frac{y-l}{2(m-l)}, & if\, l \leq y \leq m, \\ \frac{y+n-2m}{2(n-m)}, & if\, m \leq y \leq n, \\ 1, & if\, y \geq n, \end{cases}$$

is called zigzag uncertain variable. Such uncertain variable ζ is characterised by $\mathcal{Z}(l,m,n)$ where l, m, n are any real numbers with $l < m < n$.

Definition 5. *(Liu [20]) The inverse uncertainty distribution function, denoted by Ψ^{-1} of $\mathcal{Z}(l,m,n)$ is given by*

$$\Psi^{-1}(\gamma) = \begin{cases} (1-2\gamma)l + 2\gamma m, & if\, \gamma < 0.5, \\ (2-2\gamma)m + (2\gamma - 1)n, & if\, \gamma \geq 0.5. \end{cases}$$

Theorem 1. *(Liu [20]) The expected value of an uncertain variable ζ, if it exists, is provided by*

$$E[\zeta] = \int_0^1 \Psi^{-1}(\gamma) d\gamma.$$

For the zigzag uncertain variable $\mathcal{Z}(l,m,n)$, the expected value is obtained as $E[\zeta] = (l + 2m + n)/4$.

Theorem 2. *(Liu [20]) The expected value operator satisfies the linearity property $E[x\zeta + y\xi] = xE[\zeta] + yE[\xi]$, where ξ and ζ are any two independent uncertain variables and $x, y \in \mathcal{R}$.*

Definition 6. *(Liu [20]) The γ-pessimistic and γ-optimistic values of ζ are defined by*

$$\zeta_{inf}(\gamma) = inf\{t|\mathcal{M}\{\zeta \leq t\} \geq \gamma\} = \Psi^{-1}(\gamma),\ \gamma \in (0,1].$$

$$\zeta_{sup}(\gamma) = sup\{t|\mathcal{M}\{\zeta \geq t\} \geq \gamma\} = \Psi^{-1}(1-\gamma),\ \gamma \in (0,1].$$

For zigzag uncertain variable $\mathcal{Z}(l,m,n)$, we have:

$$\zeta_{sup}(\gamma) = \begin{cases} 2\gamma m + (1-2\gamma)n, & \text{if } \gamma < 0.5, \\ (2\gamma - 1)l + (2-2\gamma)m, & \text{if } \gamma \geq 0.5, \end{cases} \tag{1}$$

$$\zeta_{inf}(\gamma) = \begin{cases} (1-2\gamma)l + 2\gamma m, & \text{if } \gamma < 0.5, \\ (2-2\gamma)m + (2\gamma - 1)n, & \text{if } \gamma \geq 0.5. \end{cases} \tag{2}$$

Theorem 3. *(Liu [20]) Let ζ be an uncertain variable and $\gamma \in (0,1]$. Then we have*

(a) *$\zeta_{inf}(\gamma)$ is left-continuous and increasing function of γ.*
(b) *$\zeta_{sup}(\gamma)$ is left-continuous and decreasing function of γ.*

The fundamental problem seen in handling the uncertain variables is how to rank the uncertain numbers as there is no specific order in the uncertain environment. For this reason, four criteria were introduced by Liu [44] to rank the uncerain numbers. These ranking criteria are: Expected Value Criterion (EVC), Optimistic Value Criterion (OVC), Pessimistic Value Criterion (PVC) and Chance-Criterion (CC). Considering two uncertain variables ζ and ξ, he stated these ranking criteria as:

EVC states that $\zeta < \xi$ iff $E[\zeta] < E[\xi]$.
OVC states that $\zeta < \xi$ iff $\zeta_{sup}(\gamma) < \xi_{sup}(\gamma)$, for some $\gamma \in (0,1]$.
PVC states that $\zeta < \xi$ iff $\zeta_{inf}(\gamma) < \xi_{inf}(\gamma)$, for some $\gamma \in (0,1]$.
CC states that $\zeta < \xi$ iff $\mathcal{M}\{\zeta \geq \bar{t}\} < \mathcal{M}\{\xi \geq \bar{t}\}$ for some predefined level $\bar{t}$.

3. Problem description

This section describes the MCMOTP with an assumption of m sources and n destinations. MCMOTP concerns with developing an ideal transportation plan with an objective of obtaining the minimum of the objective vector Z^t consisting of different objectives like transportation cost, damage cost, transportation time etc.

The MCMOTP model can be mathematically formulated as given below:

Model-1:

$$\min\ Z^t = \sum_{\forall i}\sum_{\forall j}(c^t_{ij}x_{ij}), \forall t;$$

Subject to the given constraints:

$$\sum_{\forall j} x_{ij} \leq a_i,\ \forall i, \tag{3.1}$$

$$\sum_{\forall i} x_{ij} \geq b_j,\ \forall j, \tag{3.2}$$

$$x_{ij} \geq 0; \tag{3.3}$$

Here, we have have used notations $\forall\ t$ for $t = 1, 2, \cdots S$, $\forall\ i$ for $i = 1, 2, \cdots m$ and $\forall\ j$ for $j = 1, 2, \cdots n$ throughtout this paper, with S, m and n representing the total number of objectives, sources and destinations respectively. a_i represents the supplying capacity of the source i and b_j represents the demand requirements at destination j. The notation c^t_{ij} is used for representing different objective parameters like shipping cost, damage cost for a unit item to destination j from source i corresponding to objective t whereas x_{ij} represents the number of items transported from source i to destination j.

The above Model-1 assumes all the variables a_i, b_j, c^t_{ij} as constants. But in the practical situations, we are not able to define these variables accurately due to lack of information as the transportation plan is supposed to be made in advance. If the previously used information regarding the plan is available, the variables can be treated as the random variables but if we are not provided with the previous information then treating these variables as the random variables will not lead us to the appropriate results. Thus, in such cases, when we have lack of information about the historical data, we take into consideration the concepts of uncertainty theory given by Liu [20] in the objective functions.

Furthermore, the decision-makers face more complexities in making a decision when there are multiple choices/alternatives in the TP for parameters such as cost, demand and supply. These multiple alternatives for the parameters may exist due to several routes for transporting the goods or effect of climatic conditions during transportation. Therefore, in this problem, we have considered the supply and demand a_i, b_j as multi-choice parameters $\left(a_i^{(1)}, a_i^{(2)}, \cdots a_i^{(k_i)}\right)$, $\left(b_j^{(1)}, b_j^{(2)}, \cdots b_j^{(k_j)}\right)$ and objectives c^t_{ij} as uncertain objectives denoted by ζ^t_{ij}. So, the MCMOTP becomes Uncertain MCMOTP, denoted by UMCMOTP.

4. Uncertain model of MCMOTP with multi-choices in constraints

Replacing the uncertain variables ζ^t_{ij} and multi-choices $\left(a_i^{(1)}, a_i^{(2)}, \cdots a_i^{(k_i)}\right)$, $\left(b_j^{(1)}, b_j^{(2)}, \cdots b_j^{(k_j)}\right)$ in the objective functions and constraints of Model-1, to get the following UMCMOTP Model-2:

Model-2:

$$\min\ Z^t(x;\zeta) = \sum_{\forall i}\sum_{\forall j}\zeta^t_{ij}x_{ij}, \forall t; \tag{4.1}$$

Subject to the given constraints:

$$\sum_{\forall j} x_{ij} \leq \left(a_i^{(1)}, a_i^{(2)}, \cdots a_i^{(k_i)}\right),\ \forall i, \tag{4.2}$$

$$\sum_{\forall i} x_{ij} \geq \left(b_j^{(1)}, b_j^{(2)}, \cdots b_j^{(k_j)}\right),\ \forall j, \tag{4.3}$$

$$x_{ij} \geq 0; \tag{4.4}$$

which is called the uncertain programming model.

Since this uncertain mathematical model is difficult to handle due to the presence of uncertain objectives and multi-choice constraints, we need to convert both of them (uncertain objectives and multi-choice constraints) into their deterministic forms as discussed below.

4.1. Conversion procedure for multi-choice constraints

Here, we have considered the situation when the supply or demand values are not defined by an exact number. In this framework, the use of multi-choices should therefore be used to define the value of supply and demand. As there is no existing method in the literature to handle multi-choices, Biswal and Acharya [30] provided a transformation technique for obtaining the deterministic form of the multi-choice constraints in the MOTP Model-2 because there must be a single choice for all the parameters to solve the model. Assume that the supply capacity a_i at the source i has multiple choices represented in the form $\left(a_i^{(1)}, a_i^{(2)}, \cdots a_i^{(k_i)}\right), \forall i$, where k_i is the number of multiple choices available for the parameter a_i.

Let us consider the multi-choice supply constraint (4.5) with k_i choices of supply capacity at the i^{th} origin is written as follows:

$$\sum_{j=1}^{n} x_{ij} \leq \left(a_i^{(1)}, a_i^{(2)}, \cdots a_i^{(k_i)}\right), \forall i. \tag{4.5}$$

The transformation technique presented by Biswal and Acharya [30] considers two classes of k_i for obtaining a single choice from multi-choice parameters. The first class deals with the case when $k_i = 2^{m_1}$ and the second class deals with the case when $k_i \neq 2^{m_1}$ with $m_1 = 1, 2, 3, 4$. In his paper, he has considered all the fifteen cases when $2 \leq k_i \leq 16$. Here, we have discussed only three cases of k_i taken as $k_i = 2, 3, 4$ which are shown as below:

when $k_i = 2$, the multi-choice supply constraint is represented as:

$$\sum_{j=1}^{n} x_{ij} \leq \left(a_i^{(1)}, a_i^{(2)}\right), \forall i. \tag{4.6}$$

There are two multiple choices $a_i^{(1)}, a_i^{(2)}$ for the parameter a_i from which a single choice is to be chosen. Since there are two elements in the set $\left(a_i^{(1)}, a_i^{(2)}\right)$, we need only a single binary variable $m_i^{(1)}$ to handle these two choices. Using the binary variable $m_i^{(1)}$, the constraint (4.6) can be converted to the following constraint (4.7) formulated as given below:

$$\sum_{j=1}^{n} x_{ij} \leq m_i^{(1)} a_i^{(1)} + (1 - m_i^{(1)}) a_i^{(2)}, \forall i, \tag{4.7}$$

$$m_i^{(1)} \in \{0, 1\}, \forall i.$$

With $k_i = 3$, the three multi-choices in the supply constraint are represented as:

$$\sum_{j=1}^{n} x_{ij} \leq \left(a_i^{(1)}, a_i^{(2)}, a_i^{(3)}\right), \forall i. \tag{4.8}$$

There are three known parameters $a_i^{(1)}, a_i^{(2)}, a_i^{(3)}$ in the right hand side of the equation (4.8) from which a single choice is to be selected. To deal with the multi-choice constraint (4.8), we need only two variables $m_i^{(1)}$ & $m_i^{(2)}$ because $2^1 < 3 < 2^2$. Using these two binary variables $m_i^{(1)}$ & $m_i^{(2)}$, we can transform the multi-choice constraint (4.8) to constraint (4.9) along with an additional constraint (4.10) for restricting the two binary variables $m_i^{(1)}$ & $m_i^{(2)}$.

$$\begin{aligned}\sum_{j=1}^{n} x_{ij} \leq & \left(1 - m_i^{(1)}\right)\left(1 - m_i^{(2)}\right) a_i^{(1)} + \left(1 - m_i^{(1)}\right) m_i^{(2)} a_i^{(2)} \\ & + m_i^{(1)} \left(1 - m_i^{(2)}\right) a_i^{(3)}, \forall i,\end{aligned} \tag{4.9}$$

$$m_i^{(1)} + m_i^{(2)} \leq 1, \tag{4.10}$$

$$\begin{aligned} & m_i^{(p)} \in \{0, 1\}, p = 1, 2, \\ & x_{ij} \geq 0, \forall i, \forall j. \end{aligned}$$

With $k_i = 4$, the four multi-choices in the supply constraint can be represented as:

$$\sum_{j=1}^{n} x_{ij} \leq \left(a_i^{(1)}, a_i^{(2)}, a_i^{(3)}, a_i^{(4)}\right), \forall i. \tag{4.11}$$

To handle the four known parameters $a_i^{(1)}, a_i^{(2)}, a_i^{(3)}, a_i^{(4)}$ in the right hand side of constraint (4.11), we require only two binary variables $m_i^{(1)}$ and $m_i^{(2)}$ because there are 2^2 choices in the constraint (4.11) out of which one of them is to be selected. Using these two binary variables $m_i^{(1)}$ and $m_i^{(2)}$, the constraint (4.11) can be converted into the following constraint (4.12):

$$\begin{aligned}\sum_{j=1}^{n} x_{ij} \leq & \, m_i^{(1)} m_i^{(2)} a_i^{(1)} + \left(1 - m_i^{(1)}\right) m_i^{(2)} a_i^{(2)} \\ & + m_i^{(1)} \left(1 - m_i^{(2)}\right) a_i^{(3)} \\ & + \left(1 - m_i^{(1)}\right)\left(1 - m_i^{(2)}\right) a_i^{(4)}, \forall i \\ & m_i^{(p)} \in \{0, 1\}, p = 1, 2, \\ & x_{ij} \geq 0, \forall i, \forall j.\end{aligned} \tag{4.12}$$

Similar to multiple choices for supply capacity parameters, the demand parameters can also be multi-choices involved due to factors like seasonality, taxation, product availability and pricing. The procedure of transforming the multi-choice demand constraint $\sum_{i=1}^{m} x_{ij} \geq \left(b_j^{(1)}, b_j^{(2)}, \cdots b_j^{(k_j)}\right), j = 1, 2 \cdots n$ is same as stated for multi-choice supply points.

4.2. Conversion procedure for uncertain objectives

The objectives in Model-2 consists of S different objectives like uncertain transportation cost and damage cost etc., represented by ζ_{ij}^t which are uncertain variables. As stated earlier, the basic problem in uncertain transportation problems is how to rank the uncertain variables. Thus, Liu [44] introduced four ranking criteria as: EVC, OVC, PVC and CC discussed in Section 2.

These four ranking criteria can be used to convert the uncertain objectives into their deterministic forms. In this paper, we have only utilized the expected value criterion and optimistic value criterion for converting the uncertain objectives into crisp objectives but the other two remaining criterions can also be utilized for the conversion of uncertain objectives.

a) Expected value criterion: The main idea in this criterion turns out to utilize the expected values of the uncertain variables in the objective functions. So, the expected form of the uncertain objective (4.1) in Model-2 can be written as:

$$\min\ E[Z_t] = E\left[\sum_{\forall i}\sum_{\forall j}\zeta_{ij}^t x_{ij}\right], \forall t; \qquad (4.13)$$

Theorem (1) is now used to deduce the crisp formulation of the objective as shown in equation (4.14). This crisp objective can be considered for formulating the mathematical model along with the crisp form of the multi-choice constraints (as discussed in Section 4.1). The mathematical Model-3, also known as the expected value model, is a crisp model of the uncertain Model-2.

Model-3:

$$\min\ Z_{tE} = \sum_{\forall i}\sum_{\forall j}\left(x_{ij}\int_0^1 \Psi_{\zeta_{ij}^t}^{-1}(\eta_t)d\eta_t\right), \forall t; \qquad (4.14)$$

Subject to the constraints (4.2) to (4.4).

b) Optimistic value criterion: To deal with uncertain objectives, optimistic value criterion can also be utilized to convert the uncertain variables in crisp form.

$$\min\ Z_{sup}^t(\eta_t) = \left[\sum_{\forall i}\sum_{\forall j}\zeta_{ij}^t x_{ij}\right]_{sup}(\eta_t), \forall t; \qquad (4.15)$$

The optimistic value based-objective function (4.15) can further be simplified using the equation (1) and can be equivalently written as shown in equation (4.16). The mathematical Model-4 formed with the crisp objective function (4.16) along with the crisp multi-choice constraints is labelled as optimistic value model. In objective functions (4.15), η_t are the confidence levels assumed with some fixed values.

Model-4:

$$\min\ Z_{tS} = \sum_{\forall i}\sum_{\forall j} x_{ij}\Psi_{\zeta_{ij}^t}^{-1}(1-\eta_t), \forall t; \qquad (4.16)$$

Subject to the constraints (4.2) to (4.4).

5. Solution approaches

In this section, two main classical approaches are discussed for obtaining the compromise solution of the multi-objective optimization problems which are Minimizing Distance Method (MDM) and fuzzy programming technique. These two methods are utilized to obtain the compromise solution for the crisp formulations of EV and OV Models.

5.1. Minimizing distance method

This method transforms a multi-objective problem into single objective by minimizing the sum of deviation of the ideal vector from the corresponding objective functions. In this method, Euclidean distance is used to convert the crisp multi-objective models i.e. EV Model and OV Model into their equivalent compromise model as given below:

$$\min \sqrt{\sum_{t=1}^{S}(Z_t - Z_t^o)^2}$$

subject to the constraints (4.2) to (4.4).

Here, Z_t is a generalized representation for the objective functions in both the models and Z_t^o denote the ideal objective value of the t^{th} objective function in EV and OV Models without considering other objective functions.

5.2. Fuzzy programming technique

The fuzzy programming approach introduced by Zimmerman [5] is applicable to multi-objective problems only and their solutions can be obtained using the sequential steps as defined below:

Step 1. Consider each objective function of the deterministic Models 3 and 4 as a single objective problem by ignoring all the other objectives and proceed to the next step.

Step 2. Obtain the minimum (L_t) and maximum (U_t) values for $t = 1, 2, \cdots S$ objective functions.

Step 3. Formulate the linear or exponential membership function $\mu_t(Z_t)$ for $t = 1, 2, \cdots S$ objective functions:

A Linear Membership Function (LMF) can be defined by:

$$\mu_t(Z_t) = \begin{cases} 1, & \text{if } Z_t \leq L_t, \\ \frac{U_t - Z_t}{U_t - L_t}, & \text{if } L_t < Z_t < U_t, \\ 0, & \text{if } Z_t \geq U_t, \quad \forall t. \end{cases} \tag{5.1}$$

An Exponential Membership Function (EMF) is defined by:

$$\mu_t(Z_t) = \begin{cases} 1, & \text{if } Z_t \leq L_t, \\ \dfrac{e^{-s_t\psi_t(x)} - e^{-s_t}}{1 - e^{-s_t}}, & \text{if } L_t < Z_t < U_t, \\ 0, & \text{if } Z_t \geq U_t, \quad \forall t. \end{cases} \tag{5.2}$$

where, $\psi_t(x) = \frac{Z_t - L_t}{U_t - L_t}$ and s_t is a non-zero shape parameter given by the decision-maker.

Step 4. Using the max-min operator, formulate the single-objective model as:

$$\text{Maximize } \lambda$$

Subject to the given constraints:

$$\mu_t(Z_t) \geq \lambda, \text{where } \lambda = \min \mu_t(Z_t) \geq 0. \; t = 1, 2,$$
$$\text{and the constraints (4.2) to (4.4) },$$

Step 5. This single-objective model is further solved in LINGO 18.0 optimization tool to achieve the compromise solution of the MCMOTP problem.

6. Numerical illustration of uncertain MCMOTP

Let us consider a TP in which we have three origins ($m = 3$) and three destinations ($n = 3$). In this problem, all the parameters involved with objectives like transportation cost/damage cost are all considered as independent zigzag uncertain variables. The other parameters like supplier capacities and destination demands are the parameters with multi-choices. The problem aims at finding the total number of products to be shipped from sources to destinations such that the transportation cost and damage cost of items during transportation is minimized. The uncertain data for the objectives is given in Table 1 and the multi-choices for the capacity of suppliers and demands required at destinations are listed below:

$$\tilde{a}_1 \in \{8, 10, 12\}, \qquad \tilde{a}_2 \in \{9, 10, 11, 13\},$$
$$\tilde{a}_3 \in \{12, 14\}, \qquad \tilde{b}_1 \in \{7, 8\},$$
$$\tilde{b}_2 \in \{6, 7, 8\}, \qquad \tilde{b}_3 \in \{9, 10, 11\}$$

Table 1. The shipping/damage costs for two objectives from i sources to j destinations.

ζ^1_{ij}	1	2	3	ζ^2_{ij}	1	2	3
1	(2,3,4)	(5,6,7)	(4,6,8)	1	(6,8,9)	(4,6,7)	(6,8,10)
2	(3,5,7)	(1,3,5)	(2,3,4)	2	(3,5,7)	(2,3,4)	(7,8,9)
3	(4,6,8)	(7,8,9)	(6,8,10)	3	(8,9,10)	(5,6,7)	(6,7,8)

The uncertain problem defined above consists of uncertain objectives and multi-choice constraints. The uncertain model formed with this uncertain data can be converted into its crisp models: EV and OV Models using the procedure defined in Section 4.1.These two models are solved here and their results are obtained with the two solution methodologies mentioned in Section 5.

Solution:

6.1. Expected value model

The objective functions of the Model-5 are obtained by applying the expected value operator on the zigzag uncertain variables given in the Table 1. The multi-choice constraints in Model-5 are further converted to single choice constraints using the procedure given by Biswal and Acharya [30] as described in Section 4.1.

Model-5:

$$\begin{aligned} \min Z_{1E} =& 3x_{11} + 6x_{12} + 6x_{13} + 5x_{21} + 3x_{22} + 3x_{23} + 6x_{31} \\ &+ 8x_{32} + 8x_{33}; \\ \min Z_{2E} =& 7.75x_{11} + 5.75x_{12} + 8x_{13} + 5x_{21} + 3x_{22} + 8x_{23} \\ &+ 9x_{31} + 6x_{32} + 7x_{33}; \end{aligned}$$

Subject to the given constraints:

$$\begin{aligned} &x_{11} + x_{12} + x_{13} \leq \{8, 10, 12\}; \\ &x_{21} + x_{22} + x_{23} \leq \{9, 10, 11, 13\}; \\ &x_{31} + x_{32} + x_{33} \leq \{12, 14\}; \\ &x_{11} + x_{21} + x_{31} \geq \{7, 8\}; \\ &x_{12} + x_{22} + x_{32} \geq \{6, 7, 8\}; \\ &x_{13} + x_{23} + x_{33} \geq \{9, 10, 11\}; \\ &x_{ij} \geq 0, \forall i, \forall j; \end{aligned}$$

The results obtained for the EV Model using the discussed two solution methodologies are presented here.

a) Minimizing distance method:

The results obtained using MDM are displayed below with ideal values taken as $Z^o_{1E} = 72$ and $Z^o_{2E} = 116$:

$Z^*_{1E} = 83.92890, Z^*_{2E} = 137.6891, x_{11} = 4.6142, x_{13} = 4.3858,$
$x_{21} = 2.3858, x_{22} = 6, x_{23} = 4.6142$

b) Fuzzy programming technique:

i) Using linear membership function

To apply the FPT with linear membership function, the U_t and L_t are obtained as: $L_1 = 72,\ L_2 = 116,\ U_1 = 237,\ U_2 = 296.5$ which are substituted in linear membership function (5.1) to get a single objective fuzzy model as discussed in step 5 of Section 5.2. The solution obtained for the EV Model-5 by applying the fuzzy technique procedure is: $\lambda = 0.8958525, x_{11} = 3.563134, x_{13} = 5.436866, x_{21} = 3.436866, x_{22} = 6, x_{23} = 3.563134$ and the compromise solution for the objective functions are $Z^*_{1E} = 89.18433$ and $Z^*_{2E} = 134.7986$.

Here, λ represents the minimum value amongst both the membership functions. i.e. $\lambda = \min\ (\lambda_1,\ \lambda_2)$, where $\lambda_1 = \mu_1(Z_{1E})$ and $\lambda_2 = \mu_2(Z_{2E})$.

ii) Using exponential membership function

For applying FPT with exponential membership function, the U_t and L_t values are $L_1 = 72,\ L_2 = 116,\ U_1 = 237,\ U_2 = 296.5$ used to construct an exponential membership function given in (5.2) for formulating a single objective fuzzy model discussed in step (5) of Section 5.2 for the EV Model-5. Solving the single objective fuzzy model of EV Model-5 for three different cases of shape parameters (s_1, s_2) taken as $(-2, -2)$, $(3, 2)$ and $(4, 3)$ in the exponential membership function, we get the solutions as shown in Table 2.

The graphical representation of the objective functions with respect to the linear and exponential (with three cases of shape parameters) membership functions in EV Model-5 is shown in Figure 1. In Figure 1, it is clearly seen that the compromise solution of the objective functions is achieved at their corresponding degree of satisfaction level. For example, in the case of linear membership function, the compromise solution $Z^*_{1E} = 89.18433$ and $Z^*_{2E} = 134.7986$ are obtained at membership values $\lambda_1 = 0.8958525$ and $\lambda_2 = 0.8958525$ which represents the individual degree of satisfaction for objectives Z_{1E} and Z_{2E}. The fuzzy programming solution approach gives the minimum value λ of these individual membership function values $\lambda_1,\ \lambda_2$, stating that each of the objective function posseses at least λ degree of satisfaction level. As the membership value increases and approaches to 1 for the objective functions, the objective values are improved simultaneously and approach to the best value (optimal value) of the individual objective functions. Also, for each objective function, the shape parameter values can be chosen at random until the model produces a feasible solution. Changing the shape parameter values will result in different compromise solutions.

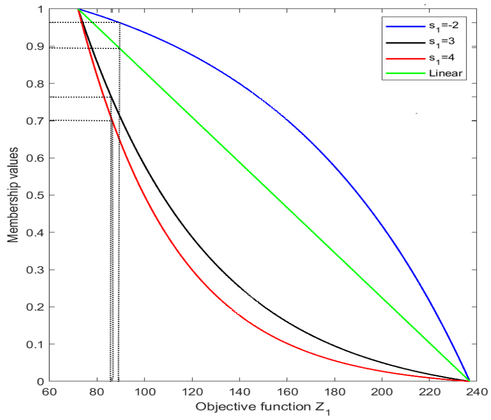

(a) Degree of satisfaction level for Z_1.

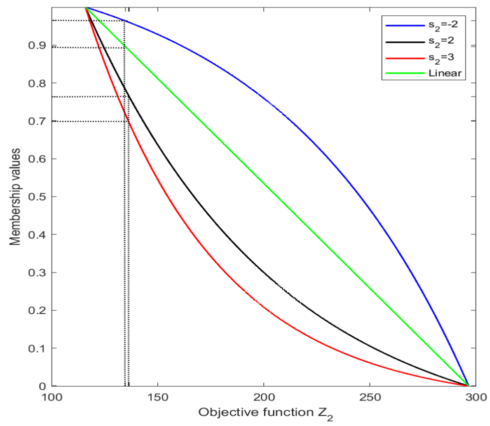

(b) Degree of satisfaction level for Z_2.

Figure 1. Graphical representation of solutions for EV Model-5 with FPT.

6.2. Optimistic value model

To formulate OV Model, we need the predetermined confidence levels $\eta_t \in (0, 1]$. Let us assume that all the confidence levels are equal to 0.9.

Model-6:

$$\begin{aligned}\min Z_{1S} =& 2.2x_{11} + 5.2x_{12} + 4.4x_{13} + 3.4x_{21} + 1.4x_{22} + 2.2x_{23}\\ &+ 4.4x_{31} + 7.2x_{32} + 6.4x_{33};\\ \min Z_{2S} =& 6.4x_{11} + 4.4x_{12} + 6.4x_{13} + 3.4x_{21} + 2.2x_{22} + 7.2x_{23}\\ &+ 8.2x_{31} + 5.2x_{32} + 6.2x_{33};\end{aligned}$$

Table 2. Solution table for (s_1, s_2) in the exponential membership function for EV Model-5.

(s_1, s_2)	Z^*_{1E}	Z^*_{2E}	$\lambda = \lambda_1 = \lambda_2$	Solution
(-2,-2)	89.18433	134.7986	0.963754	$x_{11} = 3.563134, x_{13} = 5.436866, x_{21} = 3.436866, x_{22} = 6, x_{23} = 3.563134$
(3,2)	85.95132	136.5768	0.764216	$x_{11} = 4.209737, x_{13} = 4.790263, x_{21} = 2.790263, x_{22} = 6, x_{23} = 4.209737$
(4,3)	86.46528	136.2941	0.698695	$x_{11} = 4.106944, x_{13} = 4.893056, x_{21} = 2.893056, x_{22} = 6, x_{23} = 4.106944$

Subject to the given constraints of Model-5. The solution of this multi-objective OV Model-6 can be achieved with the two solution methodologies mentioned in section 5. The results of both the methods are shown below.

a) Minimizing distance method:
The solution obtained for Model-6 using MDM is:

$$Z^*_{1S} = 62.1126, Z^*_{2S} = 105.4271, x_{11} = 2.8492, x_{13} = 6.1508,$$
$$x_{21} = 4.1508, x_{22} = 6, x_{23} = 2.8492$$

with ideal values of the objective functions taken as $Z^o_{1S} = 48$ and $Z^o_{2S} = 92.8$.

b) Fuzzy programming technique:

i) Using linear membership function

The sequential steps of the FPT can be applied to obtain the U_t and L_t values as: $L_1 = 48$, $L_2 = 92.8$, $U_1 = 189.80$, $U_2 = 260.40$. The solution obtained for the OV Model-6 using linear membership function is given as: $\lambda = 0.9129054, x_{11} = 3.367644, x_{13} = 5.632356, x_{21} = 3.632356, x_{22} = 6, x_{23} = 3.367644$ and the compromise solution for the objective functions are $Z^*_{1S} = 60.35001$ and $Z^*_{2S} = 107.3970$. Here, λ represents the minimum value amongst all these membership functions. i.e. $\lambda = \min\ (\lambda_1,\ \lambda_2)$, where $\lambda_1 = \mu_1(Z_{1S})$ and $\lambda_2 = \mu_2(Z_{2S})$.

ii) Using exponential membership function

The solutions obtained for three different cases of shape parameters $(s_1 = -2, s_2 = -2)$,$(s_1 = 3, s_2 = 2)$ and $(s_1 = 4, s_2 = 3)$ are displayed in Table 3.

The graphical representation of the linear and exponential membership function versus the objective functions in Model-6 is shown in Figure 2.

In Figure 2, it is observed that the compromise solution of both the objective functions (with linear and exponential membership function in FPT) is achieved at their corresponding individual degree of satisfaction. Say, for the linear membership function, the compromise values of the objective functions $Z^*_{1S} = 60.35001$ and $Z^*_{2S} = 107.3970$ are achieved at degree of satisfactions $\lambda_1 = 0.9129054$ and $\lambda_2 = 0.9129054$. Similarly, the compromise solution of both objective functions with three cases of shape parameters in exponential membership functions is achieved at their respective individual degrees of satisfaction, as can be seen in Figure 2.

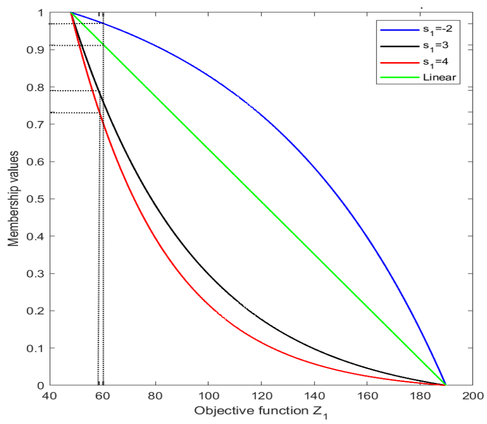

(a) Degree of satisfaction level for Z_1.

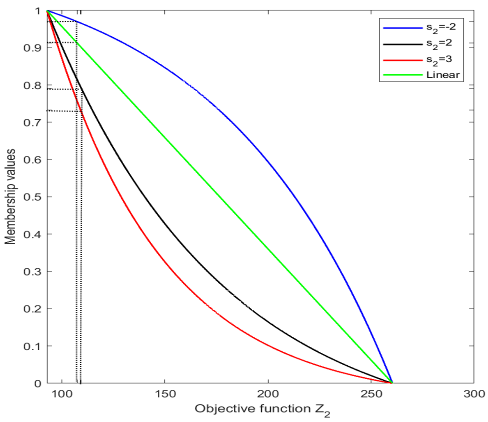

(b) Degree of satisfaction level for Z_2.

Figure 2. Graphical representation of solutions for OV Model-6 with FPT.

6.2.1. Sensitivity analysis of the objective functions in OV model

Here, the sensitivity of the objective functions is investigated in the OV Model with respect to the confidence level η_t. The complementary test is performed by variating the values of the confidence level η_t in the range $[0.1, 0.9]$ with a step

Table 3. Solution table for (s_1, s_2) in the exponential membership function for OV Model-6

(s_1, s_2)	Z_{1S}^*	Z_{2S}^*	$\lambda = \lambda_1 = \lambda_2$	Solution
(-2,-2)	60.35001	107.3970	0.970218	$x_{11} = 3.367644, x_{13} = 5.632356, x_{21} = 3.632356, x_{22} = 6, x_{23} = 3.367644$
(3,2)	58.46478	109.5041	0.790991	$x_{11} = 3.922123, x_{13} = 5.077877, x_{21} = 3.077877, x_{22} = 6, x_{23} = 3.922123$
(4,3)	58.77858	109.1534	0.732933	$x_{11} = 3.829830, x_{13} = 5.170170, x_{21} = 3.170170, x_{22} = 6, x_{23} = 3.829830$

size of 0.1 with respect to the crisp multi-choice constraints of Model-6. The results of the sensitivity analysis are shown for both the two solution methodologies. The objective values obtained during the sensitivity analysis of OV Model-6 are shown in Table 4. "CL" represents the variation of confidence level in $\eta_t : t = 1, 2$, for both the objective functions.

Table 4. Objective values obtained during the sensitivity analysis of the OV Model-6 with FPT.

CL	Z_{tS}	MDM	Fuzzy programming technique			
			EMF			LMF
			(-2,-2)	(3,2)	(4,3)	
0.1	Z_{1S}	100.9969	111.5599	107.7755	108.3744	111.5599
	Z_{2S}	161.2291	157.2987	158.7068	158.4839	157.2987
0.2	Z_{1S}	96.95949	106.3698	102.6568	103.2445	106.3698
	Z_{2S}	155.9729	152.0711	153.6106	153.3669	152.0711
0.3	Z_{1S}	92.97171	101.0594	97.4410	98.01394	101.0594
	Z_{2S}	150.5054	146.7726	148.4426	148.1782	146.7726
0.4	Z_{1S}	89.01075	95.63106	92.12848	92.68335	95.63106
	Z_{2S}	144.7999	141.4003	143.1989	142.9140	141.4003
0.5	Z_{1S}	85.23529	89.61566	86.37785	86.89344	89.61566
	Z_{2S}	138.0588	135.4306	137.3733	137.0639	135.4306
0.6	Z_{1S}	79.87618	82.29727	79.41449	79.87810	82.29727
	Z_{2S}	130.1470	128.4628	130.4682	130.1457	128.4628
0.7	Z_{1S}	74.2800	74.98182	72.44310	72.85571	74.98182
	Z_{2S}	122.0400	121.4719	123.5270	123.1930	121.4719
0.8	Z_{1S}	68.37898	67.66704	65.46099	65.82364	67.66704
	Z_{2S}	113.7778	114.4523	116.5422	116.1987	114.4523
0.9	Z_{1S}	62.11262	60.35001	58.46478	58.77854	60.35001
	Z_{2S}	105.4271	107.3970	109.5041	109.1534	107.3970

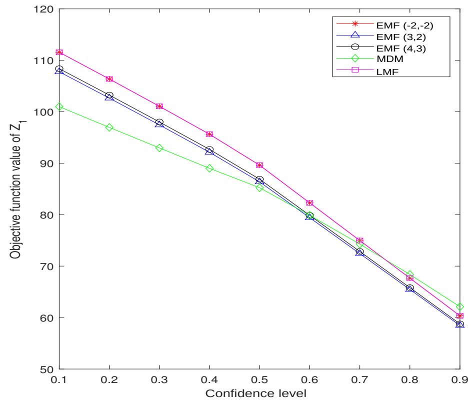

(a) Sensitivity analysis of Z_1 w.r.t η_t in the Model-6.

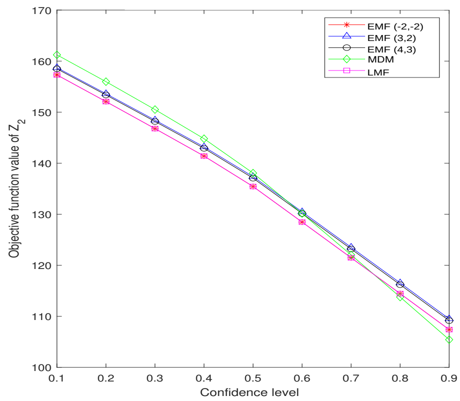

(b) Sensitivity analysis of Z_2 w.r.t η_t in the Model-6.

Figure 3. The sensitivity analysis of the objectives in OV Model-6 w.r.t η_t using FPT and MDM.

The graphical interpretation of the objective values w.r.t the confidence level η_t are shown in Figure 3. Figure 3 indicates that the objective function values are decreasing with respect to the tested confidence levels η_t for both the solution methodologies.

7. Comparison of the results

This section presents the results obtained for the Uncertain MCMOTP using the EV and OV Models. Table 5 compares the results obtained for EV and OV models with minimizing distance method and fuzzy programming technique methodologies.

Table 5. Comparison of the results obtained with two methodologies.

Model	Z_t	MDM	Fuzzy programming technique			
			EMF			LMF
			(-2,-2)	(3,2)	(4,3)	
EV Model	Z^*_{1E}	83.9290	89.1843	85.9513	86.4653	89.1843
	Z^*_{2E}	137.6891	134.7986	136.5768	136.2941	134.7986
OV Model	Z^*_{1S}	62.1126	60.3500	58.4648	58.7786	60.3500
	Z^*_{2S}	105.4271	107.3970	109.5041	109.1534	107.3970

From the results obtained with the given solution methodologies, it can be observed that neither of the method is dominating the results of the other method because if one objective approaches towards its best value then the other objective value starts worsening. Also, the EV Model gives the solution in terms of expected values of the objective functions, OV Model gives the solution in terms of optimistic values of the objective functions. The results of the OV Model obtained here are only for a single case of confidence level $\eta_t = 0.9$ in the objective function, but varying η_t in the range $(0, 1]$ can provide numerous set of solutions.

8. Conclusion

This paper developed the Uncertain Multi-choice MOTP with objectives as zigzag uncertain variables and supply and demand parameters as multi-choice parameters. The uncertain MC-MOTP model has been solved using the two crisp models: EV and OV Models. Further, the crisp models were solved using minimizing distance method and fuzzy technique (with linear and exponential membership functions). The EV Model will always lead to a single or multiple solution based on the solution methodology utilized whereas OV Model will always provide numerous solutions to the decision maker because of the confidence level η_t involved in the OV Model. In comparison to the EV Model, which does not incorporate confidence level, the OV Model may provide the decision maker with a number of alternative solutions by altering the values of the confidence level η_t between 0 and 1.

Acknowledgment

The authors express their gratitude to the anonymous reviewers and the editor for their insightful comments and suggestions. The first author is also grateful for the financial support received from the Council of Scientific and Industrial Research, File No. 09/1007(0003)/2017-EMR-I, New Delhi, India.

References

[1] Hitchcock, F. L. (1941). The distribution of a product from several sources to numerous localities. *Journal of mathematics and physics*, 20(1-4), 224-230.

[2] Ozmen, A. (2022). Multi-objective regression modeling for natural gas prediction with ridge regression and CMARS. *An International Journal of Optimization and Control: Theories & Applications*, 12(1), 56–65.

[3] Shahraki, Z., Allahdadi, M., & Mishmast Nehi, H. (2015). Fuzzy multi objective linear programming problem with imprecise aspiration level and parameters. *An International Journal of Optimization and Control: Theories & Applications*, 5(2), 81–86.

[4] Rudy, J., & Zelazny, D. (2014). Solving multi-objective job shop problem using nature-based algorithms: new Pareto approximation features. *An International Journal of Optimization and Control: Theories & Applications*, 5(1), 1–11.

[5] Zimmermann, H. J. (1978). Fuzzy programming and linear programming with several objective functions. *Fuzzy sets and systems*, 1(1), 45-55.

[6] Eghbali, H., Eghbali, M. A., & Vahidian Kamyad, A. (2012). Optimizing human diet problem based on price and taste using multi-objective fuzzy linear programming approach. *An International Journal of Optimization and Control: Theories & Applications*, 2(2), 139–151.

[7] Bit, A. K., Biswal, M. P., Alam, S. S. (1993). Fuzzy programming approach to multiobjective solid transportation problem. *Fuzzy Sets and Systems*, 57(2), 183-94.

[8] Kumar, M., Vrat, P., Shankar, R. (2006). A fuzzy programming approach for vendor selection problem in a supply chain. *International Journal of Production Economics*, 101(2), 273-85.

[9] Zadeh, L.A. (1965). Fuzzy sets. *Information and control* 8(3), 338–353.

[10] Kolmogorov, A. N., Bharucha-Reid, A. T. (2018). *Foundations of the Theory of Probability*: Second English Edition, Courier Dover Publications, New York.

[11] Moore, R.E. (1966). *Interval Analysis 4*. Englewood Cliffs: Prentice-Hall.

[12] Bhargava, A. K., Singh, S. R., & Bansal, D. (2014). Multi-objective fuzzy chance constrained fuzzy goal programming for capacitated transportation problem. *International Journal of Computer Applications*, 107(3).

[13] Giri, P. K., Maiti, M. K., & Maiti, M. (2014). Fuzzy stochastic solid transportation problem using fuzzy goal programming approach. *Computers & Industrial Engineering*, 72, 160-168.

[14] Ebrahimnejad, A. (2015). An improved approach for solving fuzzy transportation problem with triangular fuzzy numbers. *Journal of Intelligent & Fuzzy Systems*, 29(2), 963-974.

[15] Maity, G., & Roy, S. K. (2016). Solving multi-objective transportation problem with interval goal using utility function approach. *International Journal of Operational Research*, 27(4), 513-529.

[16] Roy, S. K., Ebrahimnejad, A., Verdegay, J. L., & Das, S. (2018). New approach for solving intuitionistic fuzzy multi-objective transportation problem. *Sādhanā*, 43(1), 1-12.

[17] Gupta, S., Ali, I., & Ahmed, A. (2018). Multi-objective capacitated transportation problem with

mixed constraint: a case study of certain and uncertain environment. *Opsearch*, 55(2), 447-477.

[18] Singh, S., Pradhan, A., & Biswal, M. P. (2019). Multi-objective solid transportation problem under stochastic environment. *Sādhanā*, 44(5), 1-12.

[19] Gupta, S., Ali, I., & Ahmed, A. (2020). An extended multi-objective capacitated transportation problem with mixed constraints in fuzzy environment. *International Journal of Operational Research*, 37(3), 345-376.

[20] Liu, B. (2007). Uncertainty Theory. *In Uncertainty Theory* Springer, Berlin, Heidelberg.

[21] Mou, D., Zhao, W., & Chang, X. (2013). A transportation problem with uncertain truck times and unit costs. *Industrial Engineering and Management Systems*, 12(1), 30-35.

[22] Chen, L., Peng, J., & Zhang, B. (2017). Uncertain goal programming models for bicriteria solid transportation problem. *Applied Soft Computing*, 51, 49-59.

[23] Liu, L., Zhang, B., & Ma, W. (2018). Uncertain programming models for fixed charge multi-item solid transportation problem. *Soft Computing*, 22(17), 5825-5833.

[24] Dalman, H. (2018). Uncertain programming model for multi-item solid transportation problem. *International Journal of Machine Learning and Cybernetics*, 9(4), 559-567.

[25] Mahmoodirad, A., Dehghan, R., & Niroomand, S. (2019). Modelling linear fractional transportation problem in belief degree-based uncertain environment. *Journal of Experimental & Theoretical Artificial Intelligence*, 31(3), 393-408.

[26] Chen, B., Liu, Y., & Zhou, T. (2019). An entropy based solid transportation problem in uncertain environment. *Journal of Ambient Intelligence and Humanized Computing*, 10(1), 357-363.

[27] Dalman, H. (2019). Entropy-based multi-item solid transportation problems with uncertain variables. *Soft Computing*, 23(14), 5931-5943.

[28] Zhao, G., & Pan, D. (2020). A transportation planning problem with transfer costs in uncertain environment. *Soft Computing*, 24(4), 2647-2653.

[29] Chang, C. T. (2007). Multi-choice goal programming. *Omega*, 35(4), 389-396.

[30] Biswal, M. P., & Acharya, S. (2009). Multi-choice multi-objective linear programming problem. *Journal of Interdisciplinary Mathematics*, 12(5), 606-637.

[31] Acharya, S., & Acharya, M. M. (2012). Generalized transformation techniques for multi-choice linear programming problems. *An International Journal of Optimization and Control: Theories & Applications*, 3(1), 45–54.

[32] Acharya, S., & Biswal, M. P. (2016). Solving multi-choice multi-objective transportation problem. *International Journal of Mathematics in Operational Research*, 8(4), 509-527.

[33] Roy, S. K., Mahapatra, D. R., & Biswal, M. P. (2012). Multi-choice stochastic transportation problem with exponential distribution. *Journal of uncertain systems*, 6(3), 200-213.

[34] Mahapatra, D. R. (2013). Multi-choice stochastic transportation problem involving weibull distribution. *An International Journal of Optimization and Control: Theories & Applications*, 4(1), 45–55.

[35] Roy, S. K. (2014). Multi-choice stochastic transportation problem involving Weibull distribution. *International Journal of Operational Research*, 21(1), 38-58.

[36] Maity, G., & Kumar Roy, S. (2016). Solving a multi-objective transportation problem with nonlinear cost and multi-choice demand. *International Journal of Management Science and Engineering Management*, 11(1), 62-70.

[37] Gupta, S., Ali, I., & Ahmed, A. (2018). Multi-choice multi-objective capacitated transportation problem-a case study of uncertain demand and supply. *Journal of Statistics and Management Systems*, 21(3), 467-491.

[38] Roy, S. K., Maity, G., Weber, G. W., & Gök, S. Z. A. (2017). Conic scalarization approach to solve multi-choice multi-objective transportation problem with interval goal. *Annals of Operations Research*, 253(1), 599-620.

[39] Nasseri, S. H., & Bavandi, S. (2020). Solving multi-objective multi-choice stochastic transportation problem with fuzzy programming approach. *In 2020 8th Iranian Joint Congress on Fuzzy and intelligent Systems (CFIS)*, IEEE, 207-210.

[40] Nayak, J., & Acharya, S. (2020). Dealing with a Transportation Problem with Multi Choice Cost Coefficients and Fuzzy Supplies and Demands. *Global Journal of Pure and Applied Mathematics*, 16(6), 783-788.

[41] Agrawal, P., & Ganesh, T. (2020). Solving Multi-choice Fractional Stochastic Transportation Problem Involving Newton's Divided Difference. *Numerical Optimization in Engineering and Sciences, Springer, Singapore*, 289-298.

[42] Vijayalakshmi, P., & Vinotha, J. M. (2020). Multi choice ecological intuitionistic fuzzy multi objective transportation problem with non linear cost. *Solid State Technology*, 63(2), 2675-2689.

[43] Agrawal, P., & Ganesh, T. (2021). Solution of stochastic transportation problem involving multi-choice random parameter using Newton's divided difference interpolation. *Journal of Information and Optimization Sciences*, 42(1), 77-91.

[44] Liu, B. (2010). *Uncertainty Theory: A Branch of Mathematics for Modeling Human Uncertainty*, Springer-Verlag, Berlin.

Vandana Kakran *received her M.Sc degree in Applied Mathematics from Maharaja Sayajiraorao University, Vadodara, Gujarat. She is currently pursuing her Ph.D degree from S.V. National Institute of Technology, Surat. Her current area of research interest is multi-objective optimization problems under uncertain environments.*

https://orcid.org/0000-0003-2889-2082

Jayesh Dhodiya *is an Associate Professor in Department of Mathematics and Humanities, SVNIT. He has received his Ph.D. degree in Mathematics from Department of Mathematics, Veer Narmad South Gujarat University Surat in 2009. He has several publications in various reputed international and national journals. Dr. Dhodiya has supervised several Ph.D. candidates and M.Sc dissertation candidates. He has successfully completed 4 Development projects with IBM Company and a research project with SVNIT. His major area of research interest lies in Operations Research, Mathematical Modelling and Simulation, Computing, Knowledge Management and Image mining.*

https://orcid.org/0000-0001-9675-412X

An International Journal of Optimization and Control: Theories & Applications (http://ijocta.balikesir.edu.tr)

An International Journal of Optimization and Control: Theories & Applications
ISSN:2146-0957 eISSN:2146-5703
Vol.12, No.2, pp.113-127 (2022)
http://doi.org/10.11121/ijocta.2022.1161

RESEARCH ARTICLE

Optimal matchday schedule for Turkish professional soccer league using nonlinear binary integer programming

Yasin Göçgün[a*], Niyazi Onur Bakır[b]

[a] *Department of Industrial Engineering, İstinye University, İstanbul, Turkey*
[b] *Department of Industrial Engineering, Altınbaş University, İstanbul, Turkey*
yasin.gocgun@istinye.edu.tr, onur.bakir@altinbas.edu.tr

ARTICLE INFO

Article History:
Received 14 September 2021
Accepted 30 March 2022
Available 12 July 2022

Keywords:
OR in sports
Sports scheduling
Integer programming

AMS Classification 2010:
90B35

ABSTRACT

Sports scheduling problems are interesting optimization problems that require the decision of who play with whom, where and when to play. In this work, we study the sports scheduling problem faced by the Turkish Football Federation. Given the schedule of games for each round of the season, the problem is to determine the match days with the goal of having a fair schedule for each team. The criteria we employ to establish this fairness are achieving an equal distribution of match days between the teams throughout the season and the ideal assignment of games to different days in each round of the tournament. The problem is formulated as a nonlinear binary integer program and is solved optimally for each week. Our results indicate that significant improvements over the existing schedule can be achieved if the optimal solution is implemented.

1. Introduction

Due to increasing popularity of sports on the globe as well as demands of stakeholders such as teams, players, TV broadcasters, their sponsors and fans, scheduling sport tournaments has become quite important. In the presence of high economic stakes, the tournament organizers are hard-pressed to design a fair schedule that strikes a reasonable balance in addressing the needs of all the stakeholders.This is indeed an enormous task because the objectives of multiple stakeholders are often in conflict and the fixtures have to be determined subject to a wide variety of constraints. Therefore, over the years, sports scheduling has turned into a challenging decision problem that can best be handled by a rigorous application of operations research methods.

The main focus of this paper is the scheduling of the Turkish Super League which is a task undertaken by the Turkish Football Federation (TFF). Each year, the TFF officials first finalize the seasonal fixture of the league which regularly includes 18 teams (although the Federation recently announced the cancellation of relegation for the 2019-20 season due to the pandemic, which implies that there are 21 participants in the 2020-21 season). To be more specific, they determine who will play with whom each week. Then, the actual schedule is determined taking into account other tournaments organized by UEFA and FIFA (governing bodies of soccer in Europe and the world, respectively) as well as the domestic Turkish Cup. Naturally, each season, number of games played by any team in the Super League is known with certainty. On the other hand, UEFA competitions and the Turkish Cup are single-elimination tournaments, so there is uncertainty about the number of rounds each team will play without getting knocked out. Therefore, determination of when league games are played is a dynamic process that has to take the most recent status of other tournaments into account. With 18 teams in the league,

*Corresponding Author

the fixture is divided into 34 weeks of play. Unless there are exceptional circumstances, games of any week are scheduled from Friday to Monday; i.e., four days of the week.

The critical aspect of this procedure is the fixture determination for its supposed influence on each team's overall performance. To illustrate, if a team is scheduled to play two consecutive games with relatively stronger teams, additional fatigue may impair the endurance of the players and cause a significant drop in performance in the latter match. This negative influence is called the carryover effect, and its minimization is one of the many issues that should be addressed in fixture determination. However, in recent years, club administrators as well as the technical staff in Turkey are also increasingly vocal in their criticism on which day of the week their next game in the fixture is scheduled. It is a widespread belief in the soccer community that not all days of play are equally beneficial. Their criticisms are centered around two main arguments: first economic, second performance related. Both arguments are parallel in claiming that scheduled matches on Fridays and Mondays are less favorable. Those that raise the economic concerns complain about the loss of revenues for the reduced attendance of spectators on the weekdays (see for instance [1], [2], [3], [4]) whereas the performance concerns are largely centered around unusual loss of points on weekdays due to various reasons. News on Beşiktaş´s unexpectedly low performance on Fridays in the season $2017-18$ after two consecutive years of league championship (see [5]) and Trabzonspor's loss of points on Fridays in the first half of $2007-2008$ (see [6]) are examples of reports that support this view on reduced performance. Other examples may be found in [7] and [8].

Given these concerns, the problem is to determine the day of each game with the objective of having a fair distribution among all the participating clubs. Since the future of other tournaments affecting the Turkish Super League is uncertain, any proposed method should be dynamic in nature. The metric of day distribution is also quite important because it will be the main element of the method that maintains fairness in the resulting schedule. Schedules of other related tournaments, and the rest period requirements add constraints to this challenging problem that we formulate as a nonlinear binary integer programming problem.

In the sections below, we first give an overview of the related literature. The third section is where we present the main problem formulation that we also solve optimally for each round of the season on the fly. In particular, using the data of the 2018-2019 season, we compare the performance of the optimal schedule generated by our program against that obtained manually by the TFF officials. An extended discussion of the results is offered in the fourth section. Section 5 concludes.

2. Literature

Constructing schedules for sports competitions has attracted the attention of academicians in the last five decades ([9]). In particular, the literature for round robin tournaments where every team has to play every other team a certain number of times is rich. We provide a short overview of the literature here, however interested reader can examine [10], [11] and [12] for extensive surveys on round robin scheduling. Various objectives are utilized for obtaining optimal/near optimal schedules for those tournaments. Examples of those objectives include (but are not limited to) minimizing rest mismatches ([13], [14]), minimizing breaks ([15], [16], [17], [18]), minimizing travel distances ([19]), and minimizing carry-over effects ([20], [21], [22]). Bulk of the literature concentrates on addressing a number of these and other objectives (such as maximizing gate revenue, attendance etc.) simultaneously subject to constraints that are specific to a particular tournament ([23], [24], [25], [26], [27], [28]).

Not surprisingly, scheduling of round robin tournaments have been handled both through various types of integer programming formulations and from the perspective of graph theory. Where theoretical formulations fail against the complexity of the problem, heuristics are employed. First, we highlight some of the previous applications of integer programming on fixture determination. [29] proposed an integer programming formulation for round robin tournaments taking into account constraints such as not allowing forbidden games and fairness constraints related to breaks as well as carryover effects. [30] studied the problem of scheduling Argentina's professional basketball leagues, considering the measure of total distance traveled by the teams. The authors formulated the problem as a variation of the Traveling Tournament Problem. In [9], the current schedule of the Korea baseball league was analyzed in the presence of measures such as the total travel distance of teams and match fairness. The author proposed an integer programming model for solving the problem, and developed a heuristic algorithm for handling large-sized problems. [17] proposed an integer programming formulation for scheduling the professional soccer league in Ecuador. The authors also developed a heuristic approach for solving the problem in a reasonable amount of time. [16] addressed the problem of scheduling the South American qualifiers to the 2018 FIFA World Cup, proposing an integer programming formulation for solving it. [20] studied the problem of minimizing weighted carry over effects formulating the underlying problem using integer programming and proposed an efficient heuristic that yields high-quality solutions. In a recent work, [22] focused on a round robin scheduling problem with the goal of minimizing carry over effects in Turkish Super League while keeping the number of breaks per team below a certain threshold, and proposed a better schedule for this league.

Applications of graph theory in round robin tournament scheduling are also widely found. In some of these applications, we observe the use of the "circle method" which ensures that each team has one game in each round and there is no unassigned game by the end of the tournament ([31], [32]). Graph theoretic studies also include articles that discuss break minimization for solving round robin scheduling problems ([33], [34]). [33] transformed the sports scheduling problem into a maximum cut problem. The authors demonstrated that their method outperforms previous methods that are based on integer and constraint programming. [34] provided theoretical results for round robin scheduling problems where the number of teams is even, making sure that the schedule is constructed with minimum number of breaks. [35] addressed football league scheduling problems in the presence of uncertainty. In their work, the authors considered several quality measures such as breaks and canceled matches. They developed a variety of proactive and reactive approaches for solving the underlying problem.

Among the objectives that have been used for a better round robin schedule, minimizing rest mismatches distinguishes itself for its natural influence on determination of matchdays given a fixture. For example, [13] introduced a "Rest Mismatch Problem" under this objective. The authors tackled the problem using integer and constraint programming models that aim to find a schedule with a minimum number of rest mismatches between the opponents, and proposed a heuristic algorithm that yields a zero-mismatch schedule in certain cases. In a more recent work, same authors focused on the problem of determining matchdays with the objective of minimizing the total rest difference (which is a slightly different objective than the one in the previous paper) given that the games in each round are known ([14]). The authors showed that the problem can be solved by solving each round separately. We should note that these two papers also have two common features with this study; first is the round by round treatment of the entire season and second is the focus on determination of the matchday.

As indicated in the introduction, an important motivation of our paper is the need to determine the matchdays in the Turkish Super League in the presence of criticisms regarding the unfair distribution of weekdays throughout the season among the fixtures of participating teams. One reason behind this concern is reduced revenues generated from games scheduled certain days of the week. The determinants of fan attendance to stadiums has received most attraction in the sports economics literature. Among the determinants that have been most often reported in empirical studies are competitive balance, variables that measure the performance of home team and the away team, various economic factors, TV broadcasting (see [36], [37], [38], [39], [40]), and the matchdays. Regarding the matchdays, [41] examined data from top European soccer leagues in Germany, Spain, and France. Their analysis revealed that all of the examined leagues have a lower attendance in games that are held on "non-frequently played" days as compared to frequently played days. In addition, the home advantage that weak teams have on non-frequent days is significantly lower than that of stronger teams. The conventional wisdom that weekday matches attract less attendance than weekend matches is also supported for the Spanish league in [42]. [43], in a comparative study across various soccer league divisions in England, reported that midweek scheduling has more negative impact on attendance in lower divisions. As far as the impact of TV broadcasting is concerned, [44] published a study on English soccer leagues as well that presents evidence for a higher degree of negative influence of satellite coverage on match attendance during weekdays rather than weekends.

2.1. Contribution

We study the matchday schedule problem for the Turkish professional soccer league that has unique features due to the needs of different stakeholders. The problem is formulated as a nonlinear binary integer programming through the use of unique fairness criteria. Particularly, an equal distribution of match days between the teams throughout the season and the ideal assignment of games to different days in each round of the tournament are taken into account in our mathematical model. We solve the underlying integer program optimally for each week and demonstrate that the optimal solution significantly outperforms the existing schedule generated manually by TFF officials.

Further, our work differs from the related work (described in [13] and [14]) in the following aspects. First, in both references, authors assign schedules to matches in the league with the objective of minimizing rest differences, whereas our model does not deal with rest difference. Second, unlike the solutions of the formulations of those work, our solution is highly dependent on the matchday schedules in all the previous rounds. Finally, there is a strong relation between the decomposed IP models of such work and the quadratic assignment problem (QAP), whereas the nature of the objective function of our model does not lend itself to the application of QAP.

We are now in a position to describe our problem and its mathematical formulation.

3. Problem description and mathematical formulation

We first provide brief information about the Turkish professional soccer league.

3.1. Turkish Professional Soccer League

The Turkish Super League (TSL) is the top tier professional soccer league of Turkey. The league regularly contains 18 teams that play with their opponents in both parts of the season, one being played at their home venue and the other at an opponent's venue. Such a tournament is called Double Round Robin Tournament. Further, teams earn three points for a win and one point for a draw, whereas no points are given for a loss.

Teams to take part in international cups are determined by the following rules. Teams ranked first and second at the end of the season qualify for the UEFA Champions League. The champion of the Turkish Cup along with teams ranked third and fourth qualify for the UEFA Europa League. These rules may be subject to change because each season the number of teams allowed to participate is redetermined by UEFA based on the overall performance of Turkish teams in five successive years before the season.

Due to the concerns indicated in the introduction, the administrators of the TSL have been facing the issue of making sure that games are fairly distributed. Since it is a quite uncommon practice of the federation in Turkey to schedule TSL games to the middle of the week, we will proceed according to the assumption that teams play Friday to Monday. There are a total of nine games in each round of play. The distribution of matches played Friday to Monday is mathematically represented as $e-f-g-h$ where e, f, g, h represent the number of games played on Friday, Saturday, Sunday and Monday, respectively. Surely, $e+f+g+h=9$. The days and hourly times of all the games during a season is scheduled by the officials of the TSL manually. On top of that, the season contains a number of rounds for which a matchday schedule has to be constructed by taking into account the games of teams attending the Champions League and the Europa League as well as the games held for the Turkish Cup from Tuesdays to Thursdays. Accordingly, a minimum of two consecutive days without any competitive encounter are inserted in between back-to-back matches (possibly in different tournaments).

Table 1. Rankings of the favorite teams in different seasons.

Season	GS	FB	BJK	MB
2014-2015	1	2	3	4
2015-2016	6	2	1	4
2016-2017	4	3	1	2
2017-2018	1	2	4	3
2018-2019	1	6	3	2

Table 2. Total number of games the favorite teams played on different days between 2014 and 2019.

Day	GS	FB	BJK	MB
Friday	20	13	18	17
Saturday	72	49	48	60
Sunday	55	76	67	68
Monday	19	29	33	22

Tables 1 and 2 display the rankings and matchday distributions of the four most successful teams between 2014 and 2019 ([45]). These teams are Galatasaray (GS), Fenerbahçe (FB), Beşiktaş (BJK), and Medipol Başakşehir (MB). Apparently, the number of games each team plays on certain days vary significantly (see Table 2). Our mathematical analysis aims to reduce this variability for these and other teams in the league. The mathematical formulation of our problem is given next.

3.2. Mathematical formulation

Our mathematical formulation is inspired by the Monden heuristic, which is used for mixed model assembly line scheduling to minimize the variation of the component parts for manufacturing end-items. This method determines the order of end items to be assembled which will make the actual usage rate of components most closely match their average usage rates ([46]). In order to choose which end item to schedule in the next assembly, all possible options are evaluated by summing the squared deviations of the actual use rates of the components. The minimum of the summed values is selected for the next assembly. The related equation is given by:

$$D_{ki} = \sqrt{\sum_{j=1}^{\beta} (\frac{K \times N_j}{Q} - X_{j,k-1} - B_{ij})^2}, \qquad (1)$$

where: D_{ki} is the deviation for end item i and order number k; β is the number of variable components; K is the number of the sequence for scheduling; N_j is the sum of components j required for the final assembly sequence; Q is the sum of the end items in the final assembly; $X_{j,k-1}$ is the cumulative number of component j used until sequence $k-1$; B_{ij} is the number of component j required to make end item i.

This method ensures that the actual usage for all components tracks closely to their average usages. We utilized Eqn. 1 in constructing the mathematical formulation of our problem. In particular, we formulate the scheduling problem faced by the TSL administrators for each round of the season as a nonlinear binary integer program, to achieve an equal matchday distribution. Monden heuristic is used for problems in a completely different domain, but there is one useful analogy which we briefly explain here. The concept of Just-in-time (JIT) manufacturing advocates a schedule in which multiple products are produced in a mixed sequence that plans for the same rate of production in any reasonable unit of time. This rate is adjusted based on incoming rate of demand. For example, consider a production environment with only three items (i.e., Item 1, Item 2, and Item 3) to produce. If in a period of 8 hours, 16 units of Item 1, 24 units of Item 2, and 32 units of Item 3 should be produced, then we schedule production of 2, 3, and 4 units per hour of Items 1, 2, and 3, respectively. In our problem, each team is analogous to a different product and each round is analogous to a different period of time where the rate of games to be played by each team on any day throughout the season is the same for establishing fairness. The details of how this works and the resulting mathematical model are provided below.

3.2.1. Parameters and decision variables

As mentioned earlier, our model is dynamic in nature. When it is used to find an equitable distribution of matchdays among the participating teams in a given round of play, it seeks to minimize the differences between the total number of times that each team has made an appearance until that round on any given day. Roughly speaking, when determining the game to be played on a Friday in any round that includes nine games, the model first compares the total number of Friday games that each team has played up to that point in the season. Then it assigns the teams with a minimal number of Friday appearances until that round to the Friday slot as long as other constraints are satisfied. In doing so, the model assumes an ideal distribution of matchdays for each team throughout season that includes 34 games in total, which is denoted by (s^*, t^*, u^*, v^*) where numbers s^* to v^* represent the total number of games played from Friday to Monday respectively. Since there are 34 weeks in any seasonal fixture, $s^* + t^* + u^* + v^* = 34$. For fairness, the ideal distribution is essentially the same for each team. Since weekend games are more preferable from the perspective of all stakeholders, ideal distribution over 34 rounds should indicate that a greater portion of games for each team to be played over the weekend. The presence of the ideal distribution establishes an objective ground for the assignment of matchdays as equally as possible in the entire season.

To emphasize, the comparative analysis indicated in the above paragraph draws an analogy with the Monden heuristic in the following sense: like we align the usage of items in production closely with their average usages, we make sure that the total number of appearances on any day of the week by the end of a specific round is as close as possible to an ideal distribution of matchdays associated with that round. Accordingly, we calculate a metric for each team to measure a matchday count deviation from an ideal and fair distribution in each round. This deviation metric, D_{dr}, $d \in DS = \{Fri, Sat, Sun, Mon\}$, $1 \leq r \leq 34$ is given below:

$$D_{dr} = \sqrt{\sum_{i=1}^{I} (x_{ird} + \sum_{k=1}^{r-1} x_{ikd} - r \times a_d)^2}, \qquad (2)$$

where

$$x_{ird} = \begin{cases} 1, & \text{if team } i \text{ has a game in round } r \text{ on day } d, \\ 0 & \text{otherwise.} \end{cases}$$

Here $i = 1, \ldots, I$, $r = 1, \ldots, R$, $d \in CD = \{Wed, Thu, Fri, Sat, Sun, Mon, Tue\}$, $I = 18$ and $R = 34$, as there are 18 teams. It will later become clear that x_{ird}'s are the decision variables of our model. Furthermore, a_d is the ideal matchday distribution per team in one round. It is calculated by dividing the ideal number of games played from Friday to Monday to the number of rounds as follows:

$$a_d = \begin{cases} \frac{s^*}{34}, & \text{if } d = \text{Fri.} \\ \frac{t^*}{34}, & \text{if } d = \text{Sat.} \\ \frac{u^*}{34}, & \text{if } d = \text{Sun.} \\ \frac{v^*}{34}, & \text{if } d = \text{Mon.} \end{cases}$$

Let us now exemplify the use of this metric. Consider a season with 34 rounds in which the ideal number of games on Saturday is 10. This ideal number is for the entire season, however, it is also an anchor to calculate the round-specific ideal for any round r. For instance, if $r = 7$, the ideal count of Saturday games (which is calculated by the term $r \times a_d$ in D_{dr}) is $7 \times 10/34 = 2.0588$. Then the value of the matchday decision variable in round $r = 7$ for any team i, $x_{i7Sat.}$, is set such that the total number of Saturday games played by team i *by the end of* round $r = 7$ (which is represented by the term $x_{ird} + \sum_{k=1}^{r-1} x_{ikd}$) is as close to 2.0588 as possible. This is repeated for any $i = 1, \ldots, 18$, and weighted against the round-specific deviation metric that we introduce in the next paragraph. The main motivation is to keep balance not only by the end of the season, but rather at each step of the way throughout the season. This is crucial because the presence of imbalance may challenge the perception of fairness when it occurs in any round of the season, not just the end.

In addition to the seasonal matchday count deviation metric, D_{dr}, there is another form of deviation that the model calculates: deviation from an ideal distribution of nine games from Friday to Monday in any round. This metric is related to the aforementioned distribution of matches that are mathematically represented as $e - f - g - h$ where e denotes the number of games played in one round on Friday, f on Saturday, g on Sunday, and h on Monday. Let $e^* - f^* - g^* - h^*$ be an ideal distribution from which our next metric measures the deviation for each round of play. This deviation metric is denoted by V_r and is computed using the below formula:

$$V_r = \sqrt{\sum_{d \in DS} \Big(\frac{\sum_{i=1}^{I} x_{ird}}{2} - b_d \Big)^2}, \qquad (3)$$

where b_d represents the ideal number of games on day d, which should be determined by the federation based on team and broadcasting company preferences. It should therefore be equal to:

$$b_d = \begin{cases} e^*, & \text{if } d = \text{Fri.} \\ f^*, & \text{if } d = \text{Sat.} \\ g^*, & \text{if } d = \text{Sun.} \\ h^*, & \text{if } d = \text{Mon.} \end{cases}$$

In (3), $\frac{\sum_{i=1}^{I} x_{ird}}{2}$ represents the total number of games on day d in round r. It is customary to schedule one match on Friday, and one on Monday (i.e., after setting $e^* = h^* = 1$) leaving the rest of the meetings to take place on Saturdays and Sundays. However the model that we propose in this paper can accommodate any pattern of play in each round based on relative importance of multiple deviations from ideal distribution in the objective function. In comparison to the seasonal matchday count deviation metric in (2), V_r has a simpler functional form. Nevertheless, V_r is essentially similar to many other deviation or distance metrics widely available in the literature; it is the square root of the sum of squared deviations from the ideal number of games in each day of the round. The main role of this metric is not to establish fairness, though. Instead, it is formulated to assign more games to weekends in each round as preferred by all the stakeholders for various reasons.

There are three parameters that represent the relative importance weights of deviations defined in this section:

w_d: weight assigned to deviation D_{dr} for each day $d \in DS = \{Fri, Sat, Sun, Mon\}$ in the objective function, $1 \leq r \leq 34$,

c_1: weight for the weighted sum of the seasonal matchday deviations, i.e., $\sum_{d \in DS} w_d \times D_{dr}$, in round $r \in \{1, ..., 34\}$,

c_2: weight assigned to deviation V_r.

One paper that we should highlight here for the presence of a methodological similarity is the study by [47]. As we mentioned in the previous section, inspired from the JIT's mixed production scheduling algorithm, our model generates a dynamically evolving matchday assignment for each team keeping a close track of the fair distribution of the available days for this purpose. A similar fairness concern is also central in the study by [47]. Their aim is to accomplish a fair assignment of referees by following criteria such as keeping a relatively balanced load of officiating throughout the season and setting up each referee to serve in an equal number of games played by each participating team. However, they do not use similar deviation metrics in their formulation, whereas the deviation functions D_{dr} $d \in DS = \{Fri, Sat, Sun, Mon\}$, $1 \le r \le 34$ and V_r are critical to the objective function in this paper.

The idea of establishing fairness by setting up each team to play an equal number of times on a given matchday (from Friday to Monday) as the season progresses is somewhat similar to the balancedness concept introduced in [48] as well. This concept requires for each team that the number of home and away games differ by at most one. Later, it was extended by [49] to ensure that in any round the difference between the number of home games played by any two teams up to that point in the schedule does not exceed a fixed number g. Such a schedule is called g-ranking-balanced. However, this concept is not directly applicable to our study for two reasons. First and foremost, they are not suitable for formulating the fairness criteria which are also the main motivations of our paper. Second, they are not practical for use in a multi-criteria analysis.

We state the entire problem formulation in the next subsection.

3.2.2. Objective function and constraints

Using the above parameters and decision variables, we solve a nonlinear binary integer program for $r = 1, \ldots, 34$. Owing to Champions League, European League, and Turkish Cup games before/after certain rounds, the constraints of the program differ from one round to another. We therefore provide the entire set of constraints for one specific round for illustrative purposes (i.e., $r = 7$). The fixture for this round is provided in Table 3. The games in this fixture were to be scheduled between September 28 and October 1, Friday to Monday. Without loss of generality, each team is assigned an arbitrary index 1 to 18. Specific constraints that should be considered are as follows: team 1 has a Champions League game the following Wednesday (October 3), teams 8, 11, and 13 have Turkish cup games on the Wednesday (September 26) before round 7, and team 7 has a Turkish Cup game on Thursday (September 27) which is also right before round 7.

The resulting nonlinear binary integer program for round 7 is expressed as follows:

$$\min c_1 \times \left(\sum_{d \in DS} w_d \times \sqrt{\sum_{i=1}^{I} (x_{ird} + \sum_{k=1}^{r-1} x_{ikd} - r \times a_d)^2} \right) + c_2 \times \sqrt{\sum_{d \in DS} \left(\frac{\sum_{i=1}^{I} x_{ird}}{2} - b_d \right)^2} \tag{4}$$

subject to:

Feasibility constraints:

$$x_{i,7,Fri} + x_{i,7,Sat} + x_{i,7,Sun} + x_{i,7,Mon} = 1, \quad i = 1, \ldots, I \tag{5}$$

$$x_{i,7,Thu} + x_{i,7,Fri} + x_{i,7,Sat} \le 1, \quad i = 1, \ldots, I \tag{6}$$

$$x_{i,7,Sun} + x_{i,7,Mon} + x_{i,7,Tue} \le 1, \quad i = 1, \ldots, I \tag{7}$$

$$x_{i,7,Wed} + x_{i,7,Thu} + x_{i,7,Fri} \le 1, \quad i = 1, \ldots, I, i \ne 1 \tag{8}$$

$$x_{i,7,Mon} + x_{i,7,Tue} + x_{i,7,Wed} \le 1, \quad i = 1, \ldots, I, i \ne 8, 11, 13 \tag{9}$$

Assignment constraints:

Table 3. Games scheduled for round 7.

Game	Home Team	Away Team	Home Team index	Away Team index
1	Galatasaray	Erzurum	1	17
2	Trabzon	Kasımpaşa	4	14
3	Alanya	Akhisar	9	18
4	Beşiktaş	Kayseri	3	10
5	Sivas	Bursa	12	16
6	Göztepe	Konya	15	8
7	Çaykur Rize	Fenerbahçe	11	6
8	Ankaragücü	Antalya	13	7
9	Başakşehir	Malatya	2	5

$$x_{1,7,d} - x_{17,7,d} = 0, \quad d \in DS \tag{10}$$
$$x_{4,7,d} - x_{14,7,d} = 0, \quad d \in DS \tag{11}$$
$$x_{9,7,d} - x_{18,7,d} = 0, \quad d \in DS \tag{12}$$
$$x_{3,7,d} - x_{10,7,d} = 0, \quad d \in DS \tag{13}$$
$$x_{12,7,d} - x_{16,7,d} = 0, \quad d \in DS \tag{14}$$
$$x_{15,7,d} - x_{8,7,d} = 0, \quad d \in DS \tag{15}$$
$$x_{11,7,d} - x_{6,7,d} = 0, \quad d \in DS \tag{16}$$
$$x_{13,7,d} - x_{7,7,d} = 0, \quad d \in DS \tag{17}$$
$$x_{2,7,d} - x_{5,7,d} = 0, \quad d \in DS \tag{18}$$

Additional constraints:

$$x_{1,7,Wed} = 1 \tag{19}$$
$$x_{7,7,Thu} = 1 \tag{20}$$
$$x_{11,7,Wed} = 1 \tag{21}$$
$$x_{13,7,Wed} = 1 \tag{22}$$
$$x_{8,7,Wed} = 1 \tag{23}$$
$$\textstyle\sum_{d \in CD} x_{i,7,d} = 1, \quad i = 1, \ldots, I, i \neq \{1, 7, 8, 11, 13\} \tag{24}$$

Note that the term $\sum_{k=1}^{r-1} x_{ikd}$ appearing in D_{dr} in (4) uses the data coming from the previous rounds. To be more specific, this term constitutes the optimal solutions of the previous rounds. Similarly, the optimal solution of the current round will be added to the data that will be input into the mathematical models of the remaining rounds. In this sense, the mathematical model of each round is connected to each other through this term.

Constraints 5 to 8 are all formulated for a similar purpose: that each team will play only one game between the days indicated by the decision variables. Constraint 5 imposes this restriction from Friday to Monday because each team has one game to play in one round. Constraint 6 does the same from Thursday to Saturday, Constraint 7 serves for a similar purpose from Sunday to Tuesday, and finally Constraint 8 from Wednesday to Friday all because of the minimum rest requirement between games. Constraint 8 excludes an index value of 1 although $x_{1,7,Wed} = 1$ because team 1 is to play a Wednesday game after round 7 whereas 8 is imposed for teams that are scheduled to play a Wednesday game before round 7. Constraint 9 ensures that each team except teams 8, 11, and 13 can have at most one game from Monday to Wednesday. Exclusion of teams 8, 11, and 13 in constraint 9 is for a similar reason why team 1 index is excluded in constraint 8. In sum, feasibility constraints should be amended in each round to reflect the implications of the two-day rest period between games.

Constraints 10 through 18 are assignment constraints created for each scheduled game (see Table 3). For instance, Constraint 10 ensures that for each day of Friday through Monday, if team 1 has a game, team 17 must also have a game on the same day; similarly if team 1 does not have a game on any of those days, team 17 must not have a game on the same day, either.

Constraints 19 through 23 state that team 1 has a game on Wednesday, team 7 has a game on Thursday, and teams 8, 11, and 13 have games on Wednesday. Note that these constraints are required to make sure that information on the Champions League and Turkish Cup fixture of the associated teams are reflected to the model. Finally, Constraint 24 ensures that each team except teams 1, 7, 8, 11, and 13 will have only one game from Wednesday to Tuesday.

As stated earlier, we solve the aforementioned mathematical model for each round by slightly revising its constraints, depending on what teams have additional games right before/after the respective round. The underlying nonlinear binary integer program is solved by AMPL via its solver, BARON. It takes less than a minute to solve our model for a given round.

Our computational results are discussed in the next section.

Table 4. Optimal and manual matchday schedules for round 7.

Game	Optimal Schedule	Manual Schedule
1	Sunday	Friday
2	Sunday	Saturday
3	Saturday	Saturday
4	Friday	Saturday
5	Sunday	Sunday
6	Saturday	Sunday
7	Sunday	Sunday
8	Monday	Monday
9	Saturday	Monday

4. Results

We compare the optimal matchday schedule obtained by AMPL, BARON with the manual schedule constructed by the TSL officials for the 2018-2019 soccer season of Turkey ([45]). The parameters of our models are set to the following values: $c_1 = c_2 = 1$; $w_{Fri} = 0.11, w_{Sat} = 0.33, w_{Sun} = 0.44, w_{Mon} = 0.11$. Weights c_1 and c_2 are the same indicating that both deviation

Table 5. Seasonal matchday distribution of games for each team obtained by the manual schedule.

Team index	Friday	Saturday	Sunday	Monday
1	7	11	13	3
2	4	10	13	7
3	5	10	13	6
4	6	13	11	4
5	4	10	16	4
6	4	11	11	8
7	3	13	13	5
8	4	11	14	5
9	4	11	12	7
10	1	17	13	3
11	3	14	12	5
12	5	13	13	3
13	4	12	14	4
14	5	11	10	8
15	5	14	12	3
16	7	10	15	2
17	4	11	15	4
18	1	11	15	7

Table 6. Seasonal matchday distribution of games for each team obtained by the optimal schedule.

Team index	Friday	Saturday	Sunday	Monday
1	5	12	15	2
2	4	11	16	3
3	3	12	15	4
4	5	12	14	3
5	4	11	16	3
6	3	12	15	4
7	3	12	15	4
8	4	12	14	4
9	4	12	15	3
10	5	12	15	2
11	3	12	16	3
12	3	12	16	3
13	3	12	16	3
14	3	12	15	4
15	3	12	16	3
16	4	12	15	3
17	4	12	15	3
18	3	12	15	4

components of objective function are equally important. As indicated in the introduction, economic and other concerns seem to support the view that weekend games are relatively more preferable and maybe more important. This is why we choose our baseline values for seasonal deviation metric weights for weekends (i.e., w_{Sat}, w_{Sun}) to be greater than weights for the weekdays (i.e., w_{Fri}, w_{Mon}).

Regarding the ideal distribution of matches, we set $e^*-f^*-g^*-h^* = 1 - 3 - 4 - 1$, and $(s^*, t^*, u^*, v^*) = (5, 12, 12, 5)$ for illustrative purposes and obtain our results accordingly. Like in the case of seasonal deviation metric weights, the relative preferability of the weekend games by the stakeholders is reflected to these ideal distributions.

We begin with the comparison of the optimal matchday schedule with the manual schedule for round 7. As observed in Table 4, the optimal schedule ensures the 1 - 3 - 4 - 1 pattern, whereas the manual schedule does not do so, yielding the pattern 1 - 3 - 3 - 2.

Table 7. Summary statistics for the manual schedule in the entire season.

Matchday	Std. Dev.	Min.	Max.
Friday	1.62	1	7
Saturday	1.85	10	17
Sunday	1.59	10	16
Monday	1.87	2	8

Table 8. Summary statistics for the optimal schedule in the entire season.

Matchday	Std. Dev.	Min.	Max.
Friday	0.77	3	5
Saturday	0.32	11	12
Sunday	0.65	14	16
Monday	0.65	2	4

Tables 5 and 7 show the day distribution of games obtained by the manual schedule for the entire season and the resulting summary statistics for each day from Friday to Monday, respectively. Similar statistics for the optimal solution obtained by solving the underlying nonlinear binary integer programs successively for the entire season are presented in Tables 6 and 8. Results indicate that the optimal solution significantly outperforms the manual schedule in terms of the standard deviation of the matchday schedule for Friday through Monday (see Tables 7 and 8). As an example, while standard deviation obtained by the manual schedule for Friday is 1.62, with minimum and maximum values being 1 and 7, standard deviation obtained by the optimal schedule for the same day is 0.77, with minimum and maximum values being 3 and 5. Finally, average reduction in standard deviation over the manual schedule over those four days is 65%.

Further, the optimal solution for each round reveals that the 1 - 3 - 4 - 1 pattern is ensured for the entire season except a few rounds. The TFF officials implement the 1 - 4 - 4 - 0 pattern in those few rounds due to the need to provide enough rest days for the teams with players who play in national games held right after those rounds. In contrast, the manual schedule deviates from this pattern in nearly half of the 34 rounds.

The seasonwide solution that we summarize in this section can be potentially improved upon by employing multi-round solutions based on gradual information flow from other tournaments, or comparing alternative solutions in earlier rounds that could bring better solutions in future rounds of the season. However, the dynamic approach we present here is a good start in exploring schedules that could mitigate the problems summarized in the introduction.

Table 9. Summary statistics for the optimal schedule ($c_2 = 0.2$).

Matchday	Std. Dev.	Min.	Max.
Friday	0.51	4	5
Saturday	0.46	12	13
Sunday	0.58	12	14
Monday	0.65	3	6

4.1. Sensitivity analysis

In order to observe the impact of weights, c_1 and c_2, on the performance of the optimal solution, we performed sensitivity analysis. As stated earlier, the base-case values for c_1 and c_2 are set to 1 (note that c_1 corresponds to seasonal deviation, whereas c_2 corresponds to round specific daily deviation). To explore the sensitivity of our results to these weights, we adjusted their relative values keeping the value of c_1 at 1. In particular, we generated different cases by gradually decrementing the value of c_2. It turned out that the results do not change when c_2 is greater than 0.2 (i.e., the seasonal matchday distribution of games for each team remains the same). This implies that the round specific daily deviation term of the objective function has more impact on the optimal solution. In other words, the model provides robust results even when we assign a significantly larger weight to striking a reasonable seasonwide balance up to a point in which seasonal deviation is at least five times more important than the round specific deviation. One may attribute this behavior to the partial compatibility of two deviation metrics in the sense of taking ideal matchday distributions that assign a higher number of games to weekends. As for the $c_2 = 0.2$ case, the optimal solution differs only slightly from the baseline case optimal solution in terms of the matchday distribution and the summary statistics for each matchday (Fri. to Mon.; see Tables 9 and 10).

Furthermore, Table 11 presents optimal seasonal and round specific daily deviations for each round for the baseline case and the $c_2 = 0.2$ case. Unsurprisingly, the baseline case optimal solution yields better results in terms of round specific deviation, whereas the $c_2 = 0.2$ case is superior in terms of

Table 10. The matchday distribution of games obtained by the optimal schedule ($c_2 = 0.2$).

Team index	Friday	Saturday	Sunday	Monday
1	5	12	13	4
2	4	12	13	5
3	4	12	14	4
4	5	12	13	4
5	5	13	12	4
6	5	12	13	4
7	4	12	13	5
8	5	12	13	4
9	5	13	12	4
10	4	12	14	4
11	5	13	12	4
12	5	12	13	4
13	5	13	13	3
14	4	12	13	5
15	4	13	13	4
16	5	12	13	4
17	5	12	13	4
18	4	12	12	6

seasonal deviation. The sensitivity analyses also revealed that decrementing c_2 even further leads to implausible results that cannot be implemented in practice due to the concerns of TFF.

5. Conclusions

In this work, we discuss the sports scheduling problem faced by the administrators of the Turkish Super League (TSL). Given the scheduled games for each round, the problem is to determine a fair matchday schedule for each round in terms of day distribution. We formulate our problem as a nonlinear binary integer program and solve the underlying problem optimally for each round. Our results reveal that the implementation of the optimal schedule can significantly improve the manual schedule constructed by the TSL officials. We observe that the results are largely robust in the relative changes between the weights of two major deviation metrics. They also illustrate the significance of the round specific matchday distribution concerns against the need for seasonal fairness.

Future research may consider measures such as rest mismatch or breaks in addition to seasonal or round specific day distribution. In this regard, uncertain and dynamic natures of these problems can be addressed using mathematical models from the field of dynamic stochastic optimization (see [50] and [51]). Additionally, it is worthwhile to investigate cases with multi-round solutions obtained as other tournaments progress or to incorporate uncertainty into such problems owing to the fact that many games are rescheduled or canceled due to bad weather conditions in popular soccer leagues.

References

[1] Sözcü (2016). *Fenerbahçe TFF'ye başvurdu (Fenerbahçe consulted TFF)* [online]. Available from: `https://skor.sozcu.com.tr/2016/12/30/fenerbahce-tffye-basvurdu-maclara-cikmayiz-tepkisi-572320/amp` [Accessed 1 September 2021].

[2] Ajansspor (2017). *Hafta içi tribünler dolmuyor (Tribunes are not full on weekdays)* [online]. Available from: `https://ajansspor.com/haber/hafta-ici-tribunler-dolmuyor-118912` [Accessed 1 September 2021].

[3] Habertürk (2011). *Tribünler dolmuyor (Tribunes are not full)* [online]. Available from: `https://www.haberturk.com/spor/futbol/haber/686439-tribunler-dolmuyor` [Accessed 1 September 2021].

[4] Yeniçağ (2009). *TFF'ye büyük tepki (A huge reaction against TFF)* [online]. Available from: `https://www.yenicaggazetesi.com.tr/tffye-buyuk-tepki-21521h.htm` [Accessed 1 September 2021].

[5] Sözcü (2017). *Beşiktaş'a cumalar yaramıyor (Beşiktaş does not benefit from Fridays)* [online]. Available from:

Table 11. The objective function values obtained by the optimal schedules (for the baseline case and the $c_2 = 0.2$ case, indexed as 1 and 2, respectively).

Round	Seas. Dev.$_1$	Daily Dev.$_1$	Seas. Dev.$_2$	Daily Dev.$_2$
1	1.91	0	1.91	0
2	1.99	0	1.99	0
3	2.3	0	2.3	0
4	2.24	0	2.24	0
5	2.27	0	1.97	1.4
6	2.38	0	2.18	0
7	2.87	0	2.49	0
8	3.4	0	3.08	0
9	3.09	0	3.04	0
10	3.65	0	2.74	3.45
11	3.79	0	2.93	0
12	4.26	0	3.5	0
13	4.33	0	3.56	0
14	4.89	0	3.83	0
15	5.34	0	3.99	0
16	6.02	0	3.86	3.15
17	6.25	0	4.32	0
18	6.42	0	4.57	0
19	6.71	0	4.07	2.8
20	6.51	0	4.16	0
21	6.67	0	4.58	0
22	6.65	0	4.48	0
23	6.53	0	3.85	3.75
24	6.88	0	4.16	0
25	6.8	0	4.23	0
26	6.86	0	4.42	0
27	7.08	0	4.42	0
28	7.17	0	4.05	2.45
29	7.43	0	4.31	0
30	7.73	0	3.62	3.7
31	7.8	0	3.34	1.4
32	7.9	0	2.94	3.7
33	8.3	0	3.18	0
34	8.27	0	3.5	0
average	5.37	0	3.46	0.76

https://www.goal.com/tr/amp/haber/besiktasa-cumalar-yaramiyor/1wtdm3xat35i41tzisu6ezqjv9 [Accessed 1 September 2021].

[6] Sondakika (2017). *Trabzonspor'a cuma günü oynadığı maçlar yaramıyor (Trabzonspor does not benefit from Friday matches)* [online]. Available from: `https://www.sondakika.com/haber/haber-trabzonspor-a-cuma-gunu-oynadigi-maclar-yaramiyor` [Accessed 1 September 2021].

[7] Yeniçağ (2010). *Kartala cuma yaramıyor (Kartal does not benefit from Fridays)* [online]. Available from: `https://www.fanatik.com.tr/amp/kartala-cuma-yaramiyor-175352` [Accessed 1 September 2021].

[8] Fotomaç (2018). *Başakşehire pazartesi maçları yaramıyor (Başakşehir does not benefit from Monday matches)* [online]. Available from: `https://m.fotomac.com.tr/medipol-basaksehir/2018/02/27/basaksehire-pazartesi-maclari-yaramiyor/amp` [Accessed 1 September 2021].

[9] Kim, T. (2019). Optimal approach to game scheduling of multiple round-robin tournament: Korea professional baseball league in focus. *Computers and Industrial Engineering*, 136, 95–105.

[10] Rasmussen, R.V. & Trick, M.A. (2008). Round robin scheduling—a survey. *European Journal of Operational Research*, 188(3), 617–636.

[11] Ribeiro, C.C. (2012). Sports scheduling: Problems and applications. *International Transactions in Operational Research*, 19(1-2), 201–226.

[12] Kendall, G., Knust, S., Ribeiro, C.C., & Urrutia, S. (2010). Scheduling in sports: An annotated bibliography. *Computers and Operations Research*, 37(1), 1–19.

[13] Atan, T., & Çavdaroğlu, B. (2018). Minimization of rest mismatches in round robin tournaments. *Computers and Operations Research*, 99, 78–89.

[14] Çavdaroğlu, B., & Atan, T. (2020). Determining matchdays in sports league schedule to minimize rest differences. *Operations Research Letters*, 48(3), 209–216.

[15] Rasmussen, R.V., & Trick, M.A. (2007). A Benders approach for the constrained minimum break problem. *European Journal of Operational Research*, 177(1), 198–213.

[16] Duran, G., Guajardo, M., & Saure, D. (2017). Scheduling the South American Qualifiers to the 2018 FIFA World Cup by integer programming. *European Journal of Operational Research*, 262(3), 1109–1115.

[17] Recalde, D., Torres, R., & Vaca, P. (2013). Scheduling the professional Ecuadorian football league by integer programming. *Computers and Operations Research*, 40(10), 2478–2484.

[18] Bulck, D.V., & Goossens, D. (2020). Handling fairness issues in time-relaxed tournaments with availability constraints. *Computers and Operations Research*, 115, 1048–1056.

[19] Kendall, G., & Westphal, S. (2013). Sports Scheduling: Minimizing Travel for English Football Supporters. In: A. Uyar, E. Ozcan, N. Urquhart eds. *Automated Scheduling and Planning. Studies in Computational Intelligence.* Springer, Berlin, Heidelberg, 61–90.

[20] Guedes, A.C.B., & Ribeiro, C.C. (2011). A heuristic for minimizing weighted carry-over effects in round robin tournaments. *Journal of Scheduling*, 14(6), 655–667.

[21] Januario, T., & Urrutia, S. (2016). A new neighborhood structure for round robin scheduling problems. *Computers and Operations Research*, 70, 127–139.

[22] Günneç, D., & Demir, E. (2019). Fair-fixture: Minimizing carry-over effects in football leagues. *Journal of Industrial and Management Optimization*, 15(4), 1565–1577.

[23] Durán, G., Guajardo, M. & Wolf-Yadlin, R. (2012). Operations research techniques for scheduling Chile's second division soccer league. *Interfaces*, 42(3), 273–285.

[24] Rasmussen, R.V. (2008). Scheduling a triple round robin tournament for the best Danish soccer league. *European Journal of Operational Research*, 185(2), 795–810.

[25] Goossens, D., & Spieksma, F. (2009). Scheduling the Belgian soccer league. *Interfaces*, 39(2), 109–118.

[26] Ribeiro, C.C., & Urrutia, S. (2012). Scheduling the Brazilian soccer tournament: Solution approach and practice. *Interfaces*, 42(3), 260–272.

[27] Durán, G., Guajardo, M., Miranda, J., Sauré, D., Souyris, S., Weintraub, A., & Wolf, R. (2007). Scheduling the Chilean soccer league by integer programming. *Interfaces*, 37(6), 539–552.

[28] Bartsch, T., Drexl, A., & Kròger, S. (2006). Scheduling the professional soccer leagues of Austria and Germany. *Computers and Operations Research*, 33(7), 1907–1937.

[29] Briskorn, D., & Drexl, A. (2009). IP models for round robin tournaments. *Computers and Operations Research*, 36(3), 837–852.

[30] Durán, G., Durán, S., Marenco, J., Mascialino, F., & Rey, P.A. (2019). Scheduling Argentina's professional basketball leagues: A variation on the Travelling Tournament Problem. *European Journal of Operational Research*, 275(3), 1126–1138.

[31] Haselgrove, J., & Leech, J. (1977). A tournament design problem. *The Amer. Math. Monthly*, 84(3), 198–201.

[32] de Werra, D. (1981). Scheduling in Sports. In: P. Hansen, ed. *Studies on Graphs and Discrete Programming.* North Holland, 381–395.

[33] Elf, M., & Junger, M. (2003). Minimizing breaks by maximizing cuts. *Operations Research Letters*, 31(5), 343–349.

[34] van't Hof, P., Post, G., & Briskorn, D. (2010). Constructing fair round robin tournaments with a minimum number of breaks. *Operations Research Letters*, 38(6), 592–596.

[35] Yi, X., Goossens, D., & Nobibon, F.T. (2020). Proactive and reactive strategies for football league timetabling. *European Journal of Operational Research*, 282(2), 772–785.

[36] Jane, W.J. (2014). The relationship between outcome uncertainties and match attendance: New evidence in the National Basketball Association. *Review of Industrial Organization*, 45(2), 177–200.

[37] Tainsky, S., & Winfree, J.A. (2010). Short-Run Demand and Uncertainty of Outcome in Major League Baseball. *Review of Industrial Organization*, 37(3), 197–214.

[38] Buraimo, B., & Simmons, R. (2009). A tale of two audiences: Spectators, television viewers and outcome uncertainty in Spanish football. *Journal of Economics and Business*, 61(4), 326–338.

[39] Szymanski, S. (2003). The economic design of sporting contests. *Journal of Economic Literature*, 41(4), 1137–1187.

[40] Benz, M.A., Brandes, L., & Franck, E. (2009). Do soccer associations really spend on a good thing? Empirical evidence on heterogeneity in the consumer response to match uncertainty of outcome. *Contemporary Economic Policy*, 27(2), 216–235.

[41] Goller, D., & Krumer, A. (2020). Let's meet as usual: Do games played on non-frequent days differ? Evidence from top European soccer leagues. *European Journal of Operational Research*, 286(2), 740–754.

[42] Garcia, J., & Rodriguez, P. (2002). The determinants of football match attendance revisited: Empirical evidence from the Spanish football league. *Journal of Sports Economics*, 3(1), 18–38.

[43] Forrest, D., & Simmons, R. (2006). New issues in attendance demand: The case of the English football league. *Journal of Sports Economics*, 7(3), 247–266.

[44] Baimbridge, M., Cameron, S., & Dawson, P. (1996). Satellite Television and the Demand for Football: A Whole New Ball Game? *Scottish Journal of Political Economy*, 43(3), 317–333.

[45] Turkish Football Federation (TFF) Website (2021). Available from: `https://www.tff.org` [Accessed 1 September 2021].

[46] Vollman, T., Berry, W., Whybark, D., & Jakobs, F. (2011). *Manufacturing Planning and Control for Supply Chain Management*. 5th ed. McGraw-Hill, New York.

[47] Yavuz, M., İnan, U.H., & Fığlalı, A. (2008). Fair referee assignments for professional football leagues. *Computers and Operations Research*, 35(9), 2937–2951.

[48] Knust, S., & von Thaden, M. (2006). Balanced home-away assignments. *Disrete Optimization*, 3(4), 354–365.

[49] Goossens, D.R., & Spieksma, F.C.R. (2012). Soccer schedules in Europe: an overview. *Journal of Scheduling*, 15, 641–651.

[50] Göçgün, Y. (2018). Dynamic Scheduling with Cancellations: An Application to Chemotherapy Appointment Booking. *An International Journal of Optimization and Control: Theories and Applications*, 8(2), 161-169.

[51] Göçgün, Y. (2021). Performance Comparison of Approximate Dynamic Programming Techniques for Dynamic Stochastic Scheduling. *An International Journal of Optimization and Control: Theories and Applications*, 11(2), 178-185.

Yasin Göçgün *is an associate professor at İstinye University. He received his B.S. degree and M.S. degree from the Industrial Engineering Department at Bilkent University in 2003 and 2005, respectively. After completing his doctoral studies in the Industrial and Systems Engineering Department at the University of Washington in 2010, Dr. Göçgün worked as a postdoctoral fellow in Canada between 2010 and 2014. Prior to joining the Industrial Engineering Department at İstinye University, Dr. Göçgün worked as an assistant professor in the Industrial Engineering Department at Altınbaş University between 2014 and 2020.*

`https://orcid.org/0000-0003-3005-7596`

Niyazi Onur Bakır *is an associate professor of Industrial Engineering at Altınbaş University. His research interests include decision making under uncertainty, probabilistic modeling, homeland security, and economics of information. He received a Ph.D. degree in Industrial Engineering from Texas A&M University in 2004. He holds an M.S. degree in Economics from Texas A&M and a B.S. degree in Industrial Engineering from Bilkent as well. Prior to joining Altınbaş, he served as faculty members at TOBB University of Economics and Technology and Bilkent University.*

`https://orcid.org/0000-0002-0177-269X`

An International Journal of Optimization and Control: Theories & Applications
ISSN: 2146-0957 eISSN: 2146-5703
Vol.12, No.2, pp.128-136 (2022)
https://doi.org/10.11121/ijocta.2022.1227

RESEARCH ARTICLE

Financial efficiency of companies operating in the Kosovo food sector: DEA and DEAHP

Esma Canhasi Kasemi

Faculty of Education, University of Prizren, Prizren, Kosovo
esmacanhas@uni-pz.edu.com

ARTICLE INFO

Article history:
Received: 31 January 2022
Accepted: 26 May 2022
Available Online: 12 July 2022

Keywords:
Analytic Hierarchy Process (AHP)
Data Envelopment Analysis (DEA)
Decision making criteria
Efficiency measurement
Judgment scale

AMS Classification 2010:
90C08, 62P05

ABSTRACT

Data Envelopment Analysis (DEA) evaluates a large number of input and output variables using mathematical programming techniques and analyzes the effectiveness of similar decision making units (DMU). Unlike traditional methods, the most important advantage of DEA is that the weights of input and output variables can be defined by the analyzer. In this study, the limitations of the DEA weights were determined using the AHP, which considers expert opinion. In addition, an alternative judgment scale was used for the Saaty judgment scale, which is used as a standard in the AHP method, and thus a more sensitive analysis was performed. There have been studies dealing with the comparison of judgment scales, but few studies on consistency sensitivity are needed. This point has also been addressed in this study. Subsequently, the financial efficiency of 27 companies operating in the food sector in Kosovo was evaluated with the weight-restricted DEA model, first created using the unweighted DEA model and then the AHP model, and the two models were compared. This paper is the first one of its kind since there are no previous studies regarding the examination of the financial efficiency of companies operating in the Kosovo food sector based on the DEAHP method.

1. Introduction

Determining the performance of companies is important for both company management and investors. Companies have different time periods and different management levels, and therefore have different combinations of input and output. A company with very good profitability in the short term may show poor performance in the long term due to poor marketing policies. Although financial ratios such as return on investments or return on sales reflect the financial performance of the company, they are insufficient to show the overall performance of the company. On the other hand, the biggest shortcoming of efforts to combine by weighting the set of inputs and outputs adopted to show the full performance of the business is that the given weights are subjective [1].

Many inputs are used in most companies (such as several staff, wages, working hours, and advertising budgets). Similarly, output criteria (such as profitability, market share, and growth rate) differ. It is difficult for managers to "determine which units are ineffective" by evaluating many inputs and outputs simultaneously. In this case, using mathematical programming in the solution technique, Data Envelopment Analysis (DEA), in the efficiency measurement of problems with multiple inputs and multiple outputs, offers managers an important tool in determining relative activities [2].

On the other hand, when each of the multiple input and multiple output variables to be used does not have the same importance, studies have been carried out by including these variables in the analysis with the help of the Analytic Hierarchy Process (AHP) method. In addition, DEA is a method that guides managers and decision makers in terms of what should be done to improve the efficiency of relatively ineffective decision-making units [3]. In this way, it has enabled us to achieve healthier results.

DEA has had a wide range of applications since its emergence. In addition to its use alone, its use with other techniques is frequently encountered in the literature. Some of the studies related to the DEAHP method are given below.

Stern et al. [4], concluded that DMUs, which have more than one input and output, used a two-stage method with AHP to make complete sequencing whereas the DEA method lacked. In 2007 Lee et al. [5], the AHP and DEA hybrid approach in their studies and applied in the national energy efficiency plan sector. For the selection of warehouse operator networks, Korpela et al. [6], combined AHP and DEA methods. Sevkli et al. [7], made the supplier selection study of the BEKO company by using the DEAHP approach. Using the AHP-DEA method; Wang et al. [8] conducted a study evaluating the risks of bridge shapes based on previous bridge shapes. Erpolat and Cinemre [9] evaluated the efficiency of notebook computers of different brands and models, with the hybrid method of DEA and AHP. Tseng and Lee [10] measured the relationship between human resource practices and organizational performance variables using DEA / AHP method. In 2017, Keskin and Ulaş [11] investigated the effect of self-criticism on the performance of airports using AR, AHP and DEA. Çetin et al. [12] work was evaluated as a real homework problem to the banking sector and as a generalized assignment problem. In addition, in 2019, Pradhan, Olfati [13] included a detailed literature review of AHP and DEA methods used in their studies.

In addition to the methods used in the studies mentioned above, an alternative scale to the standard scale used in the binary comparison, which is one of the AHP stages, was used in this study. In this way, it has differentiated from many studies and also has the feature of being the first study done with this method in the food sector in Kosovo.

The remainder of the paper is organized as follows. The next Section 2 presents the methodology, and the steps used are given in detail in Section 3. Finally, the conclusions, including the results of the study and suggestions for future studies, are made in the last section.

2. Methodology

Since DEA and AHP methods were used in an integrated way in the study, DEA, AHP and DEAHP methods are described in this section.

2.1. Data envelopment analysis-DEA

Data Envelopment Analysis, which is based on non-parametric, linear programming principles, is a mathematical programming method that can compare relative efficiency between organizations when there are too many inputs and outputs [14]. In other words, Data Envelopment Analysis is a linear programming-based analysis method that measures the relative efficiency levels of (DMU), which has the task of generating similar outputs using similar inputs when multiple inputs and outputs represented by different units become difficult to compare [15].

In DEA, two models work under the constant return assumption (CRS) according to the scale generally used and the variable return according to the scale (VRS) and both are evaluated as input and output side [14]. While input direction models are investigating how the most appropriate input combination should be used to produce a certain output combination most efficiently; output direction models investigate how much output composition can be achieved with a given input combination. The selection of the model to be used in DEA varies according to the scope of the research and assumptions.

The original fractional CRS model Eq. (1) evaluates the relative efficiencies of n DMUs $j=1,\dots,n$ each with m inputs and s outputs denoted by $x_{1j}, x_{2j},\dots, x_{mj}$ and $y_{1j}, y_{2j},\dots, y_{sj}$ respectively [16]. This is done so by maximizing the ratio of a weighted sum of output to the weighted sum of inputs:

$$E_k = Max \frac{\sum_{r=1}^{s} u_r y_{rk}}{\sum_{i=1}^{m} v_i x_{ik}},$$

s.t.

$$\frac{\sum_{r=1}^{s} u_r y_{rj}}{\sum_{i=1}^{m} v_i x_{ij}} \le 1,\ \ j=1,\dots,n,\ \ r=1,\dots,s \qquad (1)$$

$$u_r, v_i \ge 0,\ \text{for all } r \text{ and } i$$

In model Eq. (1), E_k is the efficiency of DMU_k and u_r and v_i are the factor weights. For computational convenience, the fractional form Eq.(1) is re-expressed in linear program (LP) form as follows which is known as input oriented CRS model:

$$E_k = Max \sum_{r=1}^{s} u_r y_{rk},$$

s.t.

$$\sum_{r=1}^{s} u_r y_{rj} - \sum_{i=1}^{m} v_i x_{ij} \le 1,\ \ j=1,\dots,n \qquad (2)$$

$$\sum_{i=1}^{m} v_i x_{ik} = 1$$

$$u_r, v_i \ge 0$$

The dual of linear program (LP) model for input oriented CRS model is as follows:

$$Min\, E_k$$

s.t

$$\sum_{j=1}^{n} \lambda_{jk} x_{ij} \le E_k x_{ik} \quad i=1,\dots,m \qquad (3)$$

$$\sum_{j=1}^{n} \lambda_{jk} y_{rj} \ge y_{rk} \quad r=1,\dots,s$$

$$\lambda_{jk} \ge 0$$

Despite many modified models since the emergence of DEA, the most widely known and used model is the Input-oriented CRS model [17].

2.2. Analytic hierarchy process –AHP

The Analytical Hierarchy Process (AHP) is a multi-criteria decision making method that has been widely used since the 1970s. It separates the existing problem into small pieces and examines the effects of the pieces on each other. As a result of this process, the weight of the parts and the order of importance of the parts are obtained. For this purpose, a comparison scale that quantitatively evaluates the effects of parts on each other was created. Parts of the problem are compared in pairs and the effects of each part on the target are obtained quantitatively. AHP method can be used for measuring in both social and physical areas [18].

These pairwise comparisons are made using a verbal scale. Subsequently, these verbal comparisons are converted into proportional evaluations using a one-to-one matching method with a numerical scale. Although many numerical binary comparison scales have been proposed since the date when the AHP method was introduced [19] the most widely used scale today due to its simplicity and clarity is Saaty (1980) [20] also known as the "Basic Scale", the 1-9 linear scale.

Table 1. Saaty's comparison scale

Definition	Importance
Equal importance	1
Weak dominance	3
Strong dominance	5
Demonstrated dominance	7
Absolute dominance	9
Intermediate values	(2,4,6,8)

Saaty (1994) argues that it is the best scale representing weight ratios. However, while some scholars working in this field deal with objectively measurable alternatives, AHP treats decision processes as subjective issues. Salo and Hämäläinen [21], demonstrated the superiority of the balanced scale by comparing only two elements. Choosing the appropriate scale is a difficult and frequently discussed issue. Some scientists claim that the choice depends on the person and the decision problem [22]. However, there is no exact rule as to which scale is better for certain decision-making problems, types of alternatives, or criteria.

In this study, comparisons made with traditional and balanced scales were used in the application part and the weights of the scale, and by comparing the results, the weights of the scale giving more consistent results were used.

Table 2. Pairwise comparison decision matrix

Scale Name	Parameter (x)	Mathematical Description	Approximate Scale Value
Traditional AHP-linear (Saaty 1980)	$\{1,2,...,9\}$	x	1; 2;3; 4; 5; 6;7;8; 9
Balanced (Salo and Hämäläinen, 1997)	$\{0.5,0.55,...,0.9\}$	$\frac{x}{(1-x)}$	1;1.22;1.5;1.86; 2.33;3;4;5.67;9

With the numerical values obtained as a result of binary comparisons, a square matrix called the "Binary Comparison Matrix" (BCM) is created. These numerical values in BCMs are used to calculate the local importance (weight) of all the compared elements within their groups.

With the number of variables to be evaluated, the binary comparison matrix is formed as shown below;

$$A = (a_{ij}) = \begin{bmatrix} a_{11} & a_{12} & \cdots & a_{1n} \\ a_{21} & a_{22} & \cdots & a_{2n} \\ \vdots & \vdots & \ddots & \vdots \\ a_{n1} & \cdots & \cdots & a_{nn} \end{bmatrix}, \quad \begin{matrix} i, j = 1, \ldots, n \\ a_{ij} > 0 \end{matrix}$$

If $a_{ij} = 1/a_{ji}$ and $a_{ii} = 1, a_{ij} = a_{ik}a_{kj}, i, j, k = 1,...,n,$ is equal, Matrix A is perfectly consistent if equality is achieved, inconsistent if not [8].

Their local weights are the cornerstone of the mathematics behind the AHP method; otherwise, sorting would not be possible. The most common methods used to calculate these values are the Eigenvalue Method and the Logarithmic Least Squares (also known as the Row Geometric Mean) Method. When the matrices are consistent, each method calculates the same priorities. After determining the local weights, the consistency of the decision maker's evaluations is evaluated for all (or at least doubtful) BCMs. The most widely known evaluation method is the Eigenvalue Method; the second most widely known method is the Geometric Consistency Index. Due to its nature, AHP contains a certain degree of inconsistency. A consistency value of up to 0.10 in the consistency ratio (CR) is acceptable. A CR value greater than 10% indicates that the decision maker should review its decisions [5].

2.3. DEA and AHP integrated models

By using the data envelopment analysis method, quantitative inputs and outputs are used to evaluate the effectiveness of decision-making units. Since the inputs and outputs determined for use in the analysis are not always equally important, instead of giving equal weight to the variables, it is extremely important to determine their advantages over each other [23]. In this case, the AHP method was used for weighting between inputs used by DMUs and between hemp of outputs produced with them. The Data Envelopment Analytical Hierarchy Process integrated method created in this way was first proposed by Ramanathan [24].

The constraint to be created for the weight-constrained data envelopment analysis is to use the analytical hierarchy process method and provide it with the weights obtained by including expert opinion in the analysis. The matrix of binary comparisons to be used in this constraint and its mathematical representation are as follows;

$$A = \begin{bmatrix} a_{11} & \cdots & a_{1s} \\ \vdots & \ddots & \vdots \\ a_{s1} & \cdots & a_{ss} \end{bmatrix}$$

If the AHP binary comparisons matrix created for the entries is A, the weight constraints of the inputs are as follows:

$$\frac{u_1}{u_2} \geq a_{12} \rightarrow u_1 \geq a_{12}u_2 \rightarrow u_1 - a_{12}u_2 \geq 0,$$

$$\vdots$$

$$\frac{u_{s-1}}{u_s} \geq a_{(s-1)s} \rightarrow u_{s-1} \geq a_{(s-1)s}u_s \rightarrow u_{s-1} - a_{(s-1)s}u_s \geq 0.$$

$$B = \begin{bmatrix} b_{11} & \cdots & b_{1m} \\ \vdots & \ddots & \vdots \\ b_{m1} & \cdots & b_{mm} \end{bmatrix}$$

If matrix B is the AHP binary comparisons matrix created for the outputs, the weighting restrictions for the outputs are as follows:

$$\frac{v_1}{v_2} \geq b_{12} \rightarrow v_1 \geq b_{12}v_2 \rightarrow v_1 - b_{12}v_2 \geq 0,$$

$$\vdots$$

$$\frac{v_{m-1}}{v_m} \geq b_{(m-1)m} \rightarrow v_{m-1} \geq b_{(m-1)m}v_m \rightarrow v_{m-1} - b_{(m-1)}v_m \geq 0.$$

By writing these inequalities in accordance with linear programming, the problem can be solved with simplex or similar algorithms [9].

The application stages for DEAHP method applied in this study are shown in Figure 1.

3. Evaluation of financial activities of 27 firms operating in the food sector in Kosovo

3.1. Purpose of the study

The food industry is one of the most important sectors for Kosovo's economy and most of the products in this sector are produced as domestic products. After the last war in Kosovo, the economic situation has caused damage to the food sector. One of the most important problems facing the food sector in Kosovo today is the lack of technology to increase the food and production capacity and the lack of appropriate marketing strategy that will affect the business plan due to insufficient funds. In recent years, new investment opportunities have emerged, and these investments have enabled the production of products such as milk and dairy products, fruits and vegetables, and cereals with new technology.

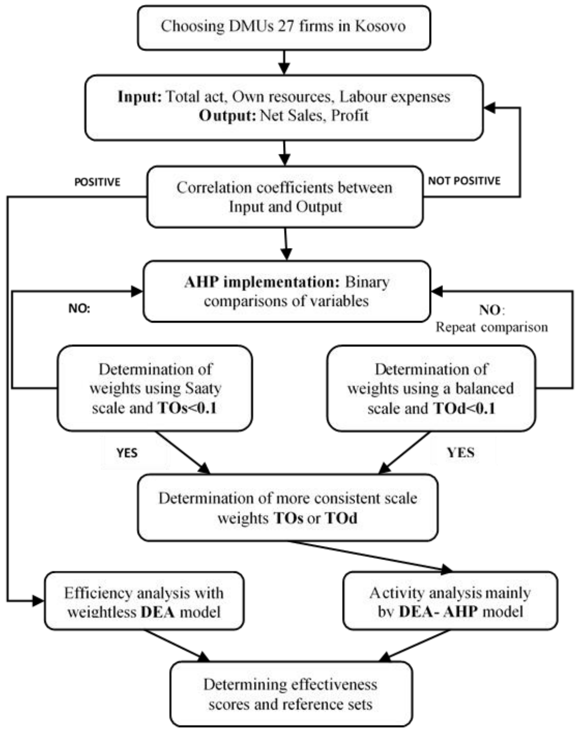

Figure 1. DEAHP method algorithm flow chart

It is thought that this study can shed light on the limited number of studies on the efficiency of the food sector in Kosovo, and also in order to increase food production companies, production and food sales and efficiency.

In this study, the financial efficiency of companies operating in the Kosovo food sector was measured by using DEA and DEAHP methods. The purpose of choosing this method is to ensure that the opinions of experts in their fields are included in the analysis while determining the financial efficiency of the companies, and at the same time to obtain healthier results. 27 companies active in this sector were included in the study. Within the scope of the study, the model and application stages in which DEA and AHP methods are used in an integrated manner are briefly explained.

3.2. Selection of DMUs

Taking into account the conditions of homogeneity of decision-making units and having the same inputs and outputs, 27 companies operating in the Kosovo food sector, with access to the balance sheet and income statement data from the Ministry of Economy and Finance, were selected as DMU.

3.3. Establishing input and output variables in DMUs

In data envelopment analysis, since different input and output groups will take different efficiency values for the same decision unit, it is necessary to determine causally related and meaningful input-outputs to the production process. For this reason, taking into account the ratios of their financial structures while conducting productivity analysis based on the financial performance of companies operating in the food sector the input and output variables of the model were determined as in Table 3.

Table 3. Input and output variables

INPUTS	OUTPUTS
Own Resources	Net Sales
Active Total	Profit
Labour Expenses	

The data of these input and output variables have been obtained from the balance sheet tables on the official website of the Ministry of Finance. Before conducting the efficiency analysis, the correlation coefficients between input and output variables will be examined first. If all the coefficients are positive and strong, the analysis phase will start.

Table 4. Correlation analysis results between ınput and output variables

	Own Resources	Active Total	Labour Excpenses	Net Sales	Profit
Own Resources	1.00				
Active Total	0.76	1.00			
Labour Excpenses	0.58	0.92	1.00		
Net Sales	0.64	0.75	0.85	1.00	
Profit	0.85	0.48	0.45	0.45	1.00

When Table 4 is examined, it is seen that there is a positive correlation between input variables and output variables. This shows that an increase in any input variable will provide an increase on the output variable. There should be no negative correlation between input and output variables.

3.4. Determining relative weights of input and output variables: application of AHP method

With the AHP method, the weights of input and output variables are determined in this section. To determine these weights, a “Financial Performance Efficiency Analysis Survey of Companies in the Food Sector” and dual criteria comparisons have been prepared. The questionnaire form prepared was done by the face-to-face interview method with the economists of the companies operating in Kosovo and included in the study. The interview was conducted with four experts, and the weight of each variable was calculated with the Expert Choice package program according to their answers to the questionnaires.

Here, the comparisons made using the traditional and balanced scale values proposed by Saaty and the weights obtained by taking their geometric averages are shown below. The experts participating in the questionnaire could not determine their opinion only according to the Saaty scale, it was calculated by making the necessary changes to the balanced scale. Table 5 shows the percentage importance values, ranks and CR values obtained by using both scales of the input variables, calculated based on the pairwise comparison matrices. One of the important criteria that AHP takes into account is CR. As stated at the beginning, it was stated that this ratio was smaller than 0.10, which was sufficient for the validity of the pairwise comparison. In a study, he interpreted the performance of the scales using many scales and several performance measurement methods [25]. Measured Scale Lower CR, one of the scale performance measurement methods used: This performance measure represents the percentage of trials that have lower CR values when generated by measured scale rather than fundamental scale. According to the CR values in Table 5, we can say that Balalanced scala results have better performance.

Table 5. Input weights obtained with two scales

Input variable	Weights and rank			
	Saaty scale	Rank	Balanced scale	Rank
Own Resources	0.498	1	0.418	1
Active Total	0.187	3	0.252	3
Labour Expenses	0.315	2	0.330	2
Consistency Ratio	***0.0025***		***0.0005***	

- According to the Saaty scale, when the average percentage weights of the input variables are examined, among the input variables, “Own Resources” are in the first place with an importance value of 49.8%, “Labour Expenses” take second place and “Active Total” take the last place.
- According to the balanced scale, when the average percentage weights of input variables are analyzed, “Own Resources” is again in the first place with a 41.8% significance value.

In addition, the closeness of the priority vectors obtained with both scales according to the Saaty compatibility index was examined.

Even when vectors are not identical, they can sometimes be considered close to each other. According to Saaty (2005), “when two vectors are close, we say they are compatible”. The Saaty Compatibility Index, S, was the first developed measure of compatibility between priority vectors. This index uses the concept of the Hadamard Product, the element-wise product of two matrices [26].

The Saaty Compatibility Index, S, between vectors $\boldsymbol{x}$ and $\boldsymbol{y}$ is obtained with Equation. $S = (1/n^2)e^T A \bullet B^T$ e where n is the number of elements of the vectors, $\boldsymbol{e}$ is a column-matrix with all elements equal to 1, $a_{ij} = x_i/x_j$, $b_{ij} = y_i/y_j$ and $\bullet$ is the Hadamard Product operator [27].

One desirable property of a consistency index is that it should indicate that a vector is completely compatible with itself. For identical vectors, $S=1$. If $S \leq 1.1$, the two vectors are said to be consistent; otherwise, not.

Table 5 has two priority vectors obtained for the criteria using the Saaty and balanced scale. The corresponding elements of vectors 1 and 2 appear close to each other based on a cursory examination of their differences. So S = 1.037 for Vector 1 and 2 indicates that they are indeed compatible.

According to the percentage weights of the input variables according to both scales, the rankings or rankings of importance are the same. The slight variation in the weight distribution according to the scale is due to the inconsistency rates accumulated in the pairwise comparisons. Pairwise comparison matrices with a balanced scale had higher consistency sensitivity and significantly reduced the weight ratios of the criteria. For example, the relative ratio of "Own Resources" and "Active Total" input criteria obtained by using the Saaty scale is found as (0.498/0.187) = 2.66, while with the balanced scale (0.418/0.252) =1.66. Although the absolute differences in weight ratios are small and the ranks are the same as expected, the AHP method takes into account relative ratios, such that the above comparison illustrates one of the situations where significantly different results can occur when using different scales [28].

As stated in this study, since consistency sensitivity will be taken into consideration, input weights obtained with a balanced scale were used to be used in the next steps.

The operations performed to obtain the weights of the input variable are also performed for the output variable and the weights are determined. Since there are only two variables here, there is no inconsistency, so little difference is observed in the comparisons made with two scales.

Table 6. Output weights obtained with two scales

Output variable	Weights and Rank			
	Saaty scale	Rank	Balanced scale	Rank
Net Sales	0.362	2	0.431	2
Profit	0.638	1	0.569	1

When the average percentage weights of the output variables required for the second analysis are examined, among the output variables, "profit" is more important than the "net sales" variable with an importance value of 63%.

The weight of each variable was calculated using the expert choice package program in line with the answers given by the financial experts. Variable weights were calculated using the geometric mean method in solving the eigenvalue of the binary comparison matrix.

The matrix of geometric means of four expert opinions for input and output variables is given below. Based on this, it is given below to be used when analyzing the financial performance efficiency with the DEA weighted method in the next steps.

A pairwise comparison matrix is adapted according to the Saaty scale values.

Inputs	v_1	v_2	v_3
v_1	1.00	2.66	1.58
v_2	0.38	1.00	0.59
v_3	0.63	1.68	1.00

Outputs	u_1	u_2
u_1	1.00	0.57
u_2	1.76	1.00

$\frac{v_1}{v_2} \geq 2.66 \Rightarrow v_1 - 2.66v_2 \geq 0$, $\frac{u_1}{u_2} \geq 0.57 \Rightarrow u_1 - 0.57u_2 \geq 0$.

$\frac{v_1}{v_3} \geq 1.58 \Rightarrow v_2 - 1.58v_3 \geq 0$,

$\frac{v_2}{v_3} \geq 0.59 \Rightarrow v_2 - 0.59v_3 \geq 0$,

A pairwise comparison matrix is adapted according to the Balanced scale values.

Inputs	v_1	v_2	v_3
v_1	1.00	1.66	1.27
v_2	0.60	1.00	0.76
v_3	0.79	1.31	1.00

Outputs	u_1	u_2
u_1	1.00	0.76
u_2	1.32	1.00

$\frac{v_1}{v_2} \geq 1.66 \Rightarrow v_1 - 1.66v_2 \geq 0$, $\frac{u_1}{u_2} \geq 0.76 \Rightarrow u_1 - 0.76u_2 \geq 0$.

$\frac{v_1}{v_3} \geq 1.27 \Rightarrow v_1 - 1.27v_3 \geq 0$,

$\frac{v_2}{v_3} \geq 0.76 \Rightarrow v_2 - 0.76v_3 \geq 0$,

The constraints obtained will be included in the DEA models to be calculated and the weighted DEAHP model will be re-run with the EMS V1.3 program developed by Holger Scheel [29].

3.5. Efficiency analysis with DEA and DEAHP

The purpose of the model for input from DEA models is to investigate the most appropriate input combination. Since the main purpose of this study is to determine how much decrease (increase) should be made in the amount of input in order to improve the efficiency of ineffective firms, the input-repetitive DEA model was used under the assumption of constant return to scale. EMS V1.3 (Efficiency Measurement System) package program was used for efficiency analysis.

DEA analysis is made with the data obtained from the accessible Balance Sheet tables. Here, DMUs will form the companies in question and the naming will be DMU. The input variables are the finance data Own Resources, Active Total, Labour Excpenses and output variables Net Sales, Profit.

Table 7. Efficiency scores and reference groups

Firms	**DEA** %ES	**Reference Groups** *Benchmarks*	**DEAHP %ES**	**Reference Groups** *Benchmarks*
DMU1	64.45%	6 (2.37) 16 (0.18) 20 (0.99)	46.67%	6 (3.94)
DMU2	61.73%	6 (2.79) 7 (0.91)	41.47%	20 (2.70)
DMU3	20.57%	6 (0.06) 7 (0.11)	11.35%	20 (0.12)
DMU4	19.86%	6 (0.08) 7 (0.09)	12.00%	20 (0.12)
DMU5	99.72%	6 (0.94) 16 (0.00) 20 (0.17)	98.74%	6 (0.93) 20 (0.18)
DMU6	**100.00**	**13**	**100.00%**	**16**
DMU7	**100.00**	**6**	63.64%	6 (0.22) 20 (0.51)
DMU8	90.87%	6 (0.18) 7 (0.57) 23 (0.04)	58.96%	6 (0.30) 20 (0.32)
DMU9	53.66%	6 (0.09) 7 (0.15)	22.58%	6 (0.13) 20 (0.08)
DMU10	67.50%	6 (0.21) 11 (0.04)	28.86%	6 (0.22)
DMU11	**100.00**	**4**	45.82%	6 (0.32)
DMU12	63.97%	6 (0.38) 7 (0.04)	33.45%	20 (0.31)
DMU13	86.34%	11(1.01) 16 (1.36)	51.12%	6 (4.05)
DMU14	91.94%	11(0.79) 16 (1.15)	53.59%	6 (3.39)
DMU15	91.75%	6 (0.02) 11 (0.16) 16 (1.10)	56.63%	6 (3.08)
DMU16	**100.00**	**12**	62.99%	6 (2.74)
DMU17	64.66%	16(0.22) 20 (0.98)	47.74%	6 (1.55)
DMU18	55.79%	16(0.15) 20 (0.63)	35.34%	6 (0.15) 20 (0.65)
DMU19	73.00%	16(0.14) 20 (0.53)	41.48%	6 (0.10) 20 (0.57)
DMU20	**100.00**	**10**	**100.00%**	**16**
DMU21	88.07%	6 (0.37) 20 (0.47)	79.75%	20 (0.74)
DMU22	94.85%	6 (0.83) 20 (0.06)	83.54%	20 (0.68)
DMU23	**100.00**	**1**	73.49%	20 (0.61)
DMU24	33.40%	16(0.32) 20 (1.28)	20.16%	20 (1.55)
DMU25	33.93%	16(0.42) 20 (1.34)	19.18%	20 (1.69)
DMU26	59.53%	6 (3.63) 16 (0.52)	36.75%	6 (3.92)
DMU27	30.03%	16(0.10) 20 (1.56)	25.89%	6 (0.39) 20 (1.36)

The model was run as input-oriented in the EMS program; The scale is based on fixed returns to scale. Efficiency analysis results of the DEA method and DEAHP methods are comparatively given in Table 7.

Table 7. shows the efficiency measurement results of the DEA method and DEAHP methods comparatively consisting of five columns. For firms that are decision units in the first column, efficiency scores (% ES) and "Benchmarks" reference groups are included in the second and third columns as percentages of DEA method. The fourth and fifth columns contain efficiency scores and reference groups of DEAHP method. Firms with a 100% ES value are effective, while those with an ES value below 100% are ineffective. In the "Benchmarks" column, there are reference groups of inactive companies (referenced companies) and information showing the number of times that active companies are referenced by inactive companies. As can be seen from Table 7, 4 out of 6 companies found effective in the analysis made with DEA method were not found to be 100% effective in the analysis made with DEAHP method. However, it is seen that efficiency scores decrease with the addition of weights. Here, instead of giving equal weight to input and output variables, including the weights of these variables in the analysis with the help of AHP method provides us to reach healthier and more reliable results.

The steps to be taken for the ineffective companies, examined in this study, to become effective are shown below with an example. Here, the results obtained with the DEAHP method will be used as it performs a more sensitive analysis. DMU6 is the most important company in the reference group that the companies below the activity limit will take samples to be fully effective. The firm with the lowest efficiency score is DMU3 with an efficiency score of 11.35%. In this input-oriented method, while keeping the output level constant, the input amount is aimed to be optimum and it is determined how much the inputs should be reduced for the ineffective DMU to be effective. The target value can be found by using the percentages in the "Benchmarks" column for the improvements (reductions) of DMU27 in its inputs.

The target value is calculated as follows:

$$DMU27_i = (0.39 \times DMU6_i) + (1.36 \times DMU20_i)$$

$DMU27_i$: DMU1' Target value for the *i'* th input

$DMU6_i$: DMU6' Current value for the *i*'th input

$DMU20_i$: DMU20 Present value of the *i*'th input

0.39 : DMU6'weight

1.36 : DMU20'weight

$$DMU27_1 = (0.39 \times 4712000) + (1.36 \times 201000) = 2111040$$

As a result, the DMU27 firm has to make a 55% reduction in order to reach the target value of 2111040 calculated euro of 4712000 euro, which is the current value of the first input "own resources". In this way, the ineffective DMU will be transformed into active as a result of the improvements to be made.

Using the values in the "Benchmarks" column of other inactive decision units, calculations can be made similarly, and the target values and improvement rates of decision units can be determined.

4. Conclusion

In this work, DEA has been conducted by taking into account the relative activities of 27 companies operating in the food sector in Kosovo. DEA was made with 3 inputs and 2 outputs in the study. The input variables are the financial data: own resources, active total, labour expenses, and output variables. For the analysis, the EMS 1.3.0 package program, one of

DEA's specialized software tools, was used.First, the efficiency of the firms according to the CCR model for input was found, and their efficiency averages were also examined. Later, weights were assigned to input and output variables with the help of the analytic hierarchy process method, and efficiency analysis was repeated with data envelopment and the analytic hierarchy process integrated method. In addition, the *Balanced scale,* which is thought to reduce the inconsistencies caused by the *Saaty scale* used for AHP pairwise comparison, was included in the study. In this way, no other study was found in the food industry using different scales in the DEAHP integrated method.In the last stage, the targets that should be achieved by ineffective companies to improve their productivity have been determined.

As a result of the efficiency measurement with data envelopment analysis, 6 companies were found effective, while the efficiency scores of the other 21 companies were found to be below 100%. In the analysis made with the DEAHP method, weights were assigned to the input and output variables with the pairwise comparison matrices obtained with the help of the opinions of four statisticians, using the more consistent balanced scale, and the efficiency analysis was repeated.

As a result of the analysis, it was seen that the efficiency scores of DMU7, DMU11, DMU16 and DMU23 companies, which are effective with the DEA method, decreased by 63.64%, 45.82%, 62.99% and 73.49%, respectively, and it was determined that only DMU6 and DMU20 companies were effective. In other words, while the average efficiency score was 72% according to DEA results, this score decreased to 50% according to DEAHP results. The reason for this is that most of the data belonging to the input variables are not taken into account under the DEA method, which invites incomplete conclusions from sensitivity and incomplete interpretations of these results. This means that weighted DEAHP methods take into account the values of all input and output variables without loss, and performing the analysis in this way reduces the margin of error in producing more accurate results.

As a result, it is recommended that active companies continue to maintain their activities and that inactive companies determine the best input amounts, ie target values, by taking reference companies as a result of the analyzes made with the DEAHP method and making improvements in this direction.

Repeating these efficiency analyses not only once but regularly, finding target values and conducting studies on this subject will contribute to the improvement of the financial efficiency of companies. In addition, in future research, we are considering combining this work with other decision making methods such as DEA and fuzzy AHP, analytical network process (ANP). We will also compare the results found in this paper.

Acknowledgments

I would like to express my sincere thanks to my dear advisor Prof. Dr. Necati Özdemir for his guidance throughout this study.

References

[1] Ulucan, A. (2002). Data Envelopment Analysis Approach in Effieiency Measurement of ISO500 Companies: Evaluations Using Different Input Output Components and Different Returns to Scale. *Ankara University SBF Journal,* 57(2), 185-202.

[2] Oruc, K. O. (2008). Efficiency measurements in fuzzy environment by using data envelopment analysis and an application at universities. *Süleyman Demirel University, Doctoral dissertation.*

[3] Ozden, U. H. (2008). Efficiency evaluation of foundation universities in Turkey by using Data Envelopment Analysis (DEA), *Istanbul University Journal of the School of Business Administration,* 37(2), 167-185.

[4] Sinuany-Stern, Z., Mehrez, A., Hadad, Y. (2000). An AHP/DEA methodology for ranking decision making units, *International Transactions in Operational Research,* 2(7), 109-124.

[5] Lee, S. K., Mogi, G., Shin, S. C., Kim, J. W. (2007). An AHP/DEA integrated model for measuring the relative efficiency of energy efficiency technologies. In *IEEE International Conference on Industrial Engineering and Engineering Management*.

[6] Korpela, J., Lehmusvaara, A., Nisonen, J. (2007). Warehouse operator selection by combining AHP and DEA methodologies. *International Journal of Production Economics,* 108(1-2), 135-142.

[7] Sevkli, M., Koh, S. L., Zaim, S., Demirbag, M., Tatoglu, E. (2008). Hybrid analytical hierarchy process model for supplier selection. *Industrial Management & Data Systems,* 1(108), 122-142.

[8] Wang, Y. M., Liu, J., Elhag, T. M. (2008). An integrated AHP–DEA methodology for bridge risk assessment. *Computers & Industrial Engineering,* 54(3), 513-525.

[9] Erpolat, S., Cinemre, N. (2011). Notebook selection in a hybrid approach: data envelopment analysis based on analytic hierarchy process. *Istanbul University Journal of the School of Business Administration,* 40(2), 207-225.

[10] Lin, M. I., Lee, Y. D., Ho T. N.(2011). Applying integrated DEA/AHP to evaluate the economic performance of local governments in China. *European Journal of Operational Research*. 209(2), 129-140.

[11] Keskin, B., Ulas, E. (2017). Does privatization affect airports performance? A comparative analysis with AHP-TOPSIS and DEA. *New Trends in Finance and Accounting. Springer,* 335-345.

[12] Çetin, K., Tuzkaya, G., Vayvay, O. (2020). A mathematical model for personnel task assignment problem and an application for banking sector. *An*

International Journal of Optimization and Control: Theories & Applications (IJOCTA), 10(2), 147-158.

[13] Pradhan, S., Olfati, M. and Gokulananda, P. (2019). Integrations and applications of Analytic Hierarchy Process with Data Envelopment Analysis- a literature review. *International Journal of the Analytic Hierarchy Process.* 11(2), 228-268.

[14] Banker, R. D. Cooper, W. W., Seiford, L. M., Thrall, R. M., Zhu, J. (2004). Returns to scale in different DEA models. *European Journal of Operational Research*, 154(2), 345-362.

[15] Kocakoç, I.D. (2003). Veri zarflama analizi'ndeki ağırlık kısıtlamalarının belirlenmesinde analitik hiyerarşi sürecinin kullanımı, *Dokuz Eylul Unıversıty Faculty of Economıcs And Admınıstratıve Scıences Journal,* 18(2).

[16] Charnes, A., Cooper, W. W., Rhodes E. (1987). Measuring the efficiency of decision making units. *European Journal of Operational Research,* 2(6), 429-444.

[17] Cooper, W. W., Seiford, M. L. and Zhu, J. (2004). Handbook on Data Envelopment Analysis. Kluwer Academic Publishers, 1-39.

[18] Ozdemir, Y., Alcan, P., Basligil, H., Cakrak, D. (2018). A hybrid QFD-AHP methodology and an application for heating systems in Turkey. *An International Journal of Optimization and Control: Theories & Applications (IJOCTA)*, 8(1), 117-126.

[19] Lootsma, F.A. (1988). Numerical scaling of human judgement in pairwise-comparison methods for fuzzy multi-criteria decision analysis. *In Mathematical models for decision support. Springer*, F48, 57-88.

[20] Saaty, T. L. (1980). The analytic hierarchy process. *McGraw-Hill, New York,* 1-72.

[21] Salo, A. A., Hämäläinen, R. P. (1997). On the measurement of preferences in the analytic hierarchy process. *Journal of Multi-Criteria Decision Analysis,* 6(6), 309-319.

[22] Harker, P., Vargas, L. (1987). The Theory of Ratio Scale Estimation: Saaty's Analytic Hierarchy Process. *Management Science*, 33(11), 1383-1403.

[23] Doğan, N. Ö., Gencan, S. (2014). Performance assessment using DEA/AHP integrated method: an application on public hospitals in Ankara. *Gazi University Journal of Faculty of Economics and Administrative Sciences,* 16(2), 88-112.

[24] Ramanathan, R. (2006). Data envelopment analysis for weight derivation and aggregation in the analytic hierarchy process. *Computers & Operations Research*, 5(33), 307.

[25] Yıldırım, B. C. (2019). A New pairwise comparison scale for analytic hierarchy pprocess. *Master's thesis of Social Sciences of Middle East Technical University*.

[26] Garuti, C., & Salomon, V. A. (2012). Compatibility indices between priority vectors. *International Journal of the Analytic Hierarchy Process*, 4(2), 152-160.

[27] Saaty, T. L., Peniwati, K. (2013). Group decision-making: Drawing out and reconciling differences. Pittsburgh: PA: RWS Publications.

[28] B. Srdjevic, (2005). Combining Different Prioritization Methods in The Analytic Hierarchy Process Synthesis. *Computers & Operations Research*, 32, 1897-1919.

[29] Scheel, H. Efficiency Measurement System (Ems). Holger Scheel's Dea Page, [Online]. Available: http://www.wiso.uni-dortmund.de/lsfg/or/scheel/ems/. [Accessed 15 09 2019].

Esma Canhasi Kasemi *was born in Kosovo (Prizren) in 1985. She graduated from Gjon Bozuku High School and received her BSc, MSc from Mimar Sinan University and PhD from Balikesir University in the Department of Mathematics. She is now working in Faculty of Education, University of Prizren, Kosovo as a Research Assistant. Her research areas are optimization and operations research, evaluation of investments, multi criteria decision making.*

http://orcid.org/0000-0001-6885-6057

An International Journal of Optimization and Control: Theories & Applications
ISSN:2146-0957 eISSN:2146-5703
Vol.12, No.2, pp.137-150 (2022)
http://doi.org/10.11121/ijocta.2022.1208

RESEARCH ARTICLE

Uncertainty-based Gompertz growth model for tumor population and its numerical analysis

Aadil Rashid Sheergojri[a], Pervaiz Iqbal[a], Praveen Agarwal[b,c,d*], Necati Ozdemir[e]

[a] *Department of Mathematics and Actuarial Science, B. S.Abdur Rahman Crescent Institute of Science and Technology, Chennai, India*
[b] *Department of Mathematics, Anand International College of Engineering, Jaipur, India*
[c] *Nonlinear Dynamics Research Center (NDRC), Ajman University, Ajman, United Arab Emirates*
[d] *Department of Mathematics, International Center for Basic and Applied Sciences, Jaipur, India*
[e] *Department of Mathematics Balıkesir University, Turkey*
aadilrashid1996@gmail.com, pervaizmaths@gmail.com, goyal.praveen2011@gmail.com, nozdemir@balikesir.edu.tr

ARTICLE INFO

Article History:
Received 20 December 2021
Accepted 19 January 2022
Available 14 July 2022

Keywords:
Tumor growth modeling
Fuzzy sets
Gompertz model
Possibility distribution function

AMS Classification 2010:
93A30; 03E72

ABSTRACT

For treating cancer, tumor growth models have shown to be a valuable resource, whether they are used to develop therapeutic methods paired with process control or to simulate and evaluate treatment processes. In addition, a fuzzy mathematical model is a tool for monitoring the influences of various elements and creating behavioral assessments. It has been designed to decrease the ambiguity of model parameters to obtain a reliable mathematical tumor development model by employing fuzzy logic.The tumor Gompertz equation is shown in an imprecise environment in this study. It considers the whole cancer cell population to be vague at any given time, with the possibility distribution function determined by the initial tumor cell population, tumor net population rate, and carrying capacity of the tumor. Moreover, this work provides information on the expected tumor cell population in the maximum period. This study examines fuzzy tumor growth modeling insights based on fuzziness to reduce tumor uncertainty and achieve a degree of realism. Finally, numerical simulations are utilized to show the significant conclusions of the proposed study.

1. Introduction

A disease caused by an abnormal proliferation of cells due to unregulated cell proliferation is called cancer. Cancer is becoming increasingly common and has reached alarming levels [1]. To put it another way, cancer is not just an isolated population of mutated cells. Still, it is part of a larger tissue population that actively interacts with and disrupts a varied community of various cellular and micro-environmental interacting components that seek to maintain homeostasis [2]. Mathematical modeling of cellular mechanisms is frequently utilized to improve numeric knowledge of clinical events. This empirical evidence may be used in both experimental and clinical contexts. Tumor research is one significant field where modeling techniques are used [3]. When the system is unclear, fuzzy mathematics provides an outlet for bio-mathematical issues such as cancer to reach a realistic solution and a better and more exciting knowledge of a particular phenomenon [4, 5].

Zadeh introduced fuzzy sets in 1965 to deal with data having non-statistical uncertainty. The actual circumstances are frequently vague or ambiguous in many situations. Due to a lack of understanding, the future status of the network may not be fully known. Probability and statistics have long been used to address this sort of complexity (stochastic nature). Imprecision refers to

*Corresponding Author

uncertainty rather than a lack of knowledge about the parameter's value. A fuzzy set theory is a structured mathematical framework that allows for the precise and rigorous study of vague cognitive representations.Fuzziness may be noticed in many sectors of daily life, including engineering, medicine, metallurgy, astronomy, and so on. However, it is widespread in all areas where human judgment, evaluation, and decision-making are crucial, such as decision-making, thinking, reasoning, and so on [1, 6, 8, 17].

Uncertainty is prevalent in nearly all scientific disciplines, with a specific focus on biological phenomena, wherein complicated elements such as inheritance, habitat, availability, and so on affect the traits and development. This feature has prompted several recent contributions to develop mathematical models that integrate ambiguity to understand evolutionary processes using differential equations.The traditional perspective of uncertainty has been transformed, and the usual view regards uncertainty as undesirable in research efforts and must be eradicated by all feasible measures. The contemporary viewpoint accepts ambiguity and thinks that science should solve it [9–12]. Possibility theory focuses on ambiguity inherent in natural languages and is "possibilistic" rather than probabilistic. As a result, the term variable is employed in a broader scientific context than in a strictly mathematical context.

As shown in the prolongation, the mathematical structure of fuzzy set theory generates a suitable concept of possibility, giving a characteristic similar to that of measure theory regarding probability theory.An ambiguous restriction is an allocation of possibilities, with its membership function serving as a distribution function of possibilities, and a fuzzy attribute is affiliated with an allocation of possibilities in the same way that a probability distribution is attributed with a random variable suggested by Zadeh in this outlook [13]. Assume that the tumor cell population $n_0$is described in the sense of tumor population dynamics by a fuzzy set n_{01} with membership function$\mu_{n_{01}}(N)$.As a result, for any precise value $N = z_0$, the value $\mu_{n_{01}}(z_0)$represents the rate of probability that the dynamical system'sactual initial state of tumor takes the value z_0 given that the initial cell count of the tumor is precisely n_0. The membership function $\mu_{n_{01}}(N)$ is then the probability distribution associated with the initial state of the tumor. A detailed explanation of the condition of tumor cell number at a specified time $t > 0$ will not be required until we have accurate knowledge about the actual value of the initial tumor status. It is essential to explain a tumor's starting state using a fuzzy constraint since the initial condition is about z_0. In turn, this determines the distribution of possibilities to the outcomes expected by the initial condition.

The extended version of the fuzzy polynomial is the fuzzy equation. Since the ambiguities are explicit undefined parameters of the fuzzy equations, the fuzzy equations are more accessible to apply than regular fuzzy systems. These characteristics, on the other hand, are challenging to get.There are numerous methods for creating fuzzy equations, e.g.,crisp linear systems, extension principle, homotypic analysis, Newton's technique, fixed point methodology, α-level methods, and superimposition of sets. More recently, fuzzy fractional differential and integral equations, which may be used to solve fuzzy numbers, have been intensively investigated [14–19]. Various approaches have been proposed to comprehend the fuzzy uncertainty of differential equations. Some authors employ delay differential equations and Hukuhara–derivatives to create answers to fuzzy uncertainty. To forecast cell proliferation and tumor development models, the idea of fuzzy differential inclusion has been applied. The generalized Seikkala differentiability approach and the Zadeh extension rule are used to determine deterministic solutions in another attempt to solve fuzzy differential equations [20–27].

This study discusses the influence of fuzzy uncertainty in the Gompertz growth equation, which is used in a variety of fields, including statistical mechanics, medicine (tumor growth rate), chemistry (response models), and ecology (population growth) [28, 29]. The Gompertz model, probably second only to the logistic model, is amongst the most widely utilized sigmoid models for fitting growth data and other data. The Gompertz equation was initially designed for actuarial analysis, but it was eventually adopted as a growth curve. According to the literature, the Gompertz model has been used for many phenomena, including plant, bird, fish, and other animal development and tumor and bacterial growth. The Gompertz model is a particular instance of the four-parameter Richards model, and therefore belongs to the Richards family of three-parameter sigmoidal growth models, among famous models like the negative exponential, logistic, and von Bertalanffy. The literature has several parametrizations and re-parameterizations of the Gompertz model. Still, no comprehensive study of them and their characteristics have been done, but the Gompertz model showed the probability density function [30, 31]. Here, we'll gradually clarify the variance in the possibility distribution function, and then we'll decide on the optimal choice of that fuzzy variable, which will result in distinct outcomes.

Uncertainties remain in ecological modeling and must be considered to improve model confidence. For example, it is sometimes impossible to precisely identify the exact cell count or the bearing capability in a specified person in the difficulties of tumor population dynamics. Since the beginning condition is about n_0 or the carrying potential is approximately K_0, verbal statements often obtain information. This may be treated as an uncertain system, with the mark almost ambiguous. These verbal assertions can alternatively be regarded as fuzzy limitations on the values followed by the output characteristic. Since the beginning of cancer research, finding models to predict tumor progression has been critical. Several techniques have been proposed; however, there is no consensus on how tumor cells grow. This is a significant problem since an accurate tumor development model is necessary to evaluate imaging techniques, enhance radiation therapy processes, and provide treatment recommendations for patients [32–34].

The primary purpose of this research is to construct a fuzzy mathematical model based on fuzzy set theory to describe tumor growth and the concept of the possibility distribution function. A similar framework on the initial state of the tumor and parameters utilized in probability theory to address fuzzy uncertainty has been established here. For deterministic outcomes, we may implement the Zadeh extension principle to the early stages of the tumor and its attributes and characterize fuzzy strategies by treating them as fuzzy variables in the possibility distribution function.Because of this, we need to know how many tumor cells are expected to be in each network structure to compute the overall impact of this fuzzy uncertainty.Calculating the desired level to the deterministic solution describes the predicted level of the initial state and parameters. In addition, the Gompertz growth model predicts the absolute growth rate using fuzzy numbers, which are described in the restricted assertions.This work reveals novel ideas and aims that might make the model more practical and suitable.The fuzzy approaches will also aid in the early detection of tumors, which will allow us to customize the medication to the tumor patient. Also, to support the created model,numerical simulation has been presented. The framework of the tumor growth model is depicted in Fig.1.

This paper is organized as follows. In section 2some preliminaries on fuzzy sets, fuzzy variables and their transformation required to determine the solution of the Gompertz model are addressed.Section 3 deals with the Gompertz model of tumor growth with the projected level of the fuzzy variable and its net population rate.Section 4 explains the tumor state at time $t > \ 0$ in an imprecise environment, and section 5 shows our significant findings with a numerical simulation. The significance of our findings is explored in section 6. The managerial insights are discussed in section 7, and the conclusion is presented in section 8.

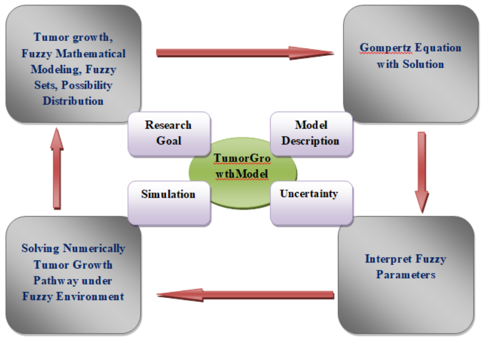

Figure 1. The framework of the tumor growth model.

2. Preliminaries for the proposed work

2.1. Fuzzy theory

Definition 1. *Let$X$ be a non-empty universal set, then a fuzzy set N is defined by a pair $(X,\ \mu_N(X))$ where, $\mu_N\,(X) : X \to [0, 1]$ for each $u \in X$, $\ \mu_N(X)$ is called the membership grade function of u defined in N.*

A fuzzy set N in X is defined by a membership function$f_N(u)$that correlates any real number in the interval [0, 1] with every point in X, to a value of $f_N(u)$ at u reflecting the membership degree of u in N. Also for any $\alpha \in [0,\ 1]$, the set of points of X where $X_\alpha = \{u \in X \mid \mu_N(u) \geq \alpha\}$ is known as an α-cut set or theα-level set of the fuzzy set $A$and the crisp set that contains all the items of X with nonzero membership grades in N is the support of a fuzzy set N within a universal set X. For $\alpha = 0$, the support of A is the same as the strong α-cut of N.

Now, let us represent the set of fuzzy subsets of $X \subset R$ by $F(X)$, where the α-cuts for each $\alpha \in [0,\ 1]$ are non-void, bounded, closed, and are simply connected. Here's how we may get the distance among two fuzzy sets $a, b \in F(X)$,

$$d_{\infty}(a,b) = \underset{\alpha\in[0,1]}{\operatorname{Sup}} \; d_p\left([a]^{\alpha},[b]^{\alpha}\right), \qquad (1)$$

where for compact sets$d_p$is the Hausdorff distance [5, 6, 22, 35, 36].

We also symbolize the characteristic function of the set M by $\chi\{M\}$.

Definition 2. *(Fuzzy variables) Fuzzy variables are more realistic than crisp variables because they reflect measurement uncertainty in experimental data. Data based on fuzzy variables offer us more accurate information regarding actual occurrences than data based on crisp variables, which is a fascinating contradiction. Albert Einstein well-articulated this crucial aspect in 1921 as in the following phrase: In terms of referring to reality, mathematical laws are unreliable. And, to the best of their knowledge, they do not refer to fact.*

The name fuzzy variable was chosen because it performs the same role in the current development as the random variable in probability theory. In contrast, we argue that this is a far better explanation for a fuzzy set on the real line [37], [38].

Now, on the value of a flexible rate, the possibility distribution function is produced by a fuzzy subset a of X, represented through the membership grade$\mu_a : X \to [0,\ 1]$. To put it another way, if $\varPsi$is a fuzzy variable, then $\mu_a(N)$ is the highest level to which the actual value N may go.However, $\mu_a(N) = 0$ means that the parameter $\varPsi$cannot conclude the value N in the sense of possibility theory. With assignment $\varPsi = N$, the amount $\mu_a(N)$ indicates the degree of possibility, where specific$N$ values are more likely than others. The nearest the value of $\mu_a(N)$ is 1, the more likely that N is the variable's actual value.

The possibility measure of M is determined by $Pos_{\mu} = Sup_{N\in M}\mu_{\alpha}(N)$, provided the subset $M \subset XNec_{\mu}(M) = 1 - Pos_{\mu}(M^c)$ where M^c stands for$M$ in X X complement set and by pointing out that $Pos_{\mu}(M)$ is a test of the possibility of assuming values in M by the fuzzy variable.It is easily verifiable that $Pos_{\mu}(\phi) = 0$ and $Pos_{\mu}(X) = 1$ [22], [35], [36].

In addition, based on the possibility and necessity measures, we provide a third index called the credibility measure, which is as follows:

$$Cr_{\mu}(M) = \frac{1}{2}\left(Pos_{\mu}(M) + Nec_{\mu}(M)\right) \qquad (2)$$

To obtain a typical representation of a fuzzy variable $\varPsi$ on the credibility space, it is necessary to establish the definition of its probable or the expected value, which can be labeled as $E[\varPsi] = \int_0^{+\infty} Cr_{\mu}\{\varPsi \geq r\}\,dr - \int_{-\infty}^{0} Cr\{\varPsi \leq r\}\,dr$, the expected value is not specified for any real number r,if the right-hand side of this equation is of nature $(\infty - \infty)$, that is at least one of the two integrals must be finite.It is noted that the concept of $Pos\,(M),\quad Nec(M)\ and\ Cr(M)$of the fuzzy variable $\varPsi$ relies on the possibility distribution function μ_a.

Suppose a random variable replaces a fuzzy variable $\varPsi$ and the probability measure Pr replaces Cr, then we have

$$\int_0^{+\infty} Pr_{\mu}\{\varPsi \geq r\}\,dr - \int_{-\infty}^{0} Pr\{\varPsi \leq r\}\,dr = \int_{-\infty}^{+\infty} N\varphi(N)\,dN,$$

this is identically the anticipated random variable value, suggesting that the description of the expected return of a fuzzy vector is equivalent to the description of the expected return of a random vector.

Now, if we specify the quantities $\varPsi'_{\alpha} = inf\{N : \mu_a(N) \geq \alpha\}$ and $\varPsi''_{\alpha} = \{N : \mu_a(N) \geq \alpha\}\ \forall\ \alpha > 0$, for the non-negative set X of real numbers, then equation (2) becomes $E[\Psi] = \frac{1}{2}\int\limits_0^1 \left(\Psi'_{\alpha} + \Psi''_{\alpha}\right) d\alpha$, given that Ψ'_{α} and Ψ''_{α} are finite and since Ψ is a fuzzy normalized variable,the α-negative value and the α-positive value of Ψ are respectively Ψ' and Ψ'' [35-38].

Definition 3. *(Fuzzy variable Transformation) The machine designing process contains a lot of uncertain data, and both random variables and fuzzy variables may be used to express uncertainty. The issue of uncertainty in the fuzzy variables might be handled using the idea of the cut-set of fuzzy mathematics by transforming from the fuzzy system to the general class [39].*

Now, related to specific subsets of the real numbers assume that$h$is a continuous function and if $\varPsi$ is a fuzzy variable, then $\rho = h(\varPsi)$, and there is a simple method of describing the possibility distribution function $\mu_{h(a)}(N)$ to $h(\varPsi)$ from the distribution $\mu_a(N)$of $\varPsi$. For a given $M \subset X$, $\varPsi$ considers a value on $h^{-1}(M)$ if and only if $h(\varPsi)$ considers values on M. So by interpretation, the ability to assign characters in $h^{-1}(M)$is similar to the ability of $h(\varPsi)$to assign characters in M.Because of this,for the fuzzy variable$\rho = h(\varPsi)$, it points out that $Pos_{\rho}(M) = \operatorname{Sup}_{p\in M}\mu_{\hat{h}(a)}(p) = \operatorname{Sup}_{N\in h^{-1}(M)}\mu_a(N) = Pos_{\varPsi}\left(h^{-1}(M)\right)$ and hence we can achieve a function by considering

$$\mu_{\hat{h}(a)}(p) = \underset{N\in h^{-1}(p)}{\operatorname{Sup}} \mu_a(N) \qquad (3)$$

It is observed that equation (3) is the depiction of the Zadeh extension of h. As a result, we represent the possibility distribution function of $h(\Psi)$ by $\mu_{\hat{h}(a)}(p)$ [40].

Now, by [41], if a fuzzy variable $\rho = h(\Psi)$ and h be a monotonic (strictly increasing or decreasing) function and the integrals $\int_0^1 h\left(\Psi'_\alpha\right) d\alpha$ and $\int_0^1 h\left(\Psi''_\alpha\right) d\alpha$ are finite; then the expected value can be determined by

$$E\left[h(\Psi)\right] = \frac{1}{2}\int_0^1 \left[h\left(\Psi'_\alpha\right) + h\left(\Psi''_\alpha\right)\right] d\alpha. \quad (4)$$

Someone may now be confronted with the issue of ambiguity regarding various elements in dynamic tumor nature and specific procedures.Assume that,μ_{a_1} and μ_{a_2} be the possibility distribution functions for the fuzzy variables Ψ_1 and Ψ_2 accordingly defined on the set X. Such factors describe a fuzzy variable on $X \times X$, that is $\rho = (\Psi_1, \Psi_2)$ and

$$\mu_a(N,p) = min\left\{\mu_{a_1}(N), \mu_{a_2}(p)\right\} \quad (5)$$

provides its combined possibility distribution function $\mu_a : X \times X \to [0, 1]$.

3. Tumor growth in a fuzzy environment using the Gompertz model

The Gompertz model, probably second to the logistic model, is one of the most often used sigmoid models for fitting growth data and other data. With application to tumor growth, several dynamic growth rate functions have been discussed. Gompertz growth has been demonstrated to recreate cell growth that slows with population density and thus is appropriate to observe tumor growth slowdown with tumor size.The growth rate is calculated by taking the negative logarithm of the present size of the population and dividing it by the carrying capacity:

$$\begin{aligned} &\dot{N}(t) = -\gamma N(t)\, log\left(\frac{N(t)}{K}\right);\ t > 0, \\ &N(0) = n_0, \quad \gamma > 0 \ \ and\ K > n_0 \end{aligned} \quad (6)$$

here $N(t)$denotes the tumor cell concentration in the target organism, $\dot{N}(t)$ denotes the derivative of N concerning time $t \neq 0$,γ indicates the net rate of tumor replication, and $K > 0$ denotes the tumor carrying capacity or the volume at which it stabilizes when the resource supply remains constant. Even though such parameters are commonly regarded as trustworthy, it is critical in creating realistic and empirical models to assess the uncertainty associated with their inherent variance or complexity. The genesis of the Gompertz model has been disputed for years; numerous independent investigations have found a strong and a substantial connection between the Gompertz model parameters and in either experimental systems or human data, and some researchers hypothesized that this would indicate a consistent maximum tumor size across tumor kinds within a species.

The dynamics of $N(t)$ over time are defined by the Gompertz model. In this context, a significant query that frequently arises in research is when $N(t)$ approaches a particular interest value.The solution of equation (**??**) is given by

$$\delta_t(n_0,\ \gamma,\ K) = Ke^{-ln}\left(\frac{K}{N_0}\right)e^{-\gamma t} \quad (7)$$

It has already been established that dealing with parameter inaccuracy is not always suitable due to a lack of comprehensive knowledge or estimation failure. A basic technique of coping with Gompertz equation uncertainties (6) is utilized to obtain these parameter estimations by utilizing the equation(7) to calculate the average approximations and to assess the complexity [42,43,45–47].

Let us now suppose that the fuzzy marks constrain the parameters n_0, γ and K. In other words, we suppose that such parameters fulfill an assertion such as the fuzzy variable (Ψ) generally is a_0. So the membership grade of the fuzzy mark is roughly the probability distribution of the fuzzy variable (Ψ) as per Zadeh. As the term $\delta_t(n_0, \gamma, K)$ of equation (7) is a fuzzy variable for a specified time $t > 0$, so the termsn_0, γ and K in equation (6) are also fuzzy variables.With the help of Zadeh extension,the procedures mentioned in the earlier parts on the parameters n_0, γ and K of the possibility distribution function $\delta_t(n_0, \gamma, K)$, for a fixed $t > 0$ can be obtained.

To create a realistic and practical model, it is necessary to remember that the parameters of equation (6) are approximate owing to the assumed lack of information and the mistakes in the calculation technique inherent in the relevant issues of the tumor growth. Different approaches, such as the use of random variables, are considered to characterize these parameters.The authors occasionally evaluate the Gompertz equation (6) with changes in the carrying capacity (K).

Note: Before we go into the details of the proposed study, everyone has a question: why do we need the starting condition, coefficient, and fuzzy numbers in tumor development modeling? The reason behind this is that.

(1) **Fuzziness in the initial condition:**If we want to calculate the population of tumor cells after a particular duration of time. For this reason, we had to estimate the beginning number of the tumor cell population, which is difficult to enumerate in an exact amount due to the inaccuracy of the count. As a result, it's preferable to use the original history as a guiding parameter.

(2) **Fuzziness in the coefficient:**If the pace of growth rate at which the population of tumor cells grows is unknown, it is difficult to estimate an exact amount. The value should be treated as ambiguous for this purpose.

(3) **Fuzziness in both the initial condition and the coefficient:**If both cases are combined in a model, this case can be used as well.

(4) **Fuzziness in the carrying capacity:**As carrying capacity varies over time in response to slow environmental changes, such as climate change or ecological succession, it is seen as ambiguous.

The creation of the fuzzy parameter system based on the Gompertz growth equation (6) is demonstrated in this paper in Fig.2, as follows:

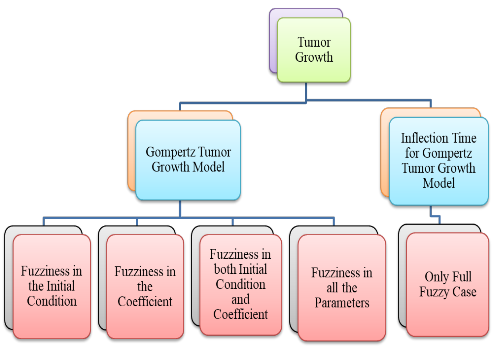

Figure 2. Fuzzy transformation mechanism of the Gompertz tumor growth model.

- *Gompertz growth equation* (6) *with fuzziness in the initial condition*n_0, *coefficient* γ *and in the initial condition* n_0 *and the coefficient* γ *together.*

The transformed model when $n_0$is taken into account as a fuzzy variable with a membership function of the possibility distribution function $\mu_{n_{01}}(N) : X \to [0,1]$, where the initial condition is limited roughly to $n_0 > 0$. However, it is suggested that the other two factors,the net growth rateγ and the carrying capacity K be specified and fixed. As a result, the Gompertz equation (6) with a fuzzy initial condition implies $\dot{N}(t)(t,\ \alpha) = -\gamma N(t)(t,\ \alpha)\ \ log\left(\frac{N(t)(t,\ \alpha)}{K}\right)$, and here $\delta_t(n_0)$ values rely on the numbers inferred by the initial condition as a fuzzy variable. Now, for a fuzzy setn_{01}, the α-*cut* of the fuzzy set $\widehat{\delta_t}(n_{01})$ having membership function $\mu_{n_{01}}(N)$ is given by the closed interval

$$\left[\widehat{\delta_t}(n_{01})\right]^{\alpha} = \left[\delta_t\left(\Psi'_{\alpha}\right),\ \ \delta_t\left(\Psi''_{\alpha}\right)\right]$$

Also, for the fuzzy variable $\delta_t(n_0)$, the expected value by using the above result can be obtained as

$$E\left[\delta_t(n_0)\right] = \frac{1}{2}\int_0^1 \left(\delta_t\left(\Psi'_{\alpha}\right) + \delta_t\left(\Psi''_{\alpha}\right)\right) d\alpha,$$

and for the membership function $\mu_{n_{01}}(N) = \chi\{[c,\ d]\}$ with the initial condition as fuzzy, the expected value is given by $E\left[\delta_t(n_0)\right] = \frac{\delta_t(c)+\delta_t(d)}{2}$. Now, the transformed model when the coefficient $\gamma$is considered a fuzzy variable and the initial condition n_0 and carrying capacity $K$is intended to be specified and fixed with a membership function of the possibility distribution function $\mu_{\gamma_1}(N) : X \to [0,1]$. Then, the Gompertz equation (6) with the fuzzy coefficient implies

$$\dot{N}(t)(t,\ \alpha) = -\gamma(\alpha)N(t)\,log\left(\frac{N(t)}{K}\right)$$

Also,the transformed model when both the initial condition n_0, coefficient γtogether are taken into account as fuzzy variables and carrying capacity$K$ is intended to be specified and fixed with a membership function of the possibility distribution function $\mu_{n_{01}}(N) : X \to [0,1]$ and $\mu_{\gamma_1}(N) : X \to [0,1]$. Then, the Gompertz equation (6) with the fuzzy initial condition$n_0$and coefficient γ implies

$$\begin{aligned}\dot{N}(t)(t,\ \alpha) = &-\gamma(\alpha)N(t)(t,\ \alpha)\\ &\times log\left(\frac{N(t)(t,\ \alpha)}{K}\right)\end{aligned}$$

- *Gompertz growth equation* (6) *with fuzziness in all parameters (full fuzzy case)*

Here, the transformation on all the three parameters, i.e., the initial condition n_0, the coefficient γ and the carrying capacity K are considered. Now, for the variables n_0, γ and K, let the fuzzy sets

$n_{01},\ \gamma_1$ and K_1 describe the fuzzy limits on the results calculated respectively. Also, define a fuzzy array $q = n_{01},\ \gamma_1,\ K_1$; where $\mu_q\left(n_0,\ \gamma,\ K\right) = \min\{\mu_{n_{01}}\left(n_0\right),\ \mu_{\gamma_1}\left(\gamma\right),\ \mu_{K_1}\left(K\right)\}$ gives the joint possibility distribution function. Now, for the fuzzy sets $n_{01},\ \gamma_1$ *and* K_1, the *α-cuts* of the fuzzy set $\widehat{\delta}_t\left(n_{01},\ \gamma_1,\ K_1\right)$ and having membership functions $\mu_{n_{01}}\left(N\right),\ \mu_{\gamma_1}\left(N\right), and\ \mu_{K_1}\left(N\right)$ is given by the closed interval

$$\left[\widehat{\delta}_t\left(n_{01},\gamma_1,K_1\right)\right]^{\alpha} = \left[\delta_t\left(\Psi_a^{'},\rho_a^{'},\nu_a^{'}\right),\delta_t\left(\Psi_a^{''},\rho_a^{''},\nu_a^{''}\right)\right].$$

Also, for the fuzzy variable $\delta_t\left(n_0,\ \gamma,\ K\right)$, the expected value by using the above result can be obtained as

$$E\left[\delta_t\left(n_0,\gamma,K\right)\right] = \frac{1}{2}\int_0^1 \left(\delta_t\left(\Psi_a^{'},\rho_a^{'},\nu_a^{'}\right),\delta_t\left(\Psi_a^{''},\rho_a^{''},\nu_a^{''}\right)\right)d\alpha$$

and for the membership function $\mu_{n_{01}}\left(N\right) = X_{[c,d]}\left(N\right)$, $\mu_{\gamma_1}\left(N\right) = X_{\left[\gamma_{01},\gamma_{02}\right]}\left(N\right)$ and $\mu_{K_1}\left(N\right) = X_{\left[K_{01},K_{02}\right]}\left(N\right)$ with an initial condition, coefficient and carrying capacity as fuzzy, the expected value is given by $E\left[\delta_t\left(n_0,\gamma,K\right)\right] = \frac{\delta_t(c,\gamma_{01},K_{01})+\delta_t(c,\gamma_{02},K_{02})}{2}$.

As a result, the Gompertz equation (6) with the fuzzy parameters $n_0,\ \gamma$ *and* K implies $\dot{N}\left(t\right)\left(t,\ \alpha\right) = -\gamma(\alpha)N\left(t\right)\left(t,\ \alpha\right)log\left(\frac{N(t)(t,\ \alpha)}{K(\alpha)}\right)$

Note: The lower α cut and the upper α cut for the fuzzy variable with the membership function $\mu_{n_{01}}\left(N\right) = \chi\left[a,\ b\right]$ of the possibility distribution function are described as

$$\Psi_\alpha^{'} = m - \left(1-\alpha\right)\theta \text{ and } \Psi_\alpha^{''} = m + \left(1-\alpha\right)\theta \quad (8)$$

where for the fuzzy interval $\chi[a,\ b]$,m is the middle term with difference θ between the middle value and the upper value of the interval [a, b].

4. Inflection time for Gompertz tumor growth model

The tumor curve development slows (moving from concave up to downward) at an inflection point)or accelerates (moving from concave down to upward). To put it another way, the inflection point aids in emphasizing the evolution that has occurred over time. Most people know that cancerous growth has a rapid beginning proliferation, which indicates that cell alterations occur rapidly throughout time. This study looks at the tumor's development and the accomplishment of carrying capacity K over time. For example,suppose the equation describes tumor size growth over time. In that case, this timespan may indicate the saturation threshold at K, since nutrients are transferred from initial growth to cell division. When it comes to cancer cells, the decreasing return rule has a specific effect on-time behavior.

Human tumor growth was once thought to be both unpredictable and rapid. A study of the development of laboratory tumors has revealed that the majority of the time, this growth rate matches a straightforward equation, such as the Gompertz equation. As a result, scientists have devised a formula to calculate the number of tumor cells within a specific period, allowing them to determine the exact growth of each cancer.As a result of this information, oncologists can design a robust recovery strategy till the tumor has had a chance to respond to treatment. In mathematical modeling, the inflection time T_i is essential because it identifies the period (or population) at which the maximum growth rate occurs, which may be used to predict future growth rates [48–50]. To get the inflection time $T_i > 0$, using Gompertz equation (6), use the following formula

$$T_i = \frac{\ln\left(-\ln(\frac{n_0}{K})\right)}{\gamma};\quad n_0 < K/2 \qquad (9)$$

Here, T_i is a fuzzy variable in the same way as $n_0,\ \gamma$ *and* K are fuzzy variables.

- *Fuzziness in the initial condition n_0, coefficient γ and in both the initial condition n_0 and coefficient γ together of the equation (9)*

The transformed model for the inflection time of the Gompertz equation (9) when n_0 is taking into account as fuzzy by a membership grade of the possibility distribution function $\mu_{n_{01}}(N) : X \to [0,1]$ with the net growth rate γ and the carrying capacity K be specified implies

$$T_i = \frac{\ln\left(-\ln(\frac{n_0(\alpha)}{K})\right)}{\gamma}$$

It is also possible to examine, for the fuzzy variable $T_i\left(n_0\right)$, the expected value while evaluating the impact of fuzzy uncertainty on the maximal tumor growth period, which is given as

$$E\left[T_i\left(n_0\right)\right] = \frac{1}{2}\int_0^1 \left(T_i\left(\Psi_\alpha^{'}\right) + T_i\left(\Psi_\alpha^{''}\right)\right)d\alpha$$

and for the membership function $\mu_{n_{01}}(N) = \chi\{[c,\ d]\}$ with the initial condition as fuzzy, the expected value is given by $E\left[T_i\left(n_0\right)\right] = \frac{T_i(c)+T_i(d)}{2}$.

Now, the transformed model when the coefficient γ is taken into account as a fuzzy variable and the initial condition n_0 and carrying capacity $K$is intended to be specified and fixed with a membership function of the possibility distribution function $\mu_{\gamma_1}(N) : X \rightarrow [0,1]$. Then, the inflection time of the Gompertz equation (9) with the fuzzy coefficient implies

$$T_i = \frac{\ln\left(-\ln(\frac{n_0}{K})\right)}{\gamma(\alpha)}$$

Also, the transformed model when both the initial condition n_0, coefficient γ are taken into account as fuzzy variables and carrying capacity K is intended to be specified and fixed with a membership function of the possibility distribution function $\mu_{n_{01}}(N) : X \rightarrow [0,1]$ and $\mu_{\gamma_1}(N) : X \rightarrow [0,1]$. Then, the inflection time of the Gompertz equation (9) with the fuzzy coefficient implies

$$T_i = \frac{\ln\left(-\ln(\frac{n_0(\alpha)}{K})\right)}{\gamma(\alpha)}.$$

- *Fuzziness in all the parameters of the equation* (9)*(full fuzzy case)*

Here, the transformation on all the three parameters, i.e., the initial condition n_0, the coefficient γ and the carrying capacity K is considered by the fuzzy sets $n_{01},\ \gamma_1\ and\ K_1$ respectively. The fuzzy set $\widehat{T_i} = \widehat{T_i}\left(n_{01},\ \gamma_1,\ K_1\right)$, where

$$\mu_{\widehat{T_i}}\left(\tau\right) = sup\left\{\mu_{n_{01}}\left(n_0,\ \gamma,\ K\right) : \left(n_0,\ \gamma,\ K\right) \in {T_i}^{-1}(\tau)\right\}$$

specifies the possibility distribution function of the fuzzy variable $T_i\left(n_0,\ \gamma,\ K\right)$. Now for the fuzzy sets $n_{01},\ \gamma_1\ and\ K_1$, the α-cut set $\widehat{T_i}\left(n_{01},\ \gamma_1,\ K_1\right)$ with the membership functions $\mu_{n_{01}}(N)$, $\mu_{\gamma_1}(N)$, and $\mu_{K_1}(N)$ is given by the closed interval $\left[\widehat{T_i}\left(n_{01}, \gamma_1, K_1\right)\right]^{\alpha} = \left[T_i\left(\Psi_a^{''}, \rho_a^{''}, \nu_a^{''}\right), \delta_t\left(\Psi_a^{'}, \rho_a^{'}, \nu_a^{'}\right)\right]$, as the function $T_i\left(n_0,\ \gamma,\ K\right)$ is increasing in K and is decreasing in $\gamma\ and\ n_0$.

So the expected value of the fuzzy variable $T_i\left(n_0,\ \gamma,\ K\right)$ may be determined by using equation (4), and it gives $E\left[T_i\left(n_0, \gamma, K\right)\right]^{\alpha} = \frac{1}{2}\int\limits_0^1 \left(T_i\left(\Psi_a^{''}, \rho_a^{''}, \nu_a^{''}\right), \delta_t\left(\Psi_a^{'}, \rho_a^{'}, \nu_a^{'}\right)\right) d\alpha$ and for the membership function $\mu_{n_{01}}(N) = \chi_{[c,\ d]}(N)$, $\mu_{\gamma_1}(N) = \chi_{[\gamma_{01},\ \ \gamma_{02}]}(N)\ and\ \mu_{K_1}(N) = \chi_{[K_{01},\ \ K_{02}]}(N)$ with an initial condition, coefficient and carrying capacity as fuzzy, the expected value is given by

$$E\left[T_i\left(n_0,\ \gamma,\ K\right)\right] = \frac{T_i\left(d,\ \gamma_{02},\ K_{01}\right) + T_i\left(c,\ \gamma_{01},\ K_{02}\right)}{2}.$$

As a result, the inflection time for the Gompertz equation (6) given by equation (9) with the fuzzy parameters $n_0,\ \gamma\ and\ K$ implies

$$T_i = \frac{\ln\left(-\ln(\frac{n_0(\alpha)}{K(\alpha)})\right)}{\gamma(\alpha)}.$$

Note: The lower α-cut and the upper α-cut are given by the equation (8), i.e.

$$\Psi_a^{'} = m - (1-\alpha)\,\theta \text{ and } \Psi_a^{''} m + (1-\alpha)\,\theta.$$

5. Numerical simulation

Numerical simulations of the Gompertz growth model under fuzzy environment for tumor development are performed in this section using the possibility distribution function. With varying growth rates and achieving the carrying capacity at different times, the net rate of tumor cell concentration fluctuates according to the lower and upper α-cuts of the possibility distribution function for the specific parameter in the Gompertz equation. We can find out how to solve the fuzzy Gompertz equation of tumor growth using the MATLAB R2019b software.

- Gompertz equation with the fuzzy initial condition:

Take $N\left(t\right) = \chi\left[3,\ 11\right]$, $\gamma = 0.15$, $K = 100$ and $t \in [0,\ 100]$. Then, the problem becomes

$$\dot{N}\left(t\right)\left(t,\ \alpha\right) = -\left(0.15\right) N(t)\left(t,\ \alpha\right) \times log\left(\frac{N\left(t\right)\left(t,\ \alpha\right)}{100}\right)$$

with initial condition $N\left(0, \alpha\right) = 7 - \left(1-\alpha\right) 4$.

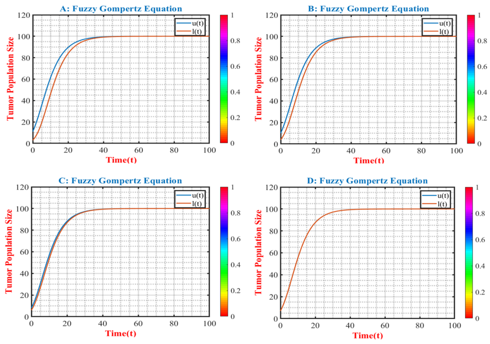

Figure 3. In this case, the system of Gompertz equation with only the initial condition as fuzzy is defined and the tumor population size as a function of time for $\alpha = 0$, $\alpha = 0.25$, $\alpha = 0.75$ and $\alpha = 1$ are illustrated.

- Gompertz equation with the fuzzy coefficient or net population rate of tumor:

Take $N(t) = 7$, $\gamma = \chi[0.1,\ 0.2]$, $K = 100$ and $t \in [0,\ 100]$.
Then, the problem becomes

$$\dot{N}(t)(t,\ \alpha) = -(0.15 - (1-\alpha)\,0.05)\,N(t) \times log\left(\frac{N(t)}{100}\right)$$

with initial condition $N(0,\alpha) = 7$.

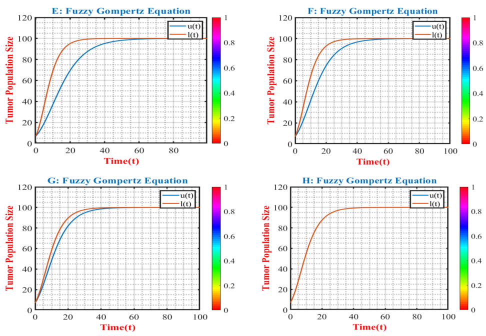

Figure 4. In this case, the system of Gompertz equation with only the coefficient as fuzzy is defined and the tumor population size as a function of time for $\alpha = 0$, $\alpha = 0.25$, $\alpha = 0.75$ and $\alpha = 1$ are illustrated.

- Gompertz equation with both the initial condition and the net population rate of the tumor as fuzzy:

Take $N(t) = \chi[3,\ 11]$, $\gamma = \chi[0.1,\ 0.2]$, $K = 100$ and $t \in [0,\ 100]$.
Then, the problem becomes

$$\dot{N}(t)(t,\ \alpha) = -(0.15 - (1-\alpha)\,0.05)\,N(t)(t,\ \alpha) \times log\left(\frac{N(t)(t,\ \alpha)}{100}\right)$$

with initial condition $N(0,\alpha) = 7 + (1-\alpha)\,4$.

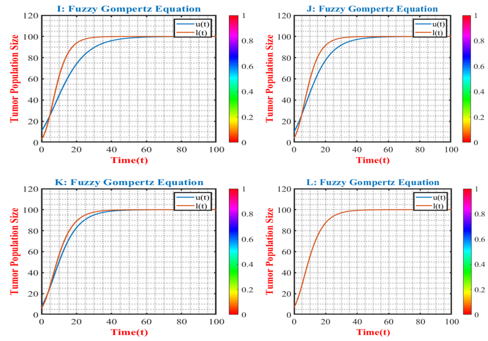

Figure 5. In this case, the system of Gompertz equation with both initial condition and the coefficient as fuzzy is defined and the tumor population size as a function of time for $\alpha = 0$, $\alpha = 0.25$, $\alpha = 0.75$ and $\alpha = 1$ are illustrated.

- Gompertz equation with all the parameters, i.e., initial condition, the net population rate of the tumor, and carrying capacity as fuzzy:

Take $N(t) = \chi[3,\ 11]$, $\gamma = \chi[0.1,\ 0.2]$, $K = \chi[90,\ 110]$ and $t \in [0,\ 100]$. Then, the problem becomes

$$\dot{N}(t)(t,\ \alpha) = -(0.15 - (1-\alpha)\,0.05)\,N(t)(t,\ \alpha) \times log\left(\frac{N(t)(t,\ \alpha)}{100 - (1-\alpha)\,10}\right)$$

with initial condition $N(0,\alpha) = 7 + (1-\alpha)\,4$.

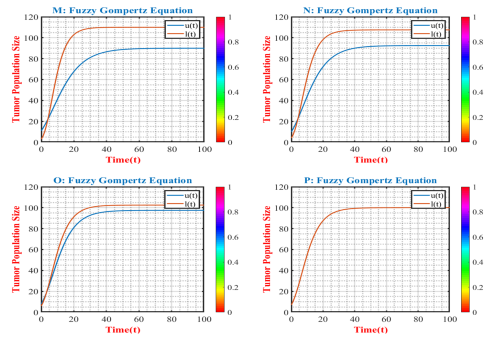

Figure 6. In this case, the system of Gompertz equation full fuzzy i.e., initial condition, coefficient and carrying capacity all are fuzzy is defined and the tumor population size as a function of time for $\alpha = 0$, $\alpha = 0.25$, $\alpha = 0.75$ and $\alpha = 1$ are illustrated.

6. Results and discussion

A fuzzy mathematical model of tumor development trajectory makes significant progress in displaying the realistic path of tumor growth with the help of a degree of accuracy.The possibility distribution function can solve the Gompertz equation for tumor development in a fuzzy environment. Upon attaining the carrying capacity at different intervals, the net tumor volume or the tumor cell concentration changes appropriately, as demonstrated by utilizing the lower and upper α-cuts for the possibility distribution function for a specific parameter of the Gompertz equation.As a result, the lower and upper α-cuts of the possibility distribution function indicate the region of ambiguity for the net tumor volume.

The absence of replication time at the beginning stages of a tumor would be attributed to a variance process or a reaction of the body to the sickness owing to some adverse effect of defensive characteristics throughout tumor cell differentiation. However, in certain situations, the defensive process would have been abducted at the start, resulting in a fast rise that is precisely proportionate to the pace of tumor development. The growth mechanism is not disrupted in the linear phase, and maximal increase happens at $K/2$, indicating that the defensive system is effectively viable. However, as tumor size increases, growth becomes more complex, and the growth rate eventually decreases, resulting in a plateau phase due to nutritional shortages, oxygen crises, and other factors.The Gompertz model extends the logistic model that includes an asymmetrical graph with an intersection point.The Gompertz model depicts the tumor's inherent phases and therefore, best deals with its development pattern.

The crisp mathematical model differs from the fuzzy mathematical model of tumor growth in the way that in the crisp model, the parameters are fixed, whereas, in the fuzzy model, the parameters are variable due to a variety of factors, including the fact that tumors are constantly evolving, resulting in changing dynamics. We can study the growth mathematically inside the binary value in a crisp mode. Still, this work shows the behavior of tumor development by modifying the initial tumor cell population, tumor net population rate, and carrying capacity of the tumor through the α-cut in a fuzzy model. This feature allows tumor load to be calculated based on the extent of accuracy, which might be extremely important for tumor staging and analysis.

Also, for the fuzzy intervals $n_0 = \chi[3,\ 11]\,,\ \gamma = \chi[0.1,\ 0.2]$ and $K = \chi[90,\ \ 110]$, it has been found that the inflection time $T_i(\alpha)$ for the Gompertz growth in a full fuzzy manner for $\alpha = 0$ is 12.24 and 4.17 as a lower and upper α-cut respectively, for $\alpha = 0.25$ is 8.8 and 5.44 as a lower and upper α-cut respectively, for $\alpha = 0.75$ is 6.4 and 7.2 as a lower and upper α-cut respectively. Finally, for $\alpha = 1$it is 6.52 for both lower and upper α-cut,which indicates the optimal time for tumor growth is also a fuzzy variable. Any variables of the possibility distribution function of fuzzy numbers must be kept in mind when measuring resemblance and its shape and midpoint are essential metrics. For the fuzzy intervals $n_0 = \chi[3,\ 11]\,,\ \gamma = \chi[0.1,\ 0.2]$ and $K = \chi[90,\ \ 110]$, the expected value of $T_i(n_0,\ \gamma,\ K)$ is given by $E[T_i(n_0,\ \gamma,\ K)] = -4.55$, means that there will be no tumor cell population, i.e., the margins don't contain cancerous cells.

7. Managerial insights

This study achieves an intelligent decision support system called fuzzy mathematical tumor growth modeling, which combines population models, mathematical modeling, and fuzzy logic. Possibility distribution functions can be utilized in decision-making, risk response, and optimization algorithms to solve the Gompertz equation of tumor development under fuzzy conditions. According to the fuzzy Gompertz equation, the tumor growth rate decreases linearly with volume until it approaches zero at carrying capacity. For example, it has been demonstrated that when reaching carrying capacity at different intervals of time, the net volume of tumor or tumor cell concentration fluctuates according to the lower and upper α-cuts of the possibility distribution function. Besides explaining tumor development in a fuzzy environment, the model also provides practical strategies for treating cancer. In real-life data, it may be utilized to analyze tumor distribution, cell count estimation, and tumor staging, which, in turn, leads to more precise targeting of treatment methods. As a continuation of this study, stochastic differential equations from the above-described models will be used to calculate and assess tumor development behavior in a fuzzy environment. It has become possible to understand clinical data with the use of new complicated mathematical models, as well. As a general rule, fuzzy logic reduces complexity in the tumor detection method by reducing the number of variables involved.

8. Conclusion

As a disease of extreme complexity, cancer's progression, remission, and treatment mechanisms are still unknown. Fuzzy mathematical modeling addresses its uncertainty and therefore gives a feasible way to cope with it in every phase. It is essential to replicate some real-life events using fuzzy mathematical modeling to obtain a more realistic representation of reality. Changing the model parameters in the tumor growth fuzzy model will lower the overall residuals, minimizing the uncertainty between the numerical predicting model and the actual results of medical studies. This study has interpreted the initial state, net population rate, and carrying capacity as a set of fuzzy variables whose possibility distribution function is determined by the membership grade of fuzzy sets. Because this method is based on facts, it may be utilized to determine the most effective prescription in less time by eliminating the uncertainty associated with tumor growth. Therefore, fuzzy mathematical modeling supports the resolution of ambiguities in calculation parameters, allowing for the differentiation of present and expected tumor growth modeling. It is also possible to improve tumor growth in a fuzzy environment by combining multiple derived principles with different fuzzy methods.This paper depicts the tumor development process numerically.

References

[1] Bekisz, S., & Geris, L. (2020). Cancer modeling: From mechanistic to data-driven approaches, and from fundamental insights to clinical applications.*Journal of Computational Science*, 46, 101198.

[2] Basanta, D., & Anderson, A. R. (2017). Homeostasis back and forth: an ecoevolutionary perspective of cancer. *Cold Spring Harbor perspectives in medicine*,7(9), a028332.

[3] Watanabe, Y., Dahlman, E. L., Leder, K. Z., & Hui, S. K. (2016). A mathematical model of tumor growth and its response to single irradiation.*Theoretical Biology and Medical Modelling*, 13(1), 1-20.

[4] Ozsahin, D. U., Uzun, B., Ozsahin, I., Mustapha, M. T., & Musa, M. S. (2020). *Fuzzy logic in medicine*. In Biomedical Signal Processing and Artificial Intelligence in Healthcare, Academic Press, 153-182.

[5] Albertos, P., Sala, A., & Olivares, M. (1998). Fuzzy logic controllers. Advantages and drawbacks *VIII international congress of automatic control*, 3, 833-844.

[6] Zimmermann, H. J. (2001). *Fuzzy Set Theory and Its Applications*. Springer Science, Business Media.

[7] Kavilal, E. G., Venkatesan, S. P., & Kumar, K. H. (2017). An integrated fuzzy approach for prioritizing supply chain complexity drivers of an Indian mining equipment manufacturer.*Resources Policy*, 51, 204-218.

[8] Bhat, S. A., & Kumar, A. (2018). Performance evaluation of outsourcing decision using a BSC and fuzzy AHP approach: A case of the Indian coal mining organization by M., Modak, K., Pathak, KK, Ghosh [Resour. Policy 52 (2017) 181-191]: Suggested modification. *Resources Policy*, 55, 29-30.

[9] Bevia, V. J., Burgos Simón, C., Cortés, J. C., & Villanueva Micó, R. J. (2021). Uncertainty Quantification of Random Microbial Growth in a Competitive Environment via Probability Density Functions. *Fractal and Fractional*, 5(2), 26.

[10] Nebot, À., Mugica, F., Martinez-Lopez, B., & Gay-Garcia, C. (2011). Fuzzy Approaches for Modeling Dynamical Ecological Systems. In *SIMULTECH*, 374-379.

[11] Marino, S., Hogue, I. B., Ray, C. J., & Kirschner, D. E. (2008). A methodology for performing global uncertainty and sensitivity analysis in systems biology. *Journal of Theoretical Biology*, 254, 178-196.

[12] Esmaili, S. S., & Nasrabadi, A. M. (2009, December). Uncertainty analysis in tumor model with fuzzy parameters. In *2009 International Conference on Computational Intelligence and Software Engineering*, 1-4.

[13] Singh, A., & Bhat, S. (2020). A note on 'A novel correlation coefficient of intuitionistic fuzzy sets based on the connection number of set pair analysis and its application'. *Authorea Preprints.*

[14] Buckley, J. J., & Qu, Y. (1990). Solving linear and quadratic fuzzy equations. *Fuzzy sets and systems*, 38(1), 43-59.

[15] Abbasbandy, S. (2006). The application of homotopy analysis method to nonlinear equations arising in heat transfer. *Physics Letters A*, 360(1), 109-113.

[16] Abbasbandy, S., & Ezzati, R. (2006). Newton's method for solving a system of fuzzy nonlinear equations. *Applied Mathematics and Computation*, 175(2), 1189-1199.

[17] Mazandarani, M., & Kamyad, A. V. (2013). Modified fractional Euler method for solving fuzzy fractional initial value problem. *Communications in Nonlinear Science and Numerical Simulation*, 18(1), 12-21.

[18] Wang, H., & Liu, Y. (2011). Existence results for fuzzy integral equations of fractional order. *Int. J. Math. Anal*, 5, 811-818.

[19] Jafari, R., & Yu, W. (2017). Fuzzy modeling for uncertainty nonlinear systems with fuzzy equations. *Mathematical problems in Engineering*, 2017.

[20] Nebot, À., Mugica, F., Martínez-López, B., & Gay-Garcia, C. (2011). Fuzzy Approaches for Modeling Dynamical Ecological Systems. In *SIMULTECH*, 374-379.

[21] Esmaili, S. S., & Nasrabadi, A. M. (2009). Uncertainty analysis in tumor model with fuzzy parameters. In *2009 International Conference on Computational Intelligence and Software Engineering*, 1-4.

[22] Zadeh, L. A. (1999). Fuzzy sets as a basis for a theory of possibility. *Fuzzy Sets and Systems*, 100, 9-34.

[23] Malinowski, M. T. (2009). On random fuzzy differential equations. *Fuzzy Sets and Systems*, 160(21), 3152-3165.

[24] Rzezuchowski, T., & Wasowski, J. (2001). Differential equations with fuzzy parameters via differential inclusions. *Journal of Mathematical Analysis and Applications*, 255(1), 177-194.

[25] Pirzada, U. M. (2018). Generalized Seikkala Differentiability and its Application to Fuzzy initial value problem. *arXiv preprint arXiv:1812.04963.*

[26] Ahmad, M. Z., Hasan, M. K., & Abbasbandy, S. (2013). Solving fuzzy fractional differential equations using Zadeh's extension principle. *The Scientific World Journal*, 2013.

[27] Buckley, J. J., & Feuring, T. (2000). Fuzzy differential equations. *Fuzzy sets and Systems*, 110(1), 43-54.

[28] Yamano, T. (2009). Statistical ensemble theory of gompertz growth model. *Entropy*, 11(4), 807-819.

[29] Kozlowski, J. (1992). Optimal allocation of resources to growth and reproduction: implications for age and size at maturity. *Trends in Ecology & Evolution*, 7(1), 15-19.

[30] Tatro, D. (2018). The Mathematics of Cancer: Fitting the Gompertz Equation to Tumor Growth.

[31] Tjorve, K. M., & Tjørve, E. (2017). The use of Gompertz models in growth analyses, and new Gompertz-model approach: An addition to the Unified-Richards family. *PloS One*, 12(6), e0178691.

[32] Halkola, A. S., Parvinen, K., Kasanen, H., Mustjoki, S., & Aittokallio, T. (2020). Modelling of killer T-cell and cancer cell subpopulation dynamics under immuno-and chemotherapies. *Journal of Theoretical Biology*, 488, 110136.

[33] Friberg, S., & Mattson, S. (1997). On the growth rates of human malignant tumors: implications for medical decision making. *Journal of Surgical Oncology*, 65(4), 284-297.

[34] Casaban, M. C., Cortés, J. C., Romero, J. V., & Roselló, M. D. (2015). Probabilistic solution of random SI-type epidemiological models using the random variable transformation technique. *Communications in Nonlinear Science and Numerical Simulation*, 24(1-3), 86-97.

[35] George, J. K., & Bo, Y. (1995). *Fuzzy Sets and Fuzzy Logic: Theory and Applications.* PHI New Delhi, 443-455.

[36] Diamond, P., & Kloeden, P. (1990). Metric spaces of fuzzy sets. *Fuzzy sets and systems*, 35(2), 241-249.

[37] Hong, D. H. (2009). Note on the expected value of a function of a fuzzy variable. *Journal of applied mathematics & informatics*, 27(3-4), 773-778.

[38] Narukawa, Y., & Torra, V. (2004). Fuzzy Measures and integrals for evaluating strategies. In *International Conference on Information Technology: Coding and Computing, 2004. Proceedings. ITCC 2004.*, 2, 162-166.

[39] Dong, Y., & Wang, A. (2006). A fuzzy reliability analysis based on the transformation between discrete fuzzy variables and discrete random variables. *International Journal of Reliability, Quality and Safety Engineering*, 13(1), 25-35.

[40] Zadeh, L. A., Klir, G. J., & Yuan, B. (1996). *Fuzzy Sets, Fuzzy Logic, and Fuzzy Systems: Selected Papers*, World Scientific, 6.

[41] Narukawa, Y., Murofushi, T., & Sugeno, M. (2000). Regular fuzzy measure and representation of comonotonically additive functional. *Fuzzy Sets and Systems*, 112(2), 177-186.

[42] Winsor, C. P. (1932). The Gompertz curve as a growth curve. *Proceedings of the National Academy of Sciences of the United States of America*, 18(1), 1.

[43] Asadi, M., Di Crescenzo, A., Sajadi, F. A., & Spina, S. (2020). A generalized Gompertz growth model with applications and related birth-death processes. *Ricerche di Matematica*, 1-36.

[44] Vaghi, C., Rodallec, A., Fanciullino, R., Ciccolini, J., Mochel, J. P., Mastri, M., ... & Benzekry, S. (2020). Population modeling of tumor growth curves and the reduced Gompertz model improve prediction of the age of experimental tumors. *PLoS Computational Biology*, 16(2), e1007178.

[45] Vaghi, C., Rodallec, A., Fanciullino, R., Ciccolini, J., Mochel, J., Mastri, M., ... & Benzekry, S. (2019). A reduced Gompertz model for predicting tumor age using a population approach. bioRxiv, 670869.

[46] Bevia, V., Burgos, C., Cortés, J. C., Navarro-Quiles, A., & Villanueva, R. J. (2020). Uncertainty quantification analysis of the biological Gompertz model subject to random fluctuations in all its parameters. *Chaos, Solitons & Fractals*, 138, 109908.

[47] Enderling, H., & AJ Chaplain, M. (2014). Mathematical modeling of tumor growth and treatment. *Current Pharmaceutical Design*, 20(30), 4934-4940.

[48] Bayat, H., Rastgo, M., Zadeh, M. M., & Vereecken, H. (2015). Particle size distribution models, their characteristics and fitting capability. *Journal of Hydrology*, 529, 872-889.

[49] Tubiana, M. (1989). Tumor cell proliferation kinetics and tumor growth rate. *Acta Oncologica*, 28(1), 113-121.

[50] Staat, C. (2020). Finding the Growth Rate of a Tumor. *Undergraduate Journal of Mathematical Modeling: One+ Two*, 10(2), 5.

Aadil Rashid Sheergojri *has received his Bachelor's degree from University of Kashmir, Srinagar (J& K), India and Master's degree from Lovely Professional University Jalandhar Punjab, India. He is presently pursuing Ph.D. in Department of Mathematics and Actuarial Science from B. S. Abdur Rahman Crescent Institute of Science and Technology, Chennai, India.His research areas include Fuzzy Logic, Fuzzy Mathematics, Mathematical Modelling, Tumor-Dynamics and Numerical Methods.*

https://orcid.org/0000-0002-7483-8709

Pervaiz Iqbal *is currently working as an Assistant Professor in the Department of Mathematics and Actuarial Science at B.S. Abdur Rahman Crescent Institute of Science & Technology, Vandalur, Chennai, 600048 since July 2017. Prior to this he was working as a Teaching Assistant in the Department of Mathematics from 2009 to 2010 at Govt. Degree College Women, Kathua, Jammu and Kashmir. He has completed his Doctor's Degree from B.S. Abdur Rahman University, Vandalur, Chennai, in the year 2017. He did his master's in Applied Mathematics from Baba Ghulam Shah Badshah University, Rajouri, Jammu and Kashmir, in the year 2009. He has published 16 papers in reputed International and National Journals and 2 Book Chapter. And he has presented 23 papers in International Conferences and 15 papers in National Conferences. His broad area of research work is Mathematical Modeling, Optimization Techniques in Operations Research and his interested area is Mathematical Modeling in Biology.*

https://orcid.org/0000-0002-3013-7206

Praveen Agarwal *was born in Jaipur (India) on August 18, 1979. After completing his schooling, he earned his Master's degree from Rajasthan University in 2000. In 2006, he earned his Ph. D. (Mathematics) atthe Malviya National Institute of Technology (MNIT) in Jaipur, India, one of the highest ranking universities in India. Dr. Agarwal has been actively involved in research as well as pedagogical activities for the last 20 years. His major research interests include Special Functions, Fractional Calculus, Numerical Analysis, Differential and Difference Equations, Inequalities, and Fixed Point Theorems. He is an excellent scholar, dedicated teacher, and prolific researcher. He has published 8 research monographs and edited volumes and more than 350 publications (with almost 100 mathematicians all over the world) in prestigious national and international mathematics journals. Dr. Agarwal worked previously either as a regular faculty or as a visiting professor and scientist in universities in several countries, including India, Germany, Turkey, South Korea, UK, Russia, Malaysia and Thailand.In summary of these few inadequate paragraphs, Dr. P. Agarwal is a visionary scientist, educator, and administrator who have contributed to the world through his long service, dedication, and tireless efforts.*

https://orcid.org/0000-0001-7556-8942

Necati Özdemir *completed his Ph.D. degree at University of Exeter in 2000, his M.Sc. degree at University of Warwick in 1997 and his undergraduate studies at Marmara University in 1992. He is a Professor in the Mathematics Department at Balıkesir University where he has been a faculty member since 2001. He was Director of Graduate School of Natural Sciences between 2015-2021. He has served on several conference and workshop program committees and served as the Co-chair for the ICAME'18, ICAME-2021. He also served as a guest editor for reputed international journals and publishers including Springer and International Journal of Nonlinear Sciences and Numerical Simulation. Frontiers in Physics, Journal of Computational and Applied Mathematics and 2 books as a editor*

https://orcid.org/0000-0002-6339-1868

An International Journal of Optimization and Control: Theories & Applications
ISSN: 2146-0957 eISSN: 2146-5703
Vol.12, No.2, pp.151-159 (2022)
https://doi.org/10.11121/ijocta.2022.1146

RESEARCH ARTICLE

Localization of an ultra wide band wireless endoscopy capsule inside the human body using received signal strength and centroid algorithm

Memduh Suveren, Rüştü Akay*, Muzaffer Kanaan

Department of Mechatronics Engineering, Erciyes University, Kayseri 38039, Turkey
msuveren@erciyes.edu.tr, akay@erciyes.edu.tr, mkanaan@erciyes.edu.tr

ARTICLE INFO

Article history:
Received: 20 August 2021
Accepted: 31 May 2022
Available Online: 26 July 2022

Keywords:
Centroid algorithm
Wireless capsule endoscopy
In-body localization
RSS based model
Body model

AMS Classification 2010:
65K10, 49M05

ABSTRACT

Wireless capsule endoscopy (WCE) is used for imaging and diagnosing diseases in the gastrointestinal (GI) system. The location of the disease detected by WCE is still an important problem. Location information is very important for the surgical or drug treatment of the detected disease. In this study, RSS-based centroid algorithm has been used in order to accurately predict the capsule position on a sample data set. The effect of different parameters such as number of sensors used on the proposed mathematical model, location of sensors on positioning is analyzed in detail. The results show that a precise position detection is possible with fewer sensors positioned correctly. As a result, the positioning error with the correctly selected sensors is reduced by approximately 55%. In addition, the performance of the proposed method was compared with the classical centroid algorithm and more than 50% improvement was achieved.

1. Introduction

Wireless capsule endoscopy (WCE) is fast becoming an important technique in modern medical imaging, allowing parts of the human body (such as the small intestine) that could not be effectively imaged using conventional techniques [1]. WCE allows the diagnosis of illnesses such as colorectal cancer, celiac disease, Crohn's disease, the sites of intestinal bleeding and other types of pathologies in the gastrointestinal (GI) tract [2, 3]. A very attractive characteristic of WCE is that, unlike conventional endoscopy techniques, it causes little to no discomfort for the patient; the patient simply has to swallow a pill-shaped camera (i.e. the endoscopy capsule), which contains all the electronics for imaging and transmission of the image data to an on-body recording unit (see Figure 1 for the general system structure). The pill-shaped camera naturally moves through the GI tract and is naturally excreted out of the body. The images captured by the capsule are sent via an on-board radio transmitter to on-body receiving antennas and from there to a recording system. The images can then be reviewed offline by a medical specialist. Although the current generation of WCE systems use the medical implant communications system (MICS) band, there are proposals calling for the use of Ultra Wide Band (UWB) technology as well [4]. The primary advantage of UWB is the low power consumption due to simple transceiver structures required [5, 6]. In another type of WCE, camera is replaced with sensors such as temperature, pressure, Potential of Hydrogen or light spectrum analyser sensors [7, 8]. WCE could locate the abnormalities in GI system. Image processing algorithms detect diseases and notify the doctors [9]. Also, some works have focused on other external localization techniques based on magnetic field [10, 11].

Current WCE systems have a significant problem in the sense that there is no way to localize the capsule as it moves through the GI tract [12]. This means that if any of the images reveal a potentially abnormal condition (such as a tumor or a lesion) there is no way to know just where in the GI tract the condition exists, making subsequent surgical interventions very difficult and more risky for the patient [13]. Thus, it is critical to come up with techniques to accurately localize the endoscopy capsule as it moves through the GI tract. Localization of a source emitting a radio frequency (RF) signal on the basis of received signal characteristics is a well-investigated topic that has received much attention in the literature [14, 15]. One example of received signal characteristics that can be used for localization purposes is the received signal

*Corresponding author

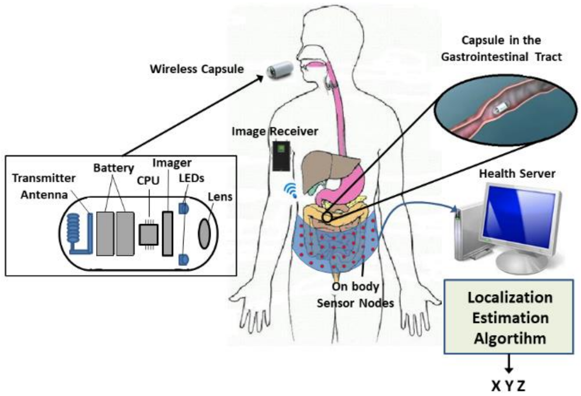

Figure 1. General system structure

strength (RSS). The usage of the RSS for localization purposes is attractive, as RSS is a very simple parameter to measure. This is why RSS has been preferred for challenging applications such as indoor localization [16]. For the in-body localization of an endoscopy capsule, however, RSS-based localization can be challenging. The in-body environment is highly non-homogeneous, consisting of different types of tissue, whose electrical conductivity and permittivity are frequency-dependent. For example, tissues such as skin, muscle, kidney, liver may have higher dielectric constant and conductivity (since these tissues contain a high amount of water), while dielectric constant and conductivity in tissues such as fat and bone with less water content may be lower. It is important to note that these parameters are also dependent on frequency [17]. This non-homogeneous environment can seriously distort UWB signals as documented by several prior studies in this area [18, 19, 20]. One way to combat these detrimental effects and obtain consistent accuracy in localization is to use more sensors (more receiving antennas) distributed over the body surface. This can provide performance gains, in a similar fashion to the diversity concept commonly used in other types of wireless communication systems [21, 22].

To explain this concept more clearly, consider the scenario of Figure 1, where the patient swallows the capsule and the signal emitted by the capsule is sensed by *N* antennas distributed over the body surface. Because of the inhomogeneity in the body environment, not all of these *N* antennas will be able to provide RSS measurements at the same quality; some will be of higher quality than others. The basic idea is to combine the measurements in such a way that higher-quality measurements have more impact on the final location estimate, while the lower-quality measurements are de-emphasized or excluded from the final location estimate altogether. There are two key questions that need to be answered in this context. First, considering the inhomogeneous nature of the in-body environment, which and how many of these *N* sensors should be used? Second, how should the measurements be combined to give an accurate location estimate? In this paper, we address these questions. To address the first question, we present a systematic analysis of which sensors have the greatest contribution to a high-accuracy location estimate. To the best of our knowledge, this paper represents the first time in open literature that such a systematic analysis has been undertaken. For the second question, we propose a nonlinear analytical model for the RSS measurements, which can be used to estimate the location of the capsule. An analysis of the localization accuracy for the proposed model is also given, on the basis of a computerized 3-D body model. In this study, centroid algorithm was used to calculate the location of the capsule from the RSS measurement data on the human body model. Although the centroid algorithm was used mostly for indoor and WSN positioning operations [23, 24], we used this algorithm for in-body localization.

The rest of this paper is organized as follows. Section 2 gives details of the simulation environment which is used for performance evaluation and details the proposed nonlinear RSS model. Results are presented in Section 3. Section 4 concludes the paper.

2. Methods and procedures

2.1. The simulation environment

In order to evaluate positioning performance within the body, a 3-D voxel model of the human body is required first. For this purpose, 3-D human model obtained from Visible Human Project is used [25]. The 3-D human body model adopted for this study came integrated into the analysis software. This model contains the location of all tissues in the human body as well as all electromagnetic properties of all tissues such as dielectric permittivity and conductivity. Since this study focused on the small intestine region, the organs such as the head, arm and leg were not included in the model in order to reduce simulation time. Figure 2 shows the 3-D voxel model of the whole body and the truncated body model to reduce the simulation time, respectively. To analyze the behavior of the electromagnetic signals in the voxel model, XFDTD™ software from Remcom Inc. was used. This software uses Finite Difference Time Domain (FDTD) techniques to numerically solve Maxwell equations and obtain the electric and magnetic field intensities in the working area by considering material properties and boundary conditions.

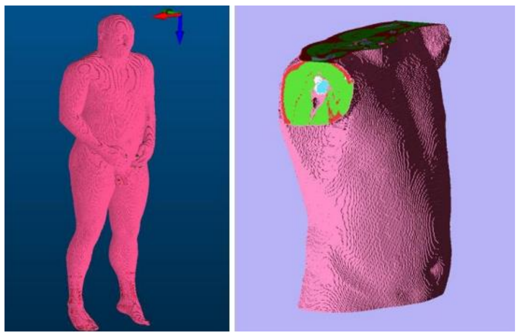

Figure 2. The whole-body model and the truncated body model used at simulations

In order to solve Maxwell's equations numerically, the body model is divided into small parts, or cells. The size of these cells, or cell size, must be calculated based on the smallest wavelength value of the signal.

This constraint, called the Courant limit, is "10 cells per wavelength", meaning that the side of each cell should be $\lambda/10$ or less at the highest frequency (shortest wavelength) of interest [18, 26]. In accordance with the Courant limit, the FDTD cell size used in the simulation was set to 1.2 mm in the x, y and z directions. The Perfectly Matched Layer (PML) boundary condition with 7 absorbing layers was also applied to prevent the reflection of the signals to the body environment. After defining the body model, the elliptic dipole type UWB antenna was placed in the simulation model. This antenna, which measures 20x12x4 mm, consists of two elliptical conductors and a dielectric case that isolates it from the body tissues [27]. A modulated gaussian pulse with center frequency of 4.1 GHz and -10 dB band width of 1.4 GHz was applied to the gap between two ellipses of the antenna. Also, the antenna input impedance was set to 50 ohm and the input power was fixed at 1mW. This applied signal satisfies to the frequency between 3.1 GHz and 4.8 GHz that known as "UWB Low Band" [28]. This band is in a range where signal attenuation is less when compared to the entire UWB band.

In the simulations, the antenna was placed in 64 different positions in the small intestine characterize the electric and magnetic field intensities within this region, as shown in Figure 3. The data for 48 of these 64 antenna position was used to optimize the parameter set for the localization algorithm and the remaining 16 positions were used to test the performance of the algorithm. In Figure 3, red and green antenna positions indicate the training and testing localizations, respectively.

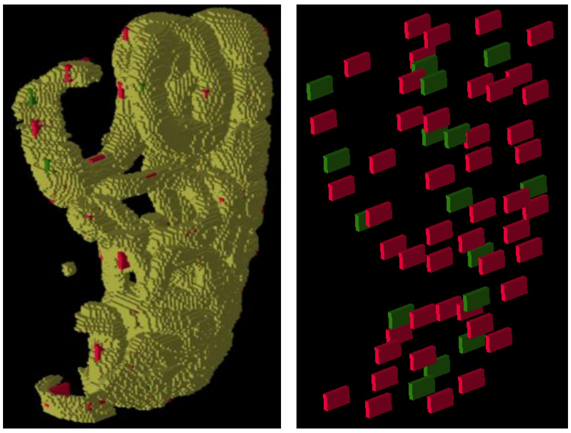

Figure 3. Small intestine in the model, test and train positions of the antenna

In order to determine the position of the wireless capsule within the small intestine, 256 point sensors are defined in the software on the body surface to observe the electric and magnetic field intension. In telecommunications, particularly in radio, signal strength refers to the magnitude of the electric field at a reference point that is at a significant distance from the transmitting antenna. This structure, defined as a point sensor in the program, represents small-size sensors that measure the amplitude and strength of electromagnetic signals in the time domain. As shown in Figure 4, each point sensor is on the body surface and sensors are arranged in 8 rows. The sensors were distributed around the body with 48 sensors on the front side, 80 on the back, 48 on the right side and 48 on the left.

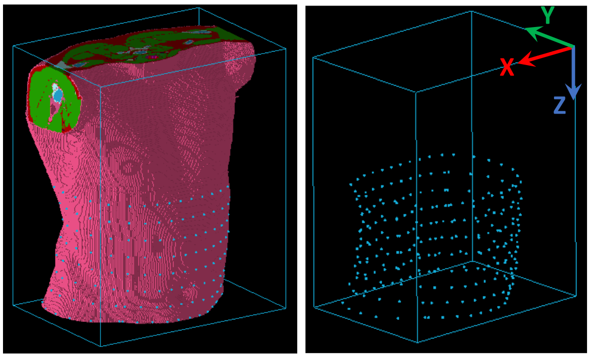

Figure 4. Sensor placement on the body model

Sensors placed on the body were used to calculate the Poynting vector. The Poynting vector, which is the vector cross product of the electric field and magnetic field intensity, is defined as,

$$\mathbf{P}(t) = \mathbf{E}(t) \times \mathbf{H}(t) \tag{1}$$

where $\mathbf{E}(t)$ and $\mathbf{H}(t)$ are the electric and magnetic intensities respectively and both are time dependent. The Poynting vector measured from each sensor gives the power density per unit area (W/m^2). 256 Poynting vectors were calculated in each of the 64 different transmitting antenna positions in the small intestine which resulted 64 x 256=16.384 data sets. The integral of the Poynting vector results in signal energy density (J/m^2) given as,

$$e = \int_t \left|\mathbf{P}(t)\right| dt \tag{2}$$

The energy density values obtained from the sensors were used to determine the position of the wireless capsule in the small intestine. Thus, the antenna position estimation was performed using a RSS-based mathematical model determined in the next section.

2.2. RSS-based in body localization using the centroid algorithm

In RSS-based positioning, energy values measured by the sensors placed on the body and the location of the sensors are used to obtain the localization of the capsule. The centroid algorithm used in positioning calculation has some similarities to the calculation of the center of the gravity for an object [29]. In this model, the energy intensity value measured by all sensors is associated with their location and the energy intensity center is calculated. Later, the position of this center point is determined as the position of the transmitter capsule antenna. In order to derive the RSS based mathematical model, the following template was proposed.

$$\hat{X}_k = \sum_{i=1}^{N} \frac{X_{S_i}\left(E_i\right)^{\alpha_x}}{\left(\sum_{j=1}^{N}\left(E_j\right)^{\alpha_x}\right)},$$
$$\hat{Y}_k = \sum_{i=1}^{N} \frac{Y_{S_i}\left(E_i\right)^{\alpha_y}}{\left(\sum_{j=1}^{N}\left(E_j\right)^{\alpha_y}\right)}, \qquad (3)$$
$$\hat{Z}_k = \sum_{i=1}^{N} \frac{Z_{S_i}\left(E_i\right)^{\alpha_z}}{\left(\sum_{j=1}^{N}\left(E_j\right)^{\alpha_z}\right)}$$

where $\left(\hat{X}_k, \hat{Y}_k, \hat{Z}_k\right)$ are the estimated coordinates of *k-th* transmitting antenna in the small intestine, $\left(X_{S_i}, Y_{S_i}, Z_{S_i}\right)$ are the coordinates of *i-th* sensor on the body, E_i is energy density which computed at Eq. (2) for *i-th* sensor. Also $\boldsymbol{\alpha} = \left[\alpha_x, \alpha_y, \alpha_z\right]$ is defined as exponent that gives nonlinearity for all coordinates and *N* is the total number of sensors with the highest energy used at model. With this model, the position of the antennas in the intestine were estimated by the known positions of the sensors and the energy density values obtained from these sensors.

The energy density values obtained from the point sensors were arranged in order of magnitude for effective localization for each transmit antenna position. Then *N* sensors with the highest energy density values were selected from the sorted data set. Thus, in the estimation of the antenna position, the effect of sensors with higher energy density values were higher, while those with lower energy density were ignored. In addition, the vector of exponents $\boldsymbol{\alpha}$, which model the nonlinear effects of the human body environment on energy density [19], increases the sensitivity of the RSS-based model. There are different types of tissues in the body and the behavior of each one is frequency dependent. This makes the human body extremely nonlinear from the perspective of electromagnetic wave propagation [19]. For this reason, nonlinearity parameter was added to the proposed model and the results were examined. In the next section, the effect of $\boldsymbol{\alpha}$ on positioning accuracy is examined in more detail. The performance of the localization model was evaluated together with range estimation errors. The localization error can be calculated using the following equation:

$$\varepsilon_k = \sqrt{\left(X_k - \hat{X}_k\right)^2 + \left(Y_k - \hat{Y}_k\right)^2 + \left(Z_k - \hat{Z}_k\right)^2} \qquad (4)$$

where $\left(X_k, Y_k, Z_k\right)$ is the real antenna location and ε_k is the localization error of *k-th* antenna location.

3. Results

The results obtained in this article are examined under three main headings. For the best performance, the results for the number of sensors, sensor topology and $\boldsymbol{\alpha}$ parameters are examined. Firstly, how many of the 256 point sensors placed on the body will be used in the positioning calculation is determined. Then, effect of the sensors distributed around the body on the positioning accuracy is examined according to the body region where the sensor is located. Finally, the effect of parameter $\boldsymbol{\alpha}$, described in the previous section, on positioning accuracy was examined. These 3 topics are discussed in detail in this section.

3.1. Effect of the number of sensors

As mentioned in the previous sections, energy values were obtained from 256 point sensors placed on the body surface. At this point, how many of these sensors should be included in the algorithm? In order to find the answer to this question, firstly, the effect of *N* used in the Eq. (3) on the localization error were investigated. While examining the effect of the number of sensors, $\boldsymbol{\alpha}$ was kept constant [1,1,1]. Considering $\boldsymbol{\alpha}$ to be constant is only for the purposes of investigating the effect of the number of sensors (*N*) on localization. The relationship between the number of sensor (*N)* and localization error is presented in Figure 5. Here, the effect of using a variable number of sensors for 64 different capsule positions is examined and the RMS value of 64 capsule localization errors for each *N* value is calculated by Eq. (4).

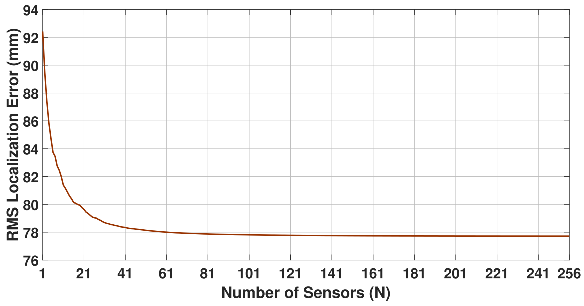

Figure 5. The relationship between number of point sensors (N) and localization error

From Figure 5, it is clearly seen that using a large number of sensors (*N*) does not affect the positioning error after a certain point. There is a 2.6% difference between using 20 sensors and 256 sensors in the model. Therefore, *N*=20 was selected in the following sections to reduce the complexity of the model. On the other hand, another important issue is that the X, Y and Z errors are different in the antenna position estimation. The next question is: what is the reason for these high localization errors? To answer this question coordinate estimation errors are calculated separately and plotted in Figure 6.

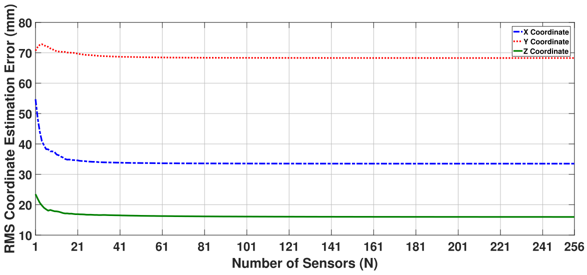

Figure 6. The relationship between number of point sensors (N) and coordinate estimation errors

As seen in Figure 6, the highest contribution to the localization error is from the Y coordinate estimate. When *N* parameter set to 20, the total localization error is 79.77 mm while the X, Y and Z antenna position estimation errors are 34.62 mm, 69.85 mm and 16.89 mm respectively. To improve these results, we have noticed that it is not sufficient to just change the number of sensors, and therefore different processes will be performed for estimating each coordinate of the capsule in the following sections.

3.2. Effect of the selected sensor region

As the localization error was very high in the previous section, we tried to reduce this error with new approaches. In order to determine the location of the capsule in the intestine, the region of the sensors were also taken into account. In other words, the effect of sensors located in different parts of the body on positioning performance has been examined. 4 different regions were examined for 256 sensors distributed around the body. As mentioned in Section 2.1, sensors were distributed around the body with 80 sensors on the front side, 80 on the back, 48 on the right side and 48 on the left as shown in Figure 7.

In this scenario, the objective is to select 20 sensors to be used in positioning calculation only from the specified body regions, not from all sensors around the body. The sensors to be included in the positioning calculation in the relevant regions are selected according to the energy density values. Thus, 20 sensors reporting the highest energy density values are included in the calculation each time. As a result, location estimation is made for 64 different capsule locations and the RMS localization errors obtained are shown in Table 1.

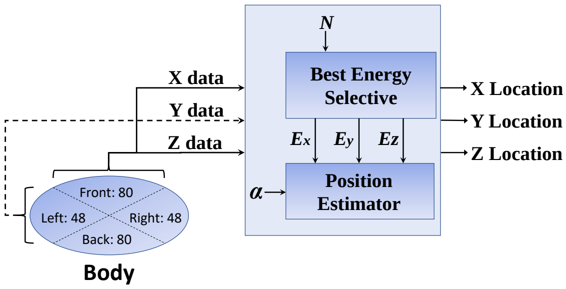

Figure 7. The final localization flow diagram

The results of Table 1 indicate that the body region on which the sensors are placed has a great influence on the positioning error. The bold marked values in the table represent the lowest errors obtained in the relevant coordinate. When the 80 sensors in front of the body are used, the X position error is 15.45 mm and the Z position error is 16.24 mm, which means a 55.4% and 3.8% improvement respectively compared to results presented in Figure 6. Also in case of the 48 sensors on the left side of the body being used, the Y position error is 28.14 mm and this provides a 59.7% improvement. According to the coordinate system given in Figure 4, the Y coordinate gives the depth information towards the inside of the body and the positioning error is higher compared to the X and Z coordinates. This is because the body is not homogeneous, and the sensor spacing and number are not the same in the lateral and anterior planes. On the other hand, it is seen that the Right-side sensors have a negative effect on the calculation of the X position and the Back sensors on the Y, Z positions. As a result, some sensors provide the better results for some coordinates, while they may have a negative impact on the other coordinates. Therefore, using all sensors together doesn't make any sense for localization estimate. The data taken from the sensors which are based on the RSS-based measurement were subjected to a flow diagram as in Figure 7.

The main takeaways from these results so far are as follows. First, it does not make sense to just use all the sensors distributed on the body surface, as they do not all provide measurements at the same quality.

Table 1. Effect of the selected sensor region on the positioning error

Sensor Location	RMS Coordinate Estimation Error			RMS Localization Error (mm)
	X (mm)	Y (mm)	Z (mm)	
Front	**15,45**	85,75	**16,24**	88,63
Left Side	126,90	**28,14**	49,17	138,98
Back	39,50	190,87	78,37	210,08
Right Side	187,02	35,34	59,63	199,45
Front + Left Side	35,34	72,71	16,30	82,47
Front + Right Side	19,24	83,47	16,77	87,29
Front + Back	16,19	79,87	16,93	83,24
Left Side + Right Side	85,31	28,97	36,66	97,27
All	34,62	69,85	16,89	**79,77**

The use of a more limited subset (selected in accordance with the flow diagram of Figure 7 will result in more accurate estimates of the capsule location. Furthermore, it is possible to accomplish this accuracy improvement at a lower overall system cost, as less on-body sensors will now need to be used. Having said that, it is possible to improve the accuracy even further by making adjustments on how the energy readings from the various sensors are incorporated into the final location estimate, as will become clear from the results of the next section.

3.3. The effect of the α parameter

All the data so far has been obtained for $\alpha_x = \alpha_y = \alpha_z = 1$. As previously mentioned, α provides a nonlinear characteristic for the mathematical model. Setting the α parameter to 0 means ignoring the effect of the energy density at the mathematical model. Similarly, making the α parameter 1 means that the energy density will provide a linear effect, making it >1 shows energy density more effective and making it <1 energy density less effective.

Some of the antenna locations to examine the effect of this parameter on the positioning error have been reserved to test the performance of algorithm. As a result, antenna locations have been decomposed for 16 and 48 antennas, as previously described in Section 2.1. Thus, the 16 antenna positions have been used to test the performance of the algorithm and remaining were used to derive the α parameters. For each alpha value, RMS value of error data obtained in 16 different capsule test positions was calculated. The test positions of the capsule were previously shown in Figure 3 (green positions). Figure 8 shows the effect of the parameter α on the individual positioning error for X, Y and Z.

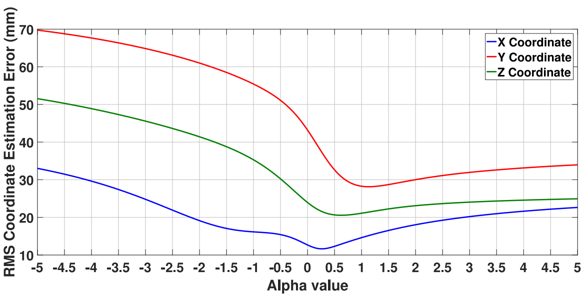

Figure 8. Alpha (α) parameter effect on the coordinate estimation errors for test points

At the Figure 8, it was tried to optimize the value of α between -5 and 5 for the test antenna locations and optimum results were obtained as $\alpha_x = 0.42$, $\alpha_y = 1.20$, $\alpha_z = 0.64$ values. In addition, when the graph was examined in a wider range between -100 and 100, it was seen that the error remained constant at very low or very large values of α.

In order to achieve the final improvement rate, these α values were used at the test locations as shown in Table 2. As a result, the RMS localization errors obtained for the number of N=20 sensors (explained in Section 3.1), the sensors selected from the body regions shown in Figure 7 (explained in Section 3.2) and the calculated optimum α values are given in Table 2.

Table 2. Effect of the ideal α parameters on the positioning error ($\alpha_1 = [1,1,1]$ and $\alpha_2 = [0.42, 1.2, 0.64]$)

Data Type	RMS(mm)		%
	α_1	α_2	Improvement
Train Antenna Loc	35,21	33,15	5,85
Test Antenna Loc.	38,19	36,88	3,43
All Antenna Loc.	35,98	34,12	5,17

From the Table 2, we can obviously find that the inclusion of 3 different alpha parameters in the mathematical model, improvement of 5.85% and 3.43% was obtained for the training and testing antenna locations, respectively. Consequently, maximum RMSE localization error of 36,88 mm has been achieved.

For a different perspective on these results, we can infer from Table 1 in Section 3.2 that, the localization error using all sensors is the 79.77mm. On the other hand, in the case of using Left-side sensors for Y data and Front sensors for X and Z data, the localization error falls to 35.98 mm for all antenna locations. Here, it is clear that a 54.9% improvement in position error of wireless capsule was achieved. Thus, it can be said that the total improvement is 57.2% by including the results obtained in Section 2.2 into the mathematical model.

3.4. Comparison of the proposed algorithm with the classical centroid algorithm

Although the centroid algorithm is frequently used in indoor positioning and WSN (Wireless Sensor Network) scenarios, it is not widely used in in-body localization. It may be instructive to compare the results to other UWB-based localization of the endoscopic capsule in the small intestine operating for the in-body context. Unfortunately, in the course of our literature search, we were unable to find any other works except [30] dealing with UWB-based in-body localization throuh centroid algorithm that would allow a direct comparison. In the [30], the path loss model was used together with the centroid algorithm for positioning, but the effects of body tissues and sensor topology on positioning were not studied. In this respect, our study fills the gap in the literature in terms of both using a realistic human model and providing capsule positioning using the RSS data directly in the centroid algorithm. For these reasons, we compared the proposed centroid algorithm with the classical centroid algorithm used in indoor positioning and examined its performance.

The classical centroid algorithm used in [31, 32] studies

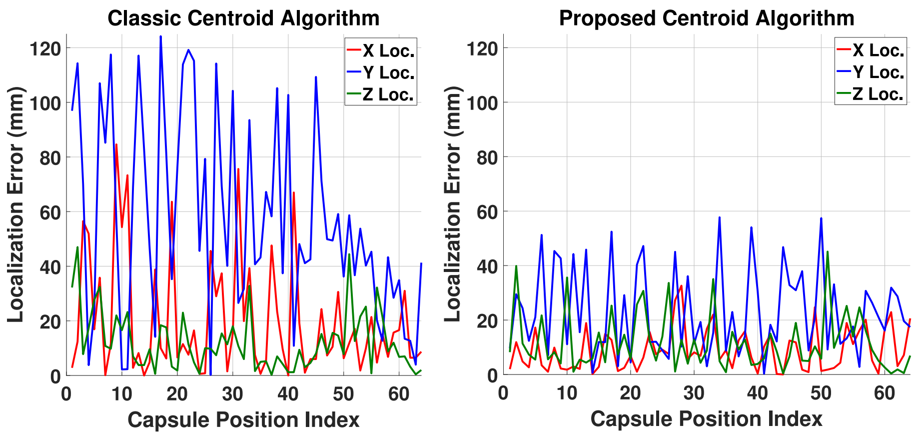

Figure 9. Localization errors of classical and proposed algorithms

is given as in Eq. 5.

$$\hat{X}_k = \sum_{i=1}^{N} \frac{X_{S_i}}{N},\ \hat{Y}_k = \sum_{i=1}^{N} \frac{Y_{S_i}}{N},\ \hat{Z}_k = \sum_{i=1}^{N} \frac{Z_{S_i}}{N} \qquad (5)$$

where N is sensor number, $\left(\hat{X}_k, \hat{Y}_k, \hat{Z}_k\right)$ are the estimated coordinates of *k-th* transmitting antenna, $\left(X_{S_i}, Y_{S_i}, Z_{S_i}\right)$ are the coordinates of *i-th* sensor. This equation basically calculates the average of the positions of N sensors with the best energy value. While comparing the performance with the classical centroid algorithm, the energy density values of 256 sensors around the body were measured for each capsule position, and the positions of the 20 sensors with the strongest energy density were used. As a result, the RMS positioning errors of the proposed centroid algorithm and the classical centroid algorithm for 64 capsule positions are shown in Figure 9. As can be seen in the Figure 9, errors are higher in the classical centroid algorithm. In terms of RMS values of X, Y, and Z localization error, the error values of the proposed centroid algorithm are 59.5%, 58.8% and 3.9% less than classic centroid algorithm, respectively. In another comparison, the cumulative probability function of the distance estimation errors was obtained as in Figure 10.

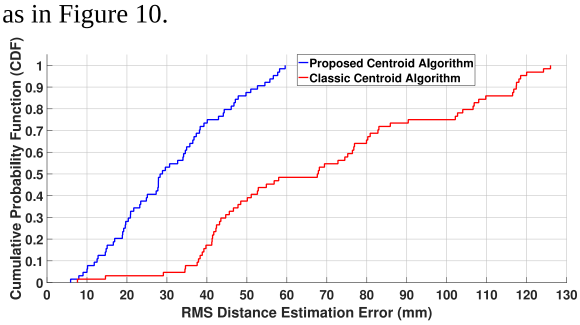

Figure 10. Comparative CDF values of localization errors

When Figure 10 is examined, the distance estimation error of the classical centroid algorithm is much higher, for example, the distance estimation error with 80% probability is below 44mm for the proposed centroid algorithm, while the error in the classical algorithm is below 104mm under the same conditions.

We end this section with comments as to how the techniques outlined in this paper can be applied in practice. If this technique is used in real life, it is possible to localize the capsule that moves within the intestine with a low error with the sensor set physically placed on the body and the simple centroid algorithm. The proposed Centroid algorithm implementation is simple, has low computational load and provides positioning with only energy density measurements. The disadvantage of this algorithm is that if the sensor positions are measured incorrectly, the positioning performance will be greatly reduced.

4. Conclusion

In this paper, we have presented a detailed study on a new RSS-based mathematical model applicable for UWB-based wireless capsule localization in the small intestine. Relationships for the mathematical model parameters, namely the N sensor number, the exponent α and the energy density have been presented. We have used the proposed mathematical model to determine the optimal location and number of the received signal sensors to improve localization accuracy. The results indicate that usage of a large number of sensors distributed all over the body surface has no beneficial impact on positioning accuracy, as all the sensors will not provide measurements at the same quality. Opportunistic deployment of a lesser number of sensors in certain parts of the body (such as the front and left sides of the torso), are seen to result in a reduction of the overall localization error, and will no doubt reduce the overall system-cost. In addition, the performance of the proposed method was compared with the classical centroid algorithm and more than 50% improvement was achieved. These results shed light on precise, cost-effective positioning of the wireless endoscopy capsule in the gastrointestinal tract with a simple RSS technique in the future.

Acknowledgment

The authors would like to acknowledge and thank the Scientific Research Projects Support Office of the Erciyes University, which has supported this work under grant number FDK-2018-7833.

References

[1] Mateen, H., Basar, R., Ahmed, A. U., & Ahmad, M. Y. (2017). Localization of wireless capsule endoscope: A systematic review. *IEEE Sensors Journal*, *17*(5), 1197-1206.

[2] Kumar, R., Zhao, Q., Seshamani, S., Mullin, G., Hager, G., & Dassopoulos, T. (2012). Assessment of crohn's disease lesions in wireless capsule endoscopy images. *IEEE Transactions on Biomedical Engineering*, 59(2), 355-362.

[3] Woods, S.P., & Constandinou, T.G. (2013). Wireless capsule endoscope for targeted drug delivery: Mechanics and design considerations. *IEEE Transactions on Biomedical Engineering* 60(4), 945-953.

[4] Davenport, D., Hernandez, M., Lewis, D., Li, H. B., McPartland, R., Omeni, O., & Astrin, A. (2011). IEEE 802.15. 6 Tutorial. *IEEE P802, 15*.

[5] Yuce, M.R., Keong, H.C., & Chae, M.S. (2009). Wideband communication for implantable and wearable systems. *IEEE transactions on microwave theory and techniques* 57(10), 2597-2604.

[6] Khaleghi, A., Chavez-Santiago, R., & Balasingham, I. (2010). Ultra-wideband pulse-based data communications for medical implants. *IET communications* 4(15), 1889-1897.

[7] Alam, M. W., Vedaei, S. S., & Wahid, K. A. (2020). A fluorescence-based wireless capsule endoscopy system for detecting colorectal cancer. *Cancers*, *12*(4), 890.

[8] Khan, A. H., Sohag, M. H. A., Vedaei, S. S., Mohebbian, M. R., & Wahid, K. A. (2020). Automatic detection of intestinal bleeding using an optical sensor for wireless capsule endoscopy. In *2020 42nd Annual International Conference of the IEEE Engineering in Medicine & Biology Society (EMBC)* (pp. 4345-4348). IEEE.

[9] Deeba, F., Bui, F. M., & Wahid, K. A. (2020). Computer-aided polyp detection based on image enhancement and saliency-based selection. *Biomedical signal processing and control*, *55*, 101530.

[10] Wang, M., Shi, Q., Song, S., Hu, C., & Meng, M. Q. H. (2019). A novel relative position estimation method for capsule robot moving in gastrointestinal tract. *Sensors*, *19*(12), 2746.

[11] Shao, G., Tang, Y., Tang, L., Dai, Q. & Guo, Y. (2019). A Novel Passive Magnetic Localization Wearable System for Wireless Capsule Endoscopy, *IEEE Sensors Journal*, 19(9), 3462-3472.

[12] Than, T.D., Alici, G., Zhou, & H., Li, W. (2012). A review of localization systems for robotic endoscopic capsules. *IEEE Transactions on Biomedical Engineering* 59(9), 2387-2399 .

[13] Pahlavan, K., Geng, Y., Cave, D. R., Bao, G., Mi, L., Agu, E., ... & Tarokh, V. (2015). A novel cyber physical system for 3-D imaging of the small intestine in vivo. *IEEE Access*, 3, 2730-2742.

[14] Wang, Y., Fu, R., Ye, Y., Khan, U., & Pahlavan, K. (2011, January). Performance bounds for RF positioning of endoscopy camera capsules. In *2011 IEEE Topical Conference on Biomedical Wireless Technologies, Networks, and Sensing Systems*, 71-74.

[15] Mao, G., Fidan, B., & Anderson, B.D. (2007). Wireless sensor network localization techniques. *Computer networks* 51(10), 2529-2553.

[16] Achroufene, A., Amirat, Y., & Chibani, A. (2018). RSS-based indoor localization using belief function theory. *IEEE Transactions on Automation Science and Engineering*, *16*(3), 1163-1180.

[17] Gabriel, C., Gabriel, S., & Corthout, Y. E. (1996). The dielectric properties of biological tissues: I. Literature survey. *Physics in medicine & biology*, 41(11), 2231.

[18] Suveren, M. (2015). *Ultra wide band (uwb) wireless systems in implant body area networks and modelling of the distance measurement error.* MSc Master thesis, Erciyes University, Kayseri.

[19] Kanaan, M., & Suveren, M. (2015). A novel frequency-dependent path loss model for ultra wideband implant body area networks. *Measurement* 68, 117-127.

[20] Kanaan, M., & Suveren, M. (2017). In-body ranging with ultra-wideband signals: Techniques and modeling of the ranging error. *Wireless Communications and Mobile Computing*, 2017.

[21] He, F., Man, H., & Wang, W. (2011). Maximal ratio diversity combining enhanced security. *IEEE Communications Letters* 15(5), 509-511.

[22] Alamouti, S. M. (1998). A simple transmit diversity technique for wireless communications. *IEEE Journal on selected areas in communications*, 16(8), 1451-1458.

[23] Liu, Y., Jin, M., & Cui, C. (2010). Modified weighted centroid localization algorithm based on rssi for wsn. *Chinese Journal of Sensors and Actuators* 23(5), 717-721

[24] Pivato, P., Palopoli, L., & Petri, D. (2011). Accuracy of rss-based centroid localization algorithms in an indoor environment. *IEEE Transactions on Instrumentation and Measurement* 60(10), 3451-3460.

[25] Ackerman, M. J., Spitzer, V. M., Scherzinger, A. L., & Whitlock, D. G. (1995). The Visible Human data set: an image resource for anatomical visualization. *Medinfo* 8, 1195-1198.

[26] Kunz, K. S., & Luebbers, R. J. (1993). *The finite difference time domain method for electromagnetics*. CRC press.

[27] Khaleghi, A., & Balasingham, I. (2009). Improving in-body ultra wideband communicationusing near-field coupling of the implanted antenna. *Microwave and Optical Technology Letters* 51(3), 585-589.

[28] Wang, Q., Masami, K., & Wang, J. (2009, September). Channel modeling and BER performance for wearable and implant UWB body area links on chest. In 2009 *IEEE International Conference on Ultra-Wideband* (316-320).

[29] Kaiser, M.J., & Morin, T.L. (1993). Algorithms for computing centroids. *Computers and operations research,* 20(2), 151-165.

[30] Hany, U., Akter, L., & Hossain, F. (2017). Degree-based wcl for video endoscopic capsule localization. *IEEE Sensors Journal,* 17(9), 2904-2916.

[31] Bulusu, N., Heidemann, J., & Estrin, D. (2000). GPS-less low-cost outdoor localization for very small devices. *IEEE personal communications*, *7*(5), 28-34.

[32] Kaur, A., Kumar, P., & Gupta, G. P. (2019). A weighted centroid localization algorithm for randomly deployed wireless sensor networks. *Journal of King Saud University-Computer and Information Sciences*, *31*(1), 82-91.

Memduh Suveren *received his M.S degree in Mechatronics Engineering from Erciyes University in 2015. He has been working as a research assistant in Mechatronics Engineering department since 2011, Erciyes University. His current research interests include Wireless Capsule Endoscopy, Ultra-Wide Band (UWB) signaling, in body localization, Magnetic Capsule localization and Electromagnetic studies.*
http://orcid.org/0000-0003-4545-5378

Rüştü Akay *received the M.S. and the Ph.D. degree in computer engineering from Erciyes University, Kayseri, Turkey, in 2006 and 2014, respectively. Since 2014 he is an Assistant Professor in the Department of Mechatronics Engineering, Erciyes University. His current research interests include evolutionary algorithm, parallel programming, intelligent control systems and their applications.*
http://orcid.org/0000-0002-3585-3332

Muzaffer Kanaan *is an associate professor of mechatronics engineering at Erciyes University, Turkey, where he has worked since 2009. He received his MS degree in electrical and computer engineering from New Jersey Institute of Technology in 1996 and PhD degrees in electrical and computer engineering from Worcester Polytechnic Institute in 2008. Between 1997-2008, he worked as a Distinguished Member of the Technical Staff at Verizon Laboratories in Waltham, MA, where he was responsible for various research and development projects related to wireless and fiber-optic communication. He has 5 U.S. Patents granted, with another two pending. His major research interests include communication and control engineering, wireless communication, with a particular focus on the application of wireless technology in medicine.*
http://orcid.org/0000-0003-4510-8392

An International Journal of Optimization and Control: Theories & Applications
ISSN:2146-0957 eISSN:2146-5703
Vol.12, No.2, pp.160-168 (2022)
http://doi.org/10.11121/ijocta.2022.1263

RESEARCH ARTICLE

Genocchi polynomials as a tool for solving a class of fractional optimal control problems

Haleh Tajadodi[a], Hossein Jafari[b*], Mahluli Naisbitt Ncube[b]

[a] *Department of Mathematics, University of Sistan and Baluchestan, Zahedan, Iran*
[b] *Department of Mathematical Sciences, University of South Africa, UNISA0003, South Africa*
tajadodi@math.usb.ac.ir, jafari.usern@gmail.com, mnncube@gmail.com

ARTICLE INFO

Article History:
Received 1 May 2022
Accepted 24 July 2022
Available 27 July 2022

Keywords:
Fractional derivative
Optimal control problems
Genocchi polynomials
Operational matrix

AMS Classification 2010:
26A33; 49Mxx; 65Dxx

ABSTRACT

In this research, we use operational matrix based on Genocchi polynomials to obtain approximate solutions for a class of fractional optimal control problems. The approximate solution takes the form of a product consisting of unknown coefficients and the Genocchi polynomials. Our main task is to compute the numerical values of the unknown coefficients. To achieve this goal, we apply the initial condition of the problem, the Tau and Lagrange multiplier methods. We do error analysis as a means to study the behaviour of the approximate solutions.

1. Introduction

In the real world, Optimal control problems are concerned with the effective allocation of limited resources, with the main objective of achieving the set goals. A classic example will be how a firm can use the limited budgets or labour hours of its employees with an overall objective of minimizing costs and maximizing revenue.

Fractional optimal control problems (FOCPs) are an extension of the optimal control problems [1–3]. In an optimal control problem, the restrictions are presented as integer order differential equations. On the other hand, in a FOCP, the restrictions are in the form of fractional differential equations.

Thus, optimal control problems are subsets of FOCPs. Imposing specific conditions on an FOCP yields the optimal control problem. As in the fractional and integer order derivatives scenario, there is a general consensus that models formulated from FOCPs capture real world phenomenon more effectively that the models constructed from Optimal control problems. However, one major drawback with FOCPs models is that they are cumbersome to solve. Generally, we solve FOCPs either indirectly or directly. Methods that solve indirectly convert the original problem into a different state, for example into a boundary value problem in Pontryagin's maximum principle. Directly solving an optimal control problem involves approximating its solution numerically.

Polynomials play a crucial role in most numerical methods for approximating differential equations. Some of them that we frequently make use of are, Legendre polynomials [4, 5], Fibonacci polynomials [6], Bernstein polynomials [7], Laguerre polynomials [8], shifted Chebyshev polynomials [9] and Genocchi polynomials [10].

The application of polynomials has also filtered through to the numerical approximation of the

*Corresponding Author

FOPCs. In [11], the authors make of the Legendre orthonormal polynomials to numerically solve FOCPs, they apply the Legendre-Gauss quadratic formula and the Lagrange multiplier method to convert the problem to a system of equations. Agrawal makes use of the fractional integration by parts, variational calculus and the Lagrange multiplier to create Euler-Lagrange equations in a quadratic numerical scheme that approximates the solutions of FOCPs [12].

Sweilam and Al-Ajami apply the Legendre polynomials as they use two different approaches to approximate the solutions of FOCPs [13]. In the first approach, they approximate the necessary optimality conditions associated with the Hamiltonian. Then, in the second approach, they employ the trapezoidal rule and the Rayleigh-Ritz to formulate a system of equations.

Rabiei, Ordokhani and Babolian applied the Bernoulli polynomials together with the Newton iterative method to approximate the solutions of one and two dimensional systems of FOCPs [14]. The same authors used the Boubaker polynomials to approximate FOCPs [15].

This research seeks to make a contribution towards the direct solution of FOCPs. In essence, we approximate the solution of the FOCPs through the use of Gennochi polynomials.

We divide our work into sections that address different aspects of the research. Section two deals with definitions and theorems that lay the necessary mathematical foundation. Section three presents our main results, we concisely describe our suggested numerical scheme. We substantiate our proposed scheme by giving practical examples in section four. Detailed explanations that cover our research findings are provided in the last section.

2. Mathematical framework

This section of the paper lays some mathematical background for the next section. We give some definitions and theorems that will be applied in section three.

Definition 1. *The Genocchi polynomial, $\mathcal{P}_q(t)$, of degree q is defined as,*

$$\mathcal{P}_q(t) = \sum_{d=0}^{q} \binom{q}{d} g_{q-d} t^d, \tag{1}$$

$g_q = 2(1-2^q)\beta_q$, g_q and β_q are Genocchi and Bernoulli numbers respectively.

The Genocchi polynomials exhibit some of the following properties,

(i) $\int_0^1 \mathcal{P}_q(t)\mathcal{P}_a(t)dt = \dfrac{2(-1)^q q! a!}{(a+q)!} g_{a+q},\ q, a \geqslant 1.$

(ii) $\mathcal{P}'_q(t) = q\mathcal{P}_{q-1}(t), \quad q \geqslant 1.$

(iii) $\mathcal{P}_q^{(d)}(t) = \begin{cases} 0 & q \leq d, \\ d!\dbinom{q}{d} g_{q-d}, & q > d. \end{cases}$

(iv) $\mathcal{P}_q(1) + \mathcal{P}_q(0) = 0, \quad q > 1.$

Definition 2. *The Caputo fractional derivative of order γ acting on $x(t)$ is defined as,*

$$D_t^\gamma x(t) = \begin{cases} \frac{1}{\Gamma(q-\gamma)}\int_0^t \frac{x(\tau)}{(t-\tau)^{1+\gamma-q}} d\tau, & q-1 < \gamma < q \\ x^{(q)}(t), & \gamma = q. \end{cases}$$

Theorem 1. *Let $f(t) \in L^2[0,1]$, $\mathcal{P}(t) = [\mathcal{P}_1(t), \mathcal{P}_2(t), \cdots, \mathcal{P}_N(t)]^T$ and $C = [c_1, c_2, \cdots, c_N]^T$, then we can approximate $f(t)$ in the form,*

$$f(t) \approx \sum_{b=0}^{N} \chi_b \mathcal{P}_b(t) = C^T \mathcal{P}(t), \tag{2}$$

with $C = \langle \mathcal{P}(t), \mathcal{P}(t)\rangle^{-1} \langle f(t), \mathcal{P}(t)\rangle$, where $\langle ., . \rangle$ denotes an inner product over the defined interval.

Theorem 2. *Suppose that $\Omega_r = span\{\mathcal{P}_1(t), \mathcal{P}_2(t), \cdots, \mathcal{P}_N(t)\} \subset H = L^2[0,1]$, and $s(t) \in C^{q+1}[0,1]$. If $s_q(t)$ is the best approximation to $s(t)$ out of Ω_r, then an analytical expression for the error can be expressed as,*

$$\| s(t) - s_q(t) \|_2 \leq \frac{\mu}{(q+1)!} \frac{1}{\sqrt{2q+3}}. \tag{3}$$

Where $\mu = max_{t\in[0,1]} \mid s^{(q+1)}(t) \mid$.

Proof. We consider the Taylor series,

$$\begin{aligned} s_1(t) &= s(0) + s'(0)t + s''(0)\frac{t^2}{2!} + \cdots \\ &+ s^{(q)}(0)\frac{t^q}{q!}. \end{aligned} \tag{4}$$

Since $s_q(t)$ is the best approximation of $s(t)$ in Ω_r, we have,

$$\begin{aligned} \| s(t)-s_q(t) \|_2 &\leq \| s(t)-s_1(t) \|_2 \\ &= \left(\int_0^1 \mid s(\tau)-s_1(\tau) \mid^2 d\tau\right)^{\frac{1}{2}} \\ &\leq \left(\int_0^1 \left(\mu \frac{\tau^{q+1}}{(q+1)!}\right)^2 d\tau\right)^{\frac{1}{2}} \\ &\leq \frac{\mu}{(q+1)!}\left(\int_0^1 \tau^{2q+2} d\tau\right)^{\frac{1}{2}} \\ &= \frac{\mu}{(q+1)!}\frac{1}{\sqrt{2q+3}}. \end{aligned}$$

Therefore, we have $\lim_{q\longrightarrow\infty} \| s(t)-s_q(t) \|_2 = 0$. This completes the proof. □

Theorem 3. *Given $\mathcal{P}(t)=[\mathcal{P}_1(t),\mathcal{P}_2(t),\cdots,\mathcal{P}_N(t)]^T$, then the $N\times N$ operational matrix of the derivative D,*

$$\mathcal{P}'(t)=D\mathcal{P}(t), \tag{5}$$

is given as,

$$D=\begin{bmatrix} 0 & 0 & 0 & \dots & 0 & 0 & 0 \\ 2 & 0 & 0 & \dots & 0 & 0 & 0 \\ 0 & 3 & 0 & \dots & 0 & 0 & 0 \\ 0 & 0 & 4 & \dots & 0 & 0 & 0 \\ \vdots & \vdots & \vdots & \dots & \vdots & \vdots & \vdots \\ 0 & 0 & 0 & \dots & N-1 & 0 & 0 \\ 0 & 0 & 0 & \dots & 0 & N & 0 \end{bmatrix}. \tag{6}$$

Corollary 1. *The q^{th} order derivative operational matrix is represented as,*

$$\mathcal{P}^{(q)}(t)=D^q\mathcal{P}(t). \tag{7}$$

Lemma 1. *If $f=1,\dots,\lceil\gamma\rceil-1$, then the derivative of order γ acting on Genocchi polynomials is given as,*

$$D^\gamma\mathcal{P}_f(t)=0, \tag{8}$$

$\lceil\gamma\rceil$ denotes the ceiling of γ, this is the least integer that is greater than γ.

Theorem 4. *The Caputo derivative of $\mathcal{P}(t)$ with order γ can be approximated as,*

$$D^\gamma\mathcal{P}(t)\simeq Z^\gamma\mathcal{P}(t), \tag{9}$$

where Z^γ is called the operational matrix of Caputo derivative based on $\mathcal{P}(t)$.

$$Z^\gamma=\begin{bmatrix} 0 & 0 & \dots & 0 \\ \vdots & \vdots & \dots & \vdots \\ 0 & 0 & \dots & 0 \\ \sum_{d=\lceil\gamma\rceil}^{\lceil\gamma\rceil}\Omega_{\lceil\gamma\rceil,1,d} & \sum_{d=\lceil\gamma\rceil}^{\lceil\gamma\rceil}\Omega_{\lceil\gamma\rceil,2,d} & \dots & \sum_{d=\lceil\gamma\rceil}^{\lceil\gamma\rceil}\Omega_{\lceil\gamma\rceil,N,d} \\ \vdots & \vdots & \dots & \vdots \\ \sum_{d=\lceil\gamma\rceil}^{f}\Omega_{f,1,d} & \sum_{d=\lceil\gamma\rceil}^{f}\Omega_{f,2,d} & \dots & \sum_{d=\lceil\gamma\rceil}^{f}\Omega_{f,N,d} \\ \vdots & \vdots & \dots & \vdots \\ \sum_{d=\lceil\gamma\rceil}^{N}\Omega_{N,1,d} & \sum_{d=\lceil\gamma\rceil}^{N}\Omega_{N,2,d} & \dots & \sum_{d=\lceil\gamma\rceil}^{N}\Omega_{N,N,d} \end{bmatrix} \tag{10}$$

Proof.

$$\begin{aligned} D^\gamma\mathcal{P}_f(t) &= \sum_{k=0}^{f}\frac{i!g_{f-d}}{(f-d)!d!}D^\gamma t^d \\ &= \sum_{d=\lceil\gamma\rceil}^{f}\frac{f!g_{f-d}}{(f-d)!\Gamma(d+1-\gamma)}t^{d-\gamma}, \end{aligned} \tag{11}$$

The term $t^{d-\gamma}$ is approximated in the form of a product that consists of coefficients and Genocchi polynomials,

$$t^{d-\gamma}=\sum_{b=1}^{N}\chi_{b,k}\mathcal{P}_b(t), \qquad d=\lceil\gamma\rceil,\cdots,f \tag{12}$$

Inserting (12) in (11) gives,

$$\begin{aligned} & D^\gamma\mathcal{P}_f(t) \\ = & \sum_{b=1}^{N}\left(\sum_{d=\lceil\gamma\rceil}^{f}\frac{f!g_{f-d}}{(f-d)!\Gamma(d+1-\gamma)}\chi_{b,d}\right) \\ \times & \mathcal{P}_f(t) \\ = & \sum_{b=1}^{N}\left(\sum_{d=\lceil\gamma\rceil}^{f}\Omega_{f,b,d}\right)\mathcal{P}_b(t), \end{aligned} \tag{13}$$

where,

$$\Omega_{f,b,d}=\frac{f!g_{f-d}}{(f-k)!\Gamma(d+1+\eta)}\chi_{b,d}. \tag{14}$$

Eq. (13) can be evaluated into the form,

$$\begin{aligned} & D^\gamma\mathcal{P}_f(t) \\ & = \left[\sum_{d=\lceil\gamma\rceil}^{f}\Omega_{\lceil\gamma\rceil,1,d}\ \sum_{d=\lceil\gamma\rceil}^{f}\Omega_{\lceil\gamma\rceil,2,d}\ \cdots\right. \\ & \left.\sum_{d=\lceil\gamma\rceil}^{f}\Omega_{\lceil\gamma\rceil,N,d}\right]\mathcal{P}(t), \\ & f=\lceil\gamma\rceil,\dots,N. \end{aligned} \tag{15}$$

Applying Lemma 1 and Eq. (15) completes the proof. □

Lemma 2. *If H denotes a Hilbert space and η is an arbitrary element of H, let $V = \{\tau_1, \tau_2, \ldots, \tau_n\}$ be a closed subspace of Hilbert space whose τ_0 is the unique best approximation to η out of V. Then*

$$\|\eta - \tau_0\|^2 = \frac{Gram(\eta, \tau_1, \tau_2, \ldots, \tau_q)}{Gram(\tau_1, \tau_2, \ldots, \tau_q)}, \tag{16}$$

with,

$$Gram(\eta, \tau_1, \tau_2, \ldots, \tau_q) = \begin{vmatrix} \langle \eta, \eta \rangle & \langle \eta, \tau_1 \rangle & \ldots & \langle \eta, \tau_q \rangle \\ \langle \tau_1, \eta \rangle & \langle \tau_1, \tau_1 \rangle & \ldots & \langle \tau_1, \tau_q \rangle \\ \vdots & \vdots & & \vdots \\ \langle \tau_q, \eta \rangle & \langle \tau_q, \tau_1 \rangle & \ldots & \langle \tau_q, \tau_q \rangle \end{vmatrix} \tag{17}$$

Proof. Kreyszig, 1978 [16].

Lemma 3. *If s_N is an approximation of $s \in L^2[0,1]$, then [17],*

$$s(t) \simeq s_N(t) = \sum_{q=1}^{N} s_q \mathcal{P}_q(t), \tag{18}$$

we define,

$$L_N(s) = \int_0^1 [s(t) - s_N(t)]^2 dt, \tag{19}$$

such that,

$$\lim_{N \longrightarrow \infty} L_N(s) = 0 \tag{20}$$

Theorem 5. *The fractional differentiation matrix has an error that is bounded as,*

$$\| W_q^\gamma \| \leq \Big| \sum_{d=\lceil \gamma \rceil}^{f} \frac{f! g_{f-d}}{(f-d)!\Gamma(d+1-\gamma)} \Big| \times \left(\frac{Gram(t^{d-\gamma}, \mathcal{P}_1(t), \ldots, \mathcal{P}_N(t))}{Gram(\mathcal{P}_1(t), \ldots, \mathcal{P}_N(t))} \right)^{\frac{1}{2}} \tag{21}$$

$$W^\gamma = D^\gamma \mathcal{P}(t) - Z^\gamma \mathcal{P}(t), \tag{22}$$

W^γ is composed of individual elements that are represented as,

$$W^\gamma = [W_q^\gamma]_{N \times 1}, \quad q = 1, \cdots, N. \tag{23}$$

Proof. Taking into consideration both Eq. (12) and Lemma 2 yields,

$$\| t^{d-\gamma} - \sum_{b=1}^{N} \chi_{b,d} \mathcal{P}_b(t) \| = \left(\frac{Gram(t^{d-\gamma}, \mathcal{P}_1(t), \ldots, \mathcal{P}_N(t))}{Gram(\mathcal{P}_1(t), \ldots, \mathcal{P}_N(t))} \right)^{\frac{1}{2}}. \tag{24}$$

Therefore, we have

$$\begin{aligned} \| W_q^\gamma \| &= \| D^\gamma \mathcal{P}(t) - Z^\gamma \mathcal{P}(t) \| \\ &\leq \Big| \sum_{d=\lceil \gamma \rceil}^{f} \frac{f! g_{f-d}}{(f-d)!\Gamma(k+1-\gamma)} \Big| \times \| t^{d-\gamma} - \sum_{b=1}^{N} \chi_{b,d} \mathcal{P}_b(t) \| \\ &\leq \Big| \sum_{d=\lceil \gamma \rceil}^{f} \frac{f! g_{f-d}}{(f-d)!\Gamma(d+1-\gamma)} \Big| \times \left(\frac{Gram(x^{d-\gamma}, \mathcal{P}_1(t), \ldots, \mathcal{P}_N(t))}{Gram(\mathcal{P}_1(t), \ldots, \mathcal{P}_N(t))} \right)^{\frac{1}{2}}. \end{aligned} \tag{25}$$

□

3. Methodology

This section constitutes the main results of this research, we discuss the algorithm of our numerical technique.
We attempt to approximate the solution of the problem,

$$min \quad \mathcal{K} = \int_0^1 \mathsf{L}(t, m(t), r(t)) dt, \tag{26}$$

with the system dynamics,

$$A\dot{m}(t) + BD_t^\gamma m(t) = f(t, m(t), r(t)), \quad 0 < \gamma \leq 1, \tag{27}$$

and the initial condition,

$$m(0) = m_0, \tag{28}$$

$A, B \neq m_0$ denote fixed real numbers, $m(t)$ and $r(t)$ are state and control variables respectively.

We express both the state and control variables as a product of coefficients to be computed and Genocchi polynomials,

$$m(t) \simeq M^T\mathcal{P}(t), \tag{29}$$
$$r(t) \simeq R^T\mathcal{P}(t). \tag{30}$$

M^T and R^T are expressed as,

$$M^T = [m_0, \cdots, m_N], \tag{31}$$
$$R^T = [r_0, \cdots, r_N]. \tag{32}$$

Introducing the derivative operator (9) in (29) means,

$$D^\gamma m(t) = X^T Z^\gamma \mathcal{P}(t). \tag{33}$$

Substituting (29) and (30) in (26) gives,

$$min \quad \mathcal{K} \simeq \int_0^1 \mathsf{L}(t, M^T\mathcal{P}(t), R^T\mathcal{P}(t))dt. \tag{34}$$

Substituting (29) and (30) in (27), thereafter applying (5) and (33), we get,

$$\begin{aligned} &AM^T D\mathcal{P}(t) + BM^T Z^\gamma \mathcal{P}(t) \\ &\quad = f(t, M^T\mathcal{P}(t), R^T\mathcal{P}(t)), \quad 0 < \gamma \leq 1. \end{aligned} \tag{35}$$

Substituting (29) in the initial condition (28) gives us,

$$M^T\mathcal{P}(0) = m_0. \tag{36}$$

We note that (36) is an equation with unknowns in M^T.

We deduce the residual $\mathcal{R}(t)$ from (35) as,

$$\begin{aligned} \mathcal{R}(t) \;=\; & AM^T D\mathcal{P}(t) + BM^T Z^\gamma \mathcal{P}(t) \\ & - f(t, M^T\mathcal{P}(t), R^T\mathcal{P}(t)). \end{aligned} \tag{37}$$

We then create a system of $N-1$ equations through the application of the Tau method as,

$$\int_0^1 \mathcal{R}(t)\mathcal{P}_b(t)dt = 0, \quad b = 1, \cdots, N-1. \tag{38}$$

The number of equations from (38) and one equation from (36) are not enough to match the number of unknowns in M^T and R^T. Thus additional equations are required, we will apply the Lagrange multipliers method to come up with more equations.
We state the Lagrange function as,

$$\begin{aligned} \mathcal{K}^*(M, R, \lambda) \;=\; & \int_0^1 \mathsf{L}(t, M^T\mathcal{P}(t), R^T\mathcal{P}(t))dt \\ & + \sum_{b=1}^{N} \lambda_b \int_0^1 \mathcal{R}(t)\mathcal{P}(t)dt, \end{aligned} \tag{39}$$

where $\lambda = [\lambda_1, \cdots, \lambda_N]^T$ are Lagrange multipliers to be determined. Imposing the extremum conditions on (39) yields,

$$\begin{aligned} &\frac{\partial \mathcal{K}^*}{\partial m_b} = 0, \quad \frac{\partial \mathcal{K}^*}{\partial r_b} = 0, \quad \frac{\partial \mathcal{K}^*}{\partial \lambda_b} = 0, \\ &b = 1, \ldots, N-1. \end{aligned} \tag{40}$$

Combining (36), equations from (38) and equations from (40), we get the sufficient number of equations that match the number of unknowns in M^T and R^T. Thus, we are able to approximate $m(t)$ and $r(t)$ in (29) and (30) respectively.

4. Illustrative examples

We support the concepts discussed in the previous section through the solution of problems and some comparison with established solutions.

Example 1. *Consider the following FOCP [11, 18]:*

$$\min \quad \mathcal{K} = \frac{1}{2}\int_0^1 3m^2(t) + r^2(t)dt, \tag{41}$$

subjected to the dynamical system,

$$\begin{aligned} &\frac{1}{4}\dot{m}(t) + \frac{3}{4}D^\gamma m(t) = m(t) - r(t) \\ &m(0) = 1. \end{aligned} \tag{42}$$

If $\gamma = 1$ the solution of (41) is,

$$\begin{aligned} m(t) &= e^{2t}(3+e^4)^{-1}(3+e^{4-4t}) \\ r(t) &= 3e^{2t}(3+e^4)^{-1}(e^{4-4t}-1) \end{aligned} \tag{43}$$

Figure 1 compares (43) with our approximate solution, as γ approaches 1, our approximate solution agrees with (43).
Figure 2, Table 1 and Table 2 display absolute errors under different conditions for Example 1. We realise that as the value of N increases, then accuracy of the proposed scheme improves.

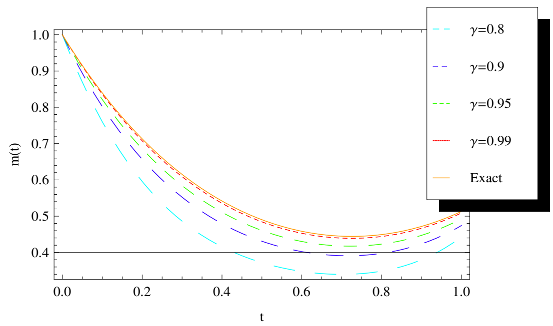

(a) Exact and approximation solutions of $m(t)$.

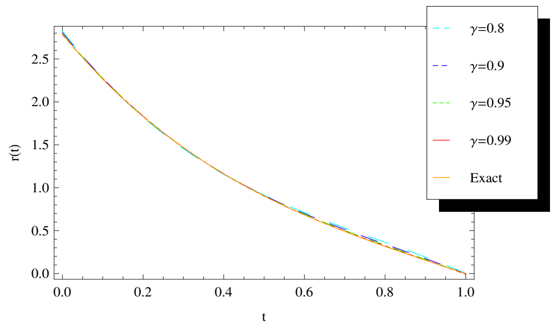

(b) Exact and approximation solutions of $r(t)$.

Figure 1. Exact and approximation solutions of $m(t)$ and $r(t)$ for $N = 5$ in Example 1.

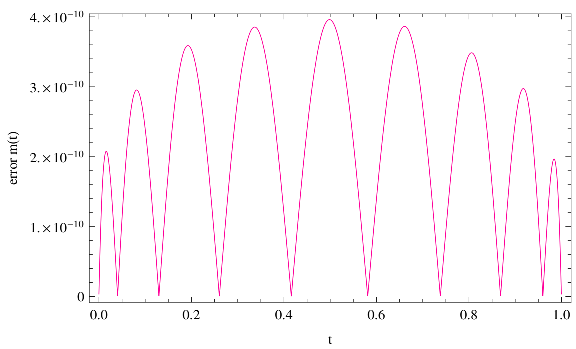

(a) Absolute errors of $m(t)$.

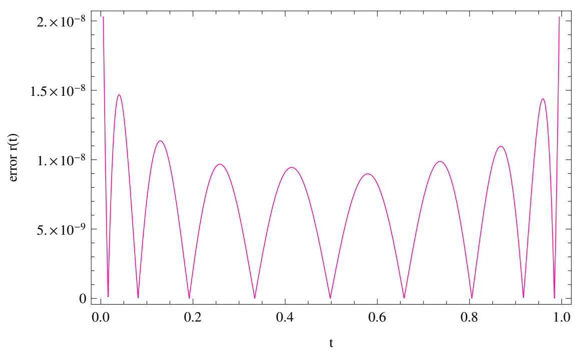

(b) Absolute errors of $r(t)$.

Figure 2. Absolute errors of $m(t)$ and $r(t)$ for $N = 10$ and $\gamma = 1$ for Example 1.

Example 2. *Suppose we have the FOCP [13],*

$$\min \quad \mathcal{K} = \int_0^1 (r(t) - m(t))^2 dt, \tag{44}$$

subjected to the dynamical system and the initial condition,

$$\begin{aligned} \dot{m}(t) + D^{\gamma} m(t) &= r(t) - m(t) + t^3 + \frac{6t^{\gamma+2}}{\Gamma(\gamma+3)} \\ m(0) &= 0, \end{aligned} \tag{45}$$

for $\gamma = 1$,

$$m(t) = r(t) = \frac{t^4}{4} \tag{46}$$

Comparison of (46) with our approximate solution is depicted in Fig. 3. Fig. 4, Table 3 and Table 4 demonstrate the behaviour of absolute errors for Example 2 under different conditions.

As we increase the number of polynomials used for approximation, the accuracy improves.

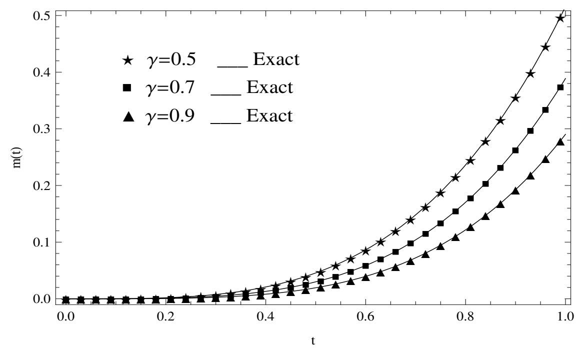

(a) Exact and approximation solutions of $m(t)$.

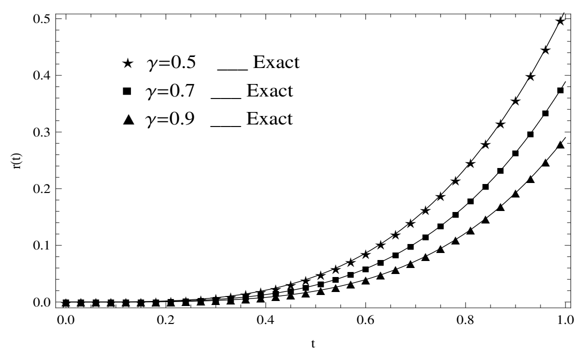

(b) Exact and approximation solutions of $r(t)$.

Figure 3. Exact and approximation solutions of $m(t)$ and $r(t)$ for $N = 5$ in Example 2.

Table 1. The absolute errors of $m(t)$ and $r(t)$ for $\gamma = 1$ for Example 1.

	m(t)			**r(t)**		
t	$N=5$	$N=8$	$N=10$	$N=5$	$N=8$	$N=10$
0.1	1.09006×10^{-4}	9.57294×10^{-8}	2.39863×10^{-10}	2.66755×10^{-3}	2.06794×10^{-16}	7.17614×10^{-9}
0.2	7.93386×10^{-5}	7.4338×10^{-9}	3.53015×10^{-10}	3.68719×10^{-3}	2.9584×10^{-6}	2.04521×10^{-9}
0.3	1.74739×10^{-4}	1.3894×10^{-7}	2.8304×10^{-10}	4.50409×10^{-4}	3.37535×10^{-7}	6.10702×10^{-9}
0.4	1.03393×10^{-4}	1.43259×10^{-8}	1.18485×10^{-10}	2.58382×10^{-3}	2.63025×10^{-6}	9.10892×10^{-9}
0.5	4.98148×10^{-5}	1.44398×10^{-7}	3.95863×10^{-10}	3.31745×10^{-3}	2.17556×10^{-7}	3.87368×10^{-10}
0.6	1.59367×10^{-4}	5.32508×10^{-9}	1.39608×10^{-10}	1.52384×10^{-3}	2.64159×10^{-6}	8.25309×10^{-9}
0.7	1.42128×10^{-4}	1.37905×10^{-7}	2.71924×10^{-10}	1.56668×10^{-3}	8.12583×10^{-8}	7.24176×10^{-9}
0.8	8.67009×10^{-6}	1.38793×10^{-8}	3.45382×10^{-10}	3.62268×10^{-3}	2.86573×10^{-6}	1.20762×10^{-9}
0.9	1.15034×10^{-4}	9.10652×10^{-8}	2.48459×10^{-10}	1.52344×10^{-3}	2.2886×10^{-6}	6.15546×10^{-9}
1	5.31549×10^{-6}	2.62501×10^{-12}	3.58774×10^{-12}	8.3610×10^{-3}	8.96794×10^{-6}	3.51907×10^{-8}

Table 2. Absolute errors of $\mathcal{K}$ at $\gamma = 1$ for Example 1.

N	$N=5$	$N=8$	$N=10$
$\lvert\mathcal{K}-\mathcal{K}_N\rvert$	3.33043×10^{-7}	1.37542×10^{-10}	1.79479×10^{-12}

Table 3. Absolute errors of J at $N = 5$ for different values of γ in Example 2.

	$\gamma=0.5$		$\gamma=0.7$		$\gamma=0.9$	
t	$N=5$	$N=8$	$N=5$	$N=8$	$N=5$	$N=8$
0.1	8.67932×10^{-5}	1.77534×10^{-6}	6.01988×10^{-5}	8.3122×10^{-7}	2.14671×10^{-5}	1.89079×10^{-7}
0.2	7.09407×10^{-5}	6.42261×10^{-7}	4.44603×10^{-5}	2.73675×10^{-7}	1.36285×10^{-5}	5.31956×10^{-8}
0.3	1.45414×10^{-4}	1.58479×10^{-6}	9.8158×10^{-5}	7.62797×10^{-7}	3.35696×10^{-5}	1.81782×10^{-7}
0.4	8.61693×10^{-5}	8.70422×10^{-7}	6.18471×10^{-5}	3.98654×10^{-7}	2.30861×10^{-5}	8.21489×10^{-8}
0.5	3.89408×10^{-5}	1.54044×10^{-6}	2.20596×10^{-5}	7.4929×10^{-7}	5.01391×10^{-6}	1.77558×10^{-7}
0.6	1.31492×10^{-3}	5.31372×10^{-7}	8.71043×10^{-5}	2.32235×10^{-7}	2.84443×10^{-5}	4.25814×10^{-8}
0.7	1.20904×10^{-4}	1.43896×10^{-6}	8.32356×10^{-5}	6.87549×10^{-7}	2.92973×10^{-5}	1.60014×10^{-7}
0.8	7.05935×10^{-6}	5.49734×10^{-7}	7.62429×10^{-6}	2.54608×10^{-7}	5.06112×10^{-6}	4.81956×10^{-8}
0.9	1.06771×10^{-4}	7.65855×10^{-7}	7.06895×10^{-5}	3.60429×10^{-7}	2.22565×10^{-5}	8.56972×10^{-8}
1	1.2497×10^{-5}	6.52598×10^{-8}	9.58809×10^{-6}	3.49445×10^{-8}	1.64419×10^{-6}	2.96755×10^{-9}

Table 4. Absolute errors of $\mathcal{K}$ at $N = 5$ for different values of γ in Example 2.

N	$\gamma=0.5$	$\gamma=0.7$	$\gamma=0.9$	$\gamma=1$
$\lvert\mathcal{K}-\mathcal{K}_N\rvert$	2.25994×10^{-31}	4.99374×10^{-30}	9.95394×10^{-32}	1.44241×10^{-31}

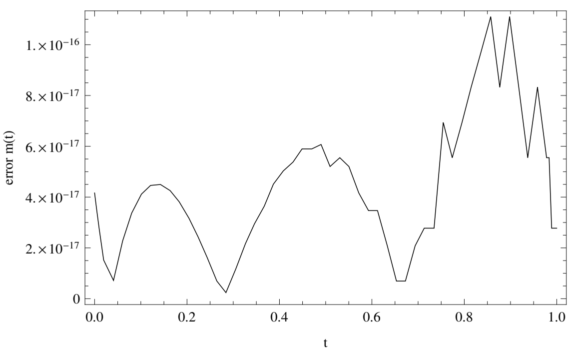

(a) Absolute errors of $m(t)$.

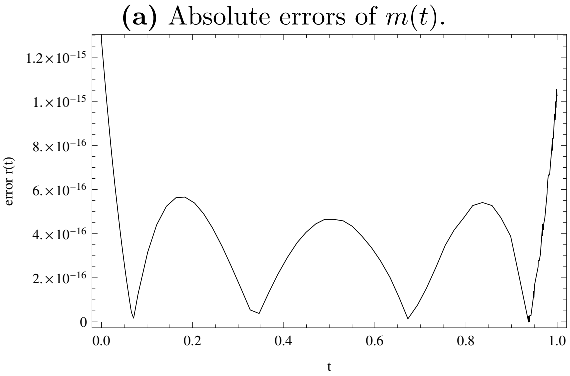

(b) Absolute errors of $r(t)$.

Figure 4. Absolute errors of $m(t)$ and $r(t)$ for $N = 5$ and $\gamma = 1$ for Example 2.

Example 3. *We intend to approximate the solution of the FOCP [14],*

$$\min \quad \mathcal{K} = \int_0^1 (m_1(t) - 1 - t^{\frac{3}{2}})^2 + (m_2(t) - 1 - t^{\frac{5}{2}})^2 + (r(t) - 0.75\pi^{\frac{1}{2}} + t^{\frac{5}{2}})^2 dt, \tag{47}$$

restricted to the conditions,

$$\dot{m}_1(t) + D^{0.5} m_1(t) = m_2(t) + r(t) + \frac{3}{2}\sqrt{t}, \tag{48}$$
$$\dot{m}_2(t) + D^{0.5} m_2(t) = \frac{5}{2} m_1(t) + \frac{15\sqrt{\pi}}{16} t^2 - \frac{5}{2},$$
$$m_1(0) = 0, \quad m_2(0) = 0,$$

whose exact solution is,

$$\begin{aligned} m_1(t) &= 1 + t^{\frac{3}{2}}, \\ m_2(t) &= \sqrt{t^5}, \\ r(t) &= \frac{15\sqrt{\pi}}{4} t - \sqrt{t^5}. \end{aligned} \tag{49}$$

Graphical comparisons of our approximate solution and (49) is depicted in Fig. 5 and fig. 6.

The absolute errors between (49) and the approximate solution are displayed in Table 5 and Table 6. Generally, the accuracy of the approximate solution improves with increasing N.

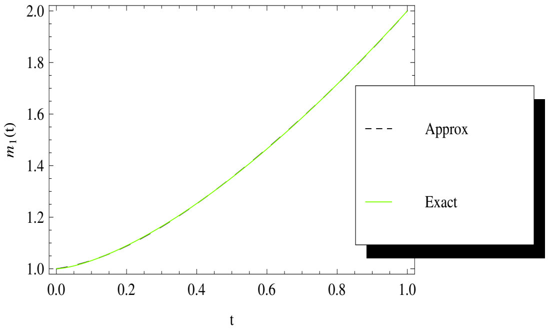

(a) Exact and approximation solutions of $m(t)$.

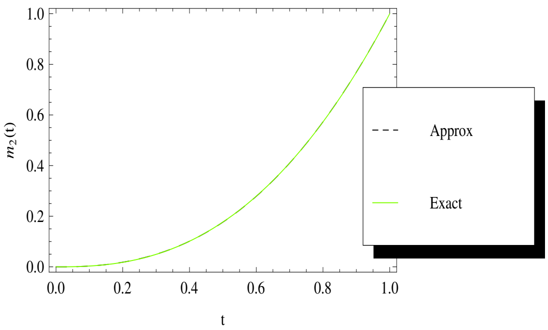

(b) Exact and approximation solutions of $r(t)$.

Figure 5. Exact and approximation solutions of $m_1(t)$ and $m_2(t)$ for $N = 5$ in Example 3.

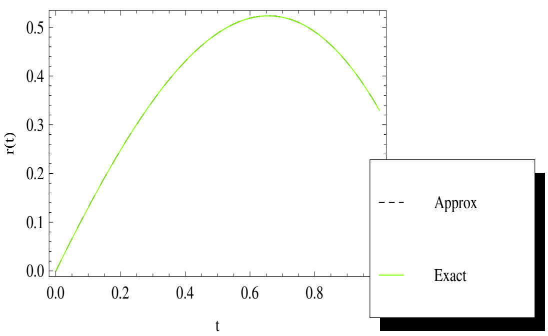

Figure 6. Exact and approximation solutions of $r(t)$ for $N = 5$ in Example 3.

5. Conclusion

We demonstrated how to apply the Genocchi polynomials in the approximation of FOCPs. The developed technique proved to give accurate and consistent results for both the state and control variables. Computed errors between our approximate solutions and the analytical solutions of specific problems were negligible, proving the accuracy of our suggested scheme. Even though the main purpose of this research was on optimal control problems of fractional order, imposing appropriate conditions on our solutions to fit that of integer order gave expected results, confirming the reliability of our approach. In light of the results emanating from this work, we are of the view that it is a worthwhile adventure to pursue the use of other polynomials in optimal control problems.

References

[1] Grzesikiewicz, W., Wakulicz, A. & Zbiciak, A. (2013). Nonlinear problems of fractional calculus in modeling of mechanical systems, *Int. J. Mech. Sci.*, 70(1), 90-98.

[2] Shah, Z., Bonyah, E., Alzahrani, E., Jan, R.& Alreshidi, N. A. (2022). Chaotic Phenomena and Oscillations in Dynamical Behaviour of Financial System via Fractional Calculus, *Complexity*, 2022, Article ID 8113760, 14 pages.

[3] Nortey, S.N., Juga, M. & Bonyah, E. (2021). Fractional order modelling of Anthrax-Listeriosis coinfection with nonsingular Mittag-Leffler law. *Scientific African*, 16, e01221.

[4] Doha, E.H., Bhrawy, A.H. & Ezz-Eldien, S.S. (2015). An efficient Legendre spectral tau matrix formulation for solving fractional subdiffusion and reaction subdiffusion equations, *J. Comput. Nonlinear Dyn.*, 10(2), 021019.

[5] Bhrawy, A., Doha, E., Ezz-Eldien, S.S. & Abdelkawy, M. (2016). A numerical technique based on the shifted Legendre polynomials for solving the time-fractional coupled KdV equations. *Calcolo*, 53, 1-17.

[6] Abd-Elhameed, W.M. & Youssri, Y.H. (2016). A novel operational matrix of Caputo fractional derivatives of Fibonacci polynomials: Spectral solutions of fractional differential equations, *Entropy*, 18, 345.

[7] Kadkhoda, N. (2020). A numerical approach for solving variable order differential equations using Bernstein polynomials, *Alexandria Engineering Journal*, 59(5), 3041-3047.

[8] Gürbüz, B. & Sezer, M. (2016). Laguerre polynomial solutions of a class of initial and boundary value problems arising in science and engineering fields. *Acta Phys. Pol.*, 130, 194-197.

[9] Sweilam, N., Nagy, A. & El-Sayed, A.A. (2016). On the numerical solution of space fractional order diffusion equation via shifted Chebyshev polynomials of the third kind, *J. King Saud Univ. Sci.*, 28, 41-47.

[10] Rigi, F. & Tajadodi, H. (2019). Numerical Approach of Fractional Abel Differential

Table 5. Absolute errors of J at $N = 5$ for different values of γ in Example 3.

	$\gamma = 0.5$		$\gamma = 0.7$		$\gamma = 0.9$	
t	$N = 5$	$N = 8$	$N = 5$	$N = 8$	$N = 5$	$N = 8$
0.1	6.82149×10^{-4}	1.42924×10^{-4}	3.77116×10^{-5}	1.47412×10^{-6}	2.9760×10^{-4}	1.45935×10^{-5}
0.2	1.3244×10^{-3}	1.83017×10^{-4}	3.27293×10^{-4}	8.71204×10^{-6}	1.31524×10^{-5}	1.67875×10^{-6}
0.3	1.52515×10^{-3}	6.9459×10^{-5}	3.0291×10^{-4}	1.57391×10^{-5}	1.99801×10^{-4}	2.93186×10^{-7}
0.4	4.62929×10^{-4}	1.2989×10^{-4}	2.04439×10^{-5}	9.14772×10^{-6}	1.73188×10^{-4}	8.39681×10^{-6}
0.5	7.85417×10^{-4}	8.84718×10^{-5}	3.58353×10^{-4}	1.12922×10^{-5}	1.98335×10^{-5}	4.46794×10^{-6}
0.6	1.3727×10^{-3}	9.80591×10^{-5}	4.62719×10^{-4}	1.49544×10^{-6}	9.6854×10^{-5}	2.31929×10^{-7}
0.7	9.56508×10^{-4}	9.28018×10^{-5}	2.35876×10^{-4}	2.50712×10^{-5}	7.70024×10^{-5}	1.72475×10^{-6}
0.8	1.72911×10^{-4}	3.6848×10^{-5}	2.02618×10^{-4}	8.3339×10^{-6}	4.89367×10^{-5}	1.97021×10^{-6}
0.9	1.02372×10^{-3}	9.84388×10^{-5}	4.72812×10^{-4}	3.47823×10^{-6}	7.70153×10^{-5}	2.24429×10^{-6}
1	1.38385×10^{-4}	2.55125×10^{-5}	9.54884×10^{-5}	9.76438×10^{-6}	4.00056×10^{-4}	1.04777×10^{-5}

Table 6. Absolute errors of $\mathcal{K}$ for different values of N in Example 3.

N	$N = 5$	$N = 8$	$N = 10$
$\lvert\mathcal{K} - \mathcal{K}_N\rvert$	1.1802×10^{-6}	4.14576×10^{-7}	2.84016×10^{-8}

Equation by Genocchi Polynomials, *International Journal of Applied and Computational Mathematics*, 5 (5), 134.

[11] Ezz-Eldien, SS., Doha, EH. & Baleanu, D. (2017). Bhrawy, AH., A numerical approach based on Legendre orthonormal polynomials for numerical solutions of fractional optimal control problems, *Journal of Vibration and Control*, 23(1), 16-30.

[12] Agrawal O.P. (2008). A quadratic numerical scheme for fractional optimal control problems, *Journal of Dynamic Systems, Measurement, and Control*, 130(1), 1-11.

[13] Sweilam, N.H. & Alajmi, T.M. (2015). Legendre spectral collocation method for solving some type of fractional optimal control problem, *J. Adv. Res.*, 6, 393-403.

[14] Rabiei, K., Ordokhani, Y. & Babolian, E. (2018). Numerical Solution of 1D and 2D Fractional Optimal Control of System via Bernoulli Polynomials, *Int. J. Appl. Comput. Math.*, 4(7).

[15] Rabiei, K., Ordokhani, Y. & Babolian, E. (2016). The Boubaker polynomials and their application to solve fractional optimal control problems, *Nonlinear Dyn.*, 88, 1013-1026.

[16] Kreyszig, E. (1978). *Introductory Functional Analysis with Applications*, New York: John Wiley and sons. Inc.

[17] Rivlin T.J. (1981). *An Introduction to the Approximation of Functions*, Dover Publications, New York.

[18] Rakhshan, S.A., Effati S. & Kamyad, A.V. (2016). Solving a class of fractional optimal control problems by the Hamilton-Jacobi-Bellman equation, *Journal of Vibration and Control*, 24 (9), 1-16.

Haleh Tajadodi *is an assistant professor in Department of Mathematics, University of Sistan and Baluchestan, Zahedan, Iran. Her research interests include: fractional differential equations, variational problems, approximation theory and iterative methods.*
https://orcid.org/0000-0001-8369-3698

Hossein Jafari *is a full professor in applied Mathematics. His research interests include: Biomathematics, fractional differential equations, Lie Symmetry and approximation methods.*
https://orcid.org/0000-0001-6807-6675

Mahluli Naisbitt Ncube *is a Ph.D. scholar at the Department of Mathematical Sciences, University of South Africa.*
https://orcid.org/0000-0001-5060-8645

An International Journal of Optimization and Control: Theories & Applications
ISSN:2146-0957 eISSN:2146-5703
Vol.12, No.2, pp.169-183 (2022)
http://doi.org/10.11121/ijocta.2022.1112

RESEARCH ARTICLE

A new generalization of Rhoades' condition

Nihal Taş, Nihal Özgür*

Department of Mathematics Balıkesir University, Turkey
nihaltas@balikesir.edu.tr, nihal@balikesir.edu.tr

ARTICLE INFO

Article History:
Received 14 September 2021
Accepted 30 March 2022
Available 27 July 2022

Keywords:
S-metric space
S-normed space
Fixed point theorem
Rhoades'condition

AMS Classification 2010:
54E35; 54E40; 54E45; 54E50

ABSTRACT

In this paper, our aim is to obtain a new generalization of the well-known Rhoades' contractive condition. To do this, we introduce the notion of an S-normed space. We extend the Rhoades' contractive condition to S-normed spaces and define a new type of contractive conditions. We support our theoretical results with necessary illustrative examples.

1. Introduction

Metric fixed point theory is important to find some applications in many areas such as topology, analysis, differential equations etc. So different generalizations of metric spaces were studied (see [1], [2], [3], [4], [5], [6] and [7]). For example, Mustafa and Sims introduced a new notion of "G-metric space" [6]. Mohanta proved some fixed point theorems for self-mappings satisfying some kind of contractive type conditions on complete G-metric spaces [5].

Recently Sedghi, Shobe and Aliouche have defined the concept of an S-metric space in [7] as follows:

Definition 1. *[7] Let X be a nonempty set and $\mathcal{S} : X \times X \times X \to [0,\infty)$ be a function satisfying the following conditions for all $x, y, z, a \in X$:*

(S1) $\mathcal{S}(x,y,z) = 0$ *if and only if* $x = y = z$,

(S2) $\mathcal{S}(x,y,z) \leq \mathcal{S}(x,x,a)+\mathcal{S}(y,y,a)+\mathcal{S}(z,z,a)$.

Then $\mathcal{S}$ is called an S-metric on X and the pair $(X,\mathcal{S})$ is called an S-metric space.

Let (X,d) be a complete metric space and T be a self-mapping of X. In [8], T is called a Rhoades' mapping if the following condition is satisfied:

$$\textbf{(R25)} \quad d(Tx,Ty) < \max\{d(x,y), d(x,Tx), d(y,Ty), d(x,Ty), d(y,Tx)\},$$

for each $x, y \in X$, $x \neq y$. Any fixed point result was not given for a Rhoades' mapping in [8]. Since then, many fixed point theorems were obtained by several authors for a Rhoades' mapping (see [9], [10] and [11]). Furthermore, the Rhoades' condition was extended on S-metric spaces and new fixed point results were presented (see [12], [13] and [14]). Now we recall the Rhoades' condition on an S-metric space.

Let $(X,\mathcal{S})$ be an S-metric space and T be a self-mapping of X. In [12] and [14], the present authors defined Rhoades' condition **(S25)** on $(X,\mathcal{S})$ as follows:

$$\textbf{(S25)} \quad \mathcal{S}(Tx,Tx,Ty) < max\{\mathcal{S}(x,x,y), \mathcal{S}(Tx,Tx,x), \mathcal{S}(Ty,Ty,y), \mathcal{S}(Ty,Ty,x), \mathcal{S}(Tx,Tx,y)\},$$

for each $x, y \in X$, $x \neq y$.

*Corresponding Author

In this paper, to obtain a new generalization of the Rhoades' condition, we introduce the notion of an S-normed space. We give some basic concepts and topological definitions related to an S-norm. Then, we study a new form of Rhoades' condition (**R25**) on S-normed spaces and obtain a fixed point theorem. In Section 2, we introduce the definition of an S-norm on X and investigate some basic properties which are needed in the sequel. We investigate the relationships among an S-norm and other known concepts by counter examples. In Section 3, we define Rhoades' condition (**NS25**) on an S-normed space. We study a fixed point theorem using the condition (**NS25**) and the notions of reflexive S-Banach space, S-normality, closure property and convexity. In Section 4, we investigate some comparisons on S-normed spaces such as the relationships between the conditions (**NR25**) and (**NS25**).

2. S-normed spaces

In this section, we introduce the notion of an S-normed space and investigate some basic concepts related to an S-norm. We study the relationships between an S-metric and an S-norm (resp. an S-norm and a norm).

Definition 2. *Let X be a real vector space. A real valued function $\|.,.,.\| : X \times X \times X \to \mathbb{R}$ is called an S-norm on X if the following conditions hold:*

(**NS1**) $\|x,y,z\| \geq 0$ *and* $\|x,y,z\| = 0$ *if and only if* $x = y = z = 0$,

(**NS2**) $\|\lambda x, \lambda y, \lambda z\| = |\lambda| \|x,y,z\|$ *for all* $\lambda \in \mathbb{R}$ *and* $x,y,z \in X$,

(**NS3**) $\|x + x', y + y', z + z'\| \leq \|0,x,z'\| + \|0,y,x'\| + \|0,z,y'\|$ *for all* $x,y,z,x',y',z' \in X$.

The pair $(X, \|.,.,.\|)$ is called an S-normed space.

Example 1. *Let $X = \mathbb{R}$ and $\|.,.,.\| : X \times X \times X \to \mathbb{R}$ be the function defined by*

$$\|x,y,z\| = |x| + |y| + |z|,$$

for all $x,y,z \in X$. Then $(X, \|.,.,.\|)$ is an S-normed space. Indeed, we show that the function $\|.,.,.\|$ satisfies the conditions (**NS1**)*,* (**NS2**) *and* (**NS3**)*.*

(**NS1**) *By the definition, clearly we have $\|x,y,z\| \geq 0$ for all $x,y,z \in X$. If $\|x,y,z\| = |x| + |y| + |z| = 0$, we obtain $x = y = z = 0$.*

(**NS2**) *Let $x,y,z \in X$ and $\lambda \in \mathbb{R}$. Then we have*

$$\begin{aligned}\|\lambda x, \lambda y, \lambda z\| &= |\lambda x| + |\lambda y| + |\lambda z| \\ &= |\lambda| |x| + |\lambda| |y| + |\lambda| |z| \\ &= |\lambda| (|x| + |y| + |z|) \\ &= |\lambda| \|x,y,z\|.\end{aligned}$$

(**NS3**) *Let $x,y,z,x',y',z' \in X$. Then we obtain*

$$\begin{aligned}\|x+x', y+y', z+z'\| &= |x+x'| + |y+y'| \\ &+ |z+z'| \\ &\leq |x| + |x'| + |y| + |y'| \\ &+ |z| + |z'| \\ &\leq |0| + |x| + |z'| \\ &+ |0| + |y| + |x'| \\ &+ |0| + |z| + |y'| \\ &= \|0,x,z'\| + \|0,y,x'\| \\ &+ \|0,z,y'\|.\end{aligned}$$

Consequently, the function $\|.,.,.\|$ satisfies the conditions (**NS1**)*,* (**NS2**)*,* (**NS3**) *and so $(X, \|.,.,.\|)$ is an S-normed space.*

Now, we show that every S-norm generates an S-metric.

Proposition 1. *Let $(X, \|.,.,.\|)$ be an S-normed space. Then the function $\mathcal{S} : X \times X \times X \to [0, \infty)$ defined by*

$$S(x,y,z) = \|x-y, y-z, z-x\| \qquad (1)$$

is an S-metric on X.

Proof. Using the condition (**NS1**), it can be easily seen that the condition (**S1**) is satisfied. We show that the condition (**S2**) is satisfied. By (**NS3**), we have

$$\begin{aligned}S(x,y,z) &= \|x-y, y-z, z-x\| \\ &= \left\| \begin{array}{c} x-a+a-y, y-a+a-z \\ , z-a+a-x \end{array} \right\| \\ &\leq \|0, x-a, a-x\| + \|0, y-a, a-y\| \\ &+ \|0, z-a, a-z\| \\ &= S(x,x,a) + S(y,y,a) + S(z,z,a),\end{aligned}$$

for all $x,y,z,a \in X$.

Then, the function $\mathcal{S}$ is an S-metric and the pair (X, S) is an S-metric space. $\square$

We call the S-metric defined in (1) as the S-metric generated by the S-norm $\|.,.,.\|$ and denoted by $S_{\|.\|}$.

Corollary 1. *Every S-normed space is an S-metric space.*

Example 2. *Let X be a nonempty set, (X,d) be a metric space and $\mathcal{S}: X\times X\times X\to[0,\infty)$ be the function defined by*

$$\mathcal{S}(x,y,z)=d(x,y)+d(x,z)+d(y,z),$$

for all $x,y,z\in X$. Then the function $\mathcal{S}$ is an S-metric on X [7].
Let $X=\mathbb{R}$. If we consider the usual metric d on X, we obtain the S-metric $\mathcal{S}$ defined as

$$\mathcal{S}(x,y,z)=|x-y|+|x-z|+|y-z|,$$

for all $x,y,z\in\mathbb{R}$. Using Proposition 1, we see that $\mathcal{S}$ is generated by the S-norm defined in Example 1. Indeed, we have

$$\begin{aligned} S(x,y,z) &= \|x-y,y-z,z-x\| \\ &= |x-y|+|y-z|+|z-x| \\ &= |x-y|+|x-z|+|y-z| \\ &= d(x,y)+d(x,z)+d(y,z), \end{aligned}$$

for all $x,y,z\in X$.

Lemma 1. *An S-metric $\mathcal{S}$ generated by an S-norm on an S-normed space X satisfies the following conditions*

(1) $\mathcal{S}(x+a,y+a,z+a)=\mathcal{S}(x,y,z)$,
(2) $\mathcal{S}(\lambda x,\lambda y,\lambda z)=|\lambda|\,\mathcal{S}(x,y,z)$,

for each $x,y,z,a\in X$ and every scalar λ.

Proof. The proof follows easily from the Proposition 1. □

We note that every S-metric can not be generated by an S-norm as we have seen in the following example:

Example 3. *Let X be a nonempty set and the function $S: X\times X\times X\to[0,\infty)$ be defined by*

$$S(x,y,z)=\begin{cases} 0 \; ; & \text{if } x=y=z \\ 1 \; ; & \text{otherwise} \end{cases},$$

for all $x,y,z\in X$. Then the function $\mathcal{S}$ is an S-metric on X. We call this S-metric is the discrete S-metric on X. The pair (X,S) is called discrete S-metric space. Now, we prove that this S-metric can not be generated by an S-norm. On the contrary, we assume that this S-metric is generated by an S-norm. Then the following equation should be satisfied :

$$S(x,y,z)=\|x-y,y-z,z-x\|,$$

for all $x,y,z\in X$.
If we consider the case $x=y\neq z$ and $|\lambda|\neq 0,1$ then we obtain

$$\begin{aligned} &S(\lambda x,\lambda y,\lambda z) \\ &=\|0,\lambda(y-z),\lambda(z-x)\|=1 \\ &\neq|\lambda|\,S(x,y,z) \\ &=|\lambda|\,\|0,y-z,z-x\|=|\lambda|, \end{aligned}$$

which is a contradiction with (**NS2**). *Consequently, this S-metric can not be generated by an S-norm.*

We use the following result in the next section.

Lemma 2. *Let $(X,\|.,.,.\|)$ be an S-normed space. We have*

$$\|0,x-y,y-x\|=\|0,y-x,x-y\|,$$

for each $x,y\in X$.

Proof. By the condition (**NS3**), we get

$$\begin{aligned} \|0,x-y,y-x\| &\leq \|0,0,0\|+\|0,0,0\| \\ +\|0,y-x,x-y\| &= \|0,y-x,x-y\| \end{aligned} \tag{2}$$

and

$$\begin{aligned} \|0,y-x,x-y\| &\leq \|0,0,0\|+\|0,0,0\| \\ +\|0,x-y,y-x\| &= \|0,x-y,y-x\|. \end{aligned} \tag{3}$$

Using (2) and (3) we obtain $\|0,x-y,y-x\|=\|0,y-x,x-y\|$. □

We recall the definition of a norm on X as follows.
Let X be a real vector space. A real valued function $\|.\|: X\to\mathbb{R}$ is called a norm on X if the following conditions hold:

(**N1**) $\|x\|\geq 0$ for all $x\in X$.
(**N2**) $\|x\|=0$ if and only if $x=0$ for all $x\in X$.
(**N3**) $\|\lambda x\|=|\lambda|\,\|x\|$ for all $\lambda\in\mathbb{R}$ and $x\in X$.
(**N4**) $\|x+y\|\leq\|x\|+\|y\|$ for all $x,y\in X$.

The pair $(X,\|.\|)$ is called a normed space.
We show that every norm generates an S-norm. We give the following proposition.

Proposition 2. *Let $(X,\|.\|)$ be a normed space and the function $\|.,.,.\|: X\times X\times X\to\mathbb{R}$ be defined by*

$$\|x,y,z\|=\|x\|+\|y\|+\|z\|, \tag{4}$$

for all $x, y, z \in X$. Then $(X, \|.,.,.\|)$ is an S-normed space.

Proof. We show that the function $\|.,.,.\|$ defined in (4) satisfies the conditions (**NS1**), (**NS2**) and (**NS3**).
(**NS1**) It is clear that $\|x, y, z\| \geq 0$ and $\|x, y, z\| = 0$ if and only if $x = y = z = 0$.

(**NS2**) Let $\lambda \in \mathbb{R}$ and $x, y, z \in X$. Then we obtain

$$\begin{aligned}\|\lambda x, \lambda y, \lambda z\| &= \|\lambda x\| + \|\lambda y\| + \|\lambda z\| \\ &= |\lambda| \|x\| + |\lambda| \|y\| + |\lambda| \|z\| \\ &= |\lambda| (\|x\| + \|y\| + \|z\|) \\ &= |\lambda| \|x, y, z\|.\end{aligned}$$

(**NS3**) Let $x, y, z, x', y', z' \in X$. Then we obtain

$$\begin{aligned}&\|x + x', y + y', z + z'\| \\ &= \|x + x'\| + \|y + y'\| + \|z + z'\| \\ &\leq \|x\| + \|x'\| + \|y\| + \|y'\| + \|z\| + \|z'\| \\ &= \|0\| + \|x\| + \|z'\| + \|0\| + \|y\| \\ &+ \|x'\| + \|0\| + \|z\| + \|y'\| \\ &= \|0, x, z'\| + \|0, y, x'\| + \|0, z, y'\|.\end{aligned}$$

Consequently, the function $\|.,.,.\|$ satisfies the conditions (**NS1**), (**NS2**), (**NS3**) and so $(X, \|.,.,.\|)$ is an S-normed space. □

We have proved that every norm on X defines an S-norm on X. We call the S-norm defined in (4) as the S-norm generated by the norm $\|.\|$. For example, the S-norm defined in Example 1 is the S-norm generated by the usual norm on $\mathbb{R}$.
There exists an S-norm which is not generated by a norm as we have seen in the following example.

Example 4. *Let X be a nonempty set and the function $\|.,.,.\| : X \times X \times X \to \mathbb{R}$ be defined by*

$$\begin{aligned}\|x, y, z\| = |x - 2y - 2z| + |y - 2x - 2z| \\ + |z - 2y - 2x|,\end{aligned}$$

for all $x, y, z \in X$. Then, the function $\|.,.,.\|$ is an S-norm on X, but it is not generated by a norm.
Now, we show that the conditions (**NS1**), (**NS2**) *and* (**NS3**) *are satisfied.*

(**NS1**) *By the definition, clearly we obtain $\|x, y, z\| \geq 0$ and $\|x, y, z\| = 0$ if and only if $x = y = z = 0$ for all $x, y, z \in X$.*

(**NS2**) *We have*

$$\begin{aligned}\|\lambda x, \lambda y, \lambda z\| &= |\lambda x - 2\lambda y - 2\lambda z| \\ &+ |\lambda y - 2\lambda x - 2\lambda z| \\ &+ |\lambda z - 2\lambda y - 2\lambda x| \\ &= |\lambda| \begin{pmatrix} |x - 2y - 2z| \\ +|y - 2x - 2z| \\ +|z - 2y - 2x| \end{pmatrix} \\ &= |\lambda| \|x, y, z\|,\end{aligned}$$

for all $\lambda \in \mathbb{R}$ and $x, y, z \in X$.

(**NS3**) *Let $x, y, z, x', y', z' \in X$. Then we obtain*

$$\begin{aligned}&\|x + x', y + y', z + z'\| \\ &= |x + x' - 2y - 2y' - 2z - 2z'| \\ &+ |y + y' - 2x - 2x' - 2z - 2z'| \\ &+ |z + z' - 2y - 2y' - 2x - 2x'| \\ &\leq |2x + 2z'| + |x - 2z'| \\ &+ |z' - 2x| + |2y + 2x'| \\ &+ |y - 2x'| + |x' - 2y| \\ &+ |2z + 2y'| + |z - 2y'| \\ &+ |y' - 2z| \\ &= \|0, x, z'\| + \|0, y, x'\| + \|0, z, y'\|.\end{aligned}$$

Consequently, the function $\|.,.,.\|$ is an S-norm on X.
On the contrary, we assume that this S-norm is generated by a norm. Then the following equation should be satisfied

$$\|x, y, z\| = \|x\| + \|y\| + \|z\|,$$

for all $x, y, z \in X$.
If we consider $\|x, 0, 0\|$ and $\|x, x, 0\|$ then we obtain

$$\begin{aligned}\|x, 0, 0\| = \|x\| = |x| + |2x| + |2x| = 5|x|, \\ \|x, x, 0\| = 2|x| = |x| + |x| + |4x| = 6|x|\end{aligned}$$

and so $\|x\| = 5|x|$ and $\|x\| = 3|x|$, which is a contradiction. Hence this S-norm is not generated by a norm.

Now we prove that every S-norm generate a norm.

Proposition 3. *Let X be a nonempty set, $(X, \|.,.,.\|)$ be an S-normed space and the function $\|.\| : X \to \mathbb{R}$ be defined as follows:*

$$\|x\| = \|0, x, 0\| + \|0, 0, x\|,$$

for all $x \in X$. Then the function $\|.\|$ is a norm on X and $(X, \|.\|)$ is a normed space.

Proof. Using the conditions (**NS1**) and (**NS2**), it is clear that we obtain the conditions (**N1**), (**N2**) and (**N3**) are satisfied.

Now, we show that the condition (**N4**) is satisfied.

(**N4**) Let $x, y \in X$. By the condition (**NS3**), we have

$$\begin{aligned}\|x+y\| &= \|0, x+y, 0\| + \|0, 0, x+y\| \\ &= \|0, x+y, 0\| + \|0, 0, y+x\| \\ &\leq \|0, 0, 0\| + \|0, x, 0\| + \|0, 0, y\| \\ &+ \|0, 0, x\| + \|0, 0, 0\| + \|0, y, 0\| \\ &= \|x\| + \|y\|.\end{aligned}$$

Consequently, the function $\|.\|$ is a norm on X and $(X, \|.\|)$ is a normed space. □

We call this norm as the norm generated by the S-norm $\|., ., .\|$.

Let X be a real vector space. New generalizations of normed spaces have been studied in recent years. For example, Khan defined the notion of a G-norm and studied some topological concepts in G-normed spaces [15]. Now we recall the definition of a G-norm and give the relationship between a G-norm and an S-norm.

Definition 3. *[15] Let X be a real vector space. A real valued function $\|., ., .\| : X \times X \times X \to \mathbb{R}$ is called a G-norm on X if the following conditions hold:*

(**NG1**) *$\|x, y, z\| \geq 0$ and $\|x, y, z\| = 0$ if and only if $x = y = z = 0$.*

(**NG2**) *$\|x, y, z\|$ is invariant under permutations of x, y, z.*

(**NG3**) *$\|\lambda x, \lambda y, \lambda z\| = |\lambda| \|x, y, z\|$ for all $\lambda \in \mathbb{R}$ and $x, y, z \in X$.*

(**NG4**) *$\|x + x', y + y', z + z'\| \leq \|x, y, z\| + \|x', y', z'\|$ for all $x, y, z, x', y', z' \in X$.*

(**NG5**) *$\|x, y, z\| \geq \|x+y, 0, z\|$ for all $x, y, z \in X$.*

The pair $(X, \|., ., .\|)$ is called a G-normed space.

Proposition 4. *Every G-normed space is an S-normed space.*

Proof. Using the conditions (**NG1**) and (**NG3**), we see that the conditions (**NS1**) and (**NS2**) are satisfied. We only show that the condition (**NS3**) is satisfied.

(**NS3**) Let $x, y, z, x', y', z' \in X$. Using the conditions (**NG2**) and (**NG4**), we obtain

$$\begin{aligned}&\|x + x', y + y', z + z'\| \\ &= \|(x + 0) + x', 0 + (y + y'), z' + z\| \\ &\leq \|x + 0, 0, 0 + z'\| + \|x', y + y', z\| \\ &= \|0, 0 + x, 0 + z'\| + \|x', y + y', z\| \\ &\leq \|0, 0, 0\| + \|0, x, z'\| + \|x', y, 0\| + \|0, y', z\| \\ &= \|0, x, z'\| + \|0, y, x'\| + \|0, z, y'\|.\end{aligned}$$

Consequently, the condition (**NS3**) is satisfied. □

The converse of Proposition 4 can not be always true as we have seen in the following example.

Example 5. *Let $X = \mathbb{R}$ and the S-norm be defined as in Example 4. If we put $x = 1$, $y = 5$ and $z = 0$, the condition (**NG5**) is not satisfied. Indeed, we have*

$$\begin{aligned}\|x, y, z\| &= |x - 2y - 2z| + |y - 2x - 2z| \\ &+ |z - 2y - 2x| \\ &= 23\end{aligned}$$

and

$$\begin{aligned}\|x + y, 0, z\| &= |x + y - 2z| + |2x + 2y + 2z| \\ &+ |z - 2y - 2x| \\ &= 30.\end{aligned}$$

Hence this S-norm is not a G-norm on $\mathbb{R}$.

Now we give the definitions of an open ball and a closed ball on an S-normed space.

Definition 4. *Let $(X, \|., ., .\|)$ be an S-normed space. For given x_0, a_1, $a_2 \in X$ and $r > 0$, the open ball $B_{a_1}^{a_2}(x_0, r)$ and the closed ball $B_{a_1}^{a_2}[x_0, r]$ are defined as follows:*

$$B_{a_1}^{a_2}(x_0, r) = \{y \in X : \|y - x_0, y - a_1, y - a_2\| < r\}$$

and

$$B_{a_1}^{a_2}[x_0, r] = \{y \in X : \|y - x_0, y - a_1, y - a_2\| \leq r\}.$$

Example 6. *Let us consider the S-normed space $(X, \|., ., .\|)$ generated by the usual norm on X, where $X = \mathbb{R}^2$ and*

$$\|x\| = \|(x_1, x_2)\| = \sqrt{x_1^2 + x_2^2},$$

for all $x \in \mathbb{R}^2$. *Then the open ball* $B_{a_1}^{a_2}(x_0, r)$ *in* $\mathbb{R}^2$ *is a 3-ellipse given by*

$$B_{a_1}^{a_2}(x_0, r) = \{y \in \mathbb{R}^2 : \|y - x_0\| + \|y - a_1\| + \|y - a_2\| < r\}.$$

If we choose $y = (y_1, y_2)$, $x_0 = (1, 1)$, $a_1 = (0, 0)$, $a_2 = (-1, -1)$ *in* $\mathbb{R}^2$ *and* $r = 5$, *then we obtain*

$$B_{a_1}^{a_2}(x_0, r) = \left\{ \begin{array}{c} y \in \mathbb{R}^2 : \sqrt{(y_1 - 1)^2 + (y_2 - 1)^2} \\ +\sqrt{y_1^2 + y_2^2} \\ +\sqrt{(y_1 + 1)^2 + (y_2 + 1)^2} < 5 \end{array} \right\}, \tag{5}$$

as shown in Figure 1a.

Now we give the following example using an S-norm which is not generated by a norm.

Example 7. *Let* $X = \mathbb{R}^2$ *and the function* $\|.,.,.\| : X \times X \times X \to \mathbb{R}$ *be defined as in Example 4. Then we have*

$$\begin{aligned} &\|x, y, z\| \\ &= |x - 2y - 2z| + |y - 2x - 2z| + |z - 2y - 2x| \\ &= \sqrt{(x_1 - 2y_1 - 2z_1)^2 + (x_2 - 2y_2 - 2z_2)^2} \\ &+ \sqrt{(y_1 - 2x_1 - 2z_1)^2 + (y_2 - 2x_2 - 2z_2)^2} \\ &+ \sqrt{(z_1 - 2y_1 - 2x_1)^2 + (z_2 - 2y_2 - 2x_2)^2}, \end{aligned}$$

for all $x = (x_1, x_2)$, $y = (y_1, y_2)$, $z = (z_1, z_2) \in \mathbb{R}^2$. *Then* $(\mathbb{R}^2, \|.,.,.\|)$ *is an* S*-normed space. The open ball* $B_{a_1}^{a_2}(x_0, r)$ *in* $\mathbb{R}^2$ *is*

$$B_{a_1}^{a_2}(x_0, r) = \{y \in \mathbb{R}^2 : \|y - x_0, y - a_1, y - a_2\| < r\}.$$

If we choose $y = (y_1, y_2)$, $x_0 = (1, 1)$, $a_1 = (0, 0)$, $a_2 = (-1, -1)$ *in* $\mathbb{R}^2$ *and* $r = 20$, *then we obtain*

$$B_{a_1}^{a_2}(x_0, r) = \left\{ \begin{array}{c} y \in \mathbb{R}^2 : \sqrt{(3y_1 + 3)^2 + (3y_2 + 3)^2} \\ +\sqrt{9y_1^2 + 9y_2^2} \\ +\sqrt{(3 - 3y_1)^2 + (3 - 3y_2)^2} < 20 \end{array} \right\}, \tag{6}$$

as shown in Figure 1b.

Definition 5. *Let* $(X, \|.,.,.\|)$ *be an* S*-normed space.*

(1) *A sequence* $\{x_n\}$ *in* X *converges to* x *if and only if*
$$\lim_{n\to\infty} \|0, x_n - x, x - x_n\| = 0.$$
That is, for each $\varepsilon > 0$ *there exists* $n_0 \in \mathbb{N}$ *such that*
$$\|0, x_n - x, x - x_n\| < \varepsilon,$$
for all $n \geq n_0$.

(2) *A sequence* $\{x_n\}$ *in* X *is called a Cauchy sequence if*
$$\lim_{n,m,l\to\infty} \|x_n - x_m, x_m - x_l, x_l - x_n\| = 0.$$
That is, for each $\varepsilon > 0$ *there exists* $n_0 \in \mathbb{N}$ *such that*
$$\|x_n - x_m, x_m - x_l, x_l - x_n\| < \varepsilon,$$
for all $n, m, l \geq n_0$.

(3) *An* S*-normed space is called complete if each Cauchy sequence in* X *converges in* X.

(4) *A complete* S*-normed space is called an* S*-Banach space.*

Proposition 5. *Every convergent sequence in an* S*-normed space is a Cauchy sequence.*

Proof. Let a sequence $\{x_n\}$ in X be convergent to x. For each $\varepsilon > 0$, there exists $n_0 \in \mathbb{N}$ such that

$$\|0, x_n - x, x - x_n\| < \frac{\varepsilon}{3},$$

for all $n \geq n_0$. We now show that for each $\varepsilon > 0$ there exists $n_0 \in \mathbb{N}$ such that

$$\|x_n - x_m, x_m - x_l, x_l - x_n\| < \varepsilon,$$

for all $n, m, l \geq n_0$. Using the condition (**NS3**), we obtain

$$\begin{aligned} &\|x_n - x_m, x_m - x_l, x_l - x_n\| \\ &= \left\| \begin{array}{c} x_n - x + x - x_m, x_m - x \\ +x - x_l, x_l - x + x - x_n \end{array} \right\| \\ &\leq \|0, x_n - x, x - x_n\| + \|0, x_m - x, x - x_m\| \\ &\quad + \|0, x_l - x, x - x_l\| \\ &< \frac{\varepsilon}{3} + \frac{\varepsilon}{3} + \frac{\varepsilon}{3} = \varepsilon. \end{aligned}$$

Consequently, the sequence $\{x_n\}$ in X is a Cauchy sequence. $\square$

The converse of Proposition 5 can not be always true as we have seen in the following example.

Example 8. *Let* $X = (0, 1) \subset \mathbb{R}$ *and the function* $\|.,.,.\| : X \times X \times X \to \mathbb{R}$ *be an* S*-norm generated by the usual norm on* X. *If we consider the sequence* $\{x_n\} = \left\{\frac{1}{n}\right\}$ *on* X, *then this sequence*

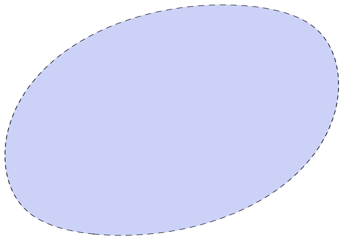

(a) The open ball which is corresponding to the S-norm defined in (5).

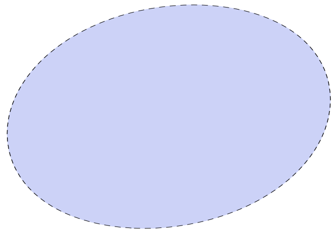

(b) The open ball which is corresponding to the S-norm defined in (6).

Figure 1. Some open balls in $(\mathbb{R}^2, \|.,.,.\|)$

is a Cauchy sequence, but it is not a convergent sequence on X.

Now we show that the sequence is a Cauchy sequence. For x_n, x_m, $x_l \in X$, we obtain

$$\begin{aligned}&\lim_{n,m,l\to\infty}\|x_n - x_m, x_m - x_l, x_l - x_n\|\\ &= \lim_{n,m,l\to\infty}\left\|\frac{1}{n}-\frac{1}{m}, \frac{1}{m}-\frac{1}{l}, \frac{1}{l}-\frac{1}{n}\right\|\\ &= \lim_{n,m,l\to\infty}\left(\left|\frac{1}{n}-\frac{1}{m}\right| + \left|\frac{1}{m}-\frac{1}{l}\right| + \left|\frac{1}{l}-\frac{1}{n}\right|\right) = 0.\end{aligned}$$

The sequence is convergent to 0 as follows:

$$\lim_{n\to\infty}\|0, x_n - x, x - x_n\| = \lim_{n\to\infty}\left\|0, \tfrac{1}{n} - 0, 0 - \tfrac{1}{n}\right\| = 0,$$

for all $x_n \in X$. But $0 \notin X$. Consequently, the sequence is not convergent on X.

3. A fixed point theorem on S-normed spaces

In this section, we introduce the Rhoades' condition on an S-normed space and denote it by (**NS25**). We prove a fixed point theorem using this contractive condition.

At first, we give some definitions and a proposition which are needed in the sequel.

Definition 6. *Let $(X, \|.,.,.\|)$ be an S-normed space and $E \subseteq X$. The closure of E, denoted by $\overline{E}$, is the set of all $x \in X$ such that there exists a sequence $\{x_n\}$ in E converging to x. If $E = \overline{E}$, then E is called a closed set.*

Definition 7. *Let $(X, \|.,.,.\|)$ be an S-normed space and $A \subseteq X$. The subset A is called bounded if there exists $r > 0$ such that*

$$\|0, x - y, y - x\| < r,$$

for all $x, y \in A$.

Definition 8. *Let $(X, \|.,.,.\|)$ be an S-normed space and $A \subseteq X$. The S-diameter of A is defined by*

$$\delta^s(A) = \sup\{\|0, x - y, y - x\| : x, y \in A\}.$$

If A is bounded then we will write $\delta^s(A) < \infty$.

Definition 9. *Let X be an S-Banach space, $A \subseteq X$ and $u \in X$.*

(1) *The S-radius of A relative to a given $u \in X$ is defined by*
$$r^s_u(A) = \sup\{\|0, u - x, x - u\| : x \in A\}.$$
(2) *The S-Chebyshev radius of A is defined by*
$$r^s(A) = \inf\{r^s_u(A) : u \in A\}.$$
(3) *The S-Chebyshev centre of A is defined by*
$$C^s(A) = \{u \in A : r^s_u(A) = r^s(A)\}.$$

By Definition 8 and Definition 9, it can be easily seen the following inequality:

$$r^s(A) \le r^s_u(A) \le \delta^s(A).$$

Definition 10. *A point $u \in A$ is called S-diametral if $r^s_u(A) = \delta^s(A)$. If $r^s_u(A) < \delta^s(A)$, then u is called non-S-diametral.*

Definition 11. *A convex subset of an S-Banach space X has S-normal structure if every S-bounded and convex subset of A having $\delta^s(A) > 0$ has at least one non-S-diametral point.*

Proposition 6. *If X is a reflexive S-Banach space, A is a nonempty, closed and convex subset of X, then $C^s(A)$ is nonempty, closed and convex.*

Proof. It can be easily seen by definition of $C^s(A)$. □

Now we introduce the Rhoades' condition (**NS25**) on an S-Banach space.

Definition 12. *Let $(X, \|.,.,.\|)$ be an S-Banach space and T be a self-mapping of X. We define*

$$(\mathbf{NS25}) \quad \|0, Tx - Ty, Ty - Tx\| < \max\left\{\begin{array}{c} \|0, x-y, y-x\|, \\ \|0, Tx-x, x-Tx\|, \\ \|0, Ty-y, y-Ty\|, \\ \|0, Ty-x, x-Ty\|, \\ \|0, Tx-y, y-Tx\| \end{array}\right\},$$

for each $x, y \in X$, $x \neq y$.

Lemma 3. *[16] Let X be a Banach space. Then X is reflexive if and only if for any decreasing sequence $\{K_n\}$ of nonempty, bounded, closed and convex subsets of X,*

$$\bigcap_{n=1}^{\infty} K_n \neq \emptyset.$$

Lemma 4. *Let X be an S-Banach space. Then X is reflexive if and only if for any decreasing sequence $\{K_n\}$ of nonempty, bounded, closed and convex subsets of X,*

$$\bigcap_{n=1}^{\infty} K_n \neq \emptyset.$$

Proof. By the definition of reflexivity the proof follows easily. □

Recall that the convex hull of a set A is denoted by $conv(A)$ and any member of this set $conv(A)$ has the form

$$\sum_{i=1}^{n} \alpha_i x_i,$$

where $x_i \in A_i, \alpha_i \geq 0$ for all $i = 1, ..., n$ and $\sum_{i=1}^{n} \alpha_i = 1$.

Now, we give the following fixed point theorem.

Theorem 1. *Let X be a reflexive S-Banach space and A be a nonempty, closed, bounded and convex subset of X, having S-normal structure. If $T : A \to A$ is a continuous self-mapping satisfying the condition* (**NS25**) *then T has a unique fixed point in A.*

Proof. At first, we show that the existence of the fixed point. Let $\mathcal{A}$ be the family of every nonempty, closed and convex subsets of A. Also we assume that if $F \in \mathcal{A}$ then $TF \subseteq F$. The family $\mathcal{A}$ is nonempty since $A \in \mathcal{A}$. We can partially order $\mathcal{A}$ by set inclusion, that is, if $F_1 \subseteq F_2$ then $F_1 \leq F_2$.

In $\mathcal{A}$, if we define a decreasing net of subsets

$$S = \{F_i : F_i \in \mathcal{A}, i \in I\},$$

then by reflexivity, this net S has nonempty intersection. Because it is a decreasing net of nonempty, closed, bounded and convex subsets of X. If we put $F_0 = \bigcap_{i \in I} F_i$ we have that F_0 is in $\mathcal{A}$ and is a lower bound of S.

Using Zorn's Lemma, there is a minimal element, denoted by F, in $\mathcal{A}$ as S is any arbitrary decreasing net in $\mathcal{A}$. We see that this F is a singleton.

Assume that $\delta^s(F) \neq \emptyset$. Since F is nonempty, closed and convex, $C^s(F)$ is a nonempty, closed and convex subset of F. We have that

$$r^s(F) < \delta^s(F),$$
$$\delta^s(C^s(F)) \leq r^s(F) < \delta^s(F)$$

and so $C^s(F)$ is a proper subset of F.

Let $(F_m)_{m \in \mathbb{N}}$ be an increasing sequence of subsets of F, defined by

$$F_1 = C^s(F) \text{ and } F_{m+1} = conv(F_m \cup TF_m),$$

for all $m \in \mathbb{N}$. If we denote the S-diameters of these sets F_k by $\delta_k^s = \delta^s(F_k)$, we show that

$$\delta_k^s \leq r^s(F),$$

for all $k \in \mathbb{N}$.

Using the (PMI), we obtain

(1) For $k = 1$,
$\delta_1^s = \delta^s(F_1) = \delta^s(C^s(F)) \leq r^s(F)$.
(2) If $\delta_k^s \leq r^s(F)$ for every $k = 1, ..., m$ then $\delta_{m+1}^s \leq r^s(F)$.

We note that

$$\begin{aligned} \delta_{m+1}^s &= \delta^s(F_{m+1}) = \delta^s(conv(F_m \cup TF_m)) \\ &= \delta^s(F_m \cup TF_m). \end{aligned}$$

By the definition of S-diameter, for any given $\varepsilon > 0$ there are x' and y' in $F_m \cup T(F_m)$ satisfying

$$\delta_{m+1}^s - \varepsilon < \|0, x' - y', y' - x'\| \leq \delta_{m+1}^s.$$

We obtain the following three cases for x', y':

(1) x', $y' \in F_m$ or
(2) $x' \in F_m$ and $y' \in TF_m$ or

(3) $x',\ y' \in TF_m$.

Redefining x' and y' as follows:

(1) $x' = x$ and $y' = y$ with $x, y \in F_m$,
(2) $x' = x$ and $y' = Ty$ with $x, y \in F_m$,
(3) $x' = Tx$ and $y' = Ty$ with $x, y \in F_m$.

We show that in any case

$$\delta^s_{m+1} - \varepsilon < r^s(F).$$

Case 1. By the definition of δ^s_m and the induction hypothesis, we obtain

$$\delta^s_{m+1} - \varepsilon < \|0, x - y, y - x\| \le \delta^s_{m+1} \le r^s(F) \quad (7)$$

and so $\delta^s_{m+1} - \varepsilon < r^s(F)$.
Case 2. We obtain

$$\delta^s_{m+1} - \varepsilon < \|0, x - Ty, Ty - x\|$$

with $x,\ y \in F_m$. Then by the definition of F_m, we have $x, y \in conv(F_{m-1} \cup TF_{m-1})$ and so there is a finite index set I such that $x = \sum\limits_{i \in I} \alpha_i x_i$, with $\sum\limits_{i \in I} \alpha_i = 1$, $\alpha_i \ge 0$ and $x_i \in F_{m-1} \cup TF_{m-1}$ for any $i \in I$. We can separate the set I in two disjoint subsets, $I = I_1 \cup I_2$, such that if $i \in I_1$ then $x_i \in F_{m-1}$ and if $i \in I_2$ then $x_i \in TF_{m-1}$.
Now redefining x_i as $x_i = Tx_i$ with $x_i \in F_{m-1}$, we obtain

$$x = \sum_{i \in I_1} \alpha_i x_i + \sum_{i \in I_2} \alpha_i T x_i.$$

Substituting in $\|0, x - Ty, Ty - x\|$, we get

$$\begin{aligned} \|0, x - Ty, Ty - x\| \le &\sum_{i \in I_1} \alpha_i \|0, x_i - Ty, Ty - x_i\| \\ &+ \sum_{i \in I_2} \alpha_i \|0, Tx_i - Ty, Ty - Tx_i\|. \end{aligned} \quad (8)$$

Applying the condition (**NS25**) to $\|0, Tx_i - Ty, Ty - Tx_i\|$, we have

$$\|0, Tx_i - Ty, Ty - Tx_i\| < \max \left\{ \begin{array}{c} \|0, x_i - y, y - x_i\|, \|0, x_i - Tx_i, Tx_i - x_i\|, \\ \|0, y - Ty, Ty - y\|, \|0, x_i - Ty, Ty - x_i\|, \\ \|0, Tx_i - y, y - Tx_i\| \end{array} \right\}. \quad (9)$$

As $x_i \in F_{m-1}$, $Tx_i, y \in F_m$, we have

$$\begin{aligned} &\|0, x_i - y, y - x_i\| \le r^s(F), \\ &\|0, x_i - Tx_i, Tx_i - x_i\| \le r^s(F), \\ &\|0, Tx_i - y, y - Tx_i\| \le r^s(F) \end{aligned}$$

and replacing in (9), we obtain

$$\|0, Tx_i - Ty, Ty - Tx_i\| < \max \left\{ \begin{array}{c} r^s(F), \\ \|0, y - Ty, Ty - y\|, \|0, x_i - Ty, Ty - x_i\| \end{array} \right\}.$$

Let us subdivide the index set I_2 in three disjoint subsets $I_2 = I_2^1 \cup I_2^2 \cup I_2^3$ such that

$$\begin{aligned} I_2^1 &= \{ i \in I_2 : \|0, Tx_i - Ty, Ty - Tx_i\| < r^s(F) \}, \\ I_2^2 &= \left\{ \begin{array}{c} i \in I_2 : \|0, Tx_i - Ty, Ty - Tx_i\| \\ < \|0, x_i - Ty, Ty - x_i\| \end{array} \right\}, \\ I_2^3 &= \left\{ \begin{array}{c} i \in I_2 : \|0, Tx_i - Ty, Ty - Tx_i\| \\ < \|0, y - Ty, Ty - y\| \end{array} \right\}. \end{aligned}$$

Then using (8), we have

$$\begin{aligned} \|0, x - Ty, Ty - x\| \le &\sum_{i \in I_1 \cup I_2^2} \alpha_i \|0, x_i - Ty, Ty - x_i\| \\ &+ \sum_{i \in I_2^1} \alpha_i r^s(F) + \sum_{i \in I_2^3} \alpha_i \|0, y - Ty, Ty - y\|. \end{aligned} \quad (10)$$

Redefining I_1, I_2 and I_3

$$\overline{I_1} = I_1 \cup I_2^2,\ \overline{I_2} = I_2^1 \text{ and } \overline{I_3} = I_2^3. \quad (11)$$

Then we have $I = \overline{I_1} \cup \overline{I_2} \cup \overline{I_3}$, with $\overline{I_j} \cap \overline{I_k} = \emptyset$. If $j \neq k$ and $\sum\limits_{i \in I} \alpha_i = 1$ then using (10), it becomes

$$\begin{aligned} \|0, x - Ty, Ty - x\| \le &\sum_{i \in \overline{I_1}} \alpha_i \|0, x_i - Ty, Ty - x_i\| \\ &+ \sum_{i \in \overline{I_2}} \alpha_i r^s(F) + \sum_{i \in \overline{I_3}} \alpha_i \|0, y - Ty, Ty - y\|. \end{aligned} \quad (12)$$

If $A_0 = \sum\limits_{i \in \overline{I_2}} \alpha_i$ and $B_0 = \sum\limits_{i \in \overline{I_3}} \alpha_i$ with $\sum\limits_{i \in \overline{I_1}} \alpha_i + A_0 + B_0 = 1$. Using (12), we have

$$\begin{aligned} \|0, x - Ty, Ty - x\| \le &\sum_{i \in \overline{I_1}} \alpha_i \|0, x_i - Ty, Ty - x_i\| \\ &+ A_0 r^s(F) + B_0 \|0, y - Ty, Ty - y\|. \end{aligned} \quad (13)$$

For each $i \in \overline{I_1}$, $x_i \in F_{m-1} = conv(F_{m-2} \cup TF_{m-2})$, there is a finite set J_i, such that

$$x_i = \sum_{j \in J_i} \beta_i^j x_i^j, \quad (14)$$

with $x_i^j \in F_{m-2} \cup TF_{m-2}$, $\beta_i^j \geq 0$ and $\sum\limits_{j \in J_i} \beta_i^j = 1$ for any $j \in J_i$. Let $J_i = J_i^1 \cup J_i^2$, with $J_i^1 \cap J_i^2 = \emptyset$ such that

$$x_i = \sum_{j \in J_i^1} \beta_i^j x_i^j + \sum_{j \in J_i^2} \beta_i^j T x_i^j. \tag{15}$$

For each $i \in \overline{I_1}$ we have

$$\begin{aligned} &\|0, x_i - Ty, Ty - x_i\| \\ &\leq \sum_{j \in J_i^1} \beta_i^j \|0, x_i^j - Ty, Ty - x_i^j\| \\ &+ \sum_{j \in J_i^2} \beta_i^j \|0, Tx_i^j - Ty, Ty - Tx_i^j\|. \end{aligned} \tag{16}$$

Applying the condition (**NS25**) to $\|0, Tx_i^j - Ty, Ty - Tx_i^j\|$, we have

$$\begin{aligned} &\|0, Tx_i^j - Ty, Ty - Tx_i^j\| \\ &< \max \left\{ \begin{array}{c} \|0, x_i^j - y, y - x_i^j\|, \\ \|0, Tx_i^j - x_i^j, x_i^j - Tx_i^j\|, \\ \|0, y - Ty, Ty - y\|, \\ \|0, Tx_i^j - y, y - Tx_i^j\|, \\ \|0, x_i^j - Ty, Ty - x_i^j\| \end{array} \right\}. \end{aligned} \tag{17}$$

Since $x_i^j \in F_{m-2}$ and $y \in F_m$, we have

$$\begin{aligned} &\|0, x_i^j - y, y - x_i^j\| \leq r^s(F), \\ &\|0, Tx_i^j - x_i^j, x_i^j - Tx_i^j\| \leq r^s(F), \\ &\|0, Tx_i^j - y, y - Tx_i^j\| \leq r^s(F). \end{aligned}$$

By (17), we obtain

$$\begin{aligned} &\|0, Tx_i^j - Ty, Ty - Tx_i^j\| \\ &< \max \left\{ \begin{array}{c} r^s(F), \|0, y - Ty, Ty - y\|, \\ \|0, x_i^j - Ty, Ty - x_i^j\| \end{array} \right\}. \end{aligned}$$

Let $J_i^2 = J_i^{2_1} \cup J_i^{2_2} \cup J_i^{2_3}$ with $J_i^{2_k} \cap J_i^{2_p} = \emptyset$ such that

$$\begin{aligned} J_i^{2_1} &= \left\{ \begin{array}{c} j \in J_i^2 : \|0, Tx_i^j - Ty, Ty - Tx_i^j\| \\ < r^s(F) \end{array} \right\}, \\ J_i^{2_2} &= \left\{ \begin{array}{c} j \in J_i^2 : \|0, Tx_i^j - Ty, Ty - Tx_i^j\| \\ < \|0, y - Ty, Ty - y\| \end{array} \right\}, \\ J_i^{2_3} &= \left\{ \begin{array}{c} j \in J_i^2 : \|0, Tx_i^j - Ty, Ty - Tx_i^j\| \\ < \|0, x_i^j - Ty, Ty - x_i^j\| \end{array} \right\}. \end{aligned}$$

Using (16), we obtain

$$\begin{aligned} &\|0, x_i - Ty, Ty - x_i\| \\ &\leq \sum_{j \in J_i^1 \cup J_i^{2_3}} \beta_i^j \|0, x_i^j - Ty, Ty - x_i^j\| \\ &+ \sum_{i \in J_i^{2_1}} \beta_i^j r^s(F) + \sum_{i \in J_i^{2_2}} \beta_i^j \|0, y - Ty, Ty - y\|. \end{aligned} \tag{18}$$

Let us denote by

$$J_1^i = J_i^1 \cup J_i^{2_3},\ J_2^i = J_i^{2_2} \text{ and } J_3^i = J_i^{2_1}.$$

Then using (18), we have

$$\begin{aligned} \|0, x_i - Ty, Ty - x_i\| &\leq \sum_{j \in J_1^i} \beta_i^j \|0, x_i^j - Ty, Ty - x_i^j\| \\ &+ \sum_{i \in J_3^i} \beta_i^j r^s(F) + \sum_{i \in J_2^i} \beta_i^j \|0, y - Ty, Ty - y\|. \end{aligned} \tag{19}$$

If $A_i = \sum\limits_{i \in J_3^i} \beta_i^j$ and $B_i = \sum\limits_{i \in J_2^i} \beta_i^j$ with $\sum\limits_{j \in J_1^i} \beta_i^j + A_i + B_i = 1$. Using (19), we obtain

$$\begin{aligned} \|0, x_i - Ty, Ty - x_i\| &\leq \sum_{j \in J_1^i} \beta_i^j \|0, x_i^j - Ty, Ty - x_i^j\| \\ &+ A_i r^s(F) + B_i \|0, y - Ty, Ty - y\|. \end{aligned} \tag{20}$$

Using (13) and $\|0, x_i - Ty, Ty - x_i\|$ by (20), we obtain

$$\begin{aligned} \|0, x - Ty, Ty - x\| &\leq \sum_{i \in \overline{I_1}} \alpha_i \sum_{j \in J_1^i} \beta_i^j \|0, x_i^j - Ty, Ty - x_i^j\| \\ &+ \left[\sum_{i \in \overline{I_1}} \alpha_i A_i + A_0 \right] r^s(F) \\ &+ \left[\sum_{i \in \overline{I_1}} \alpha_i B_i + B_0 \right] \|0, y - Ty, Ty - y\|. \end{aligned}$$

Let $A_1 = \sum\limits_{i \in \overline{I_1}} \alpha_i A_i$ and $B_1 = \sum\limits_{i \in \overline{I_1}} \alpha_i B_i$. Then we have

$$\begin{aligned} \|0, x - Ty, Ty - x\| &\leq \sum_{i \in \overline{I_1}} \alpha_i \sum_{j \in J_1^i} \beta_i^j \|0, x_i^j - Ty, Ty - x_i^j\| \\ &+ (A_1 + A_0) r^s(F) + (B_1 + B_0) \|0, y - Ty, Ty - y\|. \end{aligned} \tag{21}$$

We note that

$$\sum_{i \in \overline{I_1}} \alpha_i \sum_{j \in J_1^i} \beta_i^j + \sum_{i \in \overline{I_1}} \alpha_i A_i + A_0 + \sum_{i \in \overline{I_1}} \alpha_i B_i + B_0 = 1.$$

Let us take $K = \bigcup\limits_{i \in \overline{I_1}} \left(\bigcup\limits_{j \in J_1^i} j \right)$ and denote the scalars by ξ_k. To each k relative to the pair (i, j), x_i^j will be denoted by x_k.
Using (21), we obtain

$$\begin{aligned} \|0, x - Ty, Ty - x\| &\leq \sum_{k \in K} \xi_k \|0, x_k - Ty, Ty - x_k\| \\ &+ (A_1 + A_0) r^s(F) + (B_1 + B_0) \|0, y - Ty, Ty - y\|, \end{aligned}$$

where $\sum\limits_{k\in K}\xi_k + A_1 + A_0 + B_1 + B_0 = 1$ and $x_k \in F_{m-2}$.

Repeating this process which is done for x_k, we get

$$\begin{aligned}\|0, x-Ty, Ty-x\| &\leq \sum_{p\in P}\gamma_p\|0, x_p-Ty, Ty-x_p\| \\ &+\sum_{k=0}^{m-1}A_k r^s(F)+\sum_{k=0}^{m-1}B_k\|0, y-Ty, Ty-y\|,\end{aligned} \tag{22}$$

where $\sum\limits_{p\in P}\gamma_p + \sum\limits_{i=0}^{m-1}(A_i+B_i) = 1$ and $x_p \in F_1 = C^s(F)$.

Hence $\|0, x_p - Ty, Ty - x_p\| \leq r^s(F)$ and using (22), we obtain

$$\begin{aligned}\|0, x-Ty, Ty-x\| &\leq \sum_{k=0}^{m-1}B_k\|0, y-Ty, Ty-y\| \\ &+\left(\sum_{p\in P}\gamma_p+\sum_{k=0}^{m-1}A_k\right)r^s(F).\end{aligned} \tag{23}$$

Let us turn to $\|0, y-Ty, Ty-y\|$. Since $y \in conv(F_{m-1}\cup TF_{m-1})$, we have $y = \sum\limits_{i\in I}\alpha_i y_i$ with $\sum\limits_{i\in I}\alpha_i = 1$, $y_i \in F_{m-1}\cup TF_{m-1}$ and $\alpha_i \geq 0$ for all $i \in I$. Let $I = I_1\cup I_2$ such that $I_1\cap I_2 = \emptyset$. If $i \in I_1$ then $y_i \in F_{m-1}$ and if $i \in I_2$ then $y_i \in TF_{m-1}$. Let $y_i = Ty_i$. Then we can write

$$y = \sum_{i\in I_1}\alpha_i y_i + \sum_{i\in I_2}\alpha_i Ty_i,$$

with $y_i \in F_{m-1}$.

Substituting in $\|0, y-Ty, Ty-y\|$ we get

$$\begin{aligned}\|0, y-Ty, Ty-y\| &\leq \sum_{i\in I_1}\alpha_i\|0, y_i-Ty, Ty-y_i\| \\ &+\sum_{i\in I_2}\alpha_i\|0, Ty_i-Ty, Ty-Ty_i\|.\end{aligned} \tag{24}$$

Using the condition (**NS25**), we obtain

$$\begin{aligned}&\|0, Ty_i-Ty, Ty-Ty_i\| \\ &< \max\left\{\begin{array}{c}\|0, y_i-y, y-y_i\|, \\ \|0, y_i-Ty_i, Ty_i-y_i\|, \\ \|0, y-Ty, Ty-y\|, \\ \|0, y_i-Ty, Ty-y_i\|, \\ \|0, Ty_i-y, y-Ty_i\|\end{array}\right\}.\end{aligned} \tag{25}$$

Since $y_i \in F_{m-1}$, $y \in F_m$, we have

$$\begin{aligned}&\|0, y_i-y, y-y_i\| \leq r^s(F), \\ &\|0, y_i-Ty_i, Ty_i-y_i\| \leq r^s(F), \\ &\|0, Ty_i-y, y-Ty_i\| \leq r^s(F).\end{aligned}$$

Using (25), we obtain

$$\begin{aligned}&\|0, Ty_i-Ty, Ty-Ty_i\| \\ &< \max\left\{\begin{array}{c}r^s(F), \|0, y-Ty, Ty-y\|, \\ \|0, y_i-Ty, Ty-y_i\|\end{array}\right\}.\end{aligned}$$

Redefining the index set $I_2 = I_2^1\cup I_2^2\cup I_2^3$ with

$$\begin{aligned}I_2^1 &= \left\{\begin{array}{c}i\in I_2 : \|0, Ty_i-Ty, Ty-Ty_i\| \\ < r^s(F)\end{array}\right\}, \\ I_2^2 &= \left\{\begin{array}{c}i\in I_2 : \|0, Ty_i-Ty, Ty-Ty_i\| \\ < \|0, y-Ty, Ty-y\|\end{array}\right\}, \\ I_2^3 &= \left\{\begin{array}{c}i\in I_2 : \|0, Ty_i-Ty, Ty-Ty_i\| \\ < \|0, y_i-Ty, Ty-y_i\|\end{array}\right\}.\end{aligned}$$

Now using (24), we get

$$\begin{aligned}\|0, y-Ty, Ty-y\| &\leq \sum_{i\in I_1\cup I_2^3}\alpha_i\|0, y_i-Ty, Ty-y_i\| \\ &+\sum_{i\in I_2^1}\alpha_i r^s(F)+\sum_{i\in I_2^2}\alpha_i\|0, y-Ty, Ty-y\|.\end{aligned} \tag{26}$$

We note that if $\sum\limits_{i\in I_2^2}\alpha_i = 1$ then

$$\begin{aligned}\|0, y-Ty, Ty-y\| &\leq \|0, Ty_i-Ty, Ty-Ty_i\| \\ &< \|0, y-Ty, Ty-y\|,\end{aligned}$$

which is a contradiction.

Then $\sum\limits_{i\in I_2^2}\alpha_i < 1$ and using (26), we obtain

$$\begin{aligned}&\|0, y-Ty, Ty-y\| \\ &\leq \sum_{i\in I_1\cup I_2^3}\frac{\alpha_i}{1-\sum\limits_{i\in I_2^2}\alpha_i}\|0, y_i-Ty, Ty-y_i\| \\ &+\sum_{i\in I_2^1}\frac{\alpha_i}{1-\sum\limits_{i\in I_2^2}\alpha_i}r^s(F),\end{aligned} \tag{27}$$

with $\sum\limits_{i\in I_1\cup I_2^3}\frac{\alpha_i}{1-\sum\limits_{i\in I_2^2}\alpha_i} + \sum\limits_{i\in I_2^1}\frac{\alpha_i}{1-\sum\limits_{i\in I_2^2}\alpha_i} = 1$.

Let $I_1 = I_1\cup I_2^3$, $I_2 = I_2^1$ and $\beta_i = \dfrac{\alpha_i}{1-\sum\limits_{i\in I_2^2}\alpha_i}$.

Using (27), we obtain

$$\|0, y - Ty, Ty - y\| \leq \sum_{i \in I_1} \beta_i \|0, y_i - Ty, Ty - y_i\| + \sum_{i \in I_2} \beta_i r^s(F). \tag{28}$$

If $A_0 = \sum_{i \in I_2} \beta_i$ then using (28), we have

$$\|0, y - Ty, Ty - y\| \leq \sum_{i \in I_1} \beta_i \|0, y_i - Ty, Ty - y_i\| + A_0 r^s(F), \tag{29}$$

with $\sum_{i \in I_1} \beta_i + A_0 = 1$ and $y_i \in F_{m-1} = conv(F_{m-2} \cup TF_{m-2})$.

For each $i \in I_1$,

$$y_i = \sum_{j \in J_i^1} \gamma_i^j y_i^j + \sum_{j \in J_i^2} \gamma_i^j T y_i^j,$$

with $y_i^j \in F_{m-2}$ and $\sum_{j \in J_i^1 \cup J_i^2} \gamma_i^j = 1$. So we obtain

$$\|0, y_i - Ty, Ty - y_i\| \leq \sum_{j \in J_i^1} \gamma_i^j \|0, y_i^j - Ty, Ty - y_i^j\| + \sum_{j \in J_i^2} \gamma_i^j \|0, Ty_i^j - Ty, Ty - Ty_i^j\|. \tag{30}$$

Using the condition (**NS25**), we have

$$\|0, Ty_i^j - Ty, Ty - Ty_i^j\| < \max \left\{ \begin{array}{c} \|0, y_i^j - y, y - y_i^j\|, \\ \|0, Ty_i^j - y_i^j, y_i^j - Ty_i^j\|, \\ \|0, y - Ty, Ty - y\|, \\ \|0, Ty_i^j - y, y - Ty_i^j\|, \\ \|0, y_i^j - Ty, Ty - y_i^j\| \end{array} \right\}.$$

Since $y_i^j \in F_{m-2}$, $Ty_i^j \in F_{m-1}$ and $y \in F_m$, we can write

$$\begin{array}{l} \|0, y_i^j - y, y - y_i^j\| \leq r^s(F), \\ \|0, Ty_i^j - y_i^j, y_i^j - Ty_i^j\| \leq r^s(F), \\ \|0, Ty_i^j - y, y - Ty_i^j\| \leq r^s(F) \end{array}$$

and

$$\|0, Ty_i^j - Ty, Ty - Ty_i^j\| < \max \left\{ \begin{array}{c} r^s(F), \|0, y - Ty, Ty - y\|, \\ \|0, y_i^j - Ty, Ty - y_i^j\| \end{array} \right\}.$$

Let J_i^2 be the union of the disjoint sets $J_i^2 = J_i^{2_1} \cup J_i^{2_2} \cup J_i^{2_3}$ such that

$$J_i^{2_1} = \left\{ \begin{array}{c} j \in J_i^2 : \|0, Ty_i^j - Ty, Ty - Ty_i^j\| \\ < \|0, y_i^j - Ty, Ty - y_i^j\| \end{array} \right\},$$
$$J_i^{2_2} = \left\{ \begin{array}{c} j \in J_i^2 : \|0, Ty_i^j - Ty, Ty - Ty_i^j\| \\ < r^s(F) \end{array} \right\},$$
$$J_i^{2_3} = \left\{ \begin{array}{c} j \in J_i^2 : \|0, Ty_i^j - Ty, Ty - Ty_i^j\| \\ < \|0, y - Ty, Ty - y\| \end{array} \right\}.$$

Using (30), we obtain

$$\begin{aligned} &\|0, y_i - Ty, Ty - y_i\| \\ &\leq \sum_{j \in J_i^1 \cup J_i^{2_1}} \gamma_i^j \|0, y_i^j - Ty, Ty - y_i^j\| \\ &+ \sum_{j \in J_i^{2_2}} \gamma_i^j r^s(F) + \sum_{j \in J_i^{2_3}} \gamma_i^j \|0, y - Ty, Ty - y\|. \end{aligned} \tag{31}$$

Now redefine the index sets $J_i^1 = J_i^1 \cup J_i^{2_1}$, $J_i^2 = J_i^{2_2}$, $J_i^3 = J_i^{2_3}$ and using (31) we can write

$$\begin{aligned} &\|0, y_i - Ty, Ty - y_i\| \\ &\leq \sum_{j \in J_i^1} \gamma_i^j \|0, y_i^j - Ty, Ty - y_i^j\| \\ &+ \sum_{j \in J_i^2} \gamma_i^j r^s(F) + \sum_{j \in J_i^3} \gamma_i^j \|0, y - Ty, Ty - y\|, \end{aligned}$$

with $\sum_{j \in J_i^1} \gamma_i^j + \sum_{j \in J_i^2} \gamma_i^j + \sum_{j \in J_i^3} \gamma_i^j = 1$.

Using the (29), we obtain

$$\begin{aligned} &\|0, y - Ty, Ty - y\| \\ &\leq \sum_{i \in I_1} \beta_i \sum_{j \in J_i^1} \gamma_i^j \|0, y_i^j - Ty, Ty - y_i^j\| \\ &+ \sum_{i \in I_1} \beta_i \sum_{j \in J_i^3} \gamma_i^j \|0, y - Ty, Ty - y\| \\ &+ \left[\sum_{i \in I_1} \beta_i \sum_{j \in J_i^2} \gamma_i^j + A_0 \right] r^s(F). \end{aligned} \tag{32}$$

If $\sum_{i \in I_1} \beta_i \sum_{j \in J_i^3} \gamma_i^j = 1$ we have

$$\|0, y - Ty, Ty - y\| < \|0, y - Ty, Ty - y\|,$$

which is a contradiction.

Hence $\sum_{i \in I_1} \beta_i \sum_{j \in J_i^3} \gamma_i^j < 1$ and using (32), we obtain

$$
\begin{aligned}
&\|0, y-Ty, Ty-y\| \\
&\le \frac{\sum\limits_{i\in I_1}\beta_i\sum\limits_{j\in J_i^1}\gamma_i^j}{1-\sum\limits_{i\in I_1}\beta_i\sum\limits_{j\in J_i^3}\gamma_i^j}\|0, y_i^j-Ty, Ty-y_i^j\| \\
&\quad+\frac{\sum\limits_{i\in I_1}\beta_i\sum\limits_{j\in J_i^2}\gamma_i^j+A_0}{1-\sum\limits_{i\in I_1}\beta_i\sum\limits_{j\in J_i^3}\gamma_i^j}r^s(F),
\end{aligned}
\tag{33}
$$

with $\dfrac{\sum\limits_{i\in I_1}\beta_i\sum\limits_{j\in J_i^1}\gamma_i^j}{1-\sum\limits_{i\in I_1}\beta_i\sum\limits_{j\in J_i^3}\gamma_i^j}+\dfrac{\sum\limits_{i\in I_1}\beta_i\sum\limits_{j\in J_i^2}\gamma_i^j+A_0}{1-\sum\limits_{i\in I_1}\beta_i\sum\limits_{j\in J_i^3}\gamma_i^j}=1.$

Let $A_1=\dfrac{\sum\limits_{i\in I_1}\beta_i\sum\limits_{j\in J_i^2}\gamma_i^j+A_0}{1-\sum\limits_{i\in I_1}\beta_i\sum\limits_{j\in J_i^3}\gamma_i^j}$ and denote the index set by $K=\bigcup\limits_{i\in I_1}\left(\bigcup\limits_{j\in J_i^1}j\right)$, write ζ_k for $k\in K$ relative to (i,j), that is

$$
\zeta_k=\frac{\sum\limits_{i\in I_1}\beta_i\sum\limits_{j\in J_i^2}\gamma_i^j}{1-\sum\limits_{i\in I_1}\beta_i\sum\limits_{j\in J_i^3}\gamma_i^j}.
$$

Also we write y_k for y_i^j. Then using (33), we obtain

$$
\begin{aligned}
\|0, y-Ty, Ty-y\| &\le \sum_{k\in K}\zeta_k\|0, y_k-Ty, Ty-y_k\| \\
&\quad+(A_1+A_0)r^s(F),
\end{aligned}
$$

with $\sum\limits_{k\in K}\zeta_k+A_1+A_0=1$ and $y_k\in F_{m-2}$.

Repeating this process we get

$$
\begin{aligned}
\|0, y-Ty, Ty-y\| &\le \sum_{p\in P}\lambda_p\|0, y_p-Ty, Ty-y_p\| \\
&\quad+\sum_{k=0}^{m-1}A_k r^s(F),
\end{aligned}
$$

where $y_p\in F_1$ and $\sum\limits_{p\in P}\lambda_p+\sum\limits_{k=0}^{m-1}A_k=1$.

Then $\|0, y_p-Ty, Ty-y_p\|\le r^s(F)$ and

$$
\begin{aligned}
\|0, y-Ty, Ty-y\| &\le \left(\sum_{p\in P}\lambda_p+\sum_{k=0}^{m-1}A_k\right)r^s(F) \\
&= r^s(F).
\end{aligned}
$$

Using (23), we get

$$
\begin{aligned}
&\|0, x-Ty, Ty-x\| \\
&\le \left(\sum_{k=0}^{m-1}B_k+\sum_{p\in P}\gamma_p+\sum_{k=0}^{m-1}A_k\right)r^s(F),
\end{aligned}
$$

with $\sum\limits_{k=0}^{m-1}B_k+\sum\limits_{p\in P}\gamma_p+\sum\limits_{k=0}^{m-1}A_k=1$.

Consequently, we obtain $\|0, x-Ty, Ty-x\|\le r^s(F)$ and so

$$
\delta^s_{m+1}-\varepsilon<\|0, x-Ty, Ty-x\|\le r^s(F).
$$

Case 3. For $x, y\in F_m$, we have

$$
\begin{aligned}
&\delta^s_{m+1}-\varepsilon<\|0, Tx-Ty, Ty-Tx\| \\
&<\max\left\{\begin{array}{c}\|0, x-y, y-x\|, \\ \|0, Tx-x, x-Tx\|, \\ \|0, y-Ty, Ty-y\|, \\ \|0, x-Ty, Ty-x\|, \\ \|0, Tx-y, y-Tx\|\end{array}\right\}
\end{aligned}
\tag{34}
$$

and repeating what has been done in Case 2, we get

$$
\delta^s_{m+1}-\varepsilon<\|0, Tx-Ty, Ty-Tx\|\le r^s(F).
$$

In all three cases we have $\delta^s_{m+1}-\varepsilon<r^s(F)$. If ε tends to 0 we get $\delta^s_{m+1}\le r^s(F)$.

Let $F^\infty=\bigcup\limits_{n\in\mathbb{N}}F_n$. Then F^∞ is nonempty because $C^s(F)\ne\emptyset$. Since $F_k\subseteq F_{k+1}$, we obtain

$$
\delta^s(F^\infty)=\lim_{k\to\infty}\delta^s(F_k)\le r^s(F).
$$

As $F_k\subset F$, $F^\infty\subseteq F$ and so $\delta^s(F^\infty)\le r^s(F)$.

Using the S-normal structure of F we have $r^s(F)<\delta^s(F)$ and $\delta^s(F^\infty)<\delta^s(F)$. So F^∞ must be a proper subset of F. We obtain that F^∞ is convex and $TF^\infty\subseteq F^\infty$.

Let $M=\overline{convF^\infty}=\overline{F^\infty}$, its diameter is the same as F^∞. So we have

$$
\delta^s(M)\le r^s(F)<\delta^s(F)
$$

and M is closed, nonempty and convex proper subset of F. Since T is continuous then M is T-invariant and

$$
TM=TF^\infty\subseteq\overline{TF^\infty}\subseteq\overline{F^\infty}=M.
$$

So $M \in \mathcal{A}$ and $M \subsetneqq F$ contradicting the minimality of F. Hence, it should be $\delta^s(F) = 0$. Consequently, F has a unique fixed point under T. □

4. Some comparisons on S-normed spaces

In [12], the present authors defined Rhoades' condition (**S25**) using the notion of an S-metric. Also, they investigated relationships between the conditions (**S25**) and (**R25**) in [13].

In this section, we determine the relationships between the conditions (**S25**) (resp. (**NR25**)) and (**NS25**).

At first, we recall the Rhoades' condition on normed spaces as follows [17]:

Let $(X, \|.\|)$ be a Banach space and T be a self-mapping of X.

$$(\mathbf{NR25}) \qquad \|Tx - Ty\| < \max \left\{ \begin{array}{c} \|x-y\|, \|x-Tx\|, \\ \|y-Ty\|, \|x-Ty\|, \\ \|y-Tx\| \end{array} \right\},$$

for each $x, y \in X$, $x \neq y$.

Now we give the relationship between (**S25**) and (**NS25**) in the following proposition.

Proposition 7. *Let $(X, \|.,.,.\|)$ be an S-Banach space, $(X, S_{\|.\|})$ be the S-metric space obtained by the S-metric generated by $\|.,.,.\|$ and T be a self-mapping of X. If T satisfies the condition* (**NS25**) *then T satisfies the condition* (**S25**).

Proof. Assume that T satisfies the condition (**NS25**). Using the condition (**NS25**), we have

$$\begin{array}{l} S_{\|.\|}(Tx, Tx, Ty) = \|Tx - Tx, Tx - Ty, Ty - Tx\| \\ = \|0, Tx - Ty, Ty - Tx\| \\ < \max \left\{ \begin{array}{c} \|0, x-y, y-x\|, \|0, Tx-x, x-Tx\|, \\ \|0, Ty-y, y-Ty\|, \|0, Ty-x, x-Ty\|, \\ \|0, Tx-y, y-Tx\| \end{array} \right\} \\ = \max \left\{ \begin{array}{c} S_{\|.\|}(x,x,y), S_{\|.\|}(Tx,Tx,x), \\ S_{\|.\|}(Ty,Ty,y), S_{\|.\|}(Ty,Ty,x), \\ S_{\|.\|}(Tx,Tx,y) \end{array} \right\} \end{array}$$

and so the condition (**S25**) is satisfied by T on $(X, S_{\|.\|})$. □

Now, we give the relationship between the conditions (**NR25**) and (**NS25**) in the following proposition.

Proposition 8. *Let $(X, \|.\|)$ be a Banach space, $(X, \|.,.,.\|)$ be an S-normed space obtained by the S-norm generated by $\|.\|$ and T be a self-mapping of X. If T satisfies the condition* (**NR25**) *then T satisfies the condition* (**NS25**).

Proof. Let T satisfies the condition (**NR25**). Using the conditions (**NR25**) and (**N3**), we have

$$\begin{array}{l} \|0, Tx - Ty, Ty - Tx\| \\ = \|0\| + \|Tx - Ty\| + \|Ty - Tx\| \\ = 2\|Tx - Ty\| \\ < 2\max \left\{ \begin{array}{c} \|x-y\|, \|x-Tx\|, \\ \|y-Ty\|, \|x-Ty\|, \|y-Tx\| \end{array} \right\} \\ = \max \left\{ \begin{array}{c} 2\|x-y\|, 2\|x-Tx\|, \\ 2\|y-Ty\|, 2\|x-Ty\|, 2\|y-Tx\| \end{array} \right\} \\ = \max \left\{ \begin{array}{c} \|x-y\| + \|y-x\|, \\ \|x-Tx\| + \|Tx-x\|, \\ \|y-Ty\| + \|Ty-y\|, \\ \|x-Ty\| + \|Ty-x\|, \\ \|y-Tx\| + \|Tx-y\| \end{array} \right\} \\ = \max \left\{ \begin{array}{c} \|0, x-y, y-x\|, \\ \|0, Tx-x, x-Tx\|, \\ \|0, Ty-y, y-Ty\|, \\ \|0, Ty-x, x-Ty\|, \\ \|0, Tx-y, y-Tx\| \end{array} \right\} \end{array}$$

and so the condition (**NS25**) is satisfied. □

Finally, we give the relationship between Theorem 1 and the following theorem.

Theorem 2. *[17] Let X be a reflexive Banach space and A be a nonempty, closed, bounded and convex subset of X, having normal structure. If $T : A \to A$ is a continuous self-mapping satisfying the condition* (**NR25**) *then T has a unique fixed point in A.*

Theorem 1 and Theorem 2 coincide when X is an S-Banach space obtained by the S-norm generated by $\|.\|$. Clearly, Theorem 1 is a generalization of Theorem 2 as we have seen in Section 2 that there are S-norms which are not generated by any norm.

References

[1] Ege, Ö., Park, C., & Ansari, A. H. (2020). A different approach to complex valued G_b-metric spaces. *Advances in Difference Equations* 2020, 152. https://doi.org/10.1186/s13662-020-02605-0

[2] Ramezani, M., Ege, Ö., & De la Sen, M. (2019). A new fixedpoint theorem and a new generalized Hyers-Ulam-Rassias stability in incomplete normed spaces. *Mathematics* 2019, 7, 1117. https://doi.org/10.3390/math7111117

[3] Ege, M. E., & Alaca, C. (2015). Fixed point results and an application to homotopy in modular metric spaces. *J. Nonlinear Sci. Appl.*, 8(6), 900-908.

[4] Gupta, A. (2013). Cyclic contraction on S-metric space. *International Journal of Analysis and Applications*, 3(2) 119-130.

[5] Mohanta, S.K. (2012). Some fixed point theorems in G-metric spaces. *An. Ştiinţ. Univ. "Ovidius" Constanţa Ser. Mat.*, 20(1), 285-305.

[6] Mustafa, Z., & Sims, B. (2006). A new approach to generalized metric spaces. *J. Nonlinear Convex Anal.*, 7(2), 289-297.

[7] Sedghi, S., Shobe, N., & Aliouche, A. (2012). A generalization of fixed point theorems in S-metric spaces. *Mat. Vesnik*, 64(3), 258-266.

[8] Rhoades, B.E. (1977). A comparison of Various definitions of contractive mappings. *Trans. Amer. Math. Soc.*, 226, 257-290.

[9] Chang, S.S. (1986). On Rhoades' open questions and some fixed point theorems for a class of mappings. *Proc. Amer. Math. Soc.*, 97(2), 343-346.

[10] Chang, S.S., & Zhong, Q.C. (1990). On Rhoades' open questions. *Proc. Amer. Math. Soc.*, 109(1), 269-274.

[11] Liu, Z., Xu, Y., & Cho, Y.J. (1998). On Characterizations of fixed and common fixed points. *J. Math. Anal. Appl.*, 222, 494-504.

[12] Özgür, N.Y., & Taş, N. (2017). Some fixed point theorems on S-metric spaces. *Mat. Vesnik*, 69(1), 39-52.

[13] Özgür, N.Y., & Taş, N. (2017). Some new contractive mappings on S-metric spaces and their relationships with the mapping (**S25**). *Math. Sci.*, 11(1), 7-16.

[14] Taş, N. (2017). *Fixed point theorems and their various applications*, Ph.D. Thesis. Balıkesir University.

[15] Khan, K.A. (2014). Generalized normed spaces and fixed point theorems. *Journal of Mathematics and Computer Science*, 13, 157-167.

[16] Smulian, V. (1939). On the principle of inclusion in the space of the type (B). *Rec. Math. [Math. Sbornik]N.S. 5*, 47(2), 317-328.

[17] Oliveria, P. (2001). Two Results on Fixed Points. In: Proceedings of the Third World Congress of Nonlinear Analysts, Part 4 (Catania, 2000). Nonlinear Anal. 47 (2001) 2703-2717.

Nihal Taş *received her Ph.D. in Mathematics at Balıkesir University, Balıkesir, Turkey, in 2017. She is currently an associate professor at Balıkesir University, Balıkesir, Turkey. Her research interests include general topology, fixed point theory and soft set theory.*
https://orcid.org/0000-0002-4535-4019

Nihal Özgür *received her Ph.D. in Mathematics at Uludağ University, Bursa, Turkey, in 1999. She is currently a full professor at Balıkesir University, Balıkesir, Turkey. Her research interests include complex functions with one variable, fixed point theory and number theory.*
https://orcid.org/0000-0002-8152-1830

An International Journal of Optimization and Control: Theories & Applications
ISSN:2146-0957 eISSN:2146-5703
Vol.12, No.2, pp.184-193 (2022)
http://doi.org/10.11121/ijocta.2022.1219

RESEARCH ARTICLE

A numerical scheme for the one-dimensional neural field model

Aytül Gökçe[a*], Burcu Gürbüz[b]

[a] *Department of Mathematics, Faculty of Science and Arts, Ordu University, Ordu, Turkey*
[b] *Institute of Mathematics, Johannes Gutenberg-University, Mainz, 55128 Germany*
aytulgokce@odu.edu.tr, burcu.gurbuz@uni-mainz.de

ARTICLE INFO

Article History:
Received 24 January 2022
Accepted 28 July 2022
Available 29 July 2022

Keywords:
Neural field
Integro-differential equation
Numerical methods

AMS Classification 2010:
92B20; 34K28; 37Mxx

ABSTRACT

Neural field models, typically cast as continuum integro-differential equations, are widely studied to describe the coarse-grained dynamics of real cortical tissue in mathematical neuroscience. Studying these models with a sigmoidal firing rate function allows a better insight into the stability of localised solutions through the construction of specific integrals over various synaptic connectivities. Because of the convolution structure of these integrals, it is possible to evaluate neural field model using a pseudo-spectral method, where Fourier Transform (FT) followed by an inverse Fourier Transform (IFT) is performed, leading to an identical partial differential equation. In this paper, we revisit a neural field model with a nonlinear sigmoidal firing rate and provide an efficient numerical algorithm to analyse the model regarding finite volume scheme. On the other hand, numerical results are obtained by the algorithm.

1. Introduction

The cortex has a structure which can be viewed as a great number of macro and micro columns, each of which encapsulates laminar substructures and is considered as an elementary unit of the cortex [1, 2]. Studying columnar organisation of the cortex traces its roots back to a seminal work of Mountcastle in the 20th century, when clusters of neurons, that form cylinders of $200 - 500\mu m$, are aligned through cortical layers [1, 3]. The 20th century witnessed two breakthrough that shed lights on the foundations of theoretical neuroscience: (i) large scale cortical dynamics of the cortex relies on the dynamics of individual neurons, (ii) individual neurons can be accounted as electrical units and have an essential role to conduct signals by reacting to electrical current. Therefore the invention of multi-electrode technology provided researchers to characterise the resting state of the membrane voltage of neurons in a cortical tissue. The development of these techniques for cortical tissue had lead new research manners to analyse the electrophysiological investigations of synaptic transmission [3, 4]. Hence, large-scale spatio-temporal dynamics of neural populations which were not recognised by the scientific community till the 1980s, have been one of the primary sources in theoretical neuroscience.

Neural field models have specifically been investigated to understand the behaviour of a real cortical tissue in space and time. The history of these models is based on Beurle's pioneering work, where the study of masses of cells in the brain considering only excitatory neurons is provided, in the 1950s [5]. The bases of modern versions of these models have been conceived by Wilson and Cowan [6, 7], Amari [8, 9] and Nunez [10] in the late 1970s. Since their initial inception, neural fields have been widely analysed in one and two dimensional systems. This has mostly encapsulated the mathematical investigations and numerical analysis of space-time cortical patterns,

*Corresponding Author

and much has been studied about localised patterns, global periodic states and travelling waves. These tissue level models have shed lights into understanding of many application areas including large-scale brain rhythms [11], geometric visual hallucinations [12], motion perception [13] and short term memory [14]. For more current perspective for the analysis of neural field modelling we refer reader to a comprehensive book by Coombes et al. [15]. Neural field models have been viewed spatially extended models to mimic the macroscopic spatio-temporal dynamics of interacting neurons and written in the form of partial integro-differential equations. Using various synaptic connectivity functions between neurons and firing rate functions, these models are known to support various solutions, e.g. localised structures as well as travelling waves observed in a real cortical tissue. These continuum models have non-local nature and have been widely analysed numerically and analytically. Here we present a numerical scheme to study space-time solutions in neural fields. This provides an alternative aspect to solve the neural field equations given in the form of an integro-differential equation and comparable with its analytical representation.

Here we present an adapted numerical scheme to obtain numerical approximation to the solutions in neural fields. The numerical scheme is based on the finite volume approach and first we describe the discretisation process by working on cell centered and collocated grid of meshes. Then we provide an expression for the numerical fluxes. By the calculation of fluxes, we obtain matricial formulation. On the other hand, an approximation of the average value of f on the cell is calculated by the Gaussian quadrature. Thereafter, the Patankar matrix is defined in the matricial formulation and the system is solved by a series approach together with the help of control volume.

This chapter is organised as follows. In Sec. 2, we revisit a primer one dimensional neural field model and summarise the previous results. Then, in Sec. 3, an equivalent partial differential equation is derived with a pseudo-spectral method using Fourier Transform (FT) followed by an inverse Fourier transform (IFT). Sec. 3 is dedicated to an efficient numerical algorithm for the neural field model in partial differential equation form with an exponentially decaying synaptic kernel and sigmoidal firing rate function. Lastly, in Sec. 5, summary of the results is given with potential future directions.

2. The PIDE model

In this section, we concentrate on a minimal one-dimensional neural field equation that can be written as a partial integro-differential equation (PIDE) of the form

$$\frac{\partial v(x,t)}{\partial t} = -v(x,t) + \int_{\Omega} w(x-y) f(v(y,t)-\kappa) dy, \tag{1}$$

where $\Omega \subseteq \mathbb{R}$ is a planar domain, $x \in \Omega$ and $t \in \mathbb{R}^+$. Here the variable v stands for the synaptic activity of neuron population, the function w represents the anatomical connectivity between neurons and assumed that the connectivity depends on the Euclidean distance $|x-y|$. The function f denotes a sigmoidal type firing rate and the constant parameter κ is the firing threshold.

Typical forms for the connectivity function are often considered using exponential functions such that

$$\lim_{x\to\infty} w(x) = 0 \quad \text{and} \quad \int_{-\infty}^{\infty} w(x) \mathrm{d}x < \infty. \tag{2}$$

Therefore the kernel describing the spatial distribution of synaptic interactions can be chosen in the simplest form of

$$w(x) = \frac{1}{2\sigma} \mathrm{e}^{-|x|/\sigma}, \tag{3}$$

where w is chosen as symmetrical, e.g. $w(x) = w(-x)$ and continuous, and σ is a scaling parameter. This version of exponentially decaying connectivity function is known to support the generation of travelling front solutions which connects high activity states to a low activity states [16–18].

Besides, the firing rate non-linearity triggered by the membrane voltage is generally chosen in a smooth and monotonically increasing functional form with

$$\lim_{x\to-\infty} f(v(x,t)) = 0 \quad \text{and} \quad \lim_{x\to\infty} f(v(x,t)) = 1. \tag{4}$$

Hence, we consider an example form of such firing rate as

$$f(v(x,t)-\kappa) = \frac{1}{1+\mathrm{e}^{-\alpha(v(x,t)-\kappa)}}, \tag{5}$$

where α represents the steepness parameter and κ is the firing threshold. The form of the synaptic kernel and firing rate function is given in Fig. 1. Studying neural field models with given example of firing rate non-linearity and connectivity often allows a good understanding of the solutions as given in Fig. 2 and their stability.

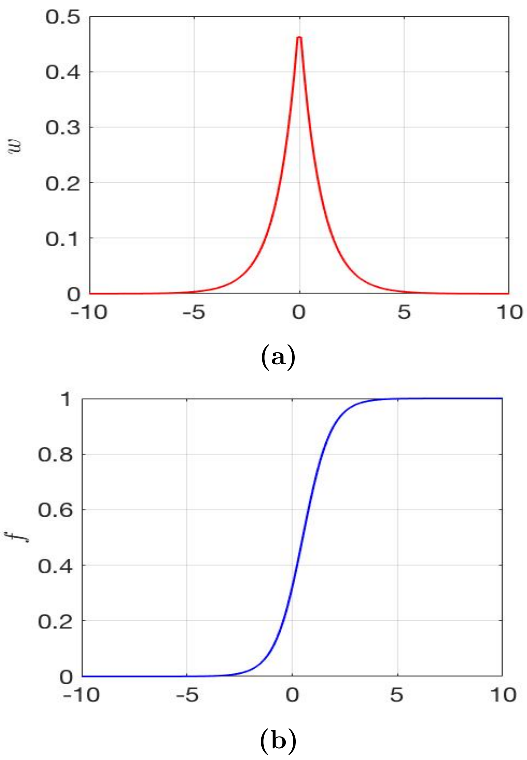

Figure 1. The synaptic kernel (a) and sigmoidal firing rate function (b) mimicking the interactions in the brain. Parameters are $\kappa = 0.5$, $\sigma = 1$ and $\mu = 1.5$.

A simplification to the model described in Eq. (1) is made by Amari, who considered a Heaviside choice of firing rate: $f(u) = H(u - \kappa)$ assuming that $f(v(x,t)) = 0$ if $v \leq \kappa$ and $f(v(x,t)) = 1$ if $v > \kappa$. Here H stands for the Heaviside function. The front solution to neural field model with a Heaviside firing rate has been studied by Coombes *et al.* for interface dynamics [18], where a typical front solution is considered as $v(x,t) > \kappa$ for $x < x_0(t)$ and $v(x,t) \leq \kappa$ for $x \geq x_0(t)$. Here $x_0(t)$ represents the evolution of interface connecting high activity state to a low activity state.

Although partial integro-differential equations (PIDE) for neural field models described in Eq. (1) are thoroughly studied in the literature for various connectivity and firing rate functions, one can also describe an identical equation of partial differential equations (PDE). This link from PIDE form to PDE form of the neural field model can be efficiently used for more straight-forward theoretical and numerical investigations [19, 20]. A large amount of analytical work has been performed on Eq. (1). Although the cortex is actually a two-dimensional domain, it is more realistic to analyse neuronal system in two dimension. However, here we focus on a one-dimensional primer to explain the numerical algorithm.

3. An equivalent PDE model

From now on our attention is directed in two folds. Firstly, using the ideas presented by Laing and Troy [20], we describe PDE which is identical to PIDE given in Eq. (1). Secondly, we provide an efficient numerical solution for the PIDE form. Owing to the convolution structure in Eq. (1), several methods have been developed to convert PIDE form to an equivalent PDE form [14]. One of these methods is applied using a Fourier transform for the convolution of the synaptic kernel and firing rate, manipulate the obtained equation. Then an inverse Fourier Transform is performed to transform the dynamics to an equivalent PDE version of the model in Eq. (1). This technique has been efficiently used to exploit dynamical systems with several standard tools [21, 22], as well as allowing for a numerical analysis of spatio-temporal neural fields in one and two dimensions.

A Fourier Transform of the convolution of synaptic kernel and firing rate functions is described as the product of their Fourier transforms. We now assume that v and v_t are continuous and integrable with $x \in \mathbb{R}$ and $t \in \mathbb{R}^+$, and follow the ideas described in [14, 20]. Thus $FT[v](p)$ can be denoted as the Fourier transform of $v(x)$ where p is the transform variable. Here the Fourier transform of the connectivity function w can be written with a rational function of p^2, e.g. $A(p^2)/B(p^2)$, where p denotes the Euclidean distance in Fourier space. Using the properties of convolution and applying FT to both sides of Eq. (1):

$$FT\left[\frac{\partial v}{\partial t} + v\right] = FT[w]FT[f(v - \kappa)], \qquad (6)$$

where $FT[\cdot]$ represents the Fourier transform. Therefore, for the kernel given in Eq. (3), it can be written that

$$FT[w] = \frac{A(p^2)}{B(p^2)} = \frac{1}{1 + \sigma^2 p^2}. \qquad (7)$$

Then Eq. (6) can be given as

$$(1 + \sigma^2 p^2)FT\left[\frac{\partial v}{\partial t} + v\right] = FT[f(v - \kappa)]. \qquad (8)$$

Taking the inverse Fourier transform, the model becomes

$$\left(1 - \sigma^2 \frac{\partial^2}{\partial x^2}\right)\left(\frac{\partial v(x,t)}{\partial t} + v(x,t)\right) = f(v(x,t) - \kappa), \qquad (9)$$

leading to

$$v_t + v - \sigma^2 v_{txx} - \sigma^2 v_{xx} = f(v - \kappa), \qquad (10)$$

where f is the sigmoidal firing rate nonlinearity given in Eq. (5) and κ is a constant threshold. Here we also used that $FT[v_{xx}] = -p^2 FT[v]$. The partial differential equation given in Eq. (10) is an equivalent version of the partial integro-differential equation given in Eq. (1) with synaptic kernel in Eq. (3) and non-linear firing rate in Eq. (5).

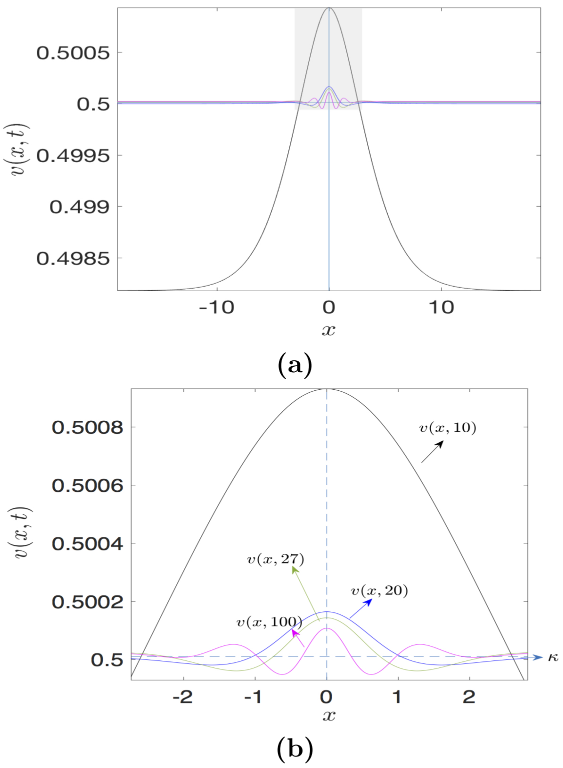

Figure 2. A bump solution $u(x,t)$ at various times: $t = 10$(black), $t = 20$ (blue), $t = 27$ (green), $t = 100$ (magenta) is shown in (a). The region that is highlighted with gray in (a) is zoomed in (b). Parameters are $\kappa = 0.5001$, $\mu = 2.5$, $\sigma = 1$ and the domain size is $L = 6\pi$. The initial condition is chosen as $u(x,0) = 2/\cosh(x)$.

In the following section we provide an efficient numerical algorithm based on finite volume approach for solving Eq. (10) with the appropriate conditions. We give detailed information about the numerical approach for the convergence results which is an effective and alternative approximation for such problems [23], [24].

4. Numerical investigation

The finite volume method is a well-known numerical approach for describing partial differential equations and to evaluate in the algebraic equations form. The typical description of the method consists of discretisation process which is for solving the partial differential equations. This is acquired a system of algebraic equations. On the other hand, the discretisation procedure can be applied for a cell centered and collocated grid of meshes depending on a geometrical and mesh construction of the problem. Thus it is clearly visible in the miscellaneous applications of the method that it is of various types of numerical algorithms regarding variable types of the equations and featured operators [25]. The method also express the conservation laws of related to the amount of unknowns in the equation which is namely indicated by the flux. In a specific case, this expression can be satisfied by the synaptic activities in a neural field studies. Namely, the flux which arrives to a control volume through the synaptic connectivity is of the contrary direction of the synaptic connectivity first existed the control volume. Therefore, we understand that the method is applied on real-world scenarios regarding the geometrical construction of the problem. As a specific example in our study, we describe the 1D problem in the neural field which is adapted to the cell centered meshes. Accordingly, the synaptic activity of neuron population in the scenario with a sigmoidal type firing rate and the related parameters can be explained concerning the meshes for the synaptic connectivities on a planar domain.

In this section, we consider the finite volume conceptualisation for the numerical investigation. The aim is to investigate the numerical solution of Eq. (10) with the suitable Dirichlet boundary conditions. Particularly, we consider first the discretisation procedure and we obtain an interpretation for the fluxes. This leads us to figure out a systematic approach for the calculation of the fluxes which is represented by the Patankar matrix in the matricial formulation.

4.1. Discretisation

We design the discretisation process on the cell centered grids (see Fig. 3). First we consider $I \in \mathbb{N}$ and the domain Ω has I cells. The cells are organised by the point-wise structures $\phi_i := [x_{i-1/2}, x_{i+1/2}]$ for $i = 1, 2, ..., N$ with $x_{i-1/2}$ and $x_{i+1/2}$.

Here we generate the figure for a 1D domain which is of the length L and it is discretised into the same size of N_x number of cells [26]. The size of the each cell is given as 0.1 and denoted by Δx_i. We contemplate with the cell-centred finite volume method for the numerical concept. Therefore, we visualise the domain with the position of the cell centered grids where interfaces are given for the cells.

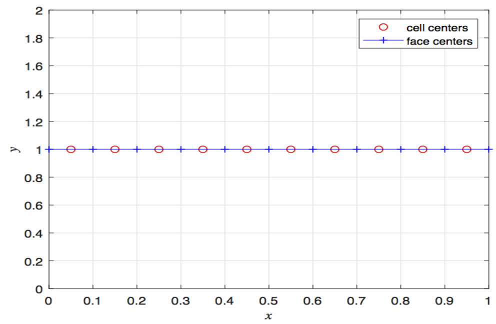

Figure 3. The discretised domain in 1D with $L = 1$ and $N_x = 10$.

Now, we design Eq. (10) on cell ϕ_i [27]. We also apply Gauss's Theorem and transform the equation into the following form [23].

$$\frac{\partial}{\partial t}\int_{\phi_i} v(x,t)\,dx + \int_{\phi_i} v(x,t)\,dx - \sigma^2\frac{\partial^3}{\partial x^2\partial t}\int_{\phi_i} v(x,t)\,dx - \sigma^2\frac{\partial^2}{\partial x^2}\int_{\phi_i} v(x,t)\,dx = f(v(x_{i+1/2},t)-\kappa) - f(v(x_{i-1/2},t)-\kappa).$$

which is alternatively shown as

$$\int_{\phi_i} v(x,t_{n+1})\,dx = \int_{\phi_i} v(x,t_n)\,dx + \int_{t_n}^{t_{n+1}} f(v(x_{i+1/2},t)-\kappa) - \int_{t_n}^{t_{n+1}} f(v(x_{i-1/2},t)-\kappa),$$

where $\Delta t := t_{n+1} - t_n$ is defined for any t_n and its successive t_{n+1} in the cell edges for a suitable number n. Then we divide equation (11) to $\frac{1}{\Delta x_i}$ where $\Delta x_i = L$.

$$\frac{1}{\Delta x_i}\int_{\phi_i} v(x,t_{n+1})\,dx = \frac{1}{\Delta x_i}\int_{\phi_i} v(x,t_n)\,dx + \frac{1}{\Delta x_i}\left(\int_{t_n}^{t_{n+1}} f(v(x_{i+1/2},t)-\kappa) - \int_{t_n}^{t_{n+1}} f(v(x_{i-1/2},t)-\kappa)\right),$$

where the numerical scheme is stated for the alternative form as

$$V_i^{n+1} = V_i^n - \frac{\Delta t}{\Delta x_i}(F_{i+1/2}^n - F_{i-1/2}^n), \tag{11}$$

where V_i^n shows us a new form of the cell averages. It is also an approximation to the average value of v at anytime $t^n := n\,\Delta t$ [28]. Alternatively, we show

$$V_i^n \approx \frac{1}{\Delta x_i}\int_{x_{i-1/2}}^{x_{i+1/2}} v(x,t_n)\,dx \equiv \frac{1}{\Delta x_i}\int_{\phi_i} v(x,t_n)\,dx. \tag{12}$$

We denote $F_{i+1/2}^n$ which is an approximation to the numerical flux through out the cell.

$$F_{i+1/2}^n \approx \frac{1}{\Delta t}\int_{t_n}^{t_{n+1}} f(v(x_{i+1/2},t)-\kappa). \tag{13}$$

On the other hand, we modify Eq. (11) as in the following form:

$$\frac{V_i^{n+1} - V_i^n}{\Delta t} + \frac{F_{i+1/2}^n - F_{i-1/2}^n}{\Delta x_i} = 0. \tag{14}$$

4.2. Numerical flux approximation

The concept of the finite volume method is included approximation to the fluxes. The conservation law is also taken into consideration. The average flux calculation is formulated by the law and also this is counted for the each cell construction [28], [29].

Here we provide an expression for the numerical flux approximation. Let us consider $x_{i+1/2}$ be an inner interface.

$$F_{i+1/2}^n = \frac{1}{2}[f(V_{i-1}^n) - f(V_i^n)], \tag{15}$$

where we have a formulation for the numerical flux. Now we define the finite volume approach on Eq. (11) and we get

$$F_i^{n+1} = F_i^n - \frac{\Delta t}{2\Delta x_i}[f(V_{i+1}^n) - f(V_{i-1}^n)]. \tag{16}$$

Then we obtain the flux expression and a different version of the expression is written as follows

$$F_i^{n+1} = \frac{1}{2}(F_{i-1}^n - F_{i+1}^n) - \frac{\Delta t}{2\Delta x_i}[f(V_{i+1}^n) - f(V_{i-1}^n)], \tag{17}$$

where $F_i^n = 1/2(F_{i-1}^n - F_{i+1}^n)$ is the average flux of F_{i-1}^n and F_{i+1}^n, respectively. Now we consider the Taylor series of $v(x,t_{n+1})$ and we get

$$
\begin{aligned}
v(x,t_{n+1}) &= v(x,t_n) + \Delta t v_t(x,t_n) \\
&+ \frac{1}{2}(\Delta t)^2 v_t t(x,t_n) + ... \\
&= v(x,t_n) - \Delta t A v_x(x,t_n) \\
&+ \frac{1}{2}(\Delta t)^2 A^2 v_x x(x,t_n) + ...,
\end{aligned}
$$

where A is the matrix which includes constant coefficients. We show the matricial formulation regarding the Taylor series results. Let us consider the first three terms of the series which are from above. We describe an essential equation from the finite difference scheme and we have the following equation [30,31].

$$
\begin{aligned}
V_i^{n+1} =& V_i^n - \frac{\Delta t}{\Delta x_i} A(V_{i+1}^n - V_{i-1}^n) \\
&+ \frac{1}{2}\left(\frac{\Delta t}{2\Delta x_i}\right)^2 A^2 (V_{i-1}^n - 2V_i^n + V_{i+1}^n).
\end{aligned} \tag{18}
$$

Now we apply finite volume scheme which is defined in Eq. (11). This gives us a clear statement for the approximation to the fluxes.

$$
F_{i-1/2}^n = \frac{1}{2} A(V_{i-1}^n - V_i^n) - \frac{1}{2}\frac{\Delta t}{\Delta x_i} A^2 (V_i^n - V_{i-1}^n). \tag{19}
$$

Thus we approximate the flux functions numerically in time $t_{n+1/2} = t_n + \frac{1}{2}\Delta t$. Briefly, we have

$$
F_{i-1/2}^n = f(V_{i-1/2}^{n+1/2}). \tag{20}
$$

For the cell centered and collocated grid of mesh, we have the form of $V_{i-1/2}^{n+1/2}$ at $\frac{1}{2}\Delta x_i$ and $\frac{1}{2}\Delta t$ as follows:

$$
V_{i-1/2}^{n+1/2} = \frac{1}{2}(V_{i-1}^n + V_{i+1}^n) - \frac{1}{2}\frac{\Delta t}{\Delta x_i}[f(V_{i+1}^n) - f(V_{i-1}^n)].
$$

Now we reduce the system and consider Eq. (11). By applying the upwind method we have

$$
V_i^{n+1} = V_i^n - \frac{\overline{\beta}\Delta t}{\Delta x_i}(V_{i+1}^n - V_i^n),
$$

and we also have

$$
F_{i-1/2}^n = \overline{\beta}^- V_i^n + \overline{\beta}^+ V_{i-1}^n,
$$

where β is a constant and $[\overline{\beta}]^- = \min(\overline{\beta}, 0)$ and $[\overline{\beta}]^+ = \max(\overline{\beta}, 0)$. Therefore we define the implicit form of the Patankar matrix $\mathbf{A} = [A_{ij}]$ [32], [33], [34].

$$
\mathbf{A} = \begin{cases}
V_{i-1}^{n+1} - V_{i-1}^n + \frac{\overline{\beta}\Delta t}{\Delta x_i}(V_i^n - V_{i-1}^n) \\
\text{for } j = i-1, \\
V_i^{n+1} - V_i^n + \frac{\overline{\beta}\Delta t}{\Delta x_i}(V_{i+1}^n - V_i^n) \\
\text{for } j = i, \\
V_{i+1}^{n+1} - V_{i+1}^n + \frac{\overline{\beta}\Delta t}{\Delta x_i}(V_{i+2}^n - V_{i+1}^n) \\
\text{for } j = i+1, \\
0, \quad \text{otherwise.}
\end{cases}
$$

Besides, we define the vectors:

$$
\begin{aligned}
\mathbf{V} &= \begin{bmatrix} v_1 & v_2 & \cdots & v_N \end{bmatrix}^T, \\
\mathbf{B}_1 &= \begin{bmatrix} f_1 & f_2 & \cdots & f_N \end{bmatrix}^T, \\
\mathbf{B}_2 &= \begin{bmatrix} k_1 & \cdots & k_{N-1} & k_N \end{bmatrix}^T,
\end{aligned}
$$

where $\mathbf{V}$ is the vector of unknowns, $\mathbf{B}_1$ is defined for the f function values and $\mathbf{B}_2$ is the vector of conditions. Consequently, we solve the system $\mathbf{AV} = \mathbf{B}_1 + \mathbf{B}_2$ by using Gaussian Elimination and we obtain the numerical results [35,36].

4.3. Convergence results

In this section, we consider the stability, consistency, and convergence of the method and implement numerical results of Eq. (10) with Dirichlet boundary conditions [37], [38], [39]. We show the difference between the approximate solution and the exact solution by the following statement.

Definition (local truncation error): Suppose that the approximate solution of the problem in (10) is replaced by the exact solution. Then by the help of Δx_i, we obtain

$$
\tau_i = \frac{1}{\Delta x_i^2}[v_{i-1} - 2v_{i-1} + v_{i+1} - f_i(v - \kappa)], \tag{21}
$$

which is the local truncation error for the approximation. The alternative representation is shown by applying the Taylor series expansion [38] and (21) becomes

$$
\tau_i = \frac{1}{12}\Delta x_i^2 v_i''' + \mathcal{O}(h^4), \tag{22}
$$

where $\tau_i = \mathcal{O}(h^2)$ as $h \to 0$ [38]. Now, we consider the following statement for the stability of the method [40].

Theorem 1. *The numerical scheme is considered as stable to solve the problem which is defined in together with the Dirichlet boundary conditions.*

Proof. The proof can be found in Section 8, LeVeque, R. J. (2002) [39]. □

We also present the consistency of the method by $||\tau^h|| \to 0$ as $h \to 0$ where $||\tau^h|| = \mathcal{O}(h^p)$ for $h = \Delta x_i$ in p-Norm and the method is considered as consistent by this approach [38]. Besides, we apply the discretisation on the cell centered and collocated grid of meshes. The numerical calculation of the fluxes gives us an understanding on matricial formulation of the implicit Patankar matrix and we have series approach to obtain the numerical solution. Briefly, the numerical algorithm is applied for the solution of the problem in this direction [41], [42]. We also apply L^1 error, $E_N = \frac{\sum_{i\in\epsilon_{el}} |\upsilon_i^N - \upsilon_i^n||\phi_i|}{\sum_{i\in\epsilon_{el}} |\upsilon_i^n||\phi_i|}$, and the error in L^∞ norm, $E_N = \frac{\sum_{i\in\epsilon_{el}} |\upsilon_i^N - \upsilon_i^n|}{\sum_{i\in\epsilon_{el}} |\upsilon_i^n|}$, respectively. where ϵ_{el} is the cell index set, υ_i^n and υ_i^N are the cell mean values of exact and approximation, respectively [41] at $t = t_{final}$. In the case the exact solution is not given, we describe truncation error which supports the finding for the comparison formula in L^1 and L^∞ norms.

We apply the procedure on Eq. (10) together with the Dirichlet boundary conditions given as 0 at $t = t_{final}$ and the parameters are given as $\kappa = 0.5$, and $\sigma = 1$.

Table 1. L^1 and L^∞ convergence results at $x = 0.2$.

N	L^1 error	L^∞ error
5	0.2514e–04	0.3509e–05
10	0.6004e–05	0.7420e–06
25	0.5038e–06	0.4081e–07
50	0.2203e–06	0.1295e–08

Table 2. L^1 and L^∞ convergence results at $x = 0.5$.

N	L^1 error	L^∞ error
5	0.2110e–04	0.3172e–05
10	0.5312e–05	0.7359e–06
25	0.4012e–06	0.4019e–07
50	0.1207e–07	0.1260e–08

Numerical results are obtained by MATLAB and Maple computer programs which show us the approximation in details. As we can see in the Table (1), (2), and (3) the approximation gives us more suitable results when the iteration increases. More specifically, we have efficient results after N=5 iteration which gives us an understanding about the performance result of the numerical scheme.

Table 3. L^1 and L^∞ convergence results at $x = 1.0$.

N	L^1 error	L^∞ error
5	0.1003e–04	0.2113e–05
10	0.4072e–05	0.5087e–06
25	0.2843e–06	0.2809e–07
50	0.0927e–07	0.0891e–08

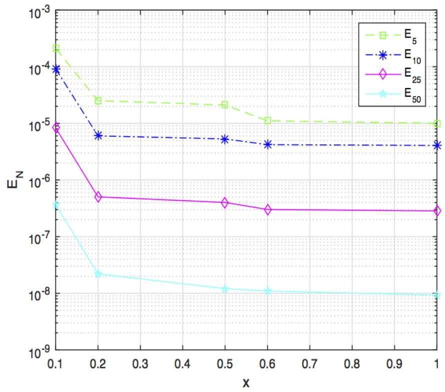

Figure 4. L^1 convergence results at $x = [0, 1]$ for $N = 5, 10, 25$, and 50.

On the other hand, Figure 4 shows us L^1 error results and we have decreasing error values by space. In the approximation we consider the analytical findings comparison with the numerical scheme result for our particular case. Figure 5 presents L^∞ error findings which is of similar effect regarding increasing x values at the final time.

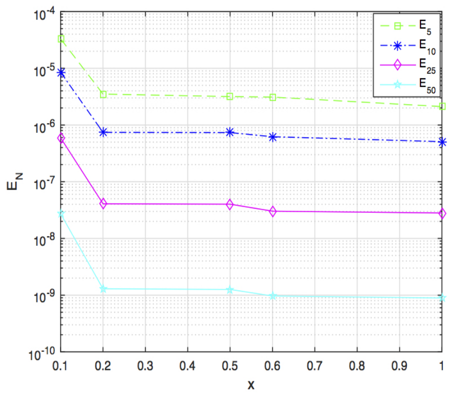

Figure 5. L^∞ convergence results at $x = [0, 1]$ for $N = 5, 10, 25$, and 50.

5. Conclusion

In this paper, we revisited a well known neural field model with a sigmoidal firing rate. We firstly provided some biological and theoretical background for the neural field model and summarised a numerical algorithm for partial differential equations. Using the ideas previously presented by Laing [14, 20], the technique to transform partial integro-differential equation to an equivalent form of partial differential equation is applied using Fourier transform followed by an inverse Fourier transform. Considering the equivalent PDE form and setting $\upsilon_t = 0$, stationary bump solutions of (1) can be obtained. Here, an exponentially decaying connectivity function and sigmoidal firing rate are taken into account for the convlution integral, see Fig. 1. The spatial derivatives in new form of the neural field model given by Eq. (9) can be computed using finite difference methods in the x direction. The system given in Eq. (9) is solved in terms of a one dimensional Mass matrix M, e.g. in the form of $Mu' = F(u)$ that allows user to compute matrix inverse in MATLAB. The PIDE model given in Eq. (1) and PDE model given in Eq. (9) are equivalent.

The numerical approach for the solution of neural fields used in this paper is based on the finite volume method which encapsulates a discretisation process to solve partial differential equation. Depending on the geometrical structure of the problem, a cell centered and collocated grid of meshes can be used for the discretisation. This approach is complemented with the Patankar matrix in the matricial formulation for the numerical investigation. As seen from the convergence results given in Figs. 4 and 5, numerical approach presented in this paper may provide an alternative direction to solve one dimensional neural fields with a better approximations when iteration increases. One straightforward extension of this work would be to consider adaptation [43, 44]. In fact, the experiments carried on cortical tissues imply that there are many metabolic processes that restrain the excitatory dynamics of neural networks. This processes differ from inhibition and called as spike frequency adaptation. The linear adaptation has been a popular modulation for investigating neural response in mean field models. Thus the numerical investigation used in this paper can be extended to include a two component neural field model including synaptic activity of a neuron population and spike frequency adaptation, see [16, 19, 20]. Another possible extension would be a numerical investigation of a two dimensional neural field model. In fact, cortex is a two dimensional structure with a few millimeter thickness. Due to its laminar organisation, the cortex is usually regarded as a two dimensional structure. Therefore it is significant to revisit a two dimensional version of the model and determine the conditions to apply the numerical investigation used here. On the other hand, the numerical investigation of a two dimensional neural field model with and without adaptation may be computationally expensive and challenging to perform in terms of algebraic equations resulting from numerical method.

Acknowledgments

Aytül Gökçe was supported by BAP (Scientific Research Projects Coordination Unit), Ordu University, through Grant No. A-2007.

References

[1] Horton, J. C., & Adams, D. L. (2005). The cortical column: a structure without a function. Philosophical Transactions of the Royal Society B: Biological Sciences, 360(1456), 837-862.

[2] DeFelipe, J., Markram, H., & Rockland, K. S. (2012). The neocortical column. Frontiers in Neuroanatomy, 6, 22.

[3] Mountcastle, V. B. (1957). Modality and topographic properties of single neurons of cat's somatic sensory cortex. Journal of Neurophysiology, 20(4), 408-434.

[4] Martin, R. (2019). Neuroscience Methods: A Guide for Advanced Students. CRC Press.

[5] Beurle, R. L. (1956). Properties of a mass of cells capable of regenerating pulses. Philosophical Transactions of the Royal Society of London. Series B, Biological Sciences, 55-94.

[6] Wilson, H. R., & Cowan, J. D. (1972). Excitatory and inhibitory interactions in localized populations of model neurons. Biophysical Journal, 12(1), 1-24.

[7] Wilson, H. R., & Cowan, J. D. (1973). A mathematical theory of the functional dynamics of cortical and thalamic nervous tissue. Kybernetik, 13(2), 55-80.

[8] Amari, S. I. (1975). Homogeneous nets of neuron-like elements. Biological Cybernetics, 17(4), 211-220.

[9] Amari, S. I. (1977). Dynamics of pattern formation in lateral-inhibition type neural fields. Biological Cybernetics, 27(2), 77-87.

[10] Nunez, P. L. (1974). The brain wave equation: a model for the EEG. Mathematical Biosciences, 21(3-4), 279-297.

[11] Coombes, S. (2010). Large-scale neural dynamics: simple and complex. NeuroImage, 52(3), 731-739.

[12] Ermentrout, G. B., & Cowan, J. D. (1979). A mathematical theory of visual hallucination patterns. Biological Cybernetics, 34(3), 137-150.

[13] Giese, M. A. (2012). Dynamic neural field theory for motion perception (Vol. 469). Springer Science & Business Media.

[14] Laing, C. R. (2014). PDE Methods for Two-Dimensional Neural Fields. In Neural Fields (pp. 153-173). Springer, Berlin, Heidelberg.

[15] Coombes, S., beim Graben, P., Potthast, R., & Wright, J. (Eds.). (2014). Neural Fields: Theory and Applications. Springer.

[16] Ermentrout, G. B., & McLeod, J. B. (1993). Existence and uniqueness of travelling waves for a neural network. Proceedings of the Royal Society of Edinburgh Section A: Mathematics, 123(3), 461-478.

[17] Coombes, S. (2005). Waves, bumps, and patterns in neural field theories. Biological Cybernetics, 93(2), 91-108.

[18] Coombes, S., Schmidt, H., & Bojak, I. (2012). Interface dynamics in planar neural field models. Journal of Mathematical Neuroscience, 2(1), 1-27.

[19] Gokce, A. (2017). The interfacial dynamics of Amari type neural field models on finite domains. (Doctoral dissertation, University of Nottingham).

[20] Laing, C. R., & Troy, W. C. (2003). PDE methods for nonlocal models. SIAM Journal on Applied Dynamical Systems, 2(3), 487-516.

[21] Laing, C. R. (2005). Spiral waves in nonlocal equations. SIAM Journal on Applied Dynamical Systems, 4(3), 588-606.

[22] Coombes, S., beim Graben, P., Potthast, R., & Wright, J. (Eds.). (2014). Neural Fields: Theory and Applications. Springer.

[23] Fedak, A. (2018). A compact fourth-order finite volume method for structured curvilinear grids. University of California, Davis.

[24] Cueto-Felgueroso, L. (2009). Finite volume methods for one-dimensional scalar conservation laws. `http://juanesgroup.mit.edu/lcueto/teach`.

[25] Zoppou, C., Knight, J. H. (1999). Analytical solution of a spatially variable coefficient advection–diffusion equation in up to three dimensions. Applied Mathematical Modelling, 23(9), 667-685.

[26] Eftekhari, A.A. et al. (2015). FVTool: a finite volume toolbox for Matlab. Zenodo. `http://doi.org/10.5281/zenodo.32745`

[27] Nordbotten, J. M. (2014). Cell-centered finite volume discretizations for deformable porous media. International Journal for Numerical Methods in Engineering, 100(6), 399-418.

[28] Mungkasi, S. (2008). Finite volume methods for the one-dimensional shallow water equations. (M. Math. Sc. thesis, Australian National University).

[29] Eymard, R., Gallouët, T., Herbin, R., Latché, J. C. (2007). Analysis tools for finite volume schemes. Proceedings of Equa Diff 11, 111-136.

[30] Versteeg, H. K., Malalasekera, W. (2007). An introduction to computational fluid dynamics: the finite volume method. Pearson Education.

[31] Abbott, M. B., Basco, D. R. (1997). Computational fluid dynamics: an introduction for engineers. Longman.

[32] Patankar, S. V. (1991). Computation of conduction and duct flow heat transfer. CRC Press.

[33] Patankar, S. V. (2018). Numerical heat transfer and fluid flow. CRC Press.

[34] Patankar, S. V. (1981). A calculation procedure for two-dimensional elliptic situations. Numerical Heat Transfer, 4(4), 409-425.

[35] Evans, L.C. (2010). Partial differential equations. American Mathematical Society, Providence, Rhode Island.

[36] Anderson, J. D., Wendt, J. (1995). Computational fluid dynamics (Vol. 206, p. 332). New York: McGraw-Hill.

[37] Morton, K. W., & Mayers, D. F. (2005). Numerical solution of partial differential equations: an introduction. Cambridge University Press.

[38] LeVeque, R. J. (2007). Finite difference methods for ordinary and partial differential equations: steady-state and time-dependent problems. Society for Industrial and Applied Mathematics.

[39] LeVeque, R. J. (2002). Finite volume methods for hyperbolic problems (Vol. 31). Cambridge university press.

[40] Badr, M., Yazdani, A., & Jafari, H. (2018). Stability of a finite volume element method for the time-fractional advection-diffusion equation. Numerical Methods for Partial Differential Equations, 34(5), 1459-1471.

[41] Syrakos, A., Goulas, A. (2006). Estimate of the truncation error of finite volume discretization of the Navier–Stokes equations on colocated grids. International journal for numerical methods in fluids, 50(1), 103-130.

[42] Fraysse, F., de Vicente, J., Valero, E. (2012). The estimation of truncation error by τ-estimation revisited. Journal of Computational Physics, 231(9), 3457-3482.

[43] Ermentrout, G. B., Folias, S. E., & Kilpatrick, Z. P. (2014). Spatiotemporal pattern formation in neural fields with linear adaptation. In Neural Fields (pp. 119-151). Springer, Berlin, Heidelberg.

[44] Benda, J., & Herz, A. V. (2003). A universal model for spike-frequency adaptation. Neural Computation, 15(11), 2523-2564.

Aytül Gökçe *is a Research Fellow at Ordu University in Turkey, working in the broad area of applied mathematics. Aytül's research is mainly devoted to dynamical systems modelling in biology and medicine, and the understanding of patterning in real life problems.*
`https://orcid.org/0000-0003-1421-3966`

Burcu Gürbüz *is a Research Associate in Johannes Gutenberg-University Mainz in Germany. Her main research interests ordinary and partial differential equations, integral and integro differential-difference equations, dynamical systems and their analysis, numerical methods, mathematical biology and scientific computation.*
`https://orcid.org/0000-0002-4253-5877`

An International Journal of Optimization and Control: Theories & Applications (http://ijocta.balikesir.edu.tr)

ISSN: 2146-0957, eISSN: 2146-5703, http://www.ijocta.org

INSTRUCTIONS FOR AUTHORS

Aims and Scope

An International Journal of Optimization and Control: Theories & Applications (IJOCTA) is a scientific, peer-reviewed, open-access journal that publishes original research papers and review articles of high scientific value in all areas of applied mathematics, optimization and control. It aims to focus on multi/inter-disciplinary research into the development and analysis of new methods for the numerical solution of real-world applications in engineering and applied sciences. The basic fields of this journal cover mathematical modeling, computational methodologies and (meta)heuristic algorithms in optimization, control theory and their applications. Note that new methodologies for solving recent optimization problems in operations research must conduct a comprehensive computational study and/or case study to show their applicability and practical relevance.

Journal Topics

The topics covered in the journal are (not limited to):

Applied Mathematics, Financial Mathematics, Control Theory, Optimal Control, Fractional Calculus and Applications, Modeling of Bio-systems for Optimization and Control, Linear Programming, Nonlinear Programming, Stochastic Programming, Parametric Programming, Conic Programming, Discrete Programming, Dynamic Programming, Nonlinear Dynamics, Stochastic Differential Equations, Optimization with Artificial Intelligence, Operational Research in Life and Human Sciences, Heuristic and Metaheuristic Algorithms in Optimization, Applications Related to Optimization in Engineering.

Submission of Manuscripts

New Submissions

Solicited and contributed manuscripts should be submitted to IJOCTA via the journal's online submission system. You need to make registration prior to submitting a new manuscript (please click here to register and do not forget to define yourself as an "Author" in doing so). You may then click on the "New Submission" link on your User Home.

IMPORTANT: If you already have an account, please click here to login. It is likely that you will have created an account if you have reviewed or authored for the journal in the past.

On the submission page, enter data and answer questions as prompted. Click on the “Next” button on each screen to save your work and advance to the next screen. The names and contact details of at least four internationally recognized experts who can review your manuscript should be entered in the "Comments for the Editor" box.

You will be prompted to upload your files: Click on the “Browse” button and locate the file on your computer. Select the description of the file in the drop down next to the Browse button. When you have selected all files you wish to upload, click the “Upload” button. Review your submission before sending to the Editors. Click the “Submit” button when you are done reviewing. Authors are responsible for verifying all files have uploaded correctly.

You may stop a submission at any phase and save it to submit later. Acknowledgment of receipt of the manuscript by IJOCTA Online Submission System will be sent to the corresponding author, including an assigned manuscript number that should be included in all subsequent correspondence. You can also log-on to submission web page of IJOCTA any time to check the status of your manuscript. You will receive an e-mail once a decision has been made on your manuscript.

Each manuscript must be accompanied by a statement that it has not been published elsewhere and that it has not been submitted simultaneously for publication elsewhere.

Manuscripts can be prepared using LaTeX (.tex) or MSWord (.docx). However, manuscripts with heavy mathematical content will only be accepted as LaTeX files.

Preferred first submission format (for reviewing purpose only) is Portable Document File (.pdf). Please find below the templates for first submission.

Click here to download Word template for first submission (.docx)

Click here to download LaTeX template for first submission (.tex)

Revised Manuscripts

Revised manuscripts should be submitted via IJOCTA online system to ensure that they are linked to the original submission. It is also necessary to attach a separate file in which a point-by-point explanation is given to the specific points/questions raised by the referees and the corresponding changes made in the revised version.

To upload your revised manuscript, please go to your author page and click on the related manuscript title. Navigate to the "Review" link on the top left and scroll down the page. Click on the "Choose File" button under the "Editor Decision" title, choose the revised article (in pdf format) that you want to submit, and click on the "Upload" button to upload the author version. Repeat the same steps to upload the "Responses to Reviewers/Editor" file and make sure that you click the "Upload" button again.

To avoid any delay in making the article available freely online, the authors also need to upload the source files (Word or LaTex) when submitting revised manuscripts. Files can be compressed if necessary. The two-column final submission templates are as follows:

Click here to download Word template for final submission (.docx)

Click here to download LaTeX template for final submission (.tex)

Authors are responsible for obtaining permission to reproduce copyrighted material from other sources and are required to sign an agreement for the transfer of copyright to IJOCTA.

Article Processing Charges

There are **no charges** for submission and/or publication.

English Editing

Papers must be in English. Both British and American spelling is acceptable, provided usage is consistent within the manuscript. Manuscripts that are written in English that is ambiguous or incomprehensible, in the opinion of the Editor, will be returned to the authors with a request to resubmit once the language issues have been improved. This policy does not imply that all papers must be written in "perfect" English, whatever that may mean. Rather, the criteria require that the intended meaning of the authors must be clearly understandable, i.e., not obscured by language problems, by referees who have agreed to review the paper.

Presentation of Papers

Manuscript style

Use a standard font of the **11-point type: Times New Roman** is preferred. It is necessary to single line space your manuscript. Normally manuscripts are expected not to exceed 25 single-spaced pages including text, tables, figures and bibliography. All illustrations, figures, and tables are placed within the text at the appropriate points, rather than at the end.

During the submission process you must enter: (1) the full title, (2) names and affiliations of all authors and (3) the full address, including email, telephone and fax of the author who is to check the proofs. Supply a brief **biography** of each author at the end of the manuscript after references.

- Include the name(s) of any **sponsor(s)** of the research contained in the paper, along with **grant number(s).**
- Enter an **abstract** of no more than 250 words for all articles.

Keywords

Authors should prepare no more than 5 keywords for their manuscript.

Maximum five **AMS Classification number** (http://www.ams.org/mathscinet/msc/msc2010.html) of the study should be specified after keywords.

Writing Abstract

An abstract is a concise summary of the whole paper, not just the conclusions. The abstract should be no more than 250 words and convey the following:

1. An introduction to the work. This should be accessible by scientists in any field and express the necessity of the experiments executed.
2. Some scientific detail regarding the background to the problem.
3. A summary of the main result.
4. The implications of the result.
5. A broader perspective of the results, once again understandable across scientific disciplines.

It is crucial that the abstract conveys the importance of the work and be understandable without reference to the rest of the manuscript to a multidisciplinary audience. Abstracts should not contain any citation to other published works.

Reference Style

Reference citations in the text should be identified by numbers in square brackets "[ ]". All references must be complete and accurate. Please ensure that every reference cited in the text is also present in the reference list (and vice versa). Online citations should include date of access. References should be listed in the following style:

Journal article

Author, A.A., & Author, B. (Year). Title of article. Title of Journal, Vol(Issue), pages.

Castles, F.G., Curtin, J.C., & Vowles, J. (2006). Public policy in Australia and New Zealand: The new global context. Australian Journal of Political Science, 41(2), 131–143.

Book

Author, A. (Year). Title of book. Publisher, Place of Publication.

Mercer, P.A., & Smith, G. (1993). Private Viewdata in the UK. 2nd ed. Longman, London.

Chapter

Author, A. (Year). Title of chapter. In: A. Editor and B. Editor, eds. Title of book. Publisher, Place of publication, pages.

Bantz, C.R. (1995). Social dimensions of software development. In: J.A. Anderson, ed. Annual review of software management and development. CA: Sage, Newbury Park, 502–510.

Internet document

Author, A. (Year). Title of document [online]. Source. Available from: URL [Accessed (date)].

Holland, M. (2004). Guide to citing Internet sources [online]. Poole, Bournemouth University. Available from: http://www.bournemouth.ac.uk/library/using/guide_to_citing_internet_sourc.html [Accessed 4 November 2004].

Newspaper article

Author, A. (or Title of Newspaper) (Year). Title of article. Title of Newspaper, day Month, page, column.

Independent (1992). Picking up the bills. Independent, 4 June, p. 28a.

Thesis

Author, A. (Year). Title of thesis. Type of thesis (degree). Name of University.

Agutter, A.J. (1995). The linguistic significance of current British slang. PhD Thesis. Edinburgh University.

Illustrations

Illustrations submitted (line drawings, halftones, photos, photomicrographs, etc.) should be clean originals or digital files. Digital files are recommended for highest quality reproduction and should follow these guidelines:

- 300 dpi or higher
- Sized to fit on journal page
- TIFF or JPEG format only
- Embedded in text files and submitted as separate files (if required)

Tables and Figures

Tables and figures (illustrations) should be embedded in the text at the appropriate points, rather than at the end. A short descriptive title should appear above each table with a clear legend and any footnotes suitably identified below.

Proofs

Page proofs are sent to the designated author using IJOCTA EProof system. They must be carefully checked and returned within 48 hours of receipt.

Offprints/Reprints

Each corresponding author of an article will receive a PDF file of the article via email. This file is for personal use only and may not be copied and disseminated in any form without prior written permission from IJOCTA.

Submission Preparation Checklist

As part of the submission process, authors are required to check off their submission's compliance with all of the following items, and submissions may be returned to authors that do not adhere to these guidelines.

1. The submission has not been previously published, nor is it before another journal for consideration (or an explanation has been provided in Comments for the Editor).
2. The paper is in PDF format and prepared using the IJOCTA's two-column template.
3. All references cited in the manuscript have been listed in the References list (and vice-versa) following the referencing style of the journal.
4. There is no copyright material used in the manuscript (or all necessary permissions have been granted).
5. Details of all authors have been provided correctly.
6. ORCID profile numbers of "all" authors are mandatory, and they are provided at the end of the manuscript as in the template (visit https://orcid.org for more details on ORCID).
7. The text adheres to the stylistic and bibliographic requirements outlined in the Author Guidelines.
8. Maximum five AMS Classification number (http://www.ams.org/mathscinet/msc/msc2010.html) of the study have been provided after keywords.
9. The names and email addresses of at least FOUR (4) possible reviewers have been indicated in "Comments for the Editor" box in "Paper Submission Step 1-Start". Please note that at least two of the recommendations should be from different countries. Avoid suggesting reviewers you have a conflict of interest.

Peer Review Process

All contributions, prepared according to the author guidelines and submitted via IJOCTA online submission system are evaluated according to the criteria of originality and quality of their scientific content. The corresponding author will receive a confirmation e-mail with a reference number assigned to the paper, which he/she is asked to quote in all subsequent correspondence.

All manuscripts are first checked by the Technical Editor using plagiarism detection software (iThenticate) to verify originality and ensure the quality of the written work. If the result is not satisfactory (i.e. exceeding the limit of 30% of overlapping), the submission is rejected and the author is notified.

After the plagiarism check, the manuscripts are evaluated by the Editor-in-Chief and can be rejected without reviewing if considered not of sufficient interest or novelty, too preliminary or out of the scope of the journal. If the manuscript is considered suitable for further evaluation, it is first sent to the Area Editor. Based on his/her opinion the paper is then sent to at least two independent reviewers. Each reviewer is allowed up to four weeks to return his/her feedback but this duration may be extended based on his/her availability. IJOCTA has instituted a blind peer review process where the reviewers' identities are not known to authors. When the reviews are received, the Area Editor gives a decision and lets the author know it together with the reviewer comments and any supplementary files.

Should the reviews be positive, the authors are expected to submit the revised version usually within two months the editor decision is sent (this period can be extended when the authors contact to the editor and let him/her know that they need extra time for resubmission). If a revised paper is not resubmitted within the deadline, it is considered as a new submission after all the changes requested by reviewers have been made. Authors are required to submit a new cover letter, a response to reviewers letter and the revised manuscript (which ideally shows the revisions made in a different color or highlighted). If a change in authorship (addition or removal of author) has occurred during the revision, authors are requested to clarify the reason for change, and all authors (including the removed/added ones) need to submit a written consent for the change. The revised version is evaluated by the Area editor and/or reviewers and the Editor-in-Chief brings a decision about final acceptance based on their suggestions. If necessary, further revision can be asked for to fulfil all the requirements of the reviewers.

When a manuscript is accepted for publication, an acceptance letter is sent to the corresponding author and the authors are asked to submit the source file of the manuscript conforming to the IJOCTA two-column final submission template. After that stage, changes of authors of the manuscript are not possible. The manuscript is sent to the Copyeditor and a linguistic, metrological and technical revision is made, at which stage the authors are asked to make the final corrections in no more than a week. The layout editor prepares the galleys and the authors receive the galley proof for final check before printing. The authors are expected to correct only typographical errors on the proofs and return the proofs within 48 hours. After the final check by the layout editor and the proofreader, the manuscript is assigned a DOI number, made publicly available and listed in the forthcoming journal issue. After printing the issue, the corresponding metadata and files published in this issue are sent to the databases for indexing.

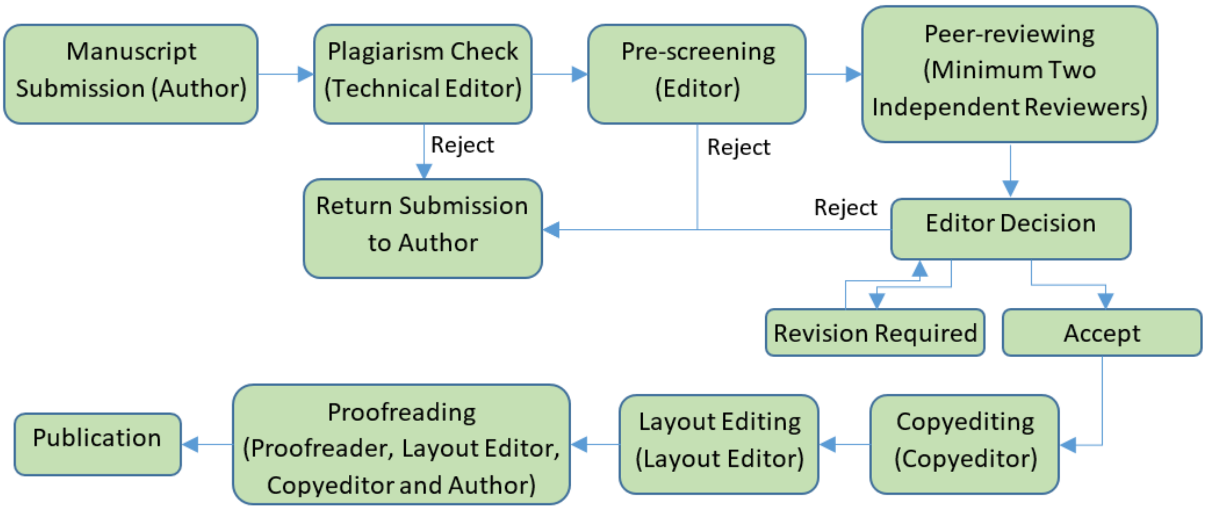

Publication Ethics and Malpractice Statement

IJOCTA is committed to ensuring ethics in publication and quality of articles. Conforming to standards of expected ethical behavior is therefore necessary for all parties (the author, the editor(s), the peer reviewer) involved in the act of publishing.

International Standards for Editors

The editors of the IJOCTA are responsible for deciding which of the articles submitted to the journal should be published considering their intellectual content without regard to race, gender, sexual orientation, religious belief, ethnic origin, citizenship, or political philosophy of the authors. The editors may be guided by the policies of the journal's editorial board and constrained by such legal requirements as shall then be in force regarding libel, copyright infringement and plagiarism. The editors may confer with other editors or reviewers in making this decision. As guardians and stewards of the research record, editors should encourage authors to strive for, and adhere themselves to, the highest standards of publication ethics. Furthermore, editors are in a unique position to indirectly foster responsible conduct of research through their policies and processes.

To achieve the maximum effect within the research community, ideally all editors should adhere to universal standards and good practices.

- Editors are accountable and should take responsibility for everything they publish.
- Editors should make fair and unbiased decisions independent from commercial consideration and ensure a fair and appropriate peer review process.
- Editors should adopt editorial policies that encourage maximum transparency and complete, honest reporting.
- Editors should guard the integrity of the published record by issuing corrections and retractions when needed and pursuing suspected or alleged research and publication misconduct.
- Editors should pursue reviewer and editorial misconduct.
- Editors should critically assess the ethical conduct of studies in humans and animals.
- Peer reviewers and authors should be told what is expected of them.
- Editors should have appropriate policies in place for handling editorial conflicts of interest.

Reference:

Kleinert S & Wager E (2011). Responsible research publication: international standards for editors. A position statement developed at the 2nd World Conference on Research Integrity, Singapore, July 22-24, 2010. Chapter 51 in: Mayer T & Steneck N (eds) Promoting Research Integrity in a Global Environment. Imperial College Press / World Scientific Publishing, Singapore (pp 317-28). (ISBN 978-981-4340-97-7) [Link].

International Standards for Authors

Publication is the final stage of research and therefore a responsibility for all researchers. Scholarly publications are expected to provide a detailed and permanent record of research. Because publications form the basis for both new research and the application of findings, they can affect not only the research community but also, indirectly, society at large. Researchers therefore have a responsibility to ensure that their publications are honest, clear, accurate, complete and balanced, and should avoid misleading, selective or ambiguous reporting. Journal editors also have responsibilities for ensuring the integrity of the research literature and these are set out in companion guidelines.

- The research being reported should have been conducted in an ethical and responsible manner and should comply with all relevant legislation.
- Researchers should present their results clearly, honestly, and without fabrication, falsification or inappropriate data manipulation.
- Researchers should strive to describe their methods clearly and unambiguously so that their findings can be confirmed by others.
- Researchers should adhere to publication requirements that submitted work is original, is not plagiarised, and has not been published elsewhere.
- Authors should take collective responsibility for submitted and published work.
- The authorship of research publications should accurately reflect individuals' contributions to the work and its reporting.
- Funding sources and relevant conflicts of interest should be disclosed.
- When an author discovers a significant error or inaccuracy in his/her own published work, it is the author's obligation to promptly notify the journal's Editor-in-Chief and cooperate with them to either retract the paper or to publish an appropriate erratum.

Reference:

Wager E & Kleinert S (2011) Responsible research publication: international standards for authors. A position statement developed at the 2nd World Conference on Research Integrity, Singapore, July 22-24, 2010. Chapter 50 in: Mayer T & Steneck N (eds) Promoting Research Integrity in a Global Environment.

Imperial College Press / World Scientific Publishing, Singapore (pp 309-16). (ISBN 978-981-4340-97-7) [Link].

Basic principles to which peer reviewers should adhere

Peer review in all its forms plays an important role in ensuring the integrity of the scholarly record. The process depends to a large extent on trust and requires that everyone involved behaves responsibly and ethically. Peer reviewers play a central and critical part in the peer-review process as the peer review assists the Editors in making editorial decisions and, through the editorial communication with the author, may also assist the author in improving the manuscript.

Peer reviewers should:

- respect the confidentiality of peer review and not reveal any details of a manuscript or its review, during or after the peer-review process, beyond those that are released by the journal;
- not use information obtained during the peer-review process for their own or any other person's or organization's advantage, or to disadvantage or discredit others;
- only agree to review manuscripts for which they have the subject expertise required to carry out a proper assessment and which they can assess within a reasonable time-frame;
- declare all potential conflicting interests, seeking advice from the journal if they are unsure whether something constitutes a relevant conflict;
- not allow their reviews to be influenced by the origins of a manuscript, by the nationality, religion, political beliefs, gender or other characteristics of the authors, or by commercial considerations;
- be objective and constructive in their reviews, refraining from being hostile or inflammatory and from making libellous or derogatory personal comments;
- acknowledge that peer review is largely a reciprocal endeavour and undertake to carry out their fair share of reviewing, in a timely manner;
- provide personal and professional information that is accurate and a true representation of their expertise when creating or updating journal accounts.

Reference:

Homes I (2013). COPE Ethical Guidelines for Peer Reviewers, March 2013, v1 [Link].

An International Journal of Optimization and Control: Theories & Applications

Volume: 12 Number: 2
July 2022

CONTENTS

ISSN 2146-0957

www.ijocta.org
editor@ijocta.org